Characterization of the Herpes Simplex Virus 1 VP11/12-tyrosine based binding motifs for Src family kinases, p85, Grb2 and Shc

by

Ulrike Strunk

A thesis submitted in partial fulfillment of the requirements for the degree of

Doctor of Philosophy

in

Virology

Department of Medical Microbiology and Immunology

University of Alberta

Abstract

Infection with HSV-1 triggers several events specifically designed to manipulate cell signal transduction pathways. Two major signaling cascades targeted by the virus are the PI3K/Akt-pathway and the TCR-signaling pathway. Prior to the studies presented in this thesis, it was known that the tegument protein VP11/12 associates with cellular proteins that are directly involved in those pathways. Specially, it was suggested that VP11/12 associates with SFKs, p85, Grb2 and Shc through specific tyrosine-based binding motifs that are located within the C-terminal region of VP11/12.

Here, we first generated point-mutated viruses with inactive binding motifs and assessed the ability of mutant VP11/12 to associate with the SFKs, p85, Grb2 and Shc. I found that inactivation of the predicted binding motifs for SFKs, Grb2 and Shc eliminated the protein-VP11/12 associations. In the case of p85, I was able to demonstrate that inactivation of the predicted p85-binding motif significantly reduced, but did not eliminate, the VP11/12-p85 interaction. From these results, it became evident that VP11/12 requires the phosphorylation of specific tyrosine-based binding motifs within its C-terminal region in order to associate with SFKs, p85, Grb2 and Shc.

Next, I determined the downstream effects of eliminating these protein-protein associations. I provide data suggesting that VP11/12 requires the recruitment and activation of SFKs to further associate with Grb2, Shc and p85 as well as to induce global phosphorylation of VP11/12. Further, I was able to demonstrate that VP11/12 must associate with SFKs, Grb2 and p85 in order to activate Akt during infection. In addition, I provide data suggesting that VP11/12 needs to associate with SFKs in order to severely reduce TCR signaling events upon transfection. Taken together, this data fully supports

the Wagner-Smiley model demonstrating that VP11/12 mimics an activated receptor in that VP11/12 associates with cellular proteins that are directly involved in the stimulation of the PI3K/Akt- as well as the TCR-signaling pathways.

To my mother and grandparents, Rolf and Ruth.

"Nothing in life is to be feared. It is only to be understood. Now is the time to understand more, so that we may fear less."

Marie Curie (1867-1934)

Acknowledgments

First I would like to thank Dr. Jim Smiley for serving as my supervisor and providing an excellent training environment. I would also like to express my thanks to all members of the Smiley lab, especially Holly Bandi, Dr. Bianca Dauber, Alexandra Mercer, Dr. Heather Eaton, Dr. Brett Duguay and Danny Gomez Ramos, for all the support and encouragement.

I would also like to acknowledge the outstanding guidance by my Ph.D. advisory committee members Dr. Hanne Ostergaard and Dr. Rob Ingham.

In addition, I would like to thank those that contributed towards my research by providing reagents, especially Dr. Hanne Ostergaard, Dr. Rob Ingham, Dr. David Leib, Dr. Wade Bresnahan, Dr. Tony Pawson and Dr. Andre Veillette.

I would also like to thank my mother and my grandparents for the support as well as teaching me that there is no substitute for hard work.

Finally, I would like to thank my close friends, Dipl. Ing. Svenja Heeren, Dr. Kinola Williams, Dr. Bettina Lehman, Debra Couwenberg, my boyfriend, Behnam Yousefi, and our cats, Bruce and Molly. You made the years fly by and words cannot express how much each of you contributed towards my life.

Table of Contents

List of Figures

List of Tables

List of Abbreviations and Symbols

Abbreviation	Meaning
A	Alanine
AG	Antigen
Akt	Protein kinase B
BAC	Bacterial artificial chromosome
BAD	Bcl-2-associated death protein
BAD	Bcl-2 associated death
C2	Membrane-interacting domain
CD	Cluster of differentiation
CeHV1	Cercopithecine Herpesvirus 1
CeHV2	Cercopithecine Herpesvirus 2
cGAS	Cyclic GMP-AMP (cGAMP) synthase
ChHV	Chimpanzee alpha-1 herpesvirus
CSK	C-terminal SRC kinase
DAG	Diacylglycerol
dH_2O	Distilled Water
DMEM	Dulbecco's modified Eagle's medium
DMSO	Dimethylsulphoxide
DNA	Deoxyribonucleic acid
DUSP	Dual specificity phosphatase
E.coli	*Escherichia coli*
EBV	Epstein-Barr Virus
EDTA	Ethylenediaminetetraacetic acid
EGFP	Enhanced green fluorescent protein
EGTA	Ethylene glycol-bis(β-aminoethyl ether)-N,N,N',N'-tetraacetic acid
ER	Endoplasmic reticulum
Erk1/2	Extracellular-signal regulated kinase ½

F	Phenylalanine
galK	Galactokinase
GDP	Guanosine diphosphate
GFP	Green fluorescent protein
Grb2	Growth factor receptor-bound protein 2
GSK3β	glycogen synthase kinase 3 beta
GST	Glutathione S-transferases
GTP	Guanosine triphosphate
HCF-1	Host cell factor 1
hCMV	Human Cytomegalovirus
HHV-6A	Human herpesvirus 6A
HHV-6B	Human herpesvirus 6B
HHV-7	Human herpesvirus 7
hpi	Hours post-infection
hpt	Hours post-transfection
HSV	Herpes Simplex Virus
HSV-1/2	Herpes Simplex Virus-1/ Herpes Simplex Virus-2
HVEM	Herpesvirus entry mediator
HVP2	Papiine herpesvirus 2
IFI-16	Interfon-gamma inducible-16
IFN	Interferon
IKK	IκB kinase
IL	Interleukin
IP	Immunoprecipitation
IP3R	IP3-receptor
IR	Internal inverted repeat
IRF	IFN response factor
ISG	IFN stimulated genes
iSh2	Inter-Sh2 domain

JAK	Janus kinase
kbp	Kilobase pairs
KCl	Potassium Cloride
KSHV	Kaposi's sarcoma-associated virus
L	Leucine
LAT	Latency-associated RNA transcript
LAT	Linker for Activation of T-cells
LB	Lysogeny broth (also known as Luria-Bertani medium)
Lck	SFK lymphocyte-specific cytoplasmic protein kinase
MAPK	Ras-mitogen associated protein kinase
MAPKK	Ras-mitogen associated protein kinase kinase
MAVS	Mitochondrial antiviral-signaling protein
McHV1	Macacine Herpesvirus 1
MEK	Erk kinase
$MgCl_2$	Magnesium Chloride
MHC1	Major histocompatibility complex 1
miRNA	Micro RNA
ms	Millisecond
MOI	Multiplicity of infection
mTOR	Mechanistic target of rapamycin
mTORC2	Mechanistic target of rapamycin complex 2
NaCl	Sodium Chloride
NEC	Nuclear egree complex
NFκB	nuclear factor κB pathway
NPC	Nuclear pore complex
Oct-1	Octamer-binding protein 1
OD	Optical density
OKT3	Antibody towards CD3
ORF	Open reading frame

ORI	Origin of replication
P	Proline
p38	stress-activated protein kinase
p85-BD	p85-binding domain
PAMP	Pathogen associated molecular pattern
PBS	Phosphate buffered saline
PCR	Polymerase chain reaction
PDCD4	Programmed cell death protein 4
PDGFR	Platelet-derived growth factor receptor
PDK1	Phosphoinositide-dependent kinase-1
PDK2	Phosphoinositide-dependent kinase-2
PI3K	Phosphatidylinositol-4,5-bisphosphate 3-kinase
PIP2	Phosphatidylinositol (4,5)-bisphosphate
PIP3	Phosphatidylinositol (3,4,5)-trisphosphate
PKC	Protein kinase C
PKR	Protein kinase RNA
PLCγ	Phospholipase γ
PMA	Phorbal ester
PRR	Pattern recognition receptor
PTB	phosphotyrosine binding
PTEN	Phosphatase and tensin homolog
pY	Phospho-Tyrosine
Raf	Murine sarcoma viral oncogene
RBD	RAS-binding domain
RNA	Ribonucleic acid
S	Serine
s	Second
S6K	Ribosomal protein S6 kinase
SDS	Sodium dodecyl sulfate

SDS-PAGE	Sodium dodecyl sulfate polyacrylamide gel electrophoresis
SFK	Src family kinase
Sh2	SRC Homology 2 Domain
Sh3	SRC Homology 3 Domain
Shc	Sh2 containing proto-oncogene
SOS	Son of sevenless
STAT	Member of the signal transducer and activator of transcription
STING	Stimulator of interferon genes
T	Threonine
TAP	Transporter associated with antigen processing
TCR	T-cell receptor
TLR	Toll-like receptor
TNF	Tumor necrosis factor
TR	Terminal Repeat
TSC1/TSC2	Tuberous sclerosis complex ½
U_L or UL	Unique long
U_s or US	Unique short
V	Volt
vhs	Virion host shutoff
VP	Virion protein
VZV	Varicella-Zoster-Virus
WT	Wild type
Y	Tyrosine
ZAP-70	Zeta-chain-associated protein kinase 70
Δ	Delta
ζ	Zeta

Chapter 1

Introduction

Preface

In this thesis I define the role of the Herpes Simplex Virus 1 (HSV-1) tegument protein VP11/12 in hijacking the phosphatidylinositol-4,5-bisphosphate-3-kinase (PI3K)/Akt-pathway and the T-cell receptor (TCR)-pathway by examining VP11/12's interactions with the signaling proteins p85, Grb2, Shc and Src family kinases (SFKs). I first determine which tyrosine-based binding motif within VP11/12 is necessary for the binding of VP11/12 to each protein. I subsequently investigate how these interactions affect the TCR- and the PI3K/Akt-pathways.

The aim of this introduction is to provide the background relevant to my thesis research. Section 1 provides a broad overview of the molecular virology of HSV-1 including taxonomy (section 1.1.1), morphology (section 1.1.2), the lytic replication cycle (section 1.1.3) and latency (section 1.1.4). Section 1.2 outlines the manipulation of host functions by HSV-1 and what was known about VP11/12 as a mediator of signaling pathways before I started my thesis research. Section 1.3 outlines my thesis rationale.

1.1 Herpesviruses

Herpesviruses share the same overall morphology but have a very broad host range including: fish, birds, mammals and reptiles [1]. Infections with herpes simplex viruses (HSVs) represent an enormous global health problem. For example, more than 67 % of the world's population is infected with Herpes Simplex Virus 1 (HSV-1) and neonatal infection can cause mortality in 60 % of the infected infants if no treatment is provided [2].

1.1.1 Taxonomy

The *Herpesviridae* family includes over 200 members and the members are grouped into three subfamilies: *Alphaherpesvirinae, Betaherpesvirinae* and *Gamma-herpesvirinae* (Fig. 1.1). This classification is based on tropism and growth, as well as the specific cell type in which the virus develops latency [1].

The *Alphaherpesvirinae* subfamily contains three viruses that infect humans: HSV-1, herpes simplex virus 2 (HSV-2) and Varicella-Zoster-virus (VZV). While HSV-1 is the causative agent of cold sores, HSV-2 is known as the causative agent of genital sores [1]. In rare cases HSV-1 and HSV-2 can infect brain tissue cells and therefore cause potentially lethal encephalitis [3]. In addition, neonatal herpes infection can lead to lasting neurologic disability or death [4]. Primary infection with VZV occurs during early childhood or adolescence and causes chickenpox. If the virus reactivates out of latency, it results in herpes zoster (shingles), which is characterized by a painful dermatomal rash. The successful design of a vaccine against herpes zoster has led to a substantial decline of this infectious disease [5].

The *Betaherpesvirinae* subfamily contains four viruses that are known to infect humans. The human cytomegalovirus (hCMV) is the prototypical member of this subfamily. It is prevalent within the population, although it is only of significant concern for infants, the elderly and immunocompromised individuals [1]. Human herpesvirus 6A (HHV-6A), 6B (HHV-6B), and 7 (HHV-7) were first classified as highly related T-lymphotropic viruses. The more recent classification is based on new research evidence, suggesting that HHV-6A and HHV-6B are distinct species due to their different epidemiology and biological characteristics [6].

The *Gammaherpesvirinae* subfamily contains two human herpesviruses: Epstein-Barr virus (EBV) and Kaposi's sarcoma-associated herpesvirus (KSHV). Both viruses infect and establish latency in lymphoid cells. EBV is the causative agent of mononucleosis [7] and KSHV is the etiological agent of Kaposi's sarcoma [8].

Given that my thesis research is focused on HSV-1, the remaining part of this introduction mainly outlines the structure and life cycle of HSV-1.

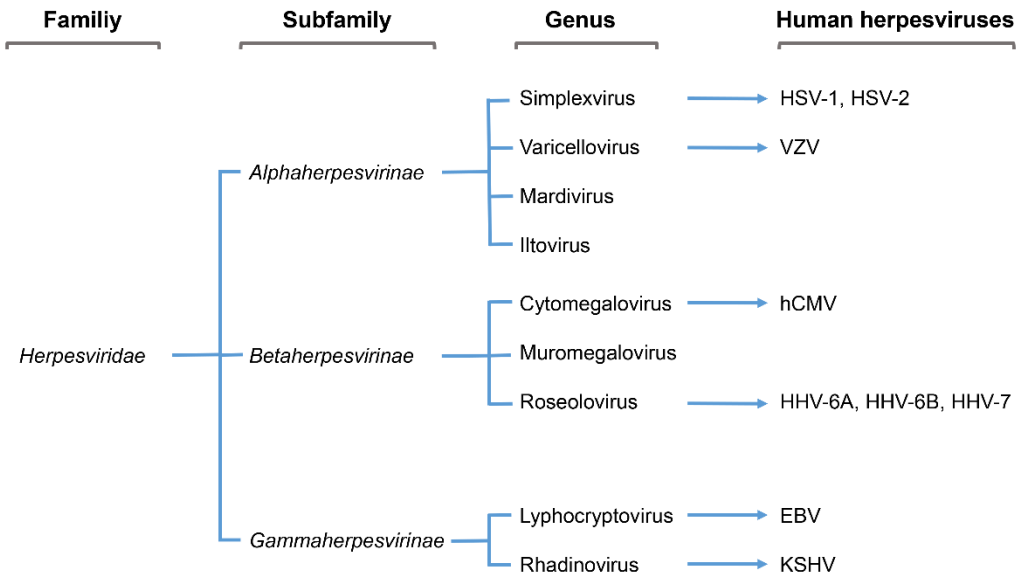

Fig. 1.1: Taxonomy of herpesviruses.

1.1.2 Structure of HSV-1

As depicted in figure 1.2, herpesviruses contain a linear double-stranded DNA genome, which is encased within an icosahedral capsid. The capsid is surrounded by a

proteinaceous layer, called the tegument, and an outer lipid bi-layer envelope containing glycoproteins. Depending on the virus, the genome size ranges from 124 to 295 kilobase pairs (kbp). The genomes of all herpesviruses contain a conserved region that codes for structural as well as non-structural genes and DNA replication proteins [1]. Each structural element is described below in more detail.

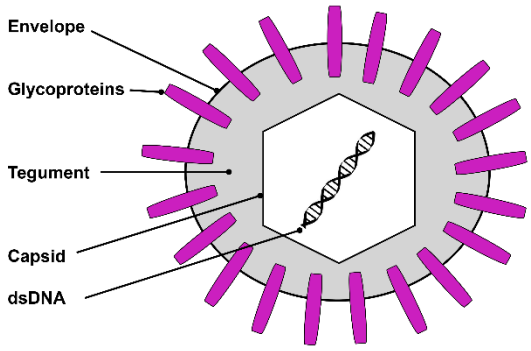

Fig. 1.2: Morphology of HSV-1.

1.1.2.1 The envelope

The envelope of HSV-1 is a lipid bi-layer derived from cellular membranes. Viral glycoproteins embedded in the envelope facilitate the fusion of the viral envelope with the cellular plasma membrane. HSV-1 envelope proteins bind directly to cellular receptors to initiate the internalization of the viral particle into the host cell. More than ten HSV-1 glycoproteins have been identified [1], but only glycoprotein B (gB), glycoprotein D (gD), glycoprotein H (gH) and glycoprotein L (gL) are necessary and sufficient to induce cell fusion [9, 10]. A detailed description of the viral entry process is given in section 1.1.3.1 of this introduction.

1.1.2.2 The tegument

The tegument is the proteinaceous layer located between the capsid and the envelope and it contains at least 20 viral proteins and some cellular proteins [11, 12]. Tegument proteins can be released into the cytoplasm or can remain associated with the injected capsid after the virion fuses with the host cell membrane [13-15]. Tegument proteins have many different functions including recruitment of cellular molecular motors, targeting of virion components to the nuclei or the cellular plasma membrane (section 1.1.3.2) as well as regulation of viral/host cell gene expression (section 1.1.3.3) [16]. The process of tegument assembly is described in section 1.1.3.5 of this introduction.

Early experiments using non-ionic fractionation suggested that the tegument consists of two layers: the inner and the outer tegument. Proteins of the inner tegument remain associated with the capsid, while proteins of the outer tegument like VP11/12 separate from the capsid during fractionation [17, 18].

Cryo-electron tomography of the viral particle showed that the tegument is not evenly distributed around the capsid (Fig. 1.3). On the proximal pole, the capsid is close to the envelope and is only separated from the envelope by a thin tegument layer. On the distal pole, the capsid is separated from the envelope by a thick tegument layer which is called the cap [19]. This asymmetry also extends to the distribution of glycoproteins as most glycoproteins form a dense cluster predominantly located at the distal pole [19]. These observations indicate that the structure of the tegument is more complex than previously predicted.

According to the spatial distribution of tegument proteins, Bohannon and colleagues suggested that tegument proteins can be subdivided into the following three classes

(Fig. 1.3): (i) proteins that symmetrically surround the capsid are termed radial distributed proteins (Fig 1.3A), (ii) proteins that are located throughout the entire tegument space are termed space filling proteins (Fig. 1.3B) and (iii) proteins that form the thick tegument layer on one side of the capsid, such as VP11/12, are termed offset/gap proteins (Fig. 1.3C) [20]. The architecture of the tegument is highly organized and can be described as a network of tegument proteins. Within this network, tegument proteins interact with each other in order to connect the capsid to the envelope [21]. A more detailed discussion of the tegument architecture and assembly is provided in section 1.1.3.5.

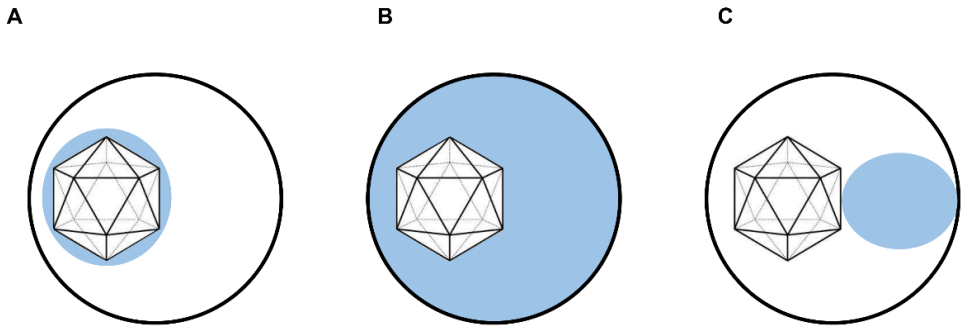

Fig. 1.3: Tegument protein distribution.

Shown is the tegument protein distribution (blue) as suggested by Bohannon and colleagues [20]. The capsid is placed asymmetrically within the tegument, as shown by *Gruenewald et al*. [19]. Tegument proteins can be subdivided into (A) radial symmetrically distributed proteins, (B) space filling proteins and (C) offset/gap asymmetrically distributed proteins. VP11/12, the tegument protein of interest to my thesis research, is described as an offset/gap tegument protein. Unlike the historical inner/outer tegument classification, this more recent model reflects the complex tegument protein distribution (figure is adapted from [20]).

The exact mechanism behind the asymmetrical placement of the capsid in the envelope is unknown, but it is suggested that the DNA portal formed by UL6 might be involved in the placement of the capsid because it is the only unique feature of the capsid [14, 22]. Further, the asymmetrical placement of the capsid might enable the two poles to serve different functions. During cell entry, the proximal pole seems to form the fusion pore

with the plasma membrane [14], whereas the distal pole is involved in the tegumentation process (section 1.1.3.5) [19].

Well characterized tegument proteins include the virion host shutoff protein vhs, a regulator of host and viral messenger RNA, VP16, a viral gene activator, and US3 and UL13, both viral protein kinases [16]. My thesis research is focused on the less well defined tegument protein VP11/12, which is encoded by the UL46 gene locus. VP11/12 is present in 1,000-2,000 copies per virion, making it one of the most abundant tegument proteins of HSV-1 [11, 23].

1.1.2.3 The capsid and the viral genome

The icosahedral capsid consists of 162 individual capsomers and is approximately 125 nm in diameter. Its function is to protect the genomic information and to assist in DNA packaging as well as release [1]. The mature capsid contains several copies of seven viral proteins. VP5 is the major capsid protein, and VP19C, VP23, VP26, UL17 and UL25 are minor capsid proteins [24]. The capsid further contains one unique single portal at one of the twelve vertexes of the icosahedron. This portal is formed by the DNA portal protein UL6 [25] and is responsible for the packaging (section 1.1.3.4) and release (1.1.3.2) of the viral genome [25, 26].

The 152 kbp HSV-1 genome [27-31] consists of one linear double-stranded DNA molecule [32] and contains two covalently linked components termed unique long (U_L) and unique short (U_S) (Fig. 1.4) [33-35], which are flanked by inverted repeats. The sequence repeat at the end of U_L (TR_L) is designated *ab*, and the internal inverted repeat (IR_L) is designated *b'a'*. The sequence repeats for U_s are designated *a'c'* (IR_s) and *ca* (TR_s) [28, 30]. The *a* sequence can be found in one or more copies (a_n) [36, 37] and it

contains no open reading frame; however, the Smiley lab and others have demonstrated that it contains signals that are essential for DNA packaging (section 1.1.3.4) [38-40]. The *b* sequence contains four open reading frames, and the *c* sequence contains only one open reading frame. Both sequences are present in two copies per genome.

The genome further contains three origins of replication, one is located within the U_L region and the other two flank the U_S region (Fig. 1.4) [41-44]. Most viral genes are only present in one copy per genome, with the U_L region encoding ~65 proteins and the U_S region encoding ~14 proteins [1].

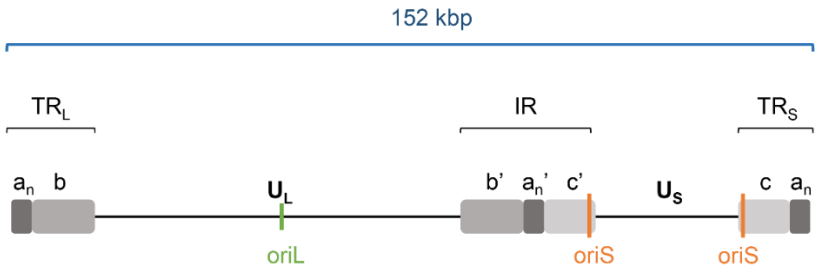

Fig. 1.4: Genomic Structure of HSV-1.

Shown is a simplified schematic structure of the linear double-stranded DNA genome of HSV-1. The U_L region, as well as the U_S region, are flanked by a terminal repeat (TR_L/TR_S) and an inverted repeat (IR), whereas IR_L contains the sequence b'a' and IR_S contains the sequence a'c'. Importantly, the *a* region can consist several sequence copies of itself (a_n). One origin of replication (ori) is located within the U_L region (oriL) and two additional origin of replication are flanking the US region (oriS). The figure is drawn to scale.

1.1.3 Lytic replication cycle

The transmission of HSV-1 depends on intimate and personal contact between a previously infected individual and a susceptible individual. In order to infect a susceptible individual the virus must come in direct contact with the mucosal surface and/or skin of

this individual. In the case of a primary HSV-1 infection, the infection site is limited to epithelial cells and transmission is induced through salvia or respiratory droplets. Initial viral replication at the entry site is followed by the establishment of latency in neurons. Viral replication within latently infected neurons is strongly limited (section 1.1.4), but following viral reactivation and anterograde transport of the viral capsid into epithelial cells, cold sores are developed at the viral replication site [1].

As outlined in figure 1.5, the HSV-1 replication cycle starts with the binding of viral glycoproteins to cellular membrane receptors (step 1). The binding initiates the fusion of the viral envelope with the cellular membrane and triggers the release of the tegument and capsid into the cytoplasm (step 2). Next, the capsid is transported towards the nucleus, and the genome is transcribed (steps 3-6). Viral capsid proteins are imported into the nucleus and the viral DNA is packed into the newly formed capsid (step 7). The capsid is then transported into the cytoplasm where it assembles its tegument and outer envelope before being released from the cell using an exocytosis based mechanism (step 8-11). In this subsection, I describe each step in more detail while highlighting the tegument assembly and tegument architecture (section 1.1.3.5).

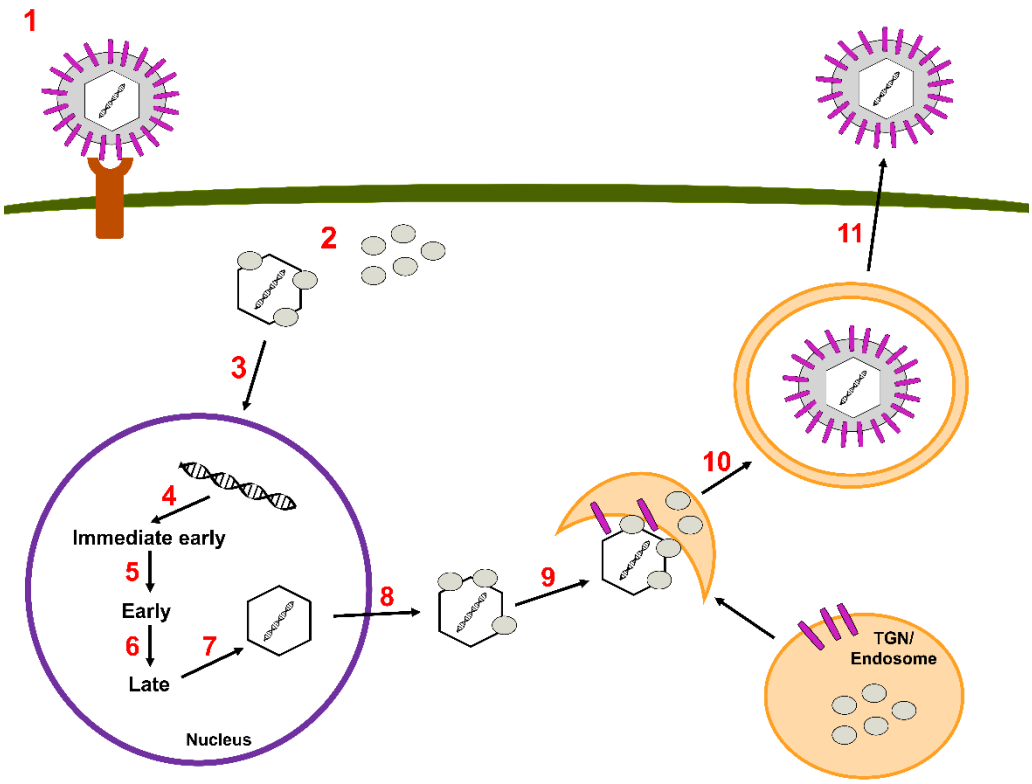

Fig. 1.5: HSV-1 lifecycle.

Shown is a simplified outline of the HSV-1 lifecycle. (1) The virus binds to cellular receptors and membrane fusion leads (2) to the release of the capsid and tegument into the cytoplasm. Inner tegument proteins remain associated with the capsid while outer tegument proteins dissociate from the capsid. (3) The genome is injected into the host cell nucleus and viral as well as host cell factors initiate viral gene transcription. (4-6) HSV-1 genes are transcribed in three kinetic classes (immediate early, early and late). Late gene products encode capsid proteins and allow (7) the formation of a new capsid within the nucleus followed by DNA packaging. (8) The mature capsid is then transported out of the nucleus into the cytoplasm and (9-10) assembles its tegument and outer envelope by budding into TGN and/or endosomal derived vesicles. Some tegument proteins might be added to the capsid within the nucleus and/or the cytoplasm. (11) The newly formed viral particle is released from the infected cell through exocytosis.

1.1.3.1 Entry

The entry of viral particles into a susceptible cell is mediated by the glycoproteins of the envelope (Fig. 1.5, step 1). The entry mechanism is highly complex and involves several temporal and spatial interactions between viral glycoproteins and cellular receptor proteins. The glycoproteins gC and gB interact with host cell receptors (glycosaminoglycans heparin sulfate, chondroitin sulfate, and dermatan sulfate) to trigger the tethering of HSV-1 virions to the cell's surface [45-50]. Once the tethering process is successful, gD associates with one entry receptor, such as herpesvirus entry mediator (HVEM) [51, 52], nectin-1, nectin-2 [53-55], or 3-O-sulfated heparin sulfate [56, 57]. The fusion machinery complex, which is composed of gB and gH/gL, then facilitates the fusion of the envelope with the cell plasma membrane [58], and the capsid and tegument are released into the cytoplasm (Fig. 1.5, step 2).

1.1.3.2 Delivery of the genome into the nucleus

The viral capsid must be actively transported through the cytoplasm towards the nucleus (Fig. 1.5, step 3), as movement within the cell is limited by viscosity as well as cellular organelles that function as steric obstacles [59]. It was first shown that the capsid is transported by a microtubule (MT) dependent mechanism [60], and a follow up study then demonstrated that the capsid can bind the microtubule motors dynein and kinesin through the inner tegument proteins UL36 and UL37 [61]. Dynein and kinesin are specialized MT associated proteins that function as motors; dynein moves cargo along minus end-directed MT and kinesin moves cargo along plus end-directed MT [62].

The initial destination of the viral capsid within the cell is the microtubule organization center (MTOC), which is reached by minus-end directed transport. The exact mode of action behind the association of the capsid with MT motors is unknown, but a study carried out by Schipke *et al* provided some insight on how the inner tegument protein UL36 might be involved in the trafficking of the capsid. The study provided evidence suggesting that UL36 remains associated with the viral capsid throughout cellular trafficking. Viruses lacking UL36 fail to transport capsids towards the nucleus [63]. After reaching the MTOC, the capsid continues its way towards the nucleus by plus-end directed transport. This second step of cellular trafficking seems to require the nuclear localization signal (NLS) of UL36, as its absence leads to accumulation of capsids at the MTOC [64].

At the nucleus, the capsid associates with the nuclear pore complex (NPC) [60, 65], which triggers the injection of the DNA into the nucleus (Fig. 1.5, step 3). This injection process involves the cellular proteins Ran-GTP and importin-beta [65], as well as the nucleoproteins Nup214 and Nup358 [66, 67]. The current data does not provide a full model for the DNA release step; however, the evidence suggests that the interaction between UL36 and Nup358 first brings the capsid and NPC closer together before the interaction between UL25 and Nup214 ultimately leads to the efficient, pressure-driven ejection of the DNA [68, 69]. After the DNA injection, the empty capsid is released into the cytosol [60] and the viral DNA adopts an end-less (most likely circular) configuration, [70-72] and cellular proteins initiate DNA chromatinization [73, 74].

1.1.3.3 Gene expression and viral genome replication

After the viral DNA is delivered into the nucleus, the viral genome can either be transcribed to induce the lytic replication cycle and produce viral particles, or it can enter the latent state, which is described in section 1.1.4.

HSV-1 gene expression occurs in a sequential order (Fig. 1.5, steps 4-6). First, immediate early (α) genes are transcribed. The gene products of this class are required for the activation of other early genes. Second, early (β) genes are transcribed and gene products of this class are essential for viral DNA replication. Lastly, leaky late ($\gamma 1$) and true late ($\gamma 2$) genes are transcribed. Late genes encode viral proteins that are required for the assembly and release of the newly formed virions. Tegument proteins are typical examples of late gene products [1].

Immediate early gene expression is initiated by the tegument protein VP16 through complex formation with the host cell factor-1 (HCF-1) and the cellular transcription factor Oct-1. This complex formation allows for the recruitment of the host RNA polymerase II to the HSV-1 genome [75-79]. The HSV-1 genome itself encodes six immediate early genes (ICP0, ICP4, ICP22, US1.5, ICP27, ICP47) and each of these genes includes a unique and crucial cis-regulatory motif (5'TAATGARAT) [80-82]. All immediate early gene products, except ICP47, are required for the activation of the early as well as late gene expression [1]. For example, ICP0 is an E3 ubiquitin ligase that antagonizes the restriction of viral gene expression by ND10 nuclear bodies and chromatin repression [83]. In addition, ICP0 targets cell signaling proteins like IFI-I6 in order to shut down

cellular signaling processes that are involved in anti-viral defence mechanisms [84, 85] and it co-activates early gene expression [86].

One of the first studies carried out to define the role of VP11/12 suggested that this tegument protein might enhance immediate early gene expression by collaborating with VP16 [87, 88]. This hypothesis was supported by evidence suggesting that VP11/12 and VP16 interact [87, 89]; however, mutant viruses lacking VP11/12 do not show any defect in immediate early gene expression [90]. Based on this observation, VP11/12 is most likely not involved in enhancing immediate early gene expression and/or its function is compensated for by another viral protein in its absence.

Early gene expression is initiated by the immediate early proteins ICP0 and ICP4, as both proteins activate early gene promotors [86, 91-93]. The majority of early genes require the expression of immediate early genes; however, UL39 seems to be the exception [94]. Some, but not all, early gene products are necessary for viral DNA replication. For example, UL9 is an origin binding protein that can bind each of the three origins of replication (Fig. 1.4) to initiate DNA replication [95-97]. Once UL9 binds an origin of replication, it starts to unwind the DNA under the support of ICP8 [98, 99]. Subsequently, UL5, UL8, and UL52 form a helicase/primase complex that further separates the double-stranded DNA and ultimately creates an oligoribonucleotide primer for the synthesis of viral DNA [100, 101]. The mechanism used to initiate DNA replication is well defined, but the mechanism used to replicate the entire genome remains to be determined. As mentioned previously, some studies suggested that the viral DNA undergoes circularization, possibly indicating a rolling circle replication mechanism [70-72]. This mode of replication would lead to the generation of long concatemeric DNA molecules, that were previously documented [102]. Nevertheless, other research studies

suggested that the observed concatemeric DNA structures might be formed as a consequence of recombination [103]. To date, the exact fate of viral DNA upon delivery into the host cell nucleus remains unknown.

The last gene group that becomes activated are genes of the leaky late ($\gamma 1$) and true late ($\gamma 2$) classes. By definition, leaky late genes do not require the synthesis of viral DNA prior to activation but true late genes do require DNA replication prior to activation [104]. The different expression pattern of these two late gene classes is most likely due to differences within the cis-acting regulatory unit of each promotor [105, 106]. The gene products of both late gene classes are either required for virion assembly, such as tegument, capsid and envelope proteins, and/or they serve as viral modulators of cellular processes that interfere with viral replication [1].

1.1.3.4 Capsid formation, DNA packaging and nuclear egress

The formation of new virions includes the following steps: importation of capsid proteins into the nucleus, capsid formation within the nucleus, packaging of viral DNA into the capsid, nuclear egress of the mature capsid and tegumentation as well as secondary envelopment in the cytoplasm. In this subsection I describe the capsid formation, DNA packaging and nuclear egress (Fig. 1.5, step 7 and 8) in more detail. The tegumentation and secondary envelopment is described in section 1.1.3.5.

First, the procapsid is assembled from the imported capsid proteins and the scaffold proteins UL26.5 and UL26. The scaffold is essential for the formation of the precursor capsid prior to encapsidation of the genome, but is not present in the mature virion [107]. In a process termed maturational cleavage, the minor scaffold protein UL26 cleaves itself as well as the major scaffold protein UL26.5. Digestion of UL26.5 and UL26 disrupts

the association with the major capsid protein VP5 [108-111], triggering the release of the scaffold and maturation of the procapsid into a mature capsid. During this process, the viral genome is packed into the capsid [112-115]. The capsid assembly itself most likely starts with the formation of the portal ring. The portal ring contains six copies of the UL6 DNA-portal protein [116], and the UL6 molecules further interact with the scaffold [117]. The UL6-scaffold interaction is thought to ensure that only one DNA portal is incorporated while the capsid is assembled [116].

The packaging of viral DNA into the capsid is mediated by the terminase complex that consist of three viral gene products (UL15, UL28, UL33) [107]. The generation of a linear unit-length genome from a concatemeric DNA molecule involves the detection of packaging sequences within the repeats that flank the U_L/U_S segments (section 1.1.2.3; Fig. 1.4) [38-40] as well as energy in form of ATP [118]. It is thought that the viral terminase complex scans along the viral DNA looking for packaging signals while it actively injects the DNA into the capsid through the portal complex, producing the mature C-capsid. Several control mechanisms are engaged during capsid formation as well as DNA packaging. If, for example, the process fails to engage the packaging mechanism, the capsid seals the scaffold inside which leads to the generation of a dead-end product termed B-capsid [107].

Once the genetic information is packed into the capsid, the capsid has to exit the nucleus and aquire its tegument and envelope before being released from the cell. This process involves an envelopment and de-envelopment step at the nucleus and is followed by a secondary envelopment step in the cytoplasm. The primary envelopment process is also termed nuclear budding, and it involves the following steps: disruption of the nuclear lamina, capsid recruitment to the inner nuclear membrane, primary envelopment of the

capsid at the inner nuclear membrane and budding of the primary enveloped capsid into the perinuclear space. Each process is controlled by the nuclear egress complex (NEC), which is comprised of UL31 and UL34. Deletion of UL31 or UL34 results in a significant reduction of viral titers [119-122].

To disrupt the nuclear lamina, the NEC triggers events that lead to the disruption of the dense fiber-like structure, which mainly consists of three types of lamins (A,B and C), in close proximity to the NEC [123-125]. The exact mechanism behind the disruption of the lamina is still unclear, but it has been suggested that UL34 recruites cellular kinases like PKC to induce phosphorylation of lamin B [126]. In addition, the viral kinase US3 is activated and leads to phosphorylation of lamin A/C [127]. It has also been proposed that the NEC interacts with lamina A/C in order to outcompete the lamin-lamin interactions that form the fiber-like structure [125, 128].

Second, the NEC is involved in recruiting the mature capsids to the inner nuclear membrane. As mentioned previously, different capsids can be found in infected cells (dead-end products or mature C capsids) and only C-capsids are exported. It was first suggested that a capsid vertex-specific complex is expressed on mature C-capsids and that this complex is recognized by the NEC [129]; however, the suggested complex was later also identified on dead-end capsid products [130, 131]. The expression of the capsid vertex-specific complex is significantly lower on dead-end capsid products, but its detection still questioned the suggested model. At this point it is unclear how the NEC distinguishes between the different capsids, but one model suggests that posttranslational modifications of specific capsid proteins might enable UL31 to selectively bind C-capsids and not to the dead-end capsid products [132].

The third step in nuclear egress involves the deformation of the inner nuclear membrane before the nascent bud can be pinched off and released into the perinuclear space. Bigalke and collegeous recently demonstrated that the NEC itself can deform the membrane as well mediate scission in the absence of any other components or chemical energy [133]. Nevertheless, the mechanisms used by the NEC are still to be determined.

Lastly, the enveloped capsid travels towards the outer nuclear membrane where the de-envelopment step occurs. The mechanism behind this step is poorly defined, but studies suggest that this step does not solely rely on the NEC [134] and may require US3 as an additional factor [135]. Once the de-enveloped capsid is released into the cytoplasm, tegumentation and secondary envelopment occur prior to the release of the viral particle.

1.1.3.5 Tegument assembly and egress of virions

The most commonly accepted model of tegumentation and secondary envelopment suggests that the majority of the inner tegument layer is constructed while the capsid is in the cytoplasmic space [136]. It is further suggested that earlier minor tegumentation steps, involving inner tegument proteins like UL36 and UL37, might occur within the nucleus, but the data is not consistent [21, 137, 138]. Subsequently, the outer tegument and secondary envelopment occurs after the capsid buds into the trans-Golgi network (TGN) or endosome derived vesicles (Fig. 1.5, step 9). Both structures contain viral glycoproteins and outer tegument proteins [139-141]. It is suggested that the presence of specific TGN and endosomal sorting signals within viral glycoproteins facilitates the accumulation of viral proteins in the TGN and endosome derived vesicles [142-145].

Tegument proteins play an important role during secondary envelopement as they interact with each other as well as with proteins of the capsid and envelope to build up

a network that links the capsid to viral envelope. The radial/inner tegument protein UL36 serves as foundation stone for this network and it interacts with the capsid protein VP5/ICP5 or the capsid vertex-specific component UL25 (Fig. 1.6) [63, 146-149]. Using optical super-resolution imaging, Laine and colleagues demonstrated that UL36 can also reach into the tegument occupied space where it interacts with UL37 or VP16 [150]. UL37 can bind to gK and therefore link the tegument to the envelope [151]. VP16 associates with VP22 in order to be connected to the envelope proteins gE and gM [152]. Organizing gap proteins like VP11/12 might assist in the formation of the tegument, but their precise role during the tegumentation process is unknown [21]. Of note, the tegument-tegument protein interactions are not limited to the ones described.

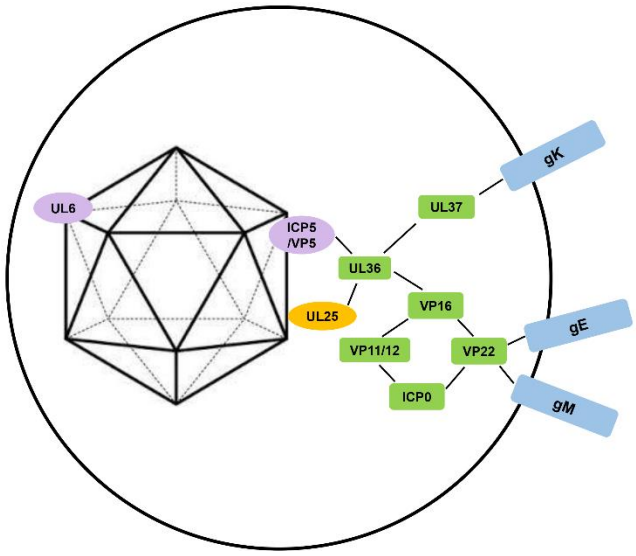

Fig. 1.6: The architecture of the tegument.

Shown is the organization of the tegument based on protein-protein interactions that form a bridge from the capsid to the envelope. The radial/inner tegument protein UL36 interacts with the capsid protein (ICP5/VP5) and/or the capsid vertex-specific component (UL25). Space filling as well as gap/outer tegument proteins then interact with UL36 or a UL36-binding partner to link the capsid to the envelope (gK, gE, gM). This figure is not drawn to scale.

In summary, the budding process does not only enable the formation of the tegument and the viral envelope, but it also creates a doubly enveloped viral transport vesicle (Fig. 1.5, step 10) that later enables the fusion of the vesicles with the plasma membrane, resulting in the release of the viral particle (Fig. 1.5, step 11) [21].

1.1.4 Latency

In all herpesviruses, an acute lytic infection is followed by a latent phase that does not support the formation of new virus particles [1]. HSV-1 establishes latent infection in the nucleus of peripheral ganglia following the retrograde transport of capsids along MTs towards the nucleus [153]. Once the viral genome is injected into the nucleus it will be maintained within the nucleus as episomes. The gene expression during latency is strongly limited in that most lytic gene expression is silenced while latency-associated RNA transcripts (LATs) expression is stimulated [1]. Research has demonstrated that the gene activation/repression is controlled by posttranslational modifications of histones that are associated with the episomes [154]. The active LAT region is enriched in euchromatin, which is the lightly packed form of chromatin, whereas the inactive lytic gene region is enriched in heterochromatin, which is the tightly packed form of chromatin [154-157]. Early studies indicated that LATs are important for controlling reactivation of the virus because deletion of the LAT promotor region did not hinder the establishment of latency, but restricted reactivation [158, 159].

In humans, reactivation can be induced by stress, like infection, fever, UV exposure or emotional stress [160]. The cellular immune system impacts the latent state, as studies have shown that T-cells play an important role in regulating the reactivation of latent viruses [161-164].

The current data suggests that the lytic-to-latent switch in neurons is regulated by the surroundings of the neuron as well as the cell type. It has been proposed that the switch is controlled by the dynamic interplay between viral and host cell transcriptional activators (to induce lytic infection) and transcriptional repressors (to establish and/or maintain latency). For example, using a primary neuronal culture system for latency and reactivation it was demonstrated that the cellular nerve growth factor-dependent signaling pathway through the PI3K/Akt axis is essential for maintaining viral latency [165-167]. The viral factor(s) that contribute to the regulation of this signaling pathway remain unknown. Interestingly, similar results were described by Wilcox and colleagues 22 years earlier [168-170], but the observations were highly criticized at the time because of the detection of low levels of lytic mRNA during latency. At that time, most researchers thought that only LATs are transcribed and accumulate within the nucleus of the latently infected neuron [171]. However, it is now well established that low levels of lytic mRNAs are detected in latently infected animal models, and that the lytic mRNAs are important to regulate the lytic-to-latent switch [172]. It has become evident that lytic mRNAs are targeted by viral and host micro-RNAs (miRNAs) in order to control the reactivation [173]. For example, the viral miRNA miR-H2 [174, 175] as well as the host miRNA miR-138 [176] were recently identified as ICP0 mRNA transcript repressors. These findings were not surprising since the LAT locus, which gives rise to the viral miRNAs, overlaps the ICP0 gene and it was suspected that LATs control the reactivation [172].

1.2 Viral manipulation of host functions

HSV-1, like many other viruses, has to encounter several aspects of the human immune system. During HSV-1 infection, viral proteins manipulate host proteins and exploit a variety of cellular signaling pathways for their own benefits. Viral proteins either shut down signaling pathways that lead to the detection and killing of infected cells, or they activate pathways that ensure cell survival and viral replication [1]. In this subsection I will first outline selected immune evasion strategies evolved by HSV-1 to escape host antiviral modulators. Subsequently, I will outline how our laboratory became interested in investigating the signaling properties of VP11/12 before I started my thesis project.

1.2.1 Escape of the innate antiviral response

In humans, the immune system consists of two arms: the non-specific innate arm and the more specific adaptive arm. During a primary infection, viral replication is first limited by the innate immune response and is finally resolved through the adaptive response [177]. HSV-1 has evolved several different strategies to escape both arms by interfering with detection and signaling molecules [178].

In the case of the innate immune response, HSV-1 directly targets the type 1 interferon signaling pathway. This pathway is a crucial line of defense and once activated, it mediates a wide range of antiviral responses. Activation of the type 1 interferon signaling pathway involves the recognition of pathogen-associated molecular patterns (PAMPs) by specific pattern recognition receptors (PRRs). Binding of PAMPs to PRRs leads to the expression of type 1 interferons, and released type 1 interferon then binds its cognate receptor and induces the production of IFN-stimulated genes (ISGs) through the JAK-

STAT pathway. PRRs relevant to the IFN response include several members of the Toll-like receptor (TLR) family as well as DNA and RNA sensors [179]. To avoid the activation of the type 1 interferon pathway, HSV-1 targets PRRs and factors that transduce the signal downstream of PRRs.

DNA-sensors that are targeted by HSV-1 include cyclic GMP-AMP (cGAMP) synthase (cGas), stimulator of interferon genes (STING) and interferon-gamma inducible-16 (IFI-16). Expression of the tegument protein vhs reduces the accumulation of cGAS [180], and expression of ICP0 and US3 affect the stability as well as function of STING [181]. In addition, ICP27 interacts with STING in order to inhibit its signaling capacity [182]. In a very recent report, Deschamps and Kalamvoki demonstrated that VP11/12 blocks the cGAS-STING sensing pathway by associating with STING. The data presented also suggested that expression of VP11/12 alone is capable of eliminating STING protein levels as well as reducing STING transcript levels [183]. IFI-16 is targeted by ICP0 to induce its proteasomal degradation; however, the data is not consistent and requires more studies in order to fully understand the interaction between ICP0 and IFI-16 [85, 184, 185]. Of note, the same study that identified VP11/12 as modulator of STING also suggested that VP11/12 reduces IFI-16 transcript levels [183].

RNA-sensors that are targeted by HSV-1 include RIG-I, TLR-3 and protein kinase RNA (PKR). RIG-I was one of the first viral RNA sensors identified and it became evident that HSV-1 directly targets this sensor. It was proposed that US11 interacts with RIG-I and hinders its function by inhibiting its complex formation with the mitochondrial antiviral-signaling protein (MAVS) [186]. Similar to RIG-I, TLR-3 is one of the best understood RNA sensors. It was demonstrated that US3 directly reduces TLR-3 expression and deletion of US3 results in a strong activation of the interferon pathway [187]. In the case

of PKR, two different viral proteins seem to be involved in dampening PKR function and/or expression. Early reports identified US11 [188] as a viral factor that limits PKR function and our laboratory and others have recently identified vhs as a negative PKR modulator [189-191].

As mentioned above, HSV-1 does not only target PRRs, but it also targets factors that are involved in signal transduction downstream of PRRs. For example, the interferon response factor 3 (IRF-3) is a crucial transcription factor that stimulates the expression of type 1 interferons in non-immune cells like fibroblasts or epithelial cells [179]. So far four viral proteins have been identified that inhibit signal transduction at the level of IRF-3: (i) US3 hyperphosphorylates IRF-3 and inhibits its dimerization as well as its translocation towards the nucleus [192], (ii) VP16 blocks IRF-3 activation through interacting with IRF-3 [193], (iii) ICP0 inhibits IRF-3 controlled transcription [194] and (iv) UL36 inhibits the dimerization of IRF-3 [195].

1.2.2 Escape of the adaptive antiviral response

Unlike the innate antiviral immune response, the adaptive antiviral immune response is more specific and consists of the T-cell mediated cellular immune response and the B-cell mediated humoral immune response [177].

Research has indicated that the B-cell humoral immune response most likely does not serve a critical role in controlling HSV-1 infection [196]. Nevertheless, HSV-1 glycoprotein gE can interfere and inactivate HSV-1 specific antibodies by directly binding to the antibody [197, 198]. In contrast to the B-cell mediated humoral response, the T-cell mediated cellular response plays a critical role in controlling HSV-1 infection. Biopsy samples have revealed that $CD8^+$T-cells infiltrate HSV lesions [199], and the infiltrating

T-cells are capable of producing interferon gamma and therefore most likely represent a HSV antigen-specific T-cell population [200]. Additional research has demonstrated that $CD4^+$ T-cells support the generation of fully functional $CD8^+$ T-cells [201], and that the HSV specific T-cell population spikes during an acute infection and rapidly decreases after the lesion is healed. Nevertheless, the specific T-cell population can remain significantly elevated for several months [202]. Lastly, some research also demonstrated that the infiltration rate of $CD8^+$ T-cells into the primary infection site strongly correlates with clearance of the virus [201].

It is therefore of no surprise that HSV-1 directly targets different essential components of T-cell activation. For example, HSV-1 directly interferes with the presentation of viral antigens by blocking the transporter associated with antigen processing (TAP) protein [203, 204] through ICP47 [205] and US3 [206]. As a non-lymphotropic virus, HSV-1 more efficiently infects T-cells through direct cell-to-cell spread from infected fibroblast cells, rather than through cell-free virus [207]. Previous research mainly carried out by the Jerome group demonstrated that HSV-1 infects T-cells and remodels T-cell receptor (TCR) signaling pathway events in order to avoid the activation of the adaptive immune response [208, 209]. Before going into detail on what was known about the viral induced remodeling process and the possible involvement of VP11/12, I want to briefly outline how cytotoxic T-cells become activated.

1.2.2.1 Activation of cytotoxic T-cells

Cytotoxic $CD8^+$ T-cells become activated once the TCR binds to a viral peptide that is presented by a major histocompatibility complex I (MHC I) (Fig. 1.7). In addition, the CD8 co-receptor will bind the invariant region of the MHC I loaded complex [210]. This

complex formation then leads to the binding of the SFK lymphocyte-specific cytoplasmic protein kinase (Lck) to the CD8 co-receptor and the non-covalent interaction of Lck with CD8 initiates the intracellular signaling cascade [211, 212]. Once Lck is activated, it phosphorylates and therefore activates the immunoreceptor tyrosine-based activation motifs (ITAMs) within the CD3 molecule. This activation allows for the recruitment and activation of Zeta-chain associated protein kinase-70 (ZAP-70) [213-215]. After the activation of ZAP-70, ZAP-70 phosphorylates and therefore activates LAT [216]. LAT is essential for the activation of: (i) calcium signaling through phospholipase Cγ1 (PLCγ1) [217], (ii) the Ras-mitogen-associated protein kinase (MAPK) pathway [217] through the Grb2/SOS complex or through RasGRP, and (iii) the PI3K/Akt pathway through p85 [218]. Of note, RasGRP is a Ras activator that becomes activated after binding to the PLCγ1 product DAG [219]. Concerning the recruitment of Grb2/SOS, a previous report suggested that Shc recruits Grb2/SOS while it is bound to the ζ chain of the TCR signaling complex [220], but an additional study then suggested that the Shc-ζ chain association is less likely due to the low affinity [221]. A newer model suggests that Lck couples Shc to the TCR signaling complex through a direct association with the PTB domain of Shc [222]. It is proposed that this association brings Shc in close proximity to ZAP-70 and phosphorylation of Shc by ZAP-70 then induces the downstream signaling events [222].

Because of its direct relevance to my project, I want to briefly outline how proteins interact with each other in order to stimulate signal transduction. One important biochemical principal in the activation of signaling pathways are direct protein-protein associations, such as the Grb2-LAT association displayed in figure 1.7. Proteins can interact with each other by recognizing tyrosine-based binding motifs. In case of the

Grb2-LAT association it was demonstrated that Grb2 binds to the YxNx motif (where 'x' is any amino acid) of LAT using its Sh2 domain [223]. A Sh2 domain is a small protein module that mediates protein-protein interactions and it can be found in adapter proteins like Grb2 or enzymes like Lck. Sh2-dependent interactions require the phosphorylation of a tyrosine within a specific tyrosine-based binding motif. In addition to Sh2 domains, Sh3 or PTB domains can also serves as interaction interfaces. PTB domains are similar to Sh2 domains, with the difference that not all PTB domains require the phosphorylation of the relevant tyrosine residue. In contrast, SH3 domains on the other hand recognize proline rich sequences and not tyrosine residues (reviewed in [224]).

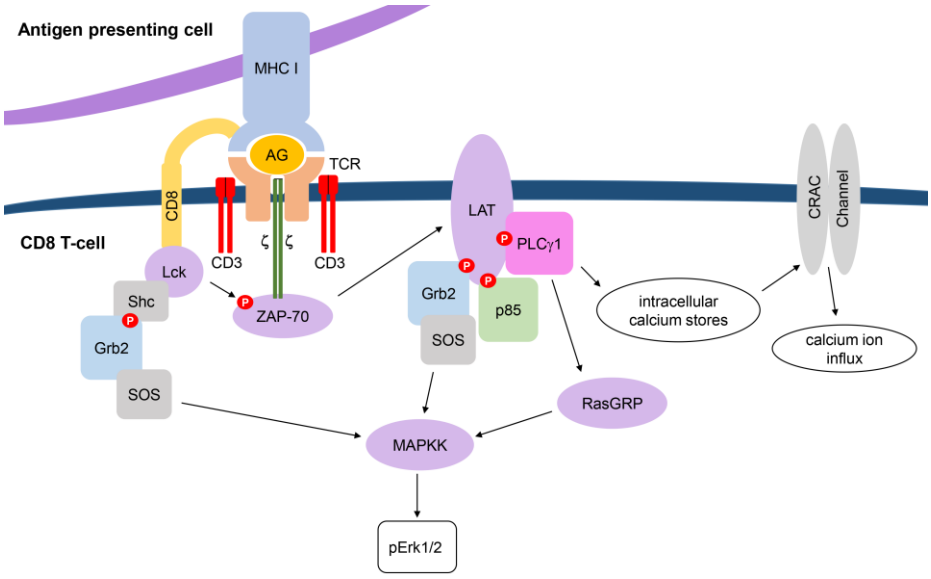

Fig. 1.7: Activation of CD8⁺ T-cells.

A T-cell becomes activated once the TCR binds to an antigen presented by an MHC I. In addition, the CD8 co-receptor will also associate with the MHC-I. These events will lead to the activation of Lck. Lck then triggers a cascade of events that involves the activation of ZAP-70. It is suggested that ZAP-70 phosphorylates Lck-bound Shc, which establishes a membrane recruitment site for Grb2/SOS in addition to the LAT Grb2/SOS recruitment site. LAT also becomes phosphorylated by ZAP-70 and functions as an adapter molecule and recruits several cellular proteins that then lead to stimulation of calcium flux and/or PI3K/Akt-signaling.

1.2.2.2 Remodeling of TCR signaling events upon HSV-1 infection

As mentioned above, research carried out in Keith Jerome's laboratory demonstrated that T-cells become inactivated upon HSV-1 infection based on remodeling of TCR signaling events [208, 209]. T-cell inactivation required the entry of HSV-1 into the T-cell, but it did not require any *de novo* protein synthesis, suggesting that tegument proteins are involved in the inactivation. The TCR signaling cascade was suppressed at the LAT level, as phosphorylation of ZAP-70 by Lck occurred normally, but a significantly reduced level of LAT phosphorylation was observed. HSV-1 infected T-cells did not display calcium flux or MAPK signaling events [208]. In a follow up study, Sloan *et al* further demonstrated that only the production of the pro-inflammatory cytokine IFNγ, tumor necrosis factor α and IL-2 was inhibited. However, the production of the tolerance-inducing cytokine IL-10, which suppresses cellular immunity, was not inhibited and occurred at levels similar to the one observed in mock infected cells [209]. It is worth mentioning that the interleukin expression pattern was based on the amount of interleukin detected in the supernatant of infected cells and was not based on intra-molecular staining. An earlier report by the same research group also suggested that inactivated $CD8^+$ cells are not apoptotic and viable, as the inactivation can be overcome by phorbol ester (PMA) stimulation. PMA is specific activator of the Protein Kinase C (PKC) and PKC is normally activated by PLC to trigger calcium release and mobilization. In addition, given that the inactivation can be overcome by PMA stimulation, it is suggested that the signaling block occurs after TCR ligation and before PKC activation. This report further indicated that three genes, including US3, might be essential to the inactivation of $CD8^+$ cells, but no mechanism was described [225]. Of note, our laboratory and others found that US3 and VP11/12 collaborate in controlling the

PI3K/Akt-pathway [226-229]; however, it remains controversial whether US3 and VP11/12 have a similar effects on the TCR-pathway (section 7.1.3.3).

Addressing the possible role of VP11/12 in damping TCR signaling events, our laboratory found in collaboration with the Jerome laboratory that deletion of VP11/12 does not restore Erk phosphorylation following TCR ligation during infection [230]; however, unpublished data by the Jerome group (personal conversation between James R. Smiley and Keith Jerome) suggest that VP11/12 is sufficient to block Erk1/2 phosphorylation and calcium flux upon overexpression in Jurkat T-cells. It is important to mention that Jurkat T-cells express CD4 instead of CD8; however, Jurkat T-cells can be directly infected by cell free virus and the TCR signaling pathway is similar to one observed in $CD8^+$ T-cells. Research described in chapter 6 of my thesis aimed to further investigate a possible role of VP11/12 in dampening TCR signaling events when VP11/12 is expressed in isolation upon transfection.

1.2.3 Signaling pathways activated by HSV-1

The evasion strategies outlined above are used by HSV-1 to inhibit signal transduction pathways in order to avoid an antiviral response. However, HSV-1 also creates a beneficial growth environment by selectively activating signaling pathways such as (i) the stress-activated protein kinase (p38) pathway, (ii) the Jun N-terminal kinase (Jnk) pathway [209, 231-233], (iii) the IκB kinase (IKK)/nuclear factor (NF)κB pathway [234] and (iv) the PI3K/Akt-pathway [228, 235, 236].

Both the p38- and Jnk-pathway are mitogen-activated protein kinase (MAPK) signaling transduction pathways and are known as stress-activated protein kinases (SAPKs) based on their role in controlling cellular stress responses [237]. It has been

demonstrated that HSV-1 activates the p38 as well the Jnk pathway in T-cells and non T-cells [209, 231-233]. In case of T-cell infection, both p38 and Jnk are active but only activation of p38 is required for the generation of IL-10 [209], a cytokine that suppresses the cellular immunity and therefore favors HSV-1 replication [238]. In case of non lymphoid cells, activation of both pathways is important for virus replication efficiency [232, 239]. It is also suggested that activation of the Jnk-pathway leads to inhibition of apoptosis through activation of the NFκB transcription factor [240, 241]. In addition, our laboratory demonstrated that activation of the p38 pathway leads to stabilization of virus induced IEX-1 mRNA, a protein known for pro- and antiapoptotic activity [242]. Importantly, activation of the p38- and Jnk-pathway can be observed as early as 3 h after infection and consistent with its kinetics, the immediate early protein ICP27 was identified as a viral modulator of these pathways [231, 242]. Nevertheless, studies carried out in Stephen Rice's laboratory suggest that in case of p38 signaling one or more viral factors, in addition to ICP27, are necessary for a robust activation of this pathway [243].

The IKK/NFκB pathway has an important role in the suppression of apoptosis by regulating the expression of many anti-apoptotic factors. NFκB itself is a transcription factor that is retained in the cytoplasm of the cell through its interaction with its inhibitor protein IκB. Activation of NFκB is initiated by the signal-induced degradation of IκB proteins through IKK. Once activated, NFκB translocates to the nucleus and interacts with the promotor regions in order to activate gene expression [244]. Early reports on the activation of NFκB during HSV-1 infection demonstrated that the entry of the virus and *de novo* protein synthesis, including the expression of ICP27, are necessary for NFκB activation [234, 240, 245, 246]. Additional reports then published that the

glycoproteins gH/gL [247] and gB [248] as well as the tegument protein UL37 [249] trigger the activation of NFκB through different mechanisms. Given the importance of IKK on the regulation of NFκB activity, it is not surprising that efficient HSV-1 replication requires the activation of IKK [234]. It was further demonstrated that activated NFκB is redirected towards the promotor of the immediate early key player gene ICP0 instead of being directed towards the promotor of IκB [250], but the exact model on how the virus guarantees the redirection of NFκB is not known.

1.2.3.1 The PI3K/Akt pathway

As mentioned in the preface of this introduction, my thesis research helped define the role of the HSV-1 tegument protein VP11/12 in hijacking the PI3K/Akt pathway. The PI3K/Akt signaling pathway modulates metabolism and promotes cell survival, growth and cap-dependent translation. Given the importance of this pathway to my thesis research, I will first outline the pathway before providing a detailed description on what was known about how HSV-1 stimulates this pathway when I started my thesis project.

Under physiological conditions, stimulation of cell surface receptors leads to the activation of the PI3K/Akt signaling cascade. For simplification, I will outline the PI3K/Akt signaling pathway that occurs following stimulation of the platelet-derived growth factor receptor (PDGFR) (Fig. 1.8). Following PDGFR stimulation, several tyrosine-based motifs within the receptor's cytoplasmic tail become auto-trans phosphorylated [251], leading to the recruitment of additional signaling proteins. For example, the specific binding motif YTHM will bind the Sh2 domain of the p85 subunit of PI3K following tyrosine phosphorylation. This interaction is essential for the activation of the PI3K/Akt pathway [252] and the binding of PI3K to the membrane-associated receptor brings it in

close proximity to its substrate, phosphatidylinositol (4,5)-bisphosphate (PIP2), which is located in the inner leaflet of the plasma membrane [253]. Phosphorylation of PIP2 by PI3K creates phosphatidylinositol (3,4,5)-triphosphate (PIP3), which in turns binds the pleckstrin homology (PH) domains of Akt and of phosphoinositide-dependent kinase-1 (PDK1). This interaction leads to the recruitment of both proteins to the plasma membrane. PDK1 then phosphorylates Akt within the activation loop at threonine 308 (T308) [254], partially activating the enzyme. In addition, Akt has to become phosphorylated at serine 473 (S473), which is located within the hydrophilic domain. This phosphorylation is carried out by either the mammalian target of rapamycin (mTOR) complex 2 (mTORC2) [255] or by other PDK2 members. Only if both residues (T308 and S473) are phosphorylated Akt can gain its full enzymatic activity. Activated Akt then translocates throughout the cell in order to phosphorylate numerous downstream targets [256].

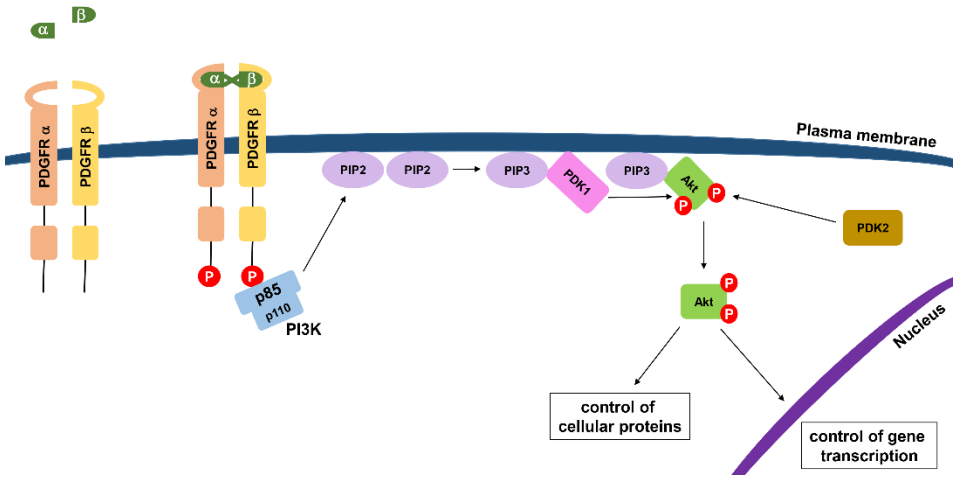

Fig. 1.8: Activation of the PI3K/Akt pathway after PDGFR stimulation.

Ligand binding (α, β) to the PDGFR induces the dimerization of the receptor and leads to auto-trans phosphorylation (P) of tyrosine-based binding motifs within its C-terminal tail. For example, the binding motif for the p85 subunit YTHM becomes activated and interacts with the PI3K subunit p85. This interaction leads to activation of PI3K, which then generates PIP3 out of PIP2. PIP3 binds and recruits Akt as well as PDK1 towards the plasma membrane. PDK1 then phosphorylates Akt at T308. To ensure full Akt activation, PDK2 will phosphorylate Akt at S473. Activated Akt can travel towards the cytoplasm and activate several different pathways overall stimulating metabolism, cell survival, growth and translation.

Following its activation, Akt phosphorylates substrates such as the glycogen synthase kinase 3 beta (GSK3β) and the Bcl-2 associated death (BAD) protein to ensure cell survival. Phosphorylation of GSK3β by Akt drives gene expression because phosphorylated GSK3β is no longer capable of inhibiting the multifactor protein β-catenin, which can interact with transcription factors to stimulate gene expression to guarantee cell survival, metabolism and migration. Phosphorylation of BAD by Akt inhibits apoptosis because phosphorylated BAD can no longer trigger the release of cytochrome c to drive apoptosis [256].

As mentioned above, the PI3K/Akt pathway is also known for promoting gene translation besides ensuring cell survival. The first step in promoting gene translation through this pathway involves the phosphorylation and inactivation of the tuberous sclerosis complex 1/2 (TSC1/2) by Akt. Once TSC1/2 is inhibited, the Ras-related small G protein Rheb-GTP functions as mTORC1 activator. mTORC1 then stimulates translation through phosphorylation of the small-molecular weight translational repressor proteins (4EBP's) and the ribosomal s6 kinase (S6K). 4EBP's interfere with the assembly of the translation initiation eIF4F complex, which becomes assembled right before cap-dependent translation. Once phosphorylated by mTORC1, 4EBP's can no longer inhibit the complex formation, thus allowing gene translation. S6K on the other side directly phosphorylates the 40S ribosomal protein S6 and the eukaryotic initiation factor 4B (eIF4B) to drive gene translation (as reviewed in [257]).

1.2.3.2 The PI3K/Akt pathway and HSV-1

Given the importance of this pathway on cell survival and gene translation, it is not surprising that many viruses including Hepatitis C virus [258], Influenza A Virus [259] and Polyoma virus [260] directly target this pathway to benefit viral growth. Roizman and colleagues were the first to demonstrate that Akt is phosphorylated at S473 during HSV-1 infection [235], indicating that HSV-1 activates the PI3K/Akt-pathway. Work in our laboratory, mainly carried out by Melany Wagner, subsequently showed that VP11/12 is essential for HSV-1-induced Akt activation [229]; however, others have demonstrated that Akt targets such as BAD are phosphorylated by the viral kinase US3 and not by Akt [226, 261, 262]. Research carried out by Dr. Heather Eaton and Kevin Quach in our laboratory further investigated the complex collaboration between VP11/12 and US3 in

manipulating the PI3K/Akt-pathway. Results of their studies are discussed in reflection of my own thesis research (section 7.1.2.1). Below I outline Melany Wagner's key findings on how VP11/12 stimulates the PI3K/Akt-pathway in combination with her VP11/12-dependent PI3K/Akt-pathway activation model, which was the starting point of my thesis research.

1.2.4 Signaling capacity of VP11/12

Before Melany Wagner started to investigate the signaling capacity of VP11/12, previous studies aimed to identify the biological function of VP11/12 based on its location within an infected cell. These data suggested that VP11/12 localizes to the perinuclear cytoplasm near a site that is thought to be the location of virion assembly [87, 263, 264]. However, VP11/12 is also able to translocate throughout the entire cytoplasm [264] and is able to associate with cellular membranes [265]. The association with cellular membranes is reversible and takes place prior to virion assembly. Data also suggest that VP11/12 associates with cellular membranes shortly after being released into the cytoplasm upon infection [264].

Our laboratory became interested in VP11/12 when it was demonstrated that HSV-1 infection inhibits the TCR-pathway [208, 209, 225] while activating Akt [235]. In collaboration with the Jerome group, our laboratory found that VP11/12 is highly tyrosine phosphorylated in lymphocyte-like cells and that this phosphorylation requires the activation of the SFK Lck. The phosphorylation state was thought to indicate activation of VP11/12, and it was therefore investigated whether VP11/12 downregulates the activation of T-cells. It was found that deletion of VP11/12 did not block the inhibition of TCR signaling during infection [230]. These results led to the conclusion that VP11/12 is

not essential for inhibiting the TCR pathway and/or that a possible role of VP11/12 is compensated for by another viral protein in the absence of VP11/12. Of note, a follow up study carried out by the Jerome group showed that VP11/12 is sufficient to block TCR-induced Erk1/2 activation as well as calcium flux upon overexpression in Jurkat T-cells (personal conversation between James R. Smiley and Keith Jerome). As mentioned in section 1.2.2, data presented in chapter 6 of my thesis aimed to reproduce the unpublished data as well as to further elucidate the role of VP11/12 in dampening TCR signaling events.

Melany Wagner continued to examine the signaling properties of VP11/12 during infection and she found that VP11/12 binds and activates Lck in T-cells. In addition, the recruitment and activation of Lck by VP11/12 led to further tyrosine phosphorylation of VP11/12 [266]. To determine if VP11/12 could possibly directly associate with SFKs, Melany decided to scan the protein sequence of VP11/12 for binding motifs using the scansite 2.0 algorithm. She was able to identify the tyrosine-based binding motifs YEEI and YETV, which were predicted to bind the Sh2 domain of SFKs. Melany then proposed that the binding of VP11/12 to SFKs predominantly occurs through the YEEI motif [266]. This hypothesis was based on a study describing that SFKs can become activated once a ligand binds the SFK Sh3 and/or Sh2 domain [267]. A ligand triggered SFK activation requires a strong affinity between the Sh2 and/or Sh3 domain of the SFK with its ligand. Proteins containing the consensus SFK Sh2 binding motif YEEI are known for their ability to successfully outcompete the inhibitory associations that keep the kinase inactive [268]. Her hypothesis was further supported by the observation that the hamster polyoma virus middle T antigen utilizes a Sh2-YEEI interaction mechanism to activate the SFK Fyn [269].

Given that SFKs are involved in many different signaling pathways, Melany suggested that VP11/12 might trigger the activation of other pathways. After determining a possible involvement of VP11/12 in different signaling cascades, she demonstrated that VP11/12 leads to Akt activation during infection of human foreskin fibroblast (HFF) cells as well as Jurkat T-cells. She also discovered that Akt activation requires PI3K and that VP11/12 associates with the regulatory subunit p85 of PI3K. Similar to the predicted tyrosine-based binding motifs for SFKs, she identified the predicted tyrosine-based binding motif YTHM for p85 within VP11/12's protein sequence. She further presented data suggesting that the VP11/12-p85 association and the VP11/12-dependent Akt activation requires SFK activity [229]. As depicted in figure 1.9, the VP11/12 protein consists of a N-terminal UL46 domain and a C-terminal region. Importantly, the predicted tyrosine-based motifs for SFKs and p85 are located in the C-terminal tail of VP11/12.

Taken together, Wagner and Smiley suggested that VP11/12 hijacks the PI3K/Akt-pathway by first recruiting and activating SFKs by interacting with the SFK Sh2 domain predominantly through YEEI. The VP11/12 dependent SFK activation then leads to further tyrosine phosphorylation of VP11/12, including the YTHM motif. Next, VP11/12 associates with the Sh2 domain of p85 though the activated YTYM motif to induce PI3K activation. Activated PI3K then leads to phosphorylation and activation of Akt, as described in subsection 1.2.3.1. In addition to the p85 and SFK tyrosine-based binding motifs identified by Melany Wagner, Jim Smiley found that VP11/12 also encodes tyrosine-based binding motifs for Grb2 and Shc within its C-terminal region (Fig. 1.9). Holly Saffran confirmed that VP11/12 associates with Grb2 and Shc, but it remained to be determined if VP11/12 interacts with Grb2 and/or Shc in addition to SFKs and p85 to activate the PI3K/Akt-signaling axis.

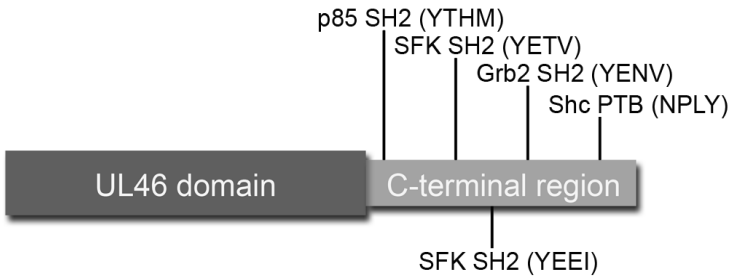

Fig. 1.9: Schematic diagram of VP11/12.

The VP11/12 protein consists of a highly conserved N-terminal UL46 domain of unknown function that can be found in all α-herpesviruses. In addition it also consists of a less-conserved C-terminal region that harbors putative tyrosine-based signaling motifs predicted by the scansite 2.0 algorithm to bind p85, SFKs, Grb2, and Shc.

1.3 Thesis rationale

At the starting point of my thesis research, there was no mechanism detailing how VP11/12 interferes with the PI3K/Akt-pathway or the TCR-pathway. In case of the PI3K/Akt-signaling axis, Melany Wagner proposed a model in which VP11/12 triggers activation of this pathway by recruiting and associating with SFKs and p85. However, the role of the predicted tyrosine-based binding motifs for both proteins had not been tested. It was also unclear if Grb2 and/or Shc were also recruited by VP11/12 to control this pathway. In case of the TCR-signaling pathway, the mechanism used by VP11/12 to hijack this pathway had not been studied yet. In summary, work mainly carried out in our laboratory raised two key questions: First, does VP11/12 interact with p85, SFKs, Grb2 and Shc through the predicted tyrosine-based binding motifs (Fig. 1.9)? Second, does VP11/12 associate with p85, SFKs, Grb2 and Shc in order to alter Akt activation

and/or TCR-signaling events? To investigate these questions, I divided my research into the following three objectives:

(1) To investigate if VP11/12 interacts with p85, SFKs, Grb2 and Shc through the predicted tyrosine-based binding motifs, as predicted by the scansite algorithm.

(2) To investigate if VP11/12, as suggested by Melany Wagner, recruits and activates SFKs in order to induce further tyrosine-phosphorylation of itself, enabling additional protein interactions. In line with this objective I also aimed to investigate if VP11/12 especially recruits p85 in order to activate Akt. Further, I aimed to investigate the possible contributions of Grb2 and Shc on the ability of VP11/12 to activate Akt.

(3) To investigate if VP11/12 is sufficient to block TCR signaling events in transfected T-cells as well as the role of the tyrosine-based binding motifs for SFKs, p85, Grb2 and Shc in inhibiting TCR signaling events.

Chapter 2

Material and Methods

2.1 List of buffers

Buffer name	Composition
10x TBS	121 g Tris, 350.4 g NaCl, bring up to 4 L with H_2O and pH to 8.0 using concentrated HCl
10x Western Blot transfer buffer	121.2 g Tris, 576 g Glycine, bring up to 4 L with H_2O
3x DNA loading buffer	100 mM Tris-HCl (pH 8.0), 10 mM EDTA, 50% Glycerol, 0.005 g bromophenol blue, 0.005 g xylene cyanol
3x SDS loading dye	15 g sucrose, 4.5 g SDS, 18.8 mL 1M Tris-HCl (pH 6.8), 26.2 mL water, 0.005 g bromophenol blue, 10 % b-mercaptoethanol (added before usage)
FLOW buffer	2% FBS, 1mM EDTA (in PBS)
GST lysis buffer	1 % Trition X-100, 20 mM Tris pH8, 2 mM EDTA, 137 mM NaCl, 10 % glycerol, protease inhibitor cocktail (Roche)
LB-medium	1% (w/v) Bacto-tryptone, 0.5% (w/v) Yeast extract, 1% (w/v) NaCl
LB-plate	LB medium, 15 g/L agar, appropriate antibiotic: 50-100 µg/mL ampicillin / 30 µg/mL / 30 µg/mL kanamycin
Lysis buffer	1 % Nonidet P-40, 0.25 % sodium deoxycholate, 150 mM sodium chloride, 1 mM EGTA, 1mM NaF, 1mM Na_3VO_4, 50 mM Tris-HCl, protease inhibitor cocktail (Roche)
PBS	137 mM NaCl, 2.7 mM KCl, 8.3 mM Sodium phosphate dibasic (Na2HPO4), 1.7 mM Potassium phosphate monobasic, adjust to pH 7.4
SDS-PAGE running buffer	25 mM Tris, 192 mM Glycine, 0.1% (w/v) SDS, adjust to pH 8.3
TAE buffer	40 mM Tris, 20 mM Sodium acetate trihydrate, 1 mM EDTA dihydrate
TBST	400 mL TBS, 4 mL Tween20, bring up to 4 L with H_2O
Urea/SDS buffer	10 mM Tris-C1 (pH 7.8), 7 M Urea, 350 mM NaCl, 10 mM EDTA, 1% (w/v) SDS
Western Blot transfer buffer	800 mL MeOH, 400 mL 10x western blot transfer buffer, 2.8 L H_2O

2.2 Mammalian cell culture

Jurkat E6-1 cells (TIB-162) and Vero cells were obtained from American Type Culture Collection (ATCC). Cre-Vero were a gift from David Leib (Dartmouth College). Cre-Vero cells constitutively express Cre recombinase. Telomerase-immortalized human foreskin fibroblasts (HFF-Tel12: HFF) were a gift from Wade Bresnahan (University of Minnesota) [270]. Jurkat E6-1 cells were grown in a complete growth medium consisting of RPMI 1640 medium (Gibco) supplemented with 10 % heat-inactivated fetal bovine serum (FBS, Sigma), 100 U/mL penicillin/streptomycin (Gibco) and 1 mM sodium pyruvate (Gibco). Vero and Cre-Vero cells were grown in Dulbecco's modified Eagle's medium (DMEM) (Gibco) supplemented with 5 % heat-inactivated FBS and 100 U/mL penicillin/streptomycin. Cre-Vero cells were additionally maintained in 400 μg/ml Hygromycin B to select for Cre recombinase expression during every fifth cell split. HFF cells were grown in DMEM supplemented with 10 % heat-inactivated FBS and were serum starved (DMEM only) twenty-four hours prior to and during infection.

2.2.1 Transfection of Cre-Vero cells with infectious BAC clones of HSV-1

Transient transfection of BACs was performed using Lipofectamine 2000 (Invitrogen) following the manufacturer's guidelines. Cre-Vero cells were grown to confluency in a 6-well plate dish. Briefly, the BAC as well as Lipofectamine 2000 were separately diluted in Opti-MEM reduced serum (Gibco) and incubated for 5 min at room temperature. Both dilutions were combined and incubated for 20 min at room temperature to allow complex formation. Next the transfection reagent was added to culture medium. Twelve hours post transfection, the transfection medium was removed and replaced with complete growth medium. The cells were harvested 48-72 hours post transfection and the

suspension was frozen at -80 °C and thawed at 37 °C two times and the suspension was vortexed after each freeze/thaw cycle. The suspension was then sonicated three times for 20 sec in a Model 550 Sonic Dismembrator (Fisher). Cell debris was separated from the virus containing supernatant via centrifugation (2000 xg, 10 min, 4 °C). Finally, the supernatant was transferred into a cyrovial and stored at -80 °C.

2.3 PCR and sequence validation

Over the course of this research project three different types of PCR were performed: (i) PCR in order to amply genes to provide proof of gene presence as well as sequence validation (standard PCR), (ii) PCR in order to perform *en passant* mutagenesis and (iii) PCR in order to perform site directed mutagenesis.

All standard PCRs were performed using Platinum *Pfx* DNA Polymerase (Invitrogen) under the following conditions: 1x *Pfx* Amplification Buffer (Invitrogen), 0.3 mM of each dNTP, 0.25-2.5 mM $MgCl_2$, 0.3 µM of each primer, 10-100 ng template DNA, 1 U *Pfx* polymerase, 3x enhancer solution (Invitrogen), dH_2O adjusted to a final volume of 50 µL. Following an initial denaturation step at 94 °C for 5 minutes, three-step cycling (95 °C for 15 seconds (denaturation), lowest primer melting temperature (Tm) minus 5 °C for 30 seconds (annealing), 68 °C - 73 °C for 1 minute per kbp of DNA (extension)) was performed for a total of 25-35 cycles followed by an incubation at 4 °C. In order to validate a sequence, the desired region was amplified using a standard PCR reaction and purified using the PCR purification kit (Qiagen). The Sanger-sequencing was carried out by the TAGC-Core (University of Alberta, tagc.med.ualberta.ca) using the indicated

sequencing primers (table 2.4). Sequences were aligned to WT sequences using ClustalOmega.

All *en passant* mutagenesis polymerase chain reactions (PCRs) were performed using *Taq* DNA Polymerase (Invitrogen) following the guidelines [271] (please see 2.4.2.1). Briefly, primers were used to generate a PCR amplicon that encodes for a selection marker cassette flanked by overlapping HSV-1 sequences containing the desired mutation. Importantly, *en passant* mutagenesis is described in detail in section 2.4 as well as in chapter 3.

All site directed mutagenesis PCRs were performed following the manufacturers guidelines (Agilent Technology, 200522). The mutagenic primers were designed to contain the desired mutation and anneal to the same sequence on opposite strands of the plasmid. The PCR protocol can be found in the manual for QuikChange II XL Site-Directed Mutagenesis Kit (Agilent Technology).

2.4 HSV-1 virus work

Table 2.1 outlines the HSV viruses used during this research. All viruses have been grown and titered in Vero cells (please see chapter 2.2.1).

Table 2.1: HSV viruses used in this study.

Name	Description	Origin
KOS-G	Wildtype HSV-1 expressing free GFP	James R Smiley [272]
KOS37	Wildtype HSV-1 derived from bacterial artificial chromosome	David Leib [273]

KOS37-UL46 GFP	KOS 37 HSV-1 derived c-terminally tagged VP11/12-EGFP fusion protein	H. Saffran (2.4.2)
KOS37-GFP UL46	KOS 37 HSV-1 derived N-terminally tagged VP11/12-EGFP fusion protein	H. Saffran (2.4.2)
KOS37-UL46 Y633F	KOS 37 HSV-1 VP11/12 with inactive YENV motif	U. Strunk (2.4.2)
KOS37-UL46 Y633F GFP	KOS 37 HSV-1 C-terminally tagged VP11/12-EGFP with inactive YENV motif	U. Strunk (2.4.2)
KOS37- GFP UL46 Y633F	KOS 37 HSV-1 N-terminally tagged VP11/12-EGFP with inactive YENV motif	U. Strunk (2.4.2)
KOS37-UL46 Y657F	KOS 37 HSV-1 VP11/12 with inactive NPLY motif	U. Strunk (2.4.2)
KOS37-UL46 Y657F GFP	KOS 37 HSV-1 C-terminally tagged VP11/12-EGFP with inactive NPLY motif	U. Strunk (2.4.2)
KOS37- GFP UL46 Y657F	KOS 37 HSV-1 N-terminally tagged VP11/12-EGFP with inactive NPLY motif	U. Strunk (2.4.2)
KOS37-UL46 Y519F	KOS 37 HSV-1 VP11/12 with inactive YTHM motif	U. Strunk (2.4.2)
KOS37-UL46 Y519F GFP	KOS 37 HSV-1 C-terminally tagged VP11/12-EGFP with inactive NPLY motif	U. Strunk (2.4.2)
KOS37-UL46 AALA	KOS 37 HSV-1 VP11/12 with an inactive proline sequence (469-472)	U. Strunk (2.4.2)
KOS37-UL46 GFP AALA	KOS 37 HSV-1 C-terminally tagged VP11/12-EGFP with an inactive proline sequence (469-472)	U. Strunk (2.4.2)
KOS37-UL46 AAPPA	KOS 37 HSV-1 VP11/12 with an inactive proline sequence (673-677)	U. Strunk (2.4.2)
KOS37-UL46 GFP AAPPA	KOS 37 HSV-1 C-terminally tagged VP11/12-EGFP with an inactive proline sequence (673-677)	U. Strunk (2.4.2)

KOS37-UL46 GFP AALA/Y519F	KOS 37 HSV-1 C-terminally tagged VP11/12-EGFP with inactive proline sequence (469-472) and inactive YTHM motif	U. Strunk (2.4.2)
KOS37-UL46 GFP Y519/AAPPA	KOS 37 HSV-1 C-terminally tagged VP11/12-EGFP with inactive YTHM motif and inactive proline sequence (673-677)	U. Strunk (2.4.2)
KOS37-UL46 GFP AALA/Y519F/AAPPA	KOS 37 HSV-1 C-terminally tagged VP11/12-EGFP with inactive proline sequence (469-472), inactive YTHM motif and inactive proline sequence (673-677)	U. Strunk (2.4.2)
KOS37-UL46 Y519F/Y633F	KOS 37 HSV-1 VP11/12 with inactive YTHM motif and inactive YENV	D. Gomez Ramos (2.4.2)
KOS37-UL46 GFP Y19F/Y633F	KOS 37 HSV-1 C-terminally tagged VP11/12-EGFP with inactive YTHM motif and inactive YENV	D. Gomez Ramos (2.4.2)
KOS37-UL46 Y624F	KOS 37 HSV-1 VP11/12 with inactive YEEI motif	H. Saffran (2.4.2)
KOS37-UL46 GFP Y624F	KOS 37 HSV-1 C-terminally tagged VP11/12-EGFP with inactive YEEI motif	H. Saffran (2.4.2)
KOS37-UL46 Y613F	KOS 37 HSV-1 VP11/12 with inactive YETV motif	U. Strunk (2.4.2)
KOS37-UL46 GFP Y613F	KOS 37 HSV-1 C-terminally tagged VP11/12-EGFP with inactive YETV motif	U. Strunk (2.4.2)
KOS37-UL46 Y613F/Y624F	KOS 37 HSV-1 VP11/12 with inactive YETV motif and inactive YEEI motif	U. Strunk (2.4.2)
KOS37-UL46 GFP Y613F/Y624F	KOS 37 HSV-1 C-terminally tagged VP11/12-EGFP with inactive YETV motif and inactive YEEI motif	U. Strunk (2.4.2)
ΔUL46	KOS37 derived VP11/12 null mutation	James R Smiley [230]

2.4.1 Preparation of virus stocks and virus stock titering

Vero cells were grown to confluency in a T150 flask. The medium was aspirated and the cells were infected with an MOI of 0.05 pfu/mL in 5 mL serum-free DMEM for 1 h at 37 °C in a 5 % CO_2 atmosphere incubator. The flask was rocked every 15 min during this absorption. Post incubation, the inoculum was aspirated and replaced with 20 mL complete DMEM growth medium. The cell attachment as well as cell shape was monitored every day after infection. Most cells showed cytopathic effects such as detachment from the growth surface as well as morphological changes three or four days post infection, at which the cells and medium were collected. The cells were pelleted via centrifugation (2000 xg, 10 min, 4 °C) and resuspended in 1 mL serum free DMEM per T150 flask. The suspension was frozen at -80 °C and thawed at 37 °C three times and the suspension was vortexed after each freeze/thaw cycle. Next, the suspension was sonicated three times for 20 sec in a Model 550 Sonic Dismembrator (Fisher). Cell debris was separated from the virus containing supernatant via centrifugation (2000 xg, 10 min, 4 °C). Finally, the supernatant was aliquoted into cryovials and stored at -80 °C.

Titration of virus stocks was carried out on Vero cells grown to confluency in a 6-well plate. The virus stocks were titered by plating ten-fold dilutions (10^{-3} to 10^{-7}) in 0.5 mL serum-free DMEM. The growth medium was aspirated and the cells were infected with the appropriate dilution for 1 h at 37 °C in a 5 % CO_2 cell-incubator. The inoculum was aspirated and replaced with 2 mL DMEM supplemented with 1 % human serum at 1 h post infection. The infection was incubated at 37 °C until plaques were visible by light microscopy (3-5 days). At this point, the medium was aspirated and the cells were fixed with methanol for 10 min at room temperature. The methanol was removed and the cells

were stained with a 10% Geimsa stain for 1-2 hours at room temperature until plaques were visible. The Geimsa stain was removed and redundant stain was washed off with water before the plaques were counted for dilutions that produced 50-100 plaques per well. Lastly, the pfu/mL was calculated based on the plaque number and dilution.

2.4.2 Preparations of mutant viruses via *en passant* mutagenesis

In order to facilitate our studies of the interactions between VP11/12 and cellular proteins, we generated KOS37 derivatives encoding N- and C-terminally tagged VP11/12-EGFP fusion proteins (KOS37-GFP UL46 and KOS37-UL46 GFP respectively), using *en passant* mutagenesis [271].

2.4.2.1 *En passant* mutagenesis

En passant mutagenesis is a two-step markerless recombination system that uses the bacteriophage λ Red recombineering system as well as inducible I-*Sce*I digestion, which originates from yeast (Fig. 2.1) [271]. This system creates a marker-less mutation in *E.coli via* site-directed homologous recombination. All mutagenesis was carried out in *E. coli* GS1784 cells that expresses the necessary enzymes for the λ Red recombination system as well as for I-*Sce*I digestion.

To introduce a specific mutation into the desired sequence, we first amplified a linear selection cassette that bears the selection marker kanamycin with an I-*Sce*I recognition site at the 5' prime end of the selection marker. The selection marker is further flanked by the target sequence regions (a, b, c and d region in figure 2.1, i) that are homologous to the target sequence. Transformation of the linear selection cassette into *E. coli* GS1784 cells will lead to incorporation of the selection cassette via the Red

recombineering system. In detail, the Red system codes for three important proteins: Exo, Beta and Gam [265, 274]. The Gam protein directly inhibits the E.coli RecBCD helicase that would degrade any linear DNA within the cell; including the PCR selection cassette [275]. Next, a homotrimer of 5'-3' exonuclease Exo protein produces a 3' single strand extension [276, 277] and this extension is protected by the Beta protein [252]. Lastly, the Beta protein will further induce the annealing of the single strand end product (linear DNA) with the complementary sequence (PCR insert) [252], finally leading to the integration of the insert into replicating DNA (BAC). The insertion of the selection cassette creates a duplication of the target sequence including the desired mutation (Fig. 2.1, ii).

During the second round of Red-mediated recombination the selection cassette will be excised, creating a seamless mutation. In detail, the second site-directed mutagenesis is initiated by the cleaving of the I-*Sce*I recognization site via the arabinose-inducible I-*Sce*I endonuclease (Fig 2.1, iii). Importantly, cleavage of the *E.coli* genome or the BAC sequence by I-*Sce*I is not expected due to the fact that the yeast based I-*Sce*I recognization site is very rarely present in bacterial or eukaryotic organisms [278]. The I-*Sce*I cleaving will ultimately expose one DNA end and therefore enable the λ Red recombineering system to induce a second recombineering step (Fig. 2.1, iv). Given that the inserted selection cassette codes for the duplicate target sequence, a second recombination will occur between the 'b' and 'c' region as described above (Fig. 2.1, v). Of note, the target sequence 'a' as well as the target sequence 'd' are used to direct the integration event to the desired region.

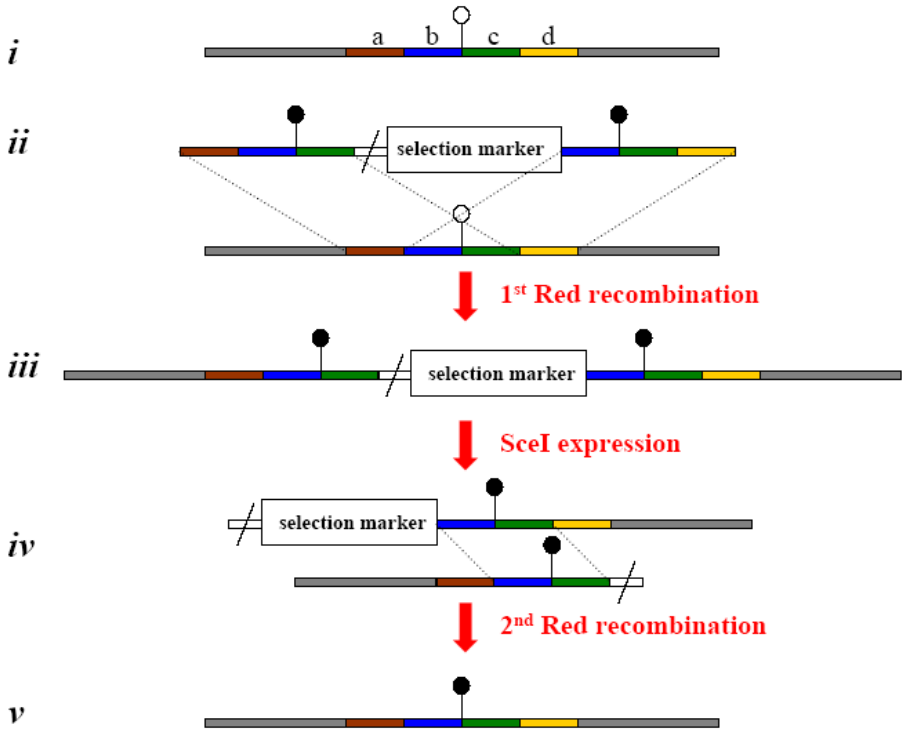

Fig. 2.1: Generation of point mutations using *en passant* mutagenesis.

The target region encoded in the BAC plasmid (i) is combined with the PCR product, which harbours the point mutation (black head) and the selection marker and the I-*Sce*I recognition site / . The combination within the bacterial cell leads to the first Red recombination step (ii). The co-integration product is characterized by the presence of the selection marker flanked by mutated sequences (iii). The co-integrate serves as product for the *in vivo Sce*I cleavage (iv), resulting in a new product that undergoes the second Red recombination (v). The final product has lost the selection marker and only harbours the mutated sequence at the desired region.

In order to perform *en passant* mutagenesis the following steps were performed: First, PCR was performed in order to generate the insertion cassette. Primers are specific for each mutation and are listed in table 2 and table 3 (section 2.4.2.2).

The PCR was carried out in a thermocycler with the following settings: initial denaturation step at 95°C for 2 minutes, 10 cycles of 30 sec at 95°C followed by 30 sec at 52°C and 1 min at 72°C, 25 cycles of 30 sec at 95°C followed by 30 sec at 68°C and 1 min at 72°C, a final extension of 5 min at 72°C before a final incubation at 4 °C.

Next, GS1784 *E. coli* bacteria with the respective BAC were prepared for recombination and electroporation. An overnight culture of the bacteria was grown at 32 °C in a bacterial shaker in the presence of 30 μg/mL chloramphenicol. 7 mL of pre-warmed LB broth (30 μg/mL chloramphenicol) was inoculated at a 1:50 ratio with the overnight culture and grown until an OD_{600} of 0.5-0.7 at 32°C and 220 rpm. The culture was transferred into a water bath shaker and kept for 15 min at 42°C and 220 rpm to induce the expression of enzymes required for the Red recombination. The culture was then transferred into an ice-bath for 20 min before being spun down at 4,500 xg for 5 min at 4 °C. The cell pellet was resuspended in 1 mL 10% ice-cold glycerol and spun down at 4,500 xg for 1 min at 4 °C. The glycerol washing and centrifugation step was performed three times before the bacteria were resuspended in 50 μL of 10% ice-cold glycerol and kept on ice.

For the transformation, approximately 100 ng of the PCR product (see above) was added to the cells. The cell suspension was then transferred into a pre-chilled 1 mm electroporation cuvette and the cells were electroporated immediately (1.5 kV, 25 μF, 200 Ω). The bacteria were removed from the cuvette and transferred into 1 mL pre-warmed LB broth and kept for 1 - 2 h in a bacterial shaker (32 °C, 220 rpm). 100 μL as

well as 900 μL of the cell suspension were plated on a LB-agar plate (30 μg/mL chloramphenicol, 30 μg/mL kanamycin). The bacteria were grown for 24 hours at 32°C.In order to identify co-integrates a colony PCR was carried out using the standard PCR protocol (2.3) and the indicated primers.

In order to resolve the co-integrate and induce the second Red recombination, positive co-integrates were grown in 1 mL LB-broth (30 μg/mL chloramphenicol) at 32 °C and 220 rpm until the solution became cloudy. 1 mL of pre-warmed LB broth (30 μg/mL chloramphenicol) containing 2 % L-arabinose was added to the solution and the solution was kept at 32 °C and 220 rpm for one hour in order to induce the I-*Sce*I gene. The cell suspension was transferred into a shaking water-bath (32°C, 220 rpm) for 30 min before being incubated at 32°C and 220 rpm for 2-3 h. The OD_{600} was measured and 10 μL of a 1:100 dilution in LB -broth (OD_{600} <0.5) or a 1:1,000 dilution in LB -broth (OD_{600} >0.5) was plated on a LB agar plate (30 μg/mL chloramphenicol, 1 % L-arabinose). The bacteria were grown at 32°C for 1-2 days, depending on the size of the bacteria colonies. In order to identify positive mutants a colony PCR was carried out using the standard PCR protocol (2.3) and indicated primers (table 2.4).

2.4.2.2 Generation of viruses using *en passant* mutagenesis

To evaluate the functions of several predicted binding motifs for cellular proteins within VP11/12, we generated mutant viruses with inactive predicted binding motifs via *en passant* mutagenesis of BAC-KOS37 clones. The mutations were generated in a WT UL46 gene as well as in the N-terminally or C-terminally EGFP-tagged UL46 genes.

Holly Saffran first modified the GFP gene to enable generation of the UL46-GFP tagged BACs (BAC-KOS37-UL46GFP or BAC-KOS37-GFP UL46). I then used those BACs as a substrate for mutagenesis.

To modify the GFP gene, Holly first engineered a silent unique AclI restriction site into EGFP coding sequences in pEGFP-C1 via Quikchange II-mediated site-directed mutagenesis (Stratagene) using oligonucleotides JRS 684 and 685 (table 2) according to the manufacturer's instructions. This mutagenesis yielded the pEGFP-C1-AclI plasmid. She then inserted the marker *I-SceI-aphAI* into this AclI site. Briefly, *the I-SceI* cassette was PCR amplified from pEPKanS using primers that included an AclI restriction site (JRS 704 and JRS 705, table 2). Following digestion with AclI, the amplimer was ligated into the AclI site of peGFP-C1-AclI to generate pEGFP-C1-AclI-sm. Of note, the *I-SceI* was inserted due to the fact that it is necessary for the incorporation of the GFP into the Ul46 gene locus via *en passant* mutagenesis (as described in chapter 2.4.2.1).

In order to generate the BAC harbouring N-terminally GFP-tagged UL46 (KOS37-GFP UL46), the EGFP cassette was PCR amplified from pEGFP-C1-AclI-sm using primers JRS 708 and JRS 709 (table 2.2) and incorporated into the KOS37 BAC via *en passant* mutagenesis (as described in chapter 2.4.2.1). The resulting BAC contains eGFP codons 1-232 fused to VP11/12 codon 2. In order to generate the BAC harbouring the C-terminally tagged UL46 (KOS36-UL46 GFP), Holly first amplified the GFP region from pEGFP-C1-AclI-sm by PCR using primers JRS 787 and JRS 788 (table 2.2) and then incorporated the PCR amplicon via *en passant* mutagenesis. The resulting construct inserts eGFP codons 1-239 between UL46 codons 710 and 711, with an additional lysine

codon (AAG) placed upstream of the insert, reconstructing the VP11/12-GFP fusion construct present in the HSV-1 KOS mutant GHSV-UL46 [264].

Table 2.2: Primers used to generate KOS37-UL46 GFP and KOS37-GFP UL46.

Primer	Sequence
JRS 684	Ctacaacagccacc**aacgtt**atatcatggccgacaag
JRS 685	Cttgtcggccatgatata**aacgtt**gtggctgttgtag
JRS 704	Ggcggc**aacgtt**tatatcatggccgacaagcagaagaacggcatcaaggtgaac aacaagattagggataacagggtaatcgattt
JRS 705	Ggcggc**aacgtt**gccagtgttacaaccaattaacc
KOS37-UL46 GFP JRS 787	AACGACGGCCCGACCAACGTCGCCGCCCTGAGCGCCCT CCTGACCAAGCTTAAgatggtgagcaagggcgaggag
JRS 788	CGACGGCAGCACGGGCGGAGGCGTTCACCGGCTCCGGC GTCCTTCGCGTTTcttgtacagctcgtccatgcc
KOS37-GFP UL46 JRS 708	gacgcggcataactccgaCCGGCGGGTCCCGACCGAACGGGCG TCACCATGgtgagcaagggcgag
JRS 709	CGTCAGGCACCGCGCCAGCCGCAGGGAGCTCGCGCCGC GCGTCCGGCGCTGCttgtacagctcgtccatgc

*HSV-1 sequences are capitalized, AclI sequences are in bold; EGFP coding sequences are lower case, ** Table is adapted from [279]

Next, I generated mutations that inactivate the VP11/12 tyrosine-based motifs at Y509, Y613, Y624, Y633 and Y657 by *en passant* mutagenesis in the context of the KOS37, KOS37-UL46 GFP, KOS37-GFP UL46 BACs. In all cases, the motifs were inactivated by converting the relevant tyrosine (Y) codon (TAC) to a phenlyalanine (F) codon (TTC). The mutagenic primers used for amplification of the I-*Sce*I-*aph*AI cassette from pEPkan-S [271] are listed in Table 3. The KOS37-derived mutant KOS37-UL46 Y633F/Y519F

was generated by introducing the Y633F mutation into a previously generated KOS37-UL46 Y519F-BAC plasmid using the primers JRS 760/JRS 761 via *en passant* mutagenesis. Mutations that inactivate the proline rich region at positions 469-472 (PPLP into AALP) and 673-677 (PPPPP into AAPPA) within VP11/12 were also generated via *en passant mutagenesis* in the context of the KOS37 and KOS37-GFP UL46 BACs. In both cases, relevant proline (P) codons (CCx) were converted to alanine (A) codons (GCx) using the primers listed in table 2.3. The KOS37-derived mutants KOS37-UL46 AALA/Y519F and KOS37-UL46 Y519F/AAPPA were generated by introducing the AALA or AAPPA mutation into the previously generated KOS37-UL46 Y519F-BAC plasmid using the primers listed in table 2.3. The KOS37-derived mutant KOS37-UL46 AALA/Y519F/AAPPA was generated by introducing the AAPPA mutation into the previously generated KOS37-UL46 AALA/Y519F-BAC plasmid using the primers JRS 853/JRS 854, listed in table 2.3. Primers JRS 754, JRS 860 and JRS 1033 (table 2.4) were used to sequence and confirm the mutation locus within the BAC-plasmid. For reconstruction of a HSV-1 virus out of a BAC-plasmid see section 2.4.3 below.

Table 2.3: Primers used to generate point mutated KOS37-UL46 viruses.

Primer	Sequence
Y519F-JRS 812	CCGAGCCCCCGCTGCGGCCACACAGCCGGCCACGTATT**T**CACGCACA
	TGGGGGAGGTGCtagggataacagggtaatcgattt
JRS 813	ACGGGCCGGGAGGCGCGGGGGCACCTCCCCCATGTGCGTG**A**AATACG
	TGGCCGGCTGTGTGgccagtgttacaaccaattaacc
Y613F-JRS 846	CGCGAACGGCACGCCCCCTACGAGGACGACGAGTCAATAT**T**CGAGAC
	GGTGAGCGAGGACGtagggataacagggtaatcgattt
JRS 847	

	TTCCTCGTAGACACGCCCCCCGTCCTCGCTCACCGTCTCG**A**ATATTGA
	CTCGTCGTCCTCGgccagtgttacaaccaattaacc
Y624F-JRS 687	GTCAATATACGAGACGGTGAGCGAGGACGGGGGGCGTGTCT**T**CGAGG
	AAATACCATGGATGCtagggataacagggtaatcgattt
	GCAGACGTTTTCGTAGACCCGCATCCATGGTATTTCCTCG**A**AGACACG
JRS 688	CCCCCCGTCCTCGgccagtgttacaaccaattaacc
Y613F/Y624F-JRS 846	CGCGAACGGCACGCCCCCTACGAGGACGACGAGTCAATAT**T**CGAGAC
	GGTGAGCGAGGACGtagggataacagggtaatcgattt
JRS 848	TTCCTCG**A**AGACACGCCCCCCGTCCTCGCTCACCGTCTCG**A**ATATTGA
	CTCGTCGTCCTCGgccagtgttacaaccaattaacc
Y633F- JRS 760	GGGGGGCGTGTCTACGAGGAAATACCATGGATGCGGGTCT**T**CGAAAAC
	GTCTGCGTGAACAtagggataacagggtaatcgattt
JRS 761	GGCCGGCGCTGCATTCGCCGTGTTCACGCAGACGTTTTCG**A**AGTCCCG
	CATCCATGGTATTgccagtgttacaaccaattaacc
Y657F-JRS 810	GCGCCGGCCTCCCCGTACATTGAGGCGGAAAATCCCCTGTT**C**GACTGG
	GGGGGATCCGCCCtagggataacagggtaatcgattt
JRS 811	GCGGCCCGGGGGGGAAAATAGGGCGGATCCCCCCCAGTCG**A**ACAGG
	GGATTTTCCGCCTCAgccagtgttacaaccaattaacc
AALA-JRS 851	TCGGGAAAAGATTCAGCGGGCGCGGCGCGACAACGAGCCC**G**CG**G**CCC
	TC**G**CCCGACCTCGCCTACACTCGACtagggataacagggtaatcgattt
JRS 852	ACCTCCGGGTGGACGCGGGGGTCGAGTGTAGGCGAGGTCGGG**C**GAG
	GG**C**CG**C**GGGCTCGTTGTCGCGCCGCGgccagtgttacaaccaattaacc
AAPPA-JRS 853	GGGGGGATCCGCCCTATTTTCCCCCCCGGGCCGCACCGGG**G**CC**G**CGC
	CCCCG**G**CGTTGAGCCCCTCGCCCGTCCTtagggataacagggtaatcgattt
JRS 854	CGTTGGCTCGATGGCGGGCGAGGACGGGCGAGGGGCTCAACG**C**CGG
	GGGCG**C**GG**C**CCCGGTGCGGCCCGGGGGGGgccagtgttacaaccaattaacc

*HSV-1 sequences are capitalized, point mutations are in bold, *I-Sce* sequence is in lower case; ** Table is adapted from [279]

2.4.3 Reconstruction of HSV-1 virus from a BAC-plasmid

We first verified the mutated sequence (see section 2.4.2) and then isolated the BAC plasmid using a large construct preparation kit (Qiagen). Next, we transfected the BAC-KOS37 constructs into Cre-Vero cells to excise the BAC and reconstruct an infectious HSV-1 clone as described in section 2.2.1. The BAC sequence is flanked by loxP sites which will be recognized by the Cre recombinase, leading to the extraction of the BAC background (Fig. 3.3).

In order to isolate a single clone, virus stocks were used to infect Cre-Vero cells grown to confluency in a 6 well plate dish by plating ten-fold dilutions (10^{-2} to 10^{-8}) in 0.5 mL serum-free DMEM per well. The growth medium was aspirated and the cells were infected with the virus dilution for 1 h at 37 °C in a 5 % CO_2 cell-incubator. The inoculum was aspirated and replaced with 2 mL DMEM supplemented with 1 % human serum 1 h post infection. The infection was incubated at 37 °C for 24 hours. Next, the Cre-Vero cells were overlaid with a 1 % agarose solution (DMEM, 5 % FBS) and kept at 37 °C until plaques were visible by light microscopy (3-5 days). Once single plaques were visible, a single plaque was isolated using a glass Pasteur pipet (Fisher) and transferred into 500 μL DMEM. The suspension was frozen at -80 °C and thawed at 37 °C three times. The suspension was vortexed after each freeze/thaw cycle and directly added to freshly cultured Cre-Vero cells (6 well plate). The procedure of infection, agarose overlay and plaque isolation was performed three times. After three rounds of plaque purification, a small scale infection was carried out in Cre-Vero cells. The cells were infected with the entire 500 μL DMEM inoculum for one hour as described above (section

2.4.1). The cells were monitored and harvested 2-3 days post infection as described in section 2.2.1. The virus stock was titered as outlined in section 2.4.1.

In order to verify the reconstruction of the HSV-1 virus from a BAC plasmid, the Cre-Vero virus stock was used to generate a virus stock grown in Vero cells. Cultivation of Vero cells as well as infection and harvesting was carried out as outlined above (section 2.4.1). A small scale infection in Vero cells was carried out with an MOI of 10 for 24 hours. The cells and media were harvested and spun down at 12,000 xg for 1 min at 4 °C. The DNA was subsequently isolating using the following Phenol/Chloroform extraction method: The cells were lysed in 500 μL Urea/SDS buffer for one minute on ice and applied to a Qiashredder (Qiagen) and spun for 13,000 xg for 2 min at 4 °C. 500 μL of a phenol/chloroform (50/50 ratio) solution was added to the aqueous suspension and the suspension was spun at 13,000 xg for 15 min at 4 °C. The upper phase layer was isolated and spun down as above after the addition of 500 μL of a phenol/chloroform solution. The upper phase layer was isolated and 500 μL chloroform was added prior a centrifugation at 13,000 xg for 5 min at 4 °C. The upper phase layer was isolated again and 1 mL isopropanol was added before the sample was kept at -80 °C for 20 min. The suspension was thawed at room temperature prior to centrifugation at 13,000 xg for 15 min at 4 °C. The pellet was resuspended in 250 μL 0.3 M Sodium Acetate, the DNA was precipitated in 750 μL 95 % ethanol and kept at -80 °C for 20 min. Subsequently, the solution was spun down at 13,000 xg for 15 min at 4 °C. The pellet was washed with 750 μL 95 % ethanol and resuspended in 50 μL EB buffer (Qiagen). The concentration and absorbance of DNA was measured using a NanoDrop2000 (Thermo Scientific). To confirm the presence of VP11/12 and GFP, a standard PCR (section 2.3) was performed on the DNA using either the primers JRS 22.1/JRS 22 or JRS 754/JRS 731. Figure 3.7

indicates the primer annealing locations. To document the absence of the BAC-plasmid, a standard PCR (section 2.3) was performed using the primers JRS 475B/476B and JRS 473B/649 (Fig. 3.9). To confirm that the sequence of interest had been mutated, DNA was sequenced using the primers JRS 754, JRS 860 and/or JRS 1033 (section 2.3). It is noted in the appendix what sequencing primer was used for each mutant.

Table 2.4: Primers used to validate the sequence of viruses after reconstruction.

Primer	Sequence
JRS 21.1	gtcgacaaacaggggaaag
JRS 22	ctggacgcggcataactc
JRS 475B	cggcatcgcaaactgcacc
JRS 476B	cgtagcaaccaggcgtttaaggg
JRS 473B	gcacaggtgttccagcagc
JRS 649	gttgcgggtagcggattgg
JRS 754	ggcggcttccggatgcg
JRS 731	ggtgtttttggttatttttattaaatctcg
JRS 754	Ggcggcttccggatgcg
JRS 860	Ctccactacgagtccatcctgc
JRS 1033	Gatggagttgagcatca

2.4.4 Infection studies

Mammalian cells were infected in serum-free medium at the multiplicity of infection (MOI), indicated in the figure legend). Virus adsorption was allowed for one hour at 37 °C. The infected plates or flasks were rocked every 15 min during the one hour incubation. In the case of adherent cells, the medium was aspirated after the one hour incubation and replaced with complete medium depending on the cell type (see section

2.1). In the case of suspension cells, the cells were spun down for 5 min at 1,000 xg at 5 °C, the medium was aspirated and the cells were resuspended in the appropriate complete medium (see section 2.2).

2.5 Chemical Inhibition of SFK activation.

Jurkat E6-1 cells were infected as indicated in serum-free RPMI-1640 supplemented with the SFK inhibitor PP2 or the inactive analogoue PP3 (10 µM; both from Calbiochem) for 1 h. Cells were then maintained in RPMI-1640 medium supplemented with 10 % heat-inactivated FBS and either PP2 or PP3 (10 µM).

2.6 DNA agarose gels

Agarose gel concentration depended on the size of the fragment of interest. To obtain the indicated agarose concentration, the appropriate amount of agarose was dissolved in 1x TAE buffer. In addition, 0.5 µg/mL of ethidium bromide (Sigma, E-8751) was added to the agarose gel solution. The gels were submerged in 1x TAE buffer. 3x DNA loading buffer was added to the DNA samples before the loading procedure. In addition to the DNA samples, a GeneRuler 1kb DNA ladder (Fermentas, SM1333) was also loaded into one well. The gels were run between 80-120 V for 60-90 min. The voltage and run time were determined by the size of the gel as well as the expected DNA fragment sizes. DNA was visualized using an ImageQuant300 imager (GE Healthcare). If required, DNA

fragments were cut out of the gel and purified using a Gel Extraction Kit (Qiagen) following the manufacturer's guidelines.

2.7 Preparation of pcDNA-UL46 constructs via site directed mutagenesis

Construction of all pcDNA-UL46 constructs was carried out using QuikChange II XL Site-Directed Mutagenesis Kit (Agilent Technology, 200522) following the manufacturer's guidelines. The primers used for the site directed mutagenesis to inactivate the VP11/12 tyrosine-based motifs at Y509, Y613, Y624, Y633 and Y657 are listed below in table 2.5. Similar to the generation of point mutated viruses (see section 2.4.2), the tyrosine based binding motif of interest was inactivated by converting the relevant tyrosine (Y) codon (TAC) to a phenlyalanine (F) codon (TTC). In order provide proof of the desired mutation, a standard PCR (section 2.3) was performed and the UL46 locus was sequenced. After their successful generation, the mutants were grown in 500 mL Luria-Bertani (LB) medium supplemented with the specific antibiotic (section 2.11) overnight and isolated using the EndoToxin Free Maxiprep Kit (Qiagen). All pcDNA-UL46 constructs were stored at -20 °C.

Table 2.5: Primers used for the construction of pcDNA3.1-UL46 mutants.

Primer	Sequence
Y519F-JRS 1012	GCCGGCCACGTATTT**C**ACGCACATGGGGG
JRS 1013	CCCCCATGTGCGT**G**AAATACGTGGCCGGC
Y613F/Y624F-JRS 990	GAGTCAATAT**T**CGAGACGGTGAGCGAGGACGGGGGGCGTGTCT**T**CGA GGAAATA
JRS 998	

	TCTTTCCTCGA**A**GACACGCCCCCCGTCCTCGCTCACCGTCTCG**A**ATATT GACTC
Y633F-JRS 1008	CATGGATGCGGGTC**T**TCGAAAACGTCTGCG
JRS 1009	CGCAGACGTTTTCG**A**AGACCCGCATCCATG
Y657F-JRS 1010	CGGAAAATCCCCTGT**T**CGACTGGGGGGGATC
JRS 1011	GATCCCCCCCAGTCG**A**ACAGGGGATTTTCCG

*HSV-1 sequences are capitalized, point mutations are in bold

2.8 Co-Immunoprecipitation

Jurkat cells were cultivated in a T25 flask at a concentration of $1x10^6$ cells/mL for the 13 h post infection (pi) and then spun down at 2,000 xg at 4 °C prior to incubation in 1 mL lysis buffer (1 % Nonidet P-40, 0.25 % sodium deoxycholate, 150 mM sodium chloride, 1 mM EGTA, 1mM NaF, 1mM Na_3VO_4, 50 mM Tris-HCl, protease inhibitor cocktail (Roche)) at 4 °C for 15 minutes (min). Post incubation, the lysates were spun down at 3,000 g for 15 min. Immunoprecipitation was carried out using 90 % of the whole cells lysate (WCL). Of note, the WCL can also be classified as a post-nucleus lysate but I will refer to it as WCL for the remaining part of this thesis. The remaining 10 % of the WCL was stored at -20 °C during the time of the immunoprecipitation. For the immunoprecipitation, antibodies were first incubated overnight with Protein G-Agarose (Roche) in phosphate buffered saline (PBS) at 4 °C, then lysates and Protein G-Agarose-conjugated antibodies were incubated at 4 °C for 3.5 h, and precipitates were washed four times with lysis buffer.

2.9 GST-pulldowns

2.9.1 Preparation of GST-fusion proteins

The following pGEX-4T-1-derived GST fusion protein expression plasmids were generous gifts from R. Ingham: GST-Grb2 Sh2 domain (human, originally from Tony Pawson), GST-Shc PTB domain (human, originally from Tony Pawson) and GST-Lck Sh2 domain (*Mus musculus*, originally from Andre Veillette). pGEX-4T-1 was from GE Health Care. All plasmids were maintained in *E. coli* BL21 cells (Stratagene). Following overnight incubation of the culture at 37 °C, the cultures were diluted in LB and grown at 37 °C to OD_{600}=0.6. Expression of GST-fusion proteins was induced by adding 1.0 mM isopropylthio-β-galactoside (IPTG; Sigma) prior to further incubation at 37 °C for 3 h. Next, the cultures were centrifuged at 5,000 xg for 20 min at 4 °C and the pellets were lysed by incubation in GST lysis buffer (1 % Trition X-100, 20 mM Tris pH8, 2 mM EDTA, 137 mM NaCl, 10 % glycerol) supplemented with protease inhibitors (Roche) for 10 min on ice. Lysates were sonicated in a Model 550 Sonic Dismembrator (Fisher) and centrifuged at 13,000 xg for 30 min at 4 °C. Clarified lysates were incubated with 3 mL glutathione-agarose beads (Sigma) at 4 °C overnight. Glutathione-agarose beads were washed three times in lysis buffer and the yield of purified GST fusion protein immobilized to glutathione-agarose was determined by sodium dodecyl sulphate polyacrylamide gel electrophoresis (SDS-PAGE) and subsequent staining with Ponceau S (Sigma).

2.9.2 GST-pulldown

Jurkat E6-1 cells were infected as indicated in the figure legends. At 13 h pi cells were lysed in 200 µL lysis buffer (1 % Triton X-100, 20 mM Tris pH8, 2 mM EDTA, 137 mM NaCl) supplemented with protease inhibitors for 15 min at 4 °C. The lysates (2x10^6 cells) were spun down at 3,000 g for 15 min at 4 °C and pre-cleared by incubation with 75 µL glutathione-agarose for 2 h at 4 °C. Pre-cleared lysates were mixed with GST fusion proteins immobilized to glutathione-agarose beads (75 µL) at 4 °C overnight. The beads were then washed three times with 200 µL lysis buffer at 4 °C, resuspended in 100 µL lysis buffer with 20 µL 3xSDS loading dye supplemented with 2-Mercaptoethanol (2-ME), and analyzed by SDS-PAGE followed by western blotting.

2.10 Western blotting

In general, the proteins in cell lysates were separated by electrophoresis. In the case of the detection of tyrosine phosphorylation, samples were separated by electrophoresis through a 10 % SDS-polyacrylamide gel. All other samples were separated by electrophoresis through an 8 % SDS-polyacrylamide gel.

Next, proteins were transferred to a nitrocellulose membrane (GE Healthcare) via a semi-dry or a wet western transfer. SDS-gels, nitrocellulose membranes as well as filter papers were incubated in transfer buffer for 2 min before the transfer. In the case of a semi-dry transfer, the transfer sandwich consisted of two filter papers, nitrocellulose membrane, SDS-gel and two filter papers. The transfer was carried out in a semi-dry transfer apparatus (Tyler) for 45 min at 450 mA. In the case of a wet-transfer, the

sandwich consisted of a sponge, two filter papers, nitrocellulose membrane, SDS-gel, two filter papers and a sponge. The transfer was carried out in a Mini Trans-Blot Cell (Biorad) for 1 h at 100V.

Following western blotting, the membrane was incubated with either 5 % BSA in TBST or 4 % skim milk in TBST for one hour at room temperature. Next, the membrane was incubated with primary antibody solution overnight at 4 °C on a rocking plate. The membrane was washed three times with TBST for 5 min at room temperature. Secondary antibody incubation was carried out at room temperature for one hour. The membrane was washed with TBST as described above. Finally, the signals were either visualized via enhanced chemiluminescence (ECL) (Thermo Scientific Pierce) or infrared imaging on an Odyssey infrared imager (Licor) as indicated in each figure legend.

2.10.1 Antibodies

Primary antibodies used for detection by western blotting included goat anti-GFP (provided by L. Berthiaume), mouse anti-ICP27 (1:5,000; Virus Corporation), mouse anti-Lck (1:1,000; Santa Cruz), mouse anti-Shc (1:2,000; BD Transduction Laboratories), mouse anti-Tyrosine phosphorylation 4G10 (1:10,000; Millipore), mouse anti-VP16 (1:50; provided by Tony Minson), rabbit anti-actin (1:5,000; Sigma), rabbit anti-Akt (1:1,000; Cell Signaling), rabbit anti-pS473 Akt (1:1,000; Cell Signaling), rabbit anti-pT308 Akt (1:1,000; Cell Signaling), rabbit anti-active SFK Y614 (1:1,000; Cell Signaling), rabbit anti-Grb2 (1:2,000; Cell Signaling), rabbit anti-p85 (1:10,000; Upstate) and rabbit HSV-2 anti-UL46 (1:10,000; provided by Yukihiro Nishiyama). Secondary antibodies included anti-mouse horseradish peroxidase (HRP) true blot (1:1,000-

1:5,000; eBioscience), anti-rabbit HRP true blot (1:2,000-1:5,000; eBioscience), donkey anti-goat HRP (1:10,000; Jackson ImmunoResearch), donkey anti-mouse IR800 (1:10,000; Rockland, Inc.), goat anti-mouse HRP (1:1,000-1:5,000; Promega), goat anti-mouse Alexa Fluor 680 (1:10,000; Invitrogen), goat anti-rabbit Alexa Fluor 680 (1:10,000; Invitrogen), goat anti-rabbit HRP (1:2,000-1:5,000; Promega) and goat anti-rabbit IR800 (1:10,000; Rockland, Inc.). Immunoprecipitation was carried out using anti-rabbit IgG (4 µg; Sigma), goat anti-GFP (1 µg; provided by L. Berthiaume), mouse anti-Grb2 (2 µg; Santa Cruz), mouse anti-Lck (1 µg; Santa Cruz), rabbit anti-p85 (4 µL, serum; Millipore) and rabbit anti-Shc (2.5 µg; BD Transduction Laboratories).

2.11 Detecting TCR signaling events using assays based on flow cytometry

2.11.1 Transfection

Transfection of Jurkat E6-1 cells was carried out via electroporation (BTX; Harvard Apparatus). Prior to the electroporation, Jurkat E6-1 cells were grown to a density of approximately $1x10^6$ cells/mL. On the day of the transfection, 30 mL of complete RPMI medium per sample was pre-equilibrated at 37 °C, 5 % CO_2 for 1 hour in a T75 flask. For the purpose of transfection, $1x10^7$ cells per sample were spun down at 1,000 xg at room temperature for 5 min. The cells were resuspended in 500 µL RPMI and incubated with the indicated amount of plasmid DNA for 5 min at room temperature in a 0.4 cm electroporation cuvettes (Fisher). The samples were electroporated at 225 V with a 8 ms time constant and three pulses (1 s between each pulse) in a BTW apparatus and incubated for another 5 min at room temperature post transfection. Finally, the cell

suspension was transferred into the pre-equilibrated medium and kept at 37 °C, 5 % CO_2 for 24 hours.

2.11.2 Detection of the phosphoErk1/2 levels

For detecting intracellular levels of phospho-Erk1/2 24 hours post transfection, the cells were spun down at 1,000 xg at room temperature for 5 min and washed once with HBSS buffer (Gibco). First, cells were resuspended and stained with a live/dead stain (Molecular Probes, L34955) in a 15 mL Falcon tube. Second, one half of the sample was incubated with 5 μg anti-human CD3 (clone OKT3, eBioscience) for 10 minutes on ice to enable the binding of the anti-human CD3 antibody to the CD3 receptor. Next, the cells were transferred to a 37 °C water bath for the indicated time in order to activate the CD3 signaling. The remaining half of the sample was treated the same way, but no anti-human CD3 antibody was added. At this point, the cells were spun down and washed once in HBSS as described above.

Next, the cells were fixed with 4 % PFA in PBS for 20 min at room temperature in the dark. Ice-cold methanol was added drop-wise to the sample until the methanol concentration reached 90 %. The samples were kept on ice for 20 min before being spun down as described above and the cells were washed in FLOW buffer (2 % FBS and 1mM EDTA in PBS) and spun down as described above.

Next, the samples were resuspended in 300 μL FLOW buffer and 100 μL was transferred into each of three wells of a 96 well plate. The cells were either left unstained (no antibody added), stained with the indicated concentration of anti-human pErk1/2 antibody (clone Milan8R, APC conjugate, eBioscience 17-9109) or with the indicated concentration of the isotype control (mouse IgG1 K-APC, eBioscience 17-4714) for 30

min at room temperature. At this point, the 96 well plate was covered with tinfoil and placed on a Titramax 101 shaker (225 rpm) for 30 min. Lastly, the cells were spun down, washed once with Flow buffer as described above and kept in the dark at 4 °C until analysis.

The detection was carried out using a Fortessa-SORP (BD) and samples were analysed via FlowJo (Windows Version 10.0.8). For gating purposes a FFS/SSC scattering plot was used to gate on the single cells. The live/dead staining was used to exclude dead cells within the single cell population. The negative control (pcDNA3.1) was used to set the GFP positive gate to 1 % for all samples. Lastly, the isotype control sample was used to set the APC positive gate to 1 % for each sample. The signal to noise graphs (S/N) are based on the median fluorescence intensity (MFI) of OKT3-stimulated cells stained with anti-human pErk1/2 antibody over non-stimulated cells stained with anti-human pErk1/2 antibody. The fold increase graphs are based on the S/N value of GFP expressing cells over non-GFP expressing cells within the same sample.

2.11.3 Calcium flux

For detecting intracellular calcium flux 24 hours post transfection, the cells were spun down at 1,000 xg at room temperature for 5 min and washed once with HBSS buffer (Gibco). First, cells were loaded with 4 μM Indo1-AM (eBioscience) in HBSS buffer. For negative controls, cells were either not loaded with Indo1-Am or loaded with Indo1-AM in the presence of 2 mM EGTA in HBSS. The cells were kept in a shaking water bath at 37 °C for 30 min, 110 rpm in the dark. The cells were spun down at 1,000 xg at room temperature for 5 min and washed with HBSS.

Next, the cells were resuspended in 2 mL HBSS, or in the case of negative loaded control in HBSS supplement with 2 mM EGTA. The cells were kept at room temperature in the dark for 15 min. Directly before the FLOW analysis, the cells were warmed to 37 °C in a water bath.

During the analysis, the background was taken for 15 sec and the sample was removed and 5 μg anti-human CD3 (clone OKT3, eBioscience) was added to each sample. The cell suspension was vortexed and placed back into the Flow machine and the calcium flux was measured for a total of 3 min.

The detection was carried out using a Fortessa-SORP (BD) and samples were analysed via FlowJo (Mac Version 9.7.6). For gating purposes, a FFS/SSC scattering blot was used to gate on single cells only. The negative control (pcDNA3.1) was used to set the GFP positive gate to 1 % for all samples. The ratio of Indo-1 violet over Indo-1 blue was determined by setting a derived parameter as follow: Indo-1 violet/Indo-1 blue on a linear scale with a maximum peak of 10. The parameter was named “Ratio Indo1”. The kinetic tool was used to plot the calcium flux for the derived parameter. Lastly, within the layout editor the calcium flux with and without EGTA was visualized for the GFP positive as well as GFP negative population within the same sample.

2.11.4 Antibodies

FLOW analysis was carried out using anti-human CD3 (clone OKT3, eBioscience 14-0037), pErk1/2 T202/Y204-APC (clone Milan8R, APC conjugate, eBioscience 17-9109) or Isotype-APC control (mouse IgG1 K-APC, eBioscience 17-4714).

Chapter 3

Generation of point mutated viruses via *en passant* mutagenesis

Portions of this chapter have been published in:

Strunk, U., et al., *Role of herpes simplex virus VP11/12 tyrosine-based motifs in binding and activation of the Src family kinase Lck and recruitment of p85, Grb2, and Shc.* J Virol, 2013. **87**(20): p. 11276-8

All experiments presented within this chapter were performed by U. Strunk with the following exceptions: the viruses KOS37-UL46 GFP, KOS37-GFP UL46, KOS37-UL46 Y624F and KOS37-UL46 GFP Y624F were generated by Holly Saffran. The viruses KOS37-UL46 Y519F/Y633F and KOS37-UL46 GFP Y519F/Y633F were generated by Danny Gomez Ramos.

Preface

Herpesviruses encode for a unique feature called the tegument. By definition, the tegument is a proteinaceous layer between the viral envelope and the DNA capsid. Tegument proteins are delivered into the cytoplasm upon infection and directly function without requiring viral protein expression [1]. Previous research carried out in the Smiley lab focused on the HSV-1 tegument protein VP11/12, which is encoded by the UL46 locus. Melany Wagner's PhD research led to the suggestion that VP11/12 might function as a growth receptor mimic: it is highly tyrosine phosphorylated in lymphocytes [230], it recruits and activates the SFK Lck in T-cells [229, 266], it recruits the p85 subunit of PI3-kinase [229] and it is essential for the activation of Akt during HSV-1 infection [229]. Wagner pointed out that the C-terminal region of VP11/12 contains tyrosine-based motifs predicted to bind the Sh2 domains of SFKs (YETV and YEEI) as well as p85 (YTHM). In addition, Holly Saffran identified one tyrosine-based motif predicted to bind the Sh2 domain of Grb2 (YENV) and one predicted to bind the PTB domain of Shc (NPLY) [279]. Of note, all sequences were identified using the scansite 2.0 algorithm [280]. Taken together, this research suggested that VP11/12 utilizes tyrosine-based binding motifs to interact with cellular proteins that are involved in signal transduction pathways.

In order to investigate the role of the predicted VP11/12 tyrosine based binding motifs for SFK, p85, Grb2 and Shc we generated point-mutated HSV-1 viruses in the context of the HSV-1 KOS37 using *en passant* mutagenesis. We inactivated each predicted tyrosine-based binding motif by converting the relevant tyrosine (Y) codon (TTA) to a

phenlyalanine (F) codon (TTC). The data presented in this chapter describes the generation of these point mutated HSV-1 viruses.

3.1 Results

3.1.1 Conservation of predicted tyrosine-based binding motifs within VP11/12

Before I started my project it was evident that VP11/12 orthologues are found in all alpha-herpesviruses, but not in beta or gamma herpes-viruses. While comparing divergent alpha-herpesviruses (HSV-1, VZV, PrV) Jim Smiley found that the N-terminal domain is conserved across all the alpha-herpesviruses; however, the C-terminal region of these diverged viruses showed no obvious sequence conservation. Importantly, every predicted tyrosine-based motifs identified by our laboratory is located in this non-conserved C-terminal tail (Fig. 1.9).

In order to support the assumption that VP11/12 might utilize the predicted tyrosine-based binding motifs to recruit cell signaling proteins, I first determined if the predicted tyrosine-binding motifs (Fig. 1.9) are conserved among closely related *Simplexviruses* (Fig. 3.1). We assumed that sequence conservation would indicate that the viruses use a similar mode of action which, in turn, would indicate functional significance. The sequences of human Herpes Simplex Virus 1 and 2 were aligned to several closely related primate herpesviruses (Chimpanzee alpha-1 herpesvirus, Cercopithecine Herpesvirus 1 and 2, Macacine Herpesvirus 1 and Papiine herpesvirus 2) using MUSCLE (http://www.ebi.ac.uk/Tools/msa/muscle/) and then visualized using GeneDoc (http://www.nrbsc.org/gfx/genedoc/). Whereas black shading within the aligment indicates sequence conservation, the rectangles indicate the predicted tyrosine-based

binding motifs. The consensus sequences for the predicted interaction partners are as followed: (i) the Sh2 domain of Grb2 specifically binds to the YxNx consensus sequence where ‘x’ is any amino acid [281, 282], (ii) the Sh2 domain of p85 specifically binds to the YxxM consensus sequence [283, 284], (iii) the PTB domain of Shc specifically binds to the NxxY consensus sequence [285] and (iii) the Sh2 domain of SFKs predominantly binds to the YEEI consensus sequence, but can also bind the YExx motif [268].

I found that the YTHM motif (p85, Y519), the YEEI motif (SFK, Y624) and the NPLY motif (Shc, Y657) are highly conserved in related *Simplexviruses*. However, the YETV motif (SFK, Y613) as well as the YENV motif (Grb2, Y633) are less well conserved (Fig. 3.1). The difference between highly conserved and less conserved is based on the amino acid that occupies the ‘x’ position in the motif. Overall the sequence alignment suggested that the tyrosine-based binding motifs might be used to interact with host signalling proteins.

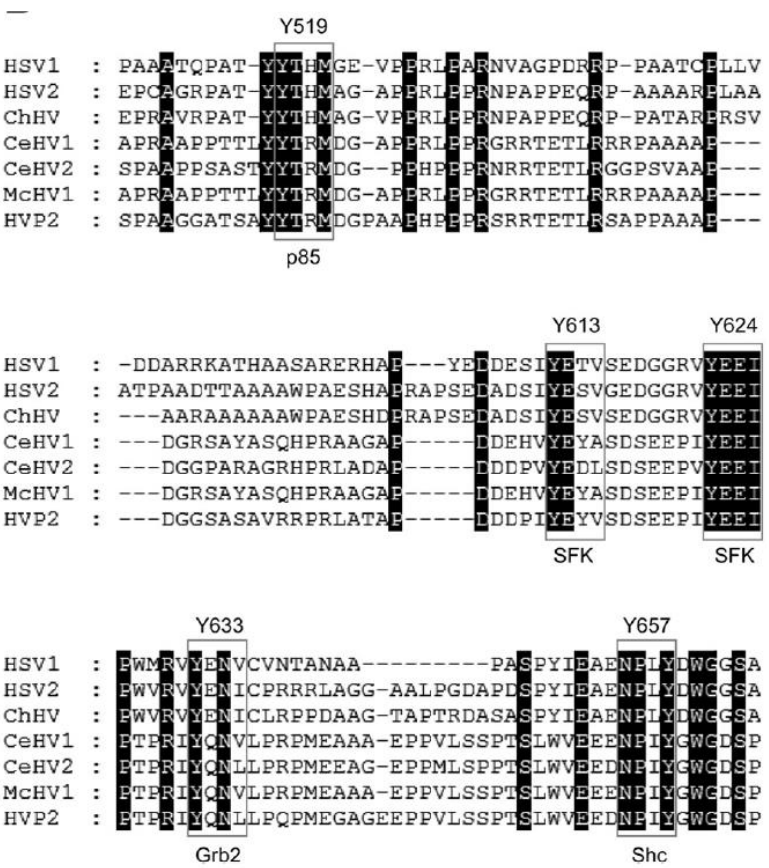

Fig. 3.1: Sequence conservation among *Simplexviruses.*

The C-terminal region is conserved in HSV-1 and closely related *simplexviruses*. Sequences were aligned using MUSCLE (http://www.ebi.ac.uk/Tools/msa/muscle/) and visualized using GeneDoc (http://www.nrbsc.org/gfx/genedoc/). HSV1/2, Herpes Simplex Virus 1/2 (ACM62269.1; AEV91385.1); ChHV, Chimpanzee alpha-1 herpesvirus (AFV26935.1); CeHV1/2, Cercopithecine Herpesvirus 1/2 (BAC58086.1; YP_164489.1); McHV1, Macacine Herpesvirus 1 (NP_851906.1); HVP2, Papiine herpesvirus 2 (YP_443893.1). Rectangles indicate the predicted tyrosine-based binding motifs and black shading indicates sequence conservation.

3.1.2 Generation of point-mutated viruses using *En passant* mutagenesis

In order to investigate the role of the predicted VP11/12 tyrosine based binding motifs for SFK, p85, Grb2 and Shc we generated point-mutated HSV-1 viruses in the context of HSV-1 KOS37 using *en passant* mutagenesis. In all cases, the motifs were inactivated by converting the relevant tyrosine (Y) codon (TTA) into a phenlyalanine (F) codon (TTC). Tyrosine and phenylalanine are structurally similar, but phenylalanine lacks the free hydroxyl group phosphorylation site. We assumed that if the binding-motif is essential for a VP11/12-host protein interaction, only WT VP11/12 will be able to interact with the predicted binding partner but not the inactive mutated virus. Table 2.1 outlines the HSV viruses generated for the purpose of this research. The data presented in this chapter describes in detail the results for the generation of the KOS37-UL46 GFP Y633F virus. As mentioned in the preface, we assumed that VP11/12 will interact with the Sh2 domain of Grb2 through its predicted tyrosine-based binding motif YENV at positon 633. For the remaining viruses, I only provide proof of the final sequence validation (appendix for chapter 3) after the reconstruction of the virus in Cre-Vero cells; similar to the one shown for KOS37-UL46 GFP Y633F in figure 3.11. Nevertheless, the generation of every virus was carried out in an identical manner.

Before I describe the generation of point-mutated viruses using *en passant* mutagenesis I want to provide a brief overview of methods previously used within the Smiley lab to generate mutated HSV-1 viruses. Since the 1990s herpesvirologists were able to clone the entire genome into a bacterial artificial chromosome (BAC). The BAC approach combines the λ phage based Red recombination system, which allows the addition of

mutations using homologous recombination, with the P1 bacteriophage based Cre-loxP system, to reconstruct infectious HSV particles (reviewed in [286]).

Over the past 15 years, several different *E. coli* strains have been used; all of them share the feature of an inducible λ phage homologous recombination system. Once the BAC is successfully generated, it will be transfected into Cre-Vero cells that constitutively express Cre recombinase. The BAC sequence are flanked by loxP sites, which will be recognized by the Cre recombinase and therefore lead to the extraction of the BAC sequence.

As mentioned above, several different BAC methods are available and they are distinguished by the specific *E. coli* strain used, as well as the marker used for the mutagenesis. Most BAC-based mutant HSV-1 viruses made in the Smiley lab prior to my work were generated using the *E.coli* SW102- galactokinase (galK) system [286] (Fig. 3.2). *E.coli* SW102 are derived from DY380 and express all necessary recombineering system proteins. The galactose operon within SW102 is fully functional with the exception of the galK enzyme. However, galK can be introduced in trans using a BAC plasmid, allowing bacterial growth when galactose is the only carbon source. Briefly, the galK cassette is amplified from a plasmid and incorporated into the desired target region using homologous recombination (Fig. 3.2A). Mutants are screened for the presence of galK (positive selection) before the second recombination step. During the second homologous recombination step the galK cassette is either removed, by introducing a short dsDNA PCR product to create a seamless deletion mutant, or the galK cassette is replaced, with a dsDNA PCR product to introduce a mutation within the desired target (Fig. 3.2B). Mutations were then selected based on the absence of the galK cassette (negative selection). The BAC plasmid encoding for the desired mutation will then be transfected into Cre-Vero cells, similar to the BACs generated using *en*

passant mutagenesis. The SW102-galK method has three major limitations. First, the second negative selection step is of very low efficiency. Second, not all of the galK-mutants carry the desired mutation due to a background of spontaneous mutations galK-mutants able to grow on the negative selection plates. Third, the desired mutation-sequence has to be PCR amplified from a pre-existing construct.

In contrast, e*n passant* mutagenesis enables the generation of point-mutations without a pre-existing construct that already contains the desired point-mutation. In addition, *en passant* mutagenesis showed a higher efficiency in our lab than the SW102-galK system. I was able to generate and fully validate single-point mutated viruses within 8 weeks at an efficiency greater than 90%. The impressive increase in efficiency is most likely due to the intra-cellular *Sce*I-arabinose based recombination (section 2.4.2.1).

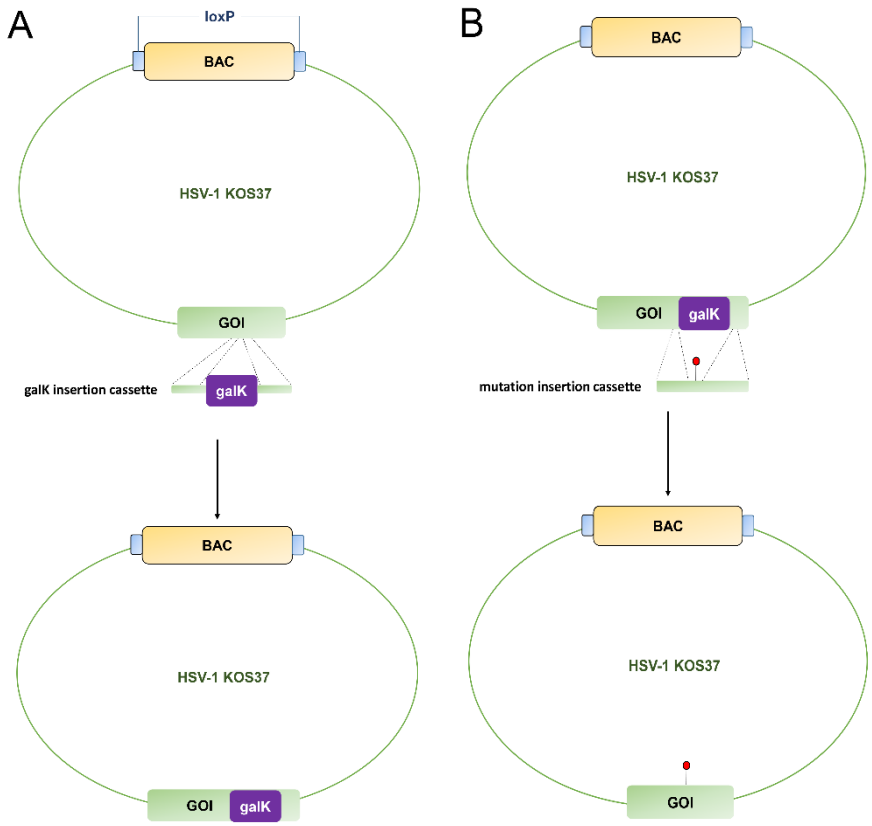

Fig. 3.2: Construction of mutant viruses using the SW102 galK system.

(A) The galK cassette needs to be amplified from a plasmid and will incorporate into the gene of interest (GOI) based on homologous recombination. The primers used for the galK cassette amplification were designed to add the HSV-1 homologous regions. Next, mutants were screened for the presence of galK. (B) In the next step, the galK cassette can either be removed, in order to create a deletion mutant, or it can be replaced, in order to introduce a mutation. Shown is the second option, where the galK cassette is replaced with the PCR amplicon harbouring the desired mutation (red). The PCR amplicon will again incorporate into the desired region based on homologous recombination. Mutants are then screened for the absence of galK. The second recombination step occurs with low efficiency and spontaneous mutations lead to false-positive mutants.

3.1.2.1 Generation of KOS37-UL46 GFP Y633F using *En passant* mutagenesis

In order to generate the KOS37-BAC without disrupting viral genes, the BAC segment was placed between the UL37 and UL38 genes [273]. The BAC region was additionally flanked with loxP sites to enable excison of the BAC sequences from the viral genome [273], as outlined below (chapter 3.1.2.2). In the case of KOS37-UL46 GFP Y633F I introduced the point-mutation into BAC-KOS37 UL46 GFP (Fig. 3.3), which was generated by Holly Saffran.

Initially I constructed a BAC-plasmid with the desired mutation at position Y633 using *en passant* mutagenesis [271]. Mutagenesis was carried out in *E. coli* GS1784cells. This specific strain expresses the necessary enzymes for the Red recombination system as well as I-*Sce*I digestion, as outlined in the chapter 2.4.2.1.

Briefly, a PCR cassette was generated that contains the viral sequence of interest flanking the kanamycin selection marker. The PCR amplicon will co-integrate into the desired sequence during the first of two recombination steps due to the sequence homology. This leads to a sequence duplication upstream as well as downstream of the selection marker (Fig. 3.4A). To ensure that the PCR amplicon was incorporated into the region of interest, a colony PCR using primers specific for the UL46 region (JRS 21.1 and JRS 22; Fig. 3.4B) was carried out after the first recombination step. The PCR products were then run on an agarose gel, and only the clones with a single band at 4 kbp were chosen for further recombination. Of note, we expected an increase of 1 kbp compared to the BAC-KOS37 UL46-GFP control sample if the PCR amplicon was inserted.

Next, single clones after the second recombination step were analyzed for the absence of the marker cassette (Fig. 3.5). Briefly, the second recombination step is initiated by cleaving the inserted selection cassette with the I-*Sce*I endonuclease. This cleavage event generates a double-stranded DNA break, which enables the λ Red recombination system to recombine the duplicated homologous regions, excising the selection cassette (Fig. 3.5A). We expected a decrease of 1 kbp compared to the BAC-KOS37 UL46-GFP control sample (Fig. 3.5B). In the following step, candidate clones were analyzed through Sanger sequencing with the indicated primer to confirm the presence of the mutation (Fig. 3.6).

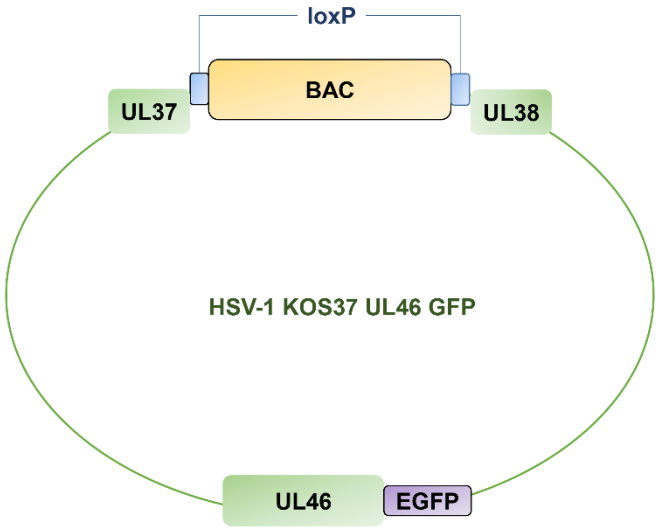

Fig. 3.3: Structure of BAC-KOS37 UL46 GFP.

The BAC region was inserted between the UL37 and UL38 gene region of HSV-1 KOS37. This placement avoids disruption of BAC as well as of viral genes. The BAC regions were flanked by loxP sites to enable the excision of the BAC region in cells expressing Cre-recombinase. This figure is adopted from [273] and it is not to scale.

A

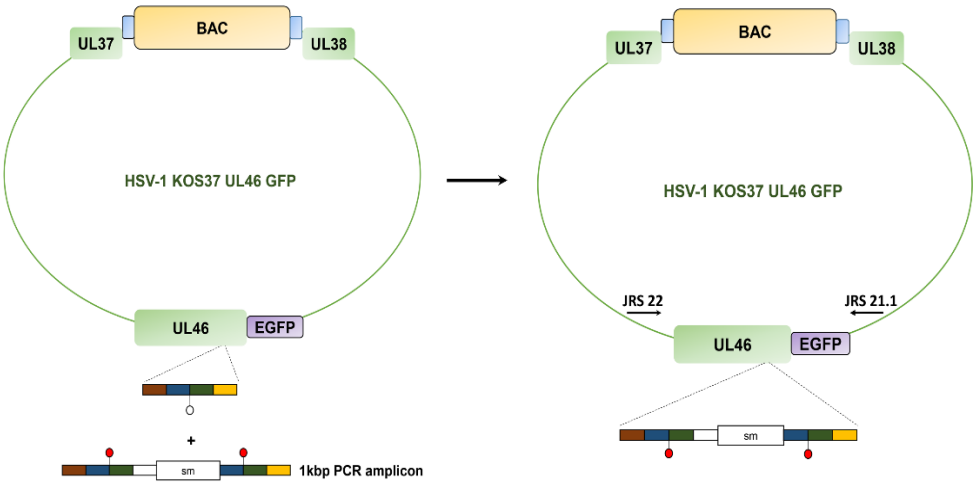

B

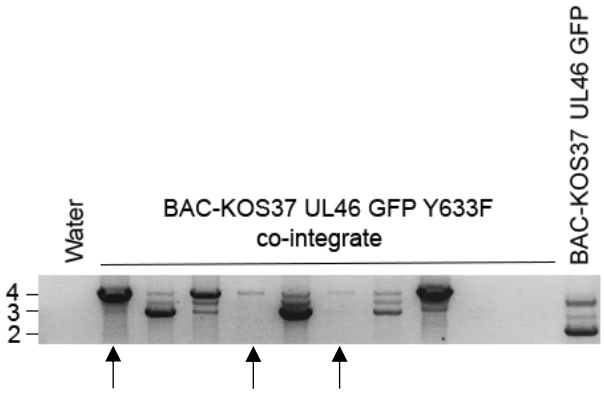

Fig 3.4: Co-Integration of the PCR product after the first Red recombination.

Shown is the co-integration event of the 1kb PCR cassette into the desired region of UL46.The region of interest is magnified and the four important sequences are colour-coded (a, brown; b, blue; c, green; d, yellow). The wildtype tyrosine sequence is shown as a white circle. The PCR integration cassette contains the selection marker that is flanked by homologous regions encoding for the desired mutation (red circle). This figure is not to scale. (B) After the first recombination step eleven single clones were screened for the co-integration of the PCR product. The integration is judged by the size of the UL46-PCR product. Water as well as the BAC-KOS37 UL46 GFP were used as controls. Only clones with a single PCR fragment of 4 kbp (arrow) were used for the second recombination step. Shown is only the portion of the agarose gel that represents PCR amplicons between 2 kbp and 4 kbp.

A

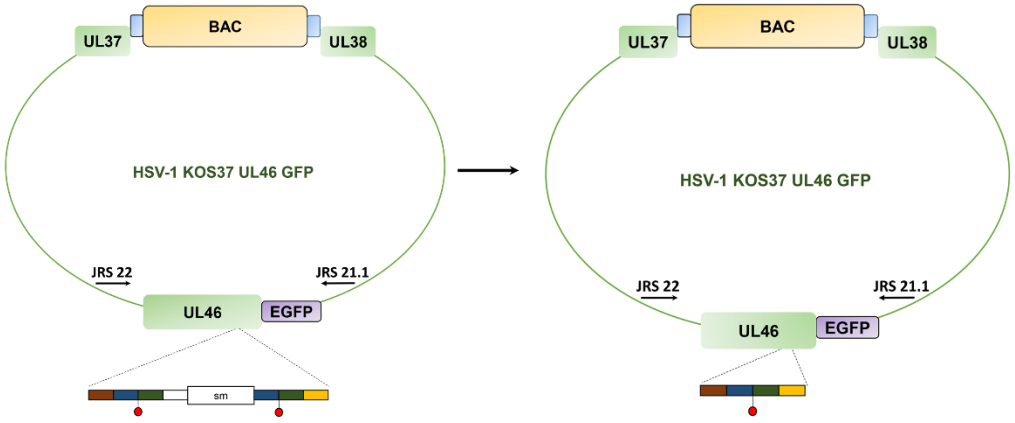

B

Fig. 3.5: Final *en passant* mutagenesis product.

(A) The selection cassette as well as the sequence duplication will be eliminated during the second recombination step. This figure is not to scale. (B) After the second recombination step three single clones were analyzed for the absence of the marker cassette. The original clone after the first recombination step was used as a control (BAC-KOS 37-UL46 GFP Y633F co-integrate). Clones with a single PCR fragment of 3 kbp were further analyzed via sequencing.

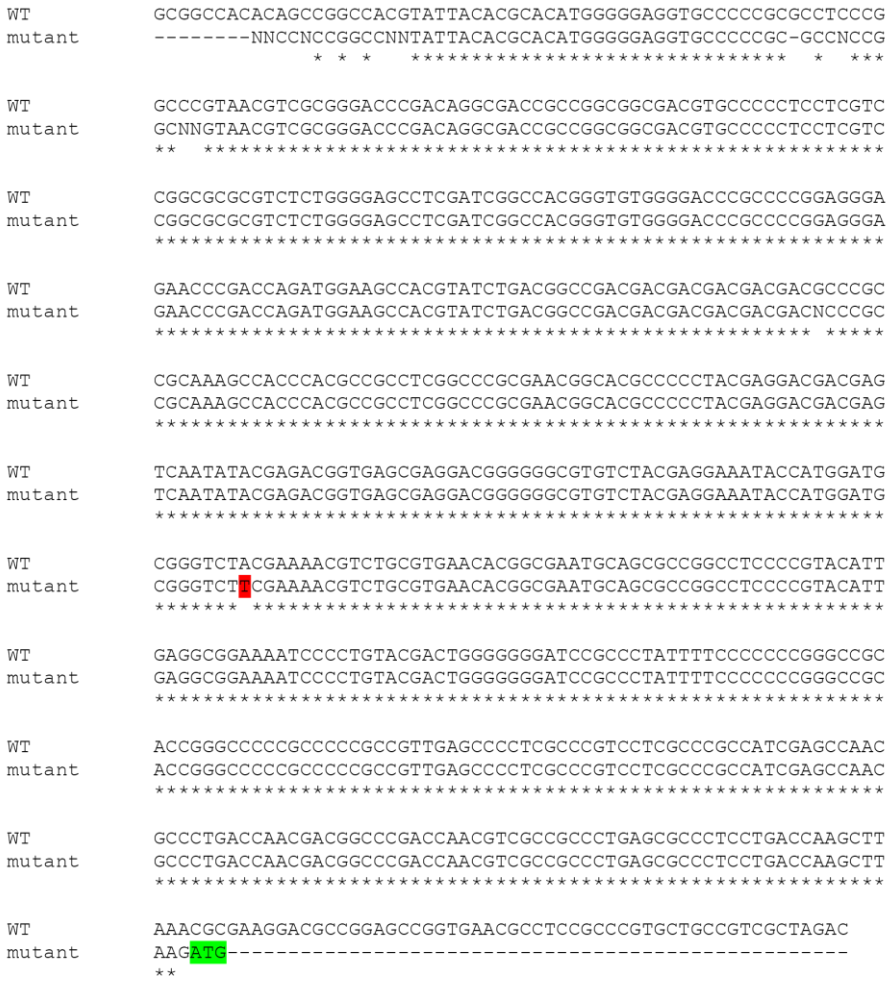

Fig. 3.6: Sequence validation of the point mutation within BAC-KOS37 UL46-GFP Y633F.

The PCR product of a single clone after the second recombination step was purified and sequenced via JRS 754. The sequence was aligned to WT HSV-1 KOS (accession number JQ673480; version JQ673480.1) in order to validate the point mutation (red). The C-terminal GFP-tag start codon is in green. Sequences were aligned using Clustal Omega.

3.1.2.2 Reconstruction of the KOS37-UL46 GFP Y633F virus

Next, BAC-KOS37-UL46 GFP Y633F was transfected into Cre-Vero cells. Cre recombinase recognizes the loxP sequences that flank the BAC sequence and leading to excision of the KOS37 genome. Passaging the virus in Cre-Vero cells and final growth of the virus in Vero cells yielded KOS37-UL46 GFP Y633F.

To confirm the presence of the correct UL46 sequence and GFP-tag, PCRs were performed on DNA from KOS37-UL46 GFP Y633F infected cells (Fig. 3.8). PCRs were carried out using either the primers (Fig. 3.7) JRS21.1 and JRS 22, which amplify the UL46 region (Fig. 3.8A), or the primers JRS 754 and JRS 731, which amplify the GFP region (Fig. 3.8B). The PCR amplicons were then analyzed using an agarose gel. The observed PCR products verified that the reconstructed virus codes for UL46 as well as the GFP-tag.

In addition, two PCRs were carried out to show that the BAC sequence had been excised from the viral genome (Fig. 3.9). One PCR was carried out using the primers JRS 475B and JRS 476B to amplify a region within the BAC sequence (BAC inside). The second PCR was carried out using the primers JRS 473B and JRS 649 to amplify the UL37 HSV-1 region (BAC outside). As described in figure 3.3, the BAC is placed between the UL37 and UL38 genes within the KOS37 genome. Primer JRS 473B binds UL37 and extends towards the N-terminus, whereas primer JRS 649 binds the UL38 gene and extends back into UL37. As expected, no BAC-DNA was amplified using the BAC inside primers on KOS37-UL46 GFP Y633F (Fig. 3.10A). This data was supported by a PCR using BAC outside primers (Fig. 3.10B). In case of KOS37-UL46 GFP Y633F I detected a single band of 0.7 kbp, which represents the UL36-UL37 region after the BAC region

was eliminated (Fig 3.10A). In case of the control sample BAC-KOS37 UL46 GFP Y633F I detected two PCR amplicons one of 3.0 kbb and of 1.0 kbp (Fig. 3.10B); however, the entire UL36-BAC-UL37 region is about 4.0 kbp. Given that the PCR settings were optimized to amplify the UL36-UL37 region and not the entire UL36-BAC-UL37 region, the observed products of 3.0 kbb and 1.0 kbp most likely represent PCR side products. Taken together, the data suggest that the BAC region was eliminated.

In combination with the PCR results for UL46 and GFP, the data indicate that KOS37-UL46 GFP Y633F was properly reconstituted from the BAC. To verify that the UL46 region encodes the Y633F mutation, I sequenced the UL46-PCR product (JRS 21.1 / JRS 22) using the sequencing primer JRS 754 and aligned the sequencing results to the sequence of WT UL46 (Fig. 3.11).

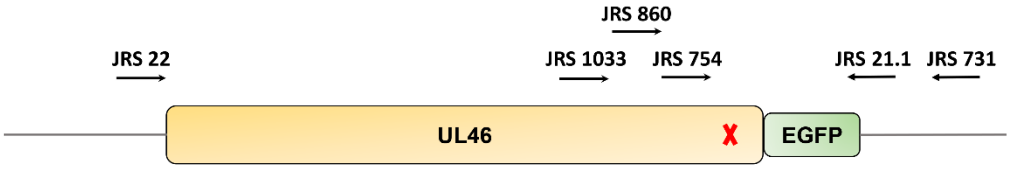

Fig. 3.7: Primer annealing sites.

This figure illustrates the annealing sites of primers used to validate viruses. The red cross indicates the location of the tyrosine-based binding motifs.

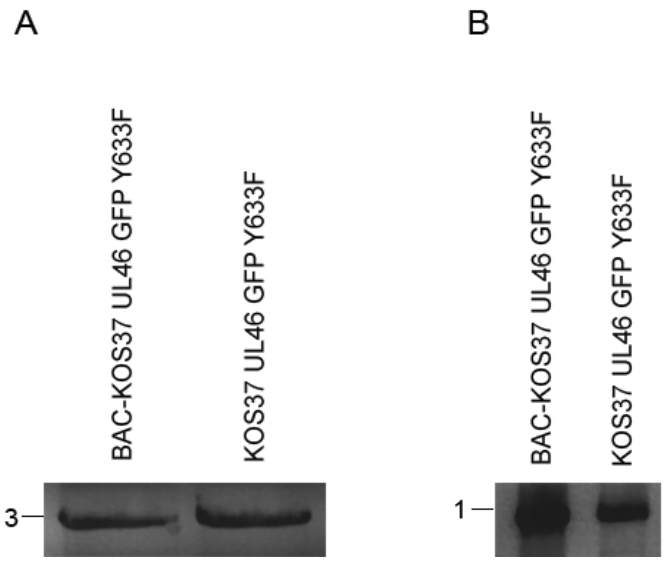

Fig. 3.8: Amplification of the UL46- and GFP-region within DNA obtained from Vero cells infected with KOS37-UL46 GFP Y633F.

DNA from KOS37-UL46 GFP Y633F infected Vero cells was used to amplify the UL46-region (A) as well as the GFP-region (B). The PCR samples were run on an agarose gel and the fragment size was compared to BAC-KOS37 UL46 GFP Y633F.

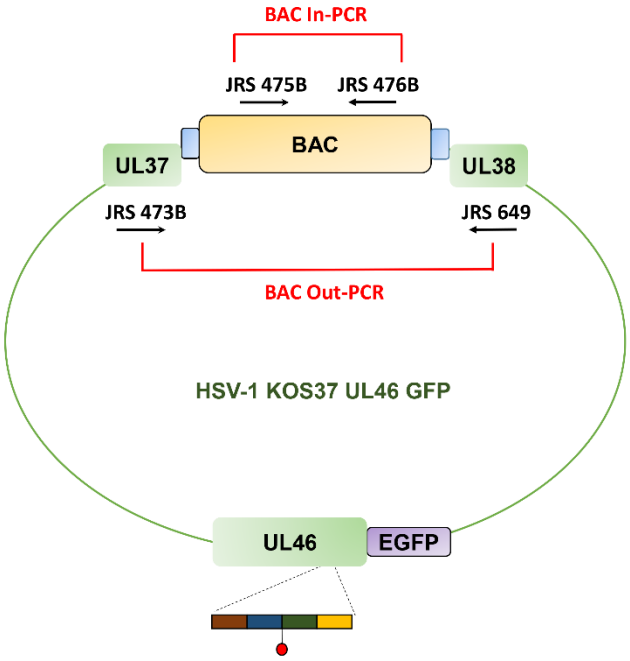

Fig. 3.9: PCR primer design to evaluate the presence of BAC.

The BAC region is flanked by loxP sites and is placed between the UL37 and UL38 region of KOS37. One primer set was designed to anneal to the BAC sequences (BAC-In PCR), whereas the second primer set was designed to anneal to the UL37 and UL38 region (BAC-Out PCR). This figure is not to scale.

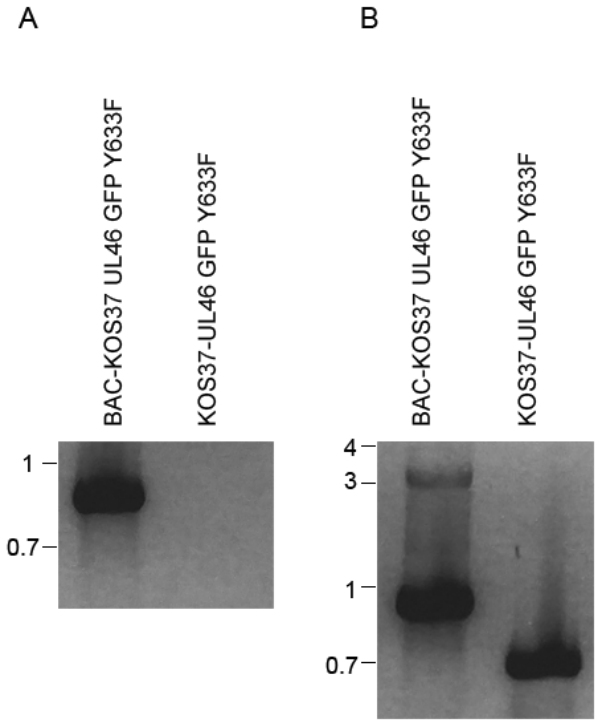

Fig. 3.10: Amplification of the BAC-region of DNA obtained from Vero cells infected with KOS37-UL46 GFP Y633F.

DNA from KOS37-UL46 GFP Y633F infected Vero cells was used to amplify a region within the BAC plasmid (A) as well as outside of the BAC region (B). The PCR samples were run on an agarose gel and the fragment size was compared to BAC-KOS37-UL46 GFP Y633F. The observed fragments for the BAC-out region in BAC-KOS37 UL46 GFP Y633F appears to be a side product of the expected 4.0 kbb fragment. PCR amplification for the BAC-out PCR was optimized to amplify the 700 bp fragment in the generated virus (KOS37-UL46 GFP Y633F) and not the larger fragment containing the BAC insert.

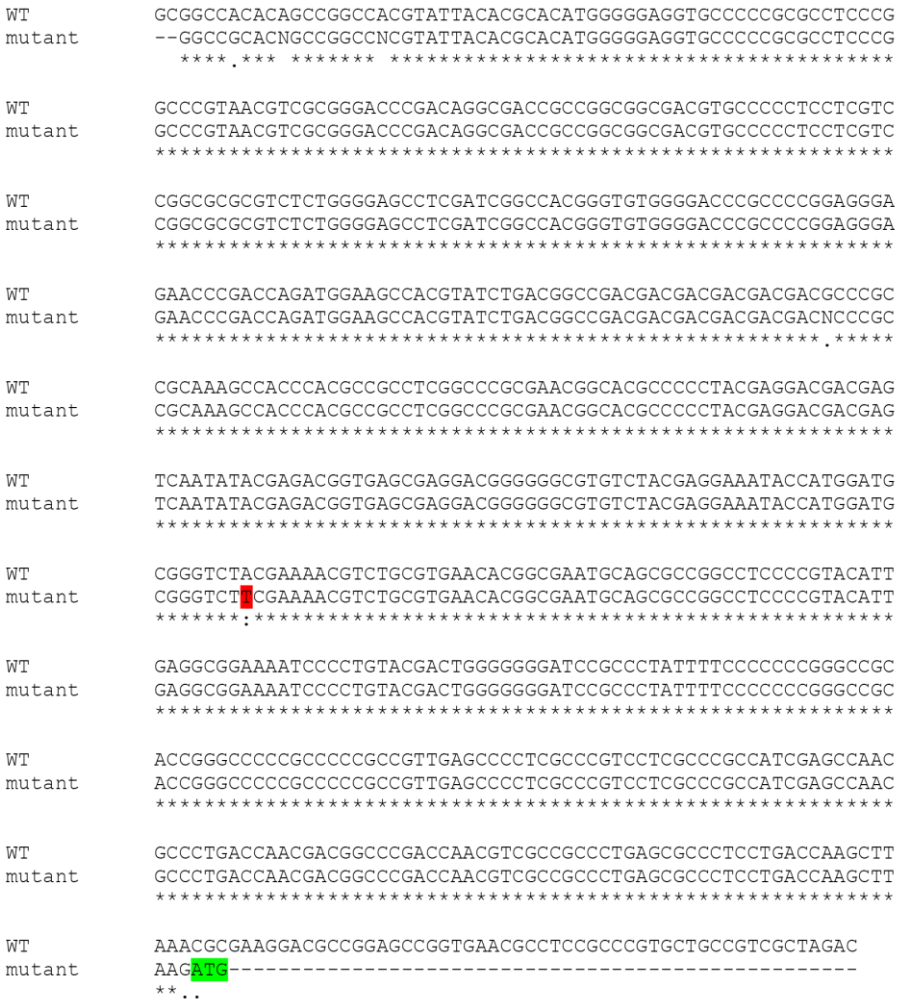

Fig. 3.11: Sequence validation of KOS37-UL46 GFP Y633F.

The UL46-PCR product was purified and sequenced using JRS 754. The sequence was aligned to WT UL46 (accession number JQ673480; version JQ673480.1) in order to verify the point mutation (red). The start codon of the C-terminal GFP-tag is in green. Sequences were aligned using Clustal Omega.

3.2 Summary

The results presented in this chapter describe the generation of viruses bearing point mutations that inactivate the tyrosine-based motifs predicted to bind SFKs, p85, Grb2 as well as Shc. Viruses were generated in order to investigate possible association of VP11/12 with cellular proteins. In addition, we aimed to investigate the effects of those possible protein-protein interactions on the ability of VP11/12 to interfere with two signaling pathways. All viruses were successfully generated using *en passant* mutagenesis in the context of a BAC that contains the entire HSV-1 KOS37 genome. Infectious viruses were then reconstructed by transfecting and passaging the virus in Cre-Vero cells to eliminate the BAC region. To finally confirm the presence of the correct UL46 sequence, the UL46 region was amplified and subjected to Sanger sequencing. If applicable, we also confirmed the presence of the GFP-tag by using a PCR specific for the GFP sequence. Lastly, we performed two sets of PCRs to confirm that the BAC was successfully eliminated.

Chapter 4

Tyrosine-based binding motifs within HSV-1 VP11/12 enable VP11/12 to associate with Src family kinase Lck, p85, Grb2 and Shc

A version of this chapter has been published in:

Strunk, U., et al., *Role of herpes simplex virus VP11/12 tyrosine-based motifs in binding and activation of the Src family kinase Lck and recruitment of p85, Grb2, and Shc.* J Virol, 2013. **87**(20): p. 11276-8

All experiments presented within this chapter were performed by U. Strunk.

Preface

The HSV-1 tegument protein VP11/12 is directly delivered into the cytoplasm and associates with both cellular membranes as well as viral capsids [265]. VP11/12 is tyrosine phosphorylated in lymphocyte cells by Src family kinases (SFKs) [229, 230]; however, the phosphorylation is less obvious in human fibroblasts [230] and monkey kidney epithelial Vero cells [228].

Melany Wagner has previously shown that the phosphorylation of VP11/12 is predominantly through the SFK Lck in lymphocyte-like Jurkat T-cells [266]. In addition, she provided evidence that VP11/12 interacts with Lck; therefore, she postulated that VP11/12 recruits and activates Lck in order to induce further tyrosine phosphorylation of itself [266]. In line with this data she further provided evidence that VP11/12 recruits p85 for the activation of Akt. In addition, she provided evidence that SFK activity is necessary for tyrosine phosphorylation of VP11/12 as well as Akt activation [229].

Based on these data, she proposed that VP11/12 recruits and activates SFKs through the consensus SFK Sh2 binding motif YEEI [266, 268] at position Y624 or the YETV potential SFK Sh2 binding motif at position Y613. Association with and activation of SFKs then leads to additional tyrosine phosphorylation of VP11/12, including the predicted p85 Sh2 binding motif YTHM at position Y519 [229]. Supported by the Wagner and Smiley model, we also hypothesized that the predicted binding motifs for the Sh2 domain of Grb2 (YENV at position Y633) as well as for the PTB domain of Shc (NPLF at position Y657) enable VP11/12 to associate with these cellular proteins [279]. Data presented in this chapter support this hypothesis and demonstrate that VP11/12 utilizes tyrosine-based binding motifs to associate with Lck, p85, Grb2 and Shc [279].

4.1 Results

4.1.1 VP11/12 associates with Grb2 and Shc in addition to Lck and p85

Before I started my project Jim Smiley found that the C-terminal region of VP11/12 contains one predicted binding motif for the Sh2 domain of Grb2 (YENV, Y633) as well one predicted binding motif for the PTB domain of Shc (NPLY, Y657). Holly Saffran then observed that VP11/12 indeed interacts with Grb2 as well as Shc in co-immunoprecipitation assays. In order to confirm these findings, I first performed co-immunoprecipitation assays with KOS37-UL46 GFP as well as with KOS37-GFP UL46. Both of these viruses express WT VP11/12, but VP11/12 is either C-terminally (KOS37-UL46 GFP) or N-terminally (KOS37-GFP UL46) fused with EGFP. We decided to fuse VP11/12 C-terminally or N-terminally to EGFP to determine if the position of the tag has an impact on the protein-protein interactions. In general fusion-tags can lead to structural changes that then can change the protein's function.

Lymphocyte-like Jurkat T-cells were either mock infected or were infected with KOS37-UL46 GFP, KOS37-GFP UL46 or with KOS-G for 13 h. KOS-G is a KOS-derived WT virus that expresses free GFP [272]. The cell extracts were co-immunoprecipitated using an anti-GFP antibody overnight and the precipitates were analyzed by western blotting using antibodies against p85, Lck, Shc, Grb2, GFP, ICP27 and actin (Fig. 4.1). Detection of GFP in the whole cell lysate (WCL) fractions demonstrated that equal levels of the VP11/12-fusion protein were expressed by KOS37-UL46 GFP and KOS37-GFP UL46. I was able to demonstrate that, as expected, the C-terminally tagged VP11/12 protein (KOS37-UL46 GFP) associates with Lck, p85, Grb2 and Shc. The N-terminally tagged VP11/12 (KOS37-GFP UL46) also associates with Lck, p85, Grb2 and Shc; however, it

seemed to associate less efficiently with p85 as well as with Shc. This finding indicates that the position of the GFP tag influences the co-immunoprecipitation efficiency. Importantly, free GFP encoded by KOS-G did not co-precipitate any of the cellular proteins, strongly suggesting that the protein-protein interactions are mediated by the VP11/12 portion of the fusion protein and not the GFP portion. Western blot detections of GFP served as control for VP11/12 expression, whereas ICP27 served as an infection control and actin served as a total loading control. The heavy chain (HC) of the antibody used to immunoprecipitate VP11/12 was cross-detected on the western blot staining for GFP. Taken together, my data confirm Hally Saffran's finding that VP11/12 interacts either indirectly or directly with Shc and Grb2 in addition to the previously described interactions with Lck [266] and p85 [229].

Based on the greater co-immunoprecipitation efficiency of p85 and Shc by the C-terminally tagged VP11/12 derivative, KOS-UL46 GFP was used in additional experiments investigating the role of the predicted tyrosine-based binding motifs in the VP11/12-host cell protein association(s). Of note, previous co-immunoprecipitation assays for Lck [266] and p85 [229] were carried out with the GHSV-UL46 virus. The GHSV-UL46 is identical to the KOS37-UL46 GFP virus, with the exception that it originates from the HSV-1 KOS strain instead of the HSV-1 KOS37 strain [264].

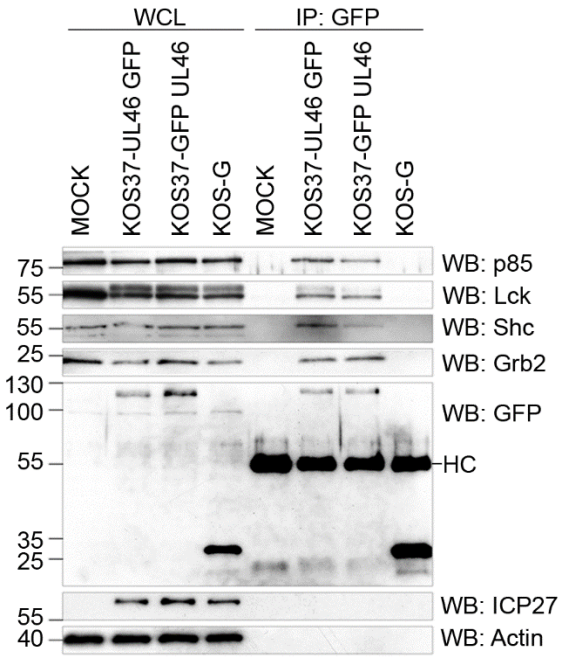

Fig. 4.1: VP11/12 associates with Grb2 and Shc in addition to Lck and p85.

Jurkat E6-1 cells were mock infected, infected with a KOS37-derived virus expressing a C-terminally GFP tagged VP11/12 (KOS37-UL46 GFP), a KOS37-derived virus expressing a N-terminally tagged VP11/12 (KOS37-GFP UL46), or a KOS-derived virus expressing free GFP (KOS-G) for 13 h. Whole cell lysates (WCL) were co-immunoprecipitated using an antibody against GFP (IP:GFP) and analyzed via Western blotting (WB) for p85, Lck, Shc, Grb2, GFP and ICP27; (HC, heavy chain). Shown is one representative experiment out of three.

4.1.2 The Role of tyrosine-based binding motifs of VP11/12 in the recruitment of Grb2, Shc, p85 and Lck

As summarized in the rationale for this chapter, I sought to address one of the key questions raised by Melany Wagner's previous research on the ability of VP11/12 to associate with cellular proteins. She suggested that tyrosine-based binding motifs within

the C-terminal region of VP11/12 are utilized to directly associate with the predicted cellular host cell protein [229, 266]. To follow up on this key question, Holly Saffran and I generated point-mutated viruses in which the predicted tyrosine-based binding motifs had been inactivated, in order to evaluate if these sequences are indeed used to enable VP11/12 to associate with the host cell proteins. I performed a series of co-immunoprecipitation assays as well as GST-pulldown assays to investigate the role of the tyrosine-based binding motifs.

4.1.2.1 VP11/12 interacts with the Sh2 domain of Grb2 through the YENV motif at position Y633

Jim Smiley identified the predicted Grb2 tyrosine-binding motif YENV at position Y633 using the scansite 2.0 algorithm. To determine if phosphorylation of the tyrosine within this putative Grb2 Sh2 binding motif is essential for the VP11/12-Grb2 association, I mutated the tyrosine codon (TTA) to a phenylalanine codon (TTC) in the context of the C-terminally tagged VP11/12 encoded by KOS37-UL46 GFP, generating KOS37-UL46 GFP Y633F. The effect of this mutation on the VP11/12-Grb2 interaction was then documented using two co-immunoprecipitation assays (Fig. 4.2) as well as one GST pull-down assay (Fig. 4.3).

For the co-immunoprecipitation assays, I mock infected Jurkat E6-1 cells or infected them with KOS37-UL46 GFP, KOS-G or KOS37-UL46 GFP Y633F for 13 h. Lysates were immunoprecipitated with an anti-GFP antibody as in figure 4.1 and then analyzed by western blotting for p85, Lck, Grb2, Shc, GFP, ICP27 and actin (Fig 4.2A).

We found that the Y633F mutation abolished the interaction between VP11/12 and Grb2 without affecting the interactions with p85, Lck, and Shc. The interaction between VP11/12 and Grb2 was also abolished in a reciprocal co-immunoprecipitation assay using an antibody against Grb2 for immunoprecipitation and western blotting for GFP to visualize the interaction (Fig. 4.2B). The reciprocal co-immunoprecipitation assay was carried out as described above, except that the lysates were immunoprecipitated using an anti-Grb2 antibody and then analyzed by western blotting for GFP, Grb2, ICP27 and actin.

To determine if the interaction between Grb2 and VP11/12 is mediated by the Sh2 domain of Grb2, Jurkat E6-1 cells were infected as above and cell extracts were incubated with glutathione-agarose beads bearing immobilized GST-Grb2 Sh2 fusion protein (Fig. 4.3).

Bound VP11/12 was then detected by western blotting using an antibody to GFP. WT VP11/12 efficiently bound to beads bearing the GST-Grb2 Sh2 domain fusion protein, whereas no interaction was observed after inactivating the YENV motif (KOS37-UL46 GFP Y633F). Importantly, WT VP11/12 did not associate with the GST portion itself and the free GFP protein encoded by KOS-G also did not bind the Sh2 domain of Grb2, or Lck or the PTB domain of Shc (Fig. 4.4). These data indicate that VP11/12 binds the Sh2 domain of Grb2 and as expected, the Y633F mutation abolished this interaction. Taken together, these data strongly suggest that VP11/12 interacts directly with the Grb2 Sh2 domain through the YENV motif at Y633. Given that Sh2 domains bind phosphorylated tyrosine residues, this interaction almost certainly requires phosphorylation of Y633.

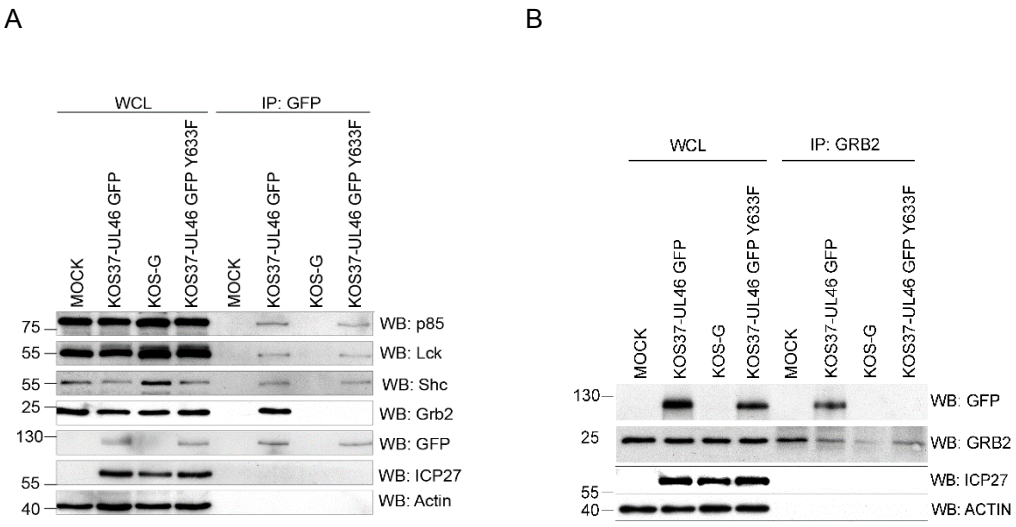

Fig. 4.2: VP11/12 requires the phosphorylation of Y633 within the YENV motif to associate with Grb2.

Jurkat E6-1 cells were mock infected or infected with the indicated viruses for 13 h. Whole cell lysates (WCL) were immunoprecipitated using an antibody against GFP (IP:GFP) and analyzed through western blotting (WB) for p85, Lck, Shc, Grb2, GFP, ICP27 and actin. Shown is one representative experiment out of four. (B) Jurkat E6-1 cells were mock infected or infected with the indicated viruses for 13 h. Whole cell lysates (WCL) were immunoprecipitated using an antibody against Grb2 (IP:Grb2) and analyzed via western blotting for GFP, Grb2, ICP27 and actin. shown is one representative experiment out of three.

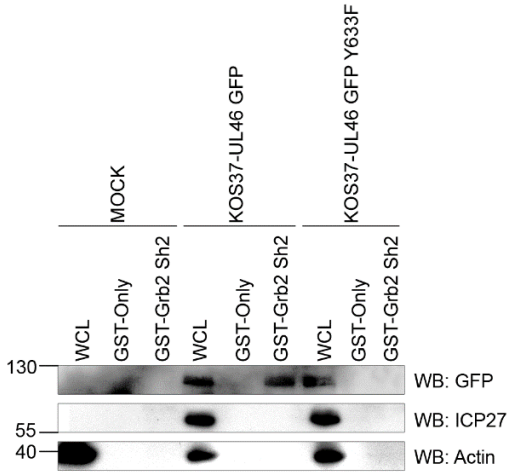

Fig. 4.3: The YENV motif at position Y633 is required for the interaction of VP11/12 with the Sh2 domain of Grb2.

Jurkat E6-1 cells were mock infected or infected with KOS37-UL46 GFP or KOS37-UL46 GFP Y633F. Cell lysates were subjected to a GST pull-down assay with the indicated GST-fusion proteins. Protein bound to the beads was analyzed for GFP, ICP27 and actin by western blotting. Shown is one representative experiment out of three.

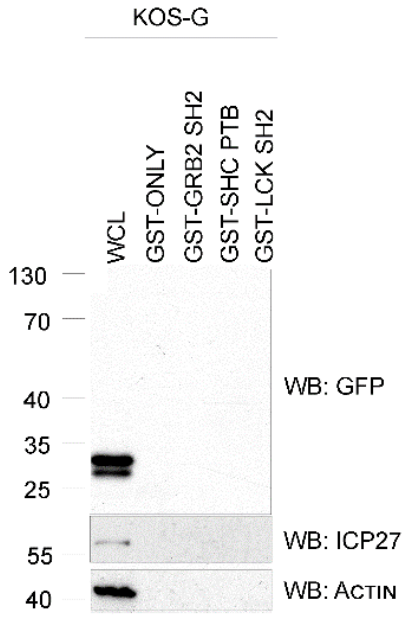

Fig. 4.4: Free GFP encoded by KOS-G does not interact with the Sh2 domain of Grb2 or Lck, or the PTB domain of Shc.

Jurkat E6-1 cells were infected with KOS-G. Cell lysates were subjected to a GFP pull-down assay with the indicated GST-fusion proteins. Protein bound to the beads was analyzed for GFP, ICP27 and actin by western blotting. Shown is one representative experiment out of three.

4.1.2.2 VP11/12 interacts with the PTB domain of Shc through the NPLF motif at position Y657

In addition to the Grb2 tyrosine-binding motif YENV at position Y633, Jim Smiley also identified the tyrosine-based binding motif NPLY at position Y657 using the scansite 2.0 algorithm. The NPLY motif was predicted to lead to an interaction with the PTB domain of Shc and Holly Saffran confirmed that VP11/12 indeed co-immunoprecipitates with Shc. I followed the same approach as used for the Grb2-YENV motif to determine if the phosphorylation of the tyrosine within this putative Shc PTB binding motif is essential for

the VP11/12-Shc association. I converted the tyrosine codon (TTA) to a phenylalanine codon (TTC) in the context of the C-terminally tagged VP11/12 encoded by KOS37-UL46 GFP, generating KOS37-UL46 GFP Y657F. The effect of this mutation on the VP11/12-Shc interaction was then documented using two co-immunoprecipitation assays (Fig. 4.5) as well as one GST pull-down assay (Fig. 4.6).

Using the co-immunoprecipitation approach as outlined for figure 4.2, I was able to document that the Y657F mutation abolished the interaction between VP11/12 and Shc. Inactivation of the NPLY motif also slightly reduced the VP11/12-p85 association, while not affecting the remaining interactions between VP11/12 with Lck or Grb2 (Fig. 4.5A). An interaction between VP11/12 and Shc was also detected in a reverse immunoprecipitation assay, using an anti-Shc antibody (Fig. 4.5B). In line with our prediction, this interaction was eliminated after inactivation of the tyrosine-based binding motif. Both co-immunoprecipitation approaches supported our assumption that VP11/12 interacts with Shc through the NPLY motif at position Y657. However, it remained to be determined if VP11/12 associates with Shc in a PTB-dependent manner.

To further assess whether the VP11/12-Shc interaction is dependent on the PTB domain of Shc, I performed a GST pull-down assay (Fig. 4.6). I was able to demonstrate that WT VP11/12 binds to beads bearing GST fused to the PTB domain of Shc, but does not bind to beads bearing GST. Importantly, the VP11/12-Shc interaction was abolished by the Y657F mutation. Moreover, the free GFP protein encoded by KOS-G did not bind the Shc PTB domain (Fig. 4.4).

Taking the co-immunoprecipitation assays as well as the GST-pulldown assays into account, my data strongly supports a model of a direct PTB-mediated interaction between VP11/12 and Shc.

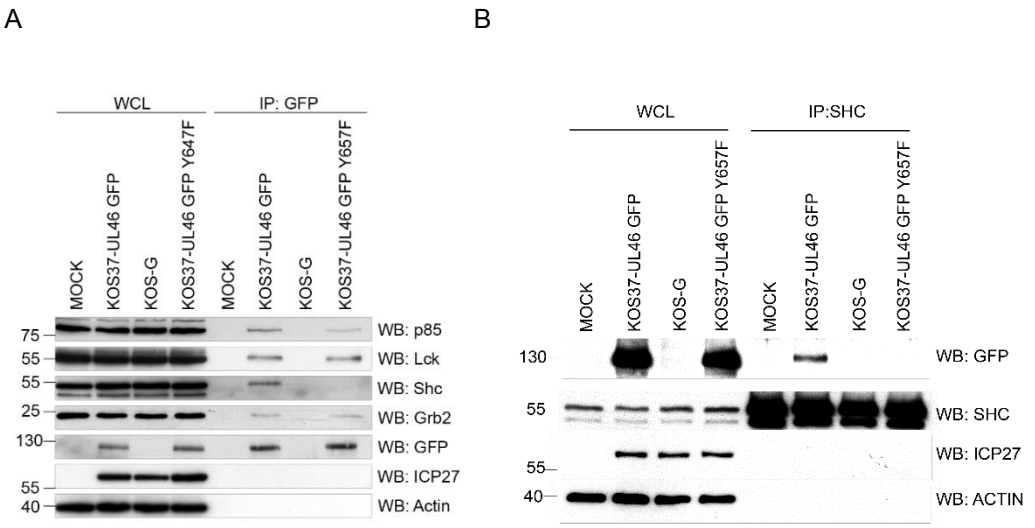

Fig. 4.5: The interaction between VP11/12 and Shc requires the NPLY motif.

(A) Extracts of Jurkat E6-1 cells infected with the indicated viruses (WCL) were precipitated with an anti-GFP antibody (IP: GFP) and analyzed by western blot for p85, Lck, Shc, Grb2, GFP, ICP27 and actin. Shown is one representative experiment out of four. (B) Extracts of Jurkat E6-1 cells infected with the indicated viruses (WCL) were precipitated with an anti-Shc antibody (IP: Shc) and analyzed by western blot for GFP, Shc, ICP27 and actin. Shown is one representative experiment out of two.

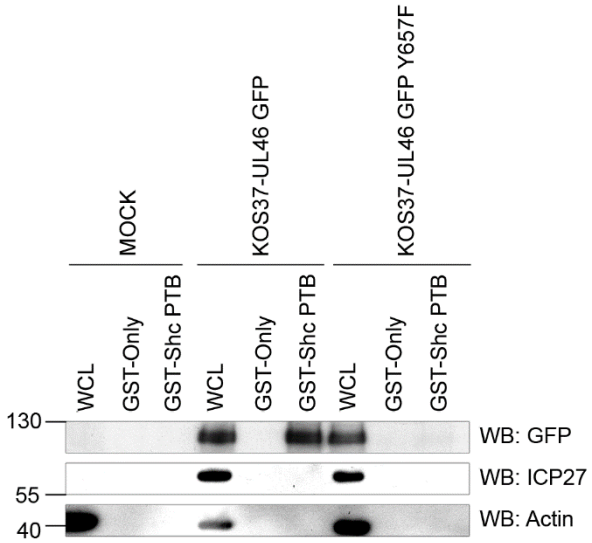

Fig. 4.6: VP11/12 associates with the PTB domain of Shc in an NPLY-dependent manner.

Extracts of Jurkat T-cells infected with KOS37-UL46 GFP or KOS37-UL46 GFP Y657F. Extracts were subjected to a GST-pulldown assay with the indicated GST-constructs and analyzed using western blotting for GFP, ICP27 and actin. Shown is one representative experiment out of three.

4.1.2.3 VP11/12 interacts with p85 through the YTHM motif at position Y519

As mentioned in the preface for this chapter, Wagner and Smiley hypothesized that VP11/12 associates with the Sh2 domain of the PI3K-regulatory subunit p85 via the YTHM motif [229]. I followed the same approach as for the predicted tyrosine-based binding motifs for Grb2 and Shc and generated a single-point mutated virus with an inactive YTHM binding motif (KOS37-UL46 GFP Y519F) and subjected the WCL to a series of co-immunoprecipitation assays.

Jurkat T-cells were infected with the indicated viruses for 13 hours. Cell lysates were either co-immunprecipitated using an antibody against GFP (IP:GFP) or an antibody against p85 (IP:p85) and analyzed via western blotting for the indicated proteins (Fig.

4.7). I found that inactivation of the YTHM motif greatly reduced, but did not eliminate, the interaction between p85 and VP11/12. Inactivation of the YTHM motif did not affect the interaction of VP11/12 with Shc (Fig. 4.7A), but the interaction of VP11/12 with Grb2 or Lck was somewhat reduced in the KOS37-UL46 GFP Y519 mutant and studies described in chapter 5.1 investigate the significance of this observation. These protein-protein interaction data confirm that the YTHM motif contributes to the interaction with p85, but also suggest that one or more additional interaction interfaces in VP11/12 may also play a role.

A B

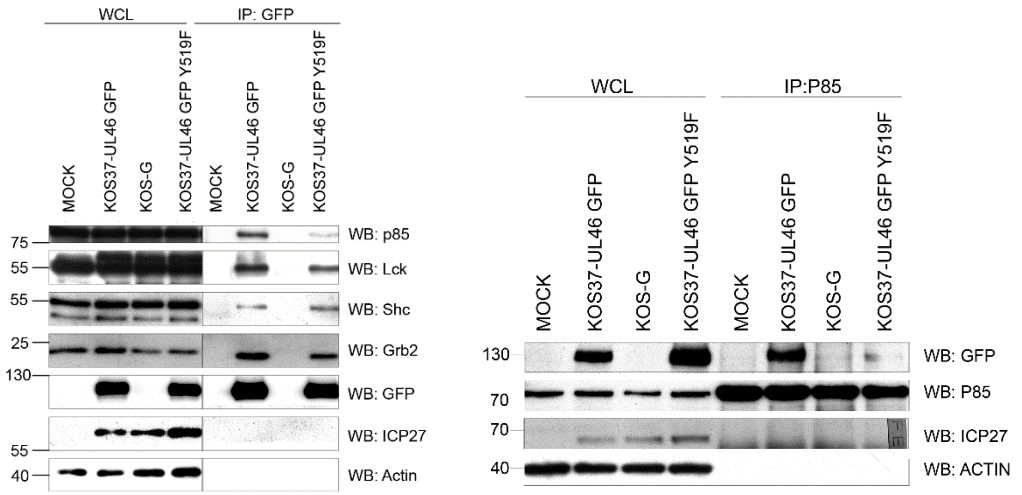

Fig. 4.7: The YTHM motif contributes towards the VP11/12-p85 association.

Extracts of Jurkat E6-1 cells infected with the indicated viruses and were precipitated with an (A) anti-GFP (IP: GFP) or an (B) anti-p85 (IP:p85). Proteins were detected using antibodies specific for the indicated proteins on a western blot. Of note, the abnormal pattern on the right in the anti ICP27 blot is the film number printed on the film by the x-ray film manufacturer. Shown are one representative experiment out of three (A) or two (B).

4.1.2.3.1 Effects of mutating proline-rich sequences predicted to bind the Sh3 domain of p85

Given the observation that inactivation of the YTHM motif reduced but did not eliminate the VP11/12-p85 association, we asked if VP11/12 might contain one or more additional binding motifs that contribute to an association with p85. Melany Wagner pointed out that VP11/12 contains two proline-rich sequences that were predicted to interact with the SH3 domain of p85, at positions 469-472 (PPLP) and at positions 673-677 (PPPPP) [236]. Both motifs encode for the consensus sequence for SH3 domains, which is either RxxPPxP (class I motif; PPPPP motif) or PPxPxR (class II motif; PPLP) [287, 288]. As reviewed in the introduction, it has been previously shown that the influenza A virus protein NS1 associates with p85 in infected cells in an Sh2- as well as an Sh3-dependent manner [259]. Shin *et al* demonstrated that, similar to HSV-1 VP11/12 [229], the influenza A virus protein stimulates the PI3K/Akt-pathway [259]. Importantly, NS1 contains one p85-Sh2-binding motif and two p85-Sh3-binding motifs and all three motifs contribute to the NS1-p85 association. However, the data presented suggest that the NS1-p85 interaction is predominantly Sh3-mediated [259]. Based on the influenza A NS1 research, I asked whether VP11/12 associates with p85 in an Sh2-Sh3 dependent manner.

To address this question I first determined if the predicted proline motifs are conserved among closely related *Simplexviruses*, as described in section 3.1.1 for the tyrosine-based binding motifs (Fig. 3.1). The sequences of several closely related primate herpesviruses were aligment as previolusly described, with the exception that the aligment as well as visualization was carried out using MUSCLE (Fig. 4.8A). Grey

shading within the aligment indicates sequence conservation and the rectangles indicate the two predicted Sh3 binding motifs. I found that only the class II binding motif (core sequence PPLP in HSV-1) is conserved among some orthologues, but not in HSV-2 and ChHV. These two viruses do not encode for the entire consensus binding motif (PPxPxR) as that the second variant amino acid between the last proline and arginine is missing. In contrast, the PPPPP motif is not conserved among the orthologues.

I then generated two double-mutated viruses in which the YTHM motif was inactivated along with one of the proline sequences (KOS37-UL46 GFP AALA/Y519F; KOS37-UL46 GFP Y519F/AAPPA). In both cases, the motifs were inactivated by converting relevant proline (P) codon into an alanine (A) codon. Also I constructed one triple-mutated virus, containing an inactive YHTM motif as well as two inactive proline sequences (KOS37-UL46 GFP AALA/Y519F/AAPPA). I infected Jurkat E6-1 cells with the indicated viruses and subjected the lysates to a co-immunoprecipitation assay using an antibody against GFP (Fig. 4.8B). Inactivation of either of the proline sequences individually to the YTHM motif did not alter VP11/12's ability to interact with p85. Unexpectedly, inactivating all three motifs (KOS37-UL46 GFP AALA/Y519F/AAPPA) led to a virus that no longer produced a detectable amount of VP11/12. The VP11/12-Shc association was not affected by the double-point mutation. Given the lack of VP11/12 expression I was not able to determine if VP11/12 associates with p85 using a similar mechanism as the influenza A virus NS1 protein. Sequence validation (figure A3.23) did not indicate any further mutations within the sequenced region. It therefore remains to be determined why the triple-point mutated virus KOS37-UL46 GFP AALA/Y519F/AAPPA fails to produce detectable levels of VP11/12 protein.

A

B

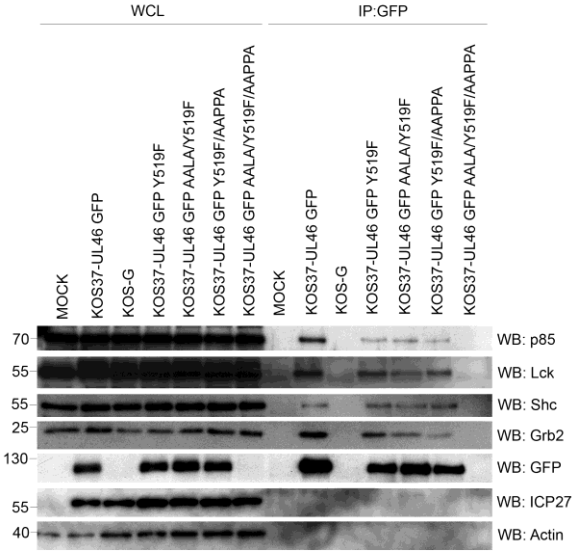

Fig. 4.8: VP11/12 might associate with p85 in a Sh2/Sh3-dependent mechanism.

(A) Sequences were aligned and visualized using MUSCLE. Rectangles indicate the predicted Sh3 binding motifs and grey shading indicates sequence conservation. (B) Jurkat E6-1 cells were infected with the indicated viruses. The WCL were precipitated with an anti-GFP antibody (IP: GFP) and proteins were detected using antibodies specific to the indicated proteins on a western blot. KOS37-UL46 GFP AALA/Y519F/AAPPA failed to produce detectable levels of VP11/12. Inactivating the YTHM motif alone had some minor effects on the ability of VP11/12 to associate with Grb2 and Lck, as pointed out for figure 4.7. Shown is one representative experiment out of two.

4.1.2.4 VP11/12 associates with the Sh2 domain of Lck through the YEEI or YETV motif

Melany Wagner's previous research demonstrated that VP11/12 interacts with Lck in Jurkat T-cells, and her model suggested that VP11/12 uses one or two tyrosine-based binding motifs to associate with the Sh2 domain of Lck [266]. Wagner and Smiley predicted that the interaction might be predominantly through the YEEI motif at position 624. To test this assumption, Holly Saffran generated the single-point mutated virus KOS37-UL46 GFP Y624F.

To determine if the interaction between VP11/12 and Lck depends only on the phosphorylation of Y624, I infected Jurkat T-cells in order to perform co-immunoprecipitation assays as well as GST-pulldown assays. After performing a co-immunoprecipitation assay, I was able to demonstrate that inactivation of the YEEI motif did not fully inhibit the association of VP11/12 with Lck (Fig. 4.9). Of note, we also used an antibody against active SFK because we wanted to determine if bound Lck is active or not. Previous work indicated that VP11/12 might recruit Lck in order to stimulate Lck activation [229, 266].

I then decided to test the possibility that the interaction of VP11/12 with Lck in T-cells either depends on the YETV motif (Y613) or both tyrosine-based binding motifs together. I generated the single point-mutated virus KOS37-UL46 GFP Y613F as well as double point-mutated virus KOS37-UL46 GFP Y613F/Y624F and performed co-immunoprecipitation assays (Fig. 4.10) as well as GST-pulldown assay (Fig. 4.11) as described above.

I found that inactivation of the YETV motif had relatively little effect on the ability of VP11/12 to co-imunoprecipitate Lck or active SFKs (Fig. 4.10A). We therefore aimed to

determine if eliminating a possible association will also lead to elimination of Lck activation. Inactivation of both binding motifs severely reduced the VP11/12-Lck association. These findings were confirmed in the reciprocal co-immunoprecipitation experiment, where Lck was immunoprecipitated (IP:Lck) and VP11/12 was detected in the immunoprecipitates (Fig. 4.10B). My co-immunoprecipitation results indicate that VP11/12 requires either the YETV motif or the YEEI motif for an association with Lck.

To further examine if VP11/12 associates with the Sh2 domain of Lck, I subjected the panel of point-mutated viruses to a GST-pulldown assay (Fig. 4.11). After infecting Jurkat T-cells with the indicated virus I observed the binding of VP11/12 to the GST-Sh2 of Lck fusion protein. Similar to the co-immunoprecipitation results I found that inactivating Y613 or Y644 reduced but did not eliminate the interaction with the Lck Sh2 domain in the GST pull-down assay. In contrast, inactivating both motifs eliminated the interactions.

Taken together, my data suggest that the interaction between VP11/12 and Lck is mediated by the Sh2-domain of Lck and requires phosphorylation of the YEEI motif or the YETV motif.

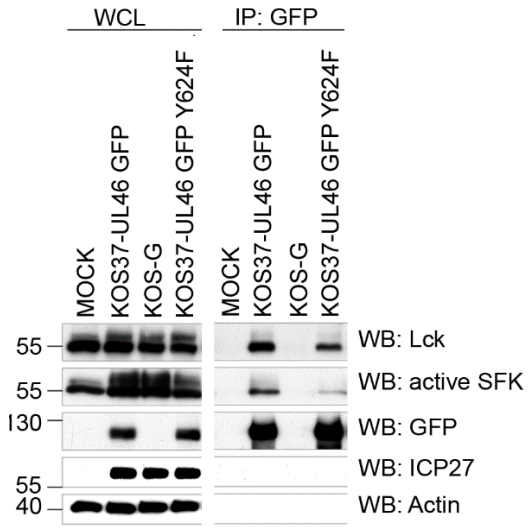

Fig. 4.9: The interaction of VP11/12 with Lck does not solely depend on the phosphorylation of the YEEI motif at position Y624.

Jurkat E6-1 cells are infected with the indicated viruses and lysates were precipitated with an anti-GFP antibody (IP: GFP). Proteins were detected using antibodies specific towards the indicated proteins on a western blot. Shown is one representative experiment out of four.

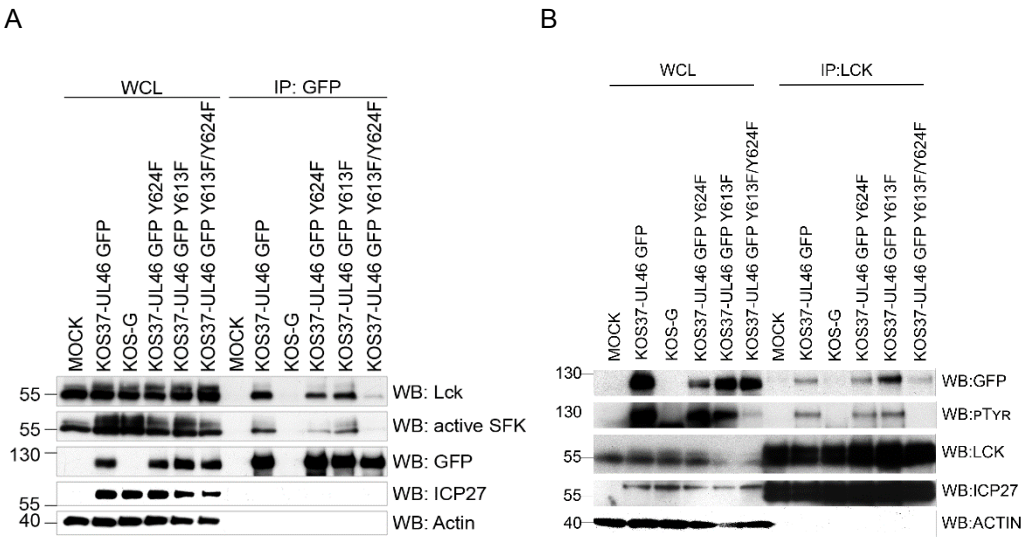

Fig. 4.10: YEEI and YETV both contribute to the association of VP11/12 with Lck.

Jurkat E6-1 cells were infected with the indicated viruses. (A) The WCL were precipitated with an anti-GFP antibody (IP: GFP) and proteins were detected using antibodies specific for the indicated proteins on a western blot. (B) The WCL were precipitated with an anti-Lck antibody (IP:Lck) and proteins were detected as indicated. Each figure represents one representative experiment out of three.

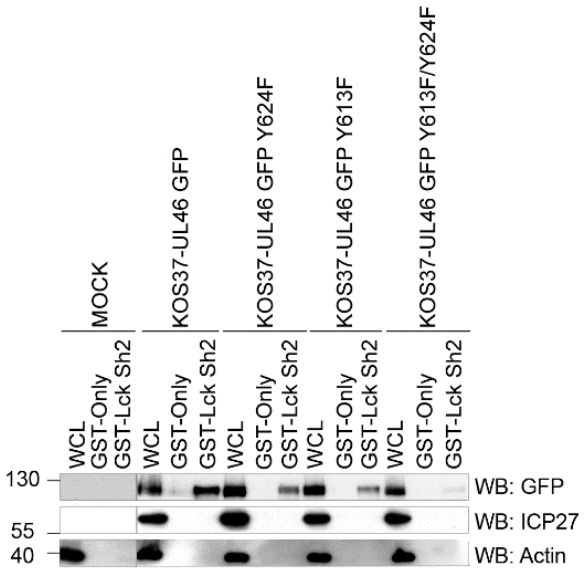

Fig. 4.11: Phosphorylation of both YEEI and YETV are required for the association of VP11/12 with the Sh2 domain of Lck.

Jurkat E6-1 cells were mock infected or infected with the indicated viruses. The cell lysates were subjected to a GST pull-down assay with the indicated GST-fusion proteins. Protein bound to the beads was analyzed for GFP, ICP27 and actin by western blot. Shown is one representative experiment out of three.

4.2 Summary

The results presented in this chapter show that HSV-1 VP11/12 associates with Lck, p85, Grb2 and Shc through specific tyrosine-based binding motifs (Fig. 4.12). The associations of VP11/12 with Grb2 and Shc were previously unpublished and rely on phosphorylation of the predicted tyrosine residue; phosphorylation of Y633 within the YENV motif leads to an association with the Sh2 domain of Grb2 while phosphorylation of Y657 within the NPLY motif leads to an association with the PTB domain of Shc. Inactivation of either binding motif abolished the VP11/12-host cell protein interaction [279].

In contrast, the association of VP11/12 with p85 and Lck was more complex than previously predicted [229]. In the case of p85 I found that inactivation of the YTHM motif at position Y519 significantly reduced, but did not eliminate, the association of VP11/12 with p85. Further, I was not able to fully investigate if VP11/12 associates with the Sh3 domain of p85 as well as its Sh2 domain due to a lack of VP11/12 expression in the mutated virus. In the case of Lck, I demonstrated that the VP11/12-Lck association requires the phosphorylation of the YEEI or the YETV binding motif. Simultaneous inactivation of both motifs created a mutant VP11/12 protein that no longer associates with the Sh2 domain of Lck. Taken together, my data supports the Wagner-Smiley model and further suggests that VP11/12 mimics an activated growth factor by directly interacting with cellular proteins that are involved in signal transduction pathways.

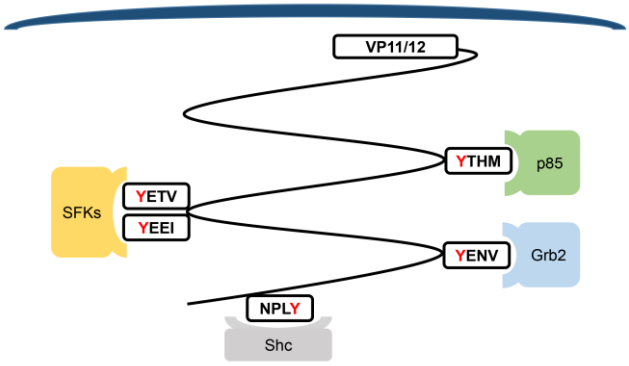

Fig. 4.12: VP11/12 requires phosphorylation of the predicted tyrosine-based binding motifs to interact with Sh2 domains of SFKs, p85 and Grb2 as well as the PTB domain of Shc.

Chapter 5

The role of tyrosine-based binding motifs for recruitment and activation of Lck and downstream binding of p85, Grb2 and Shc as well as stimulation of the PI3K/Akt-pathway by VP11/12

Portions of this chapter has been published in:

Strunk, U., et al., *Role of herpes simplex virus VP11/12 tyrosine-based motifs in binding and activation of the Src family kinase Lck and recruitment of p85, Grb2, and Shc.* J Virol, 2013. **87**(20): p. 11276-8.

Strunk, U., et al., *Role of Herpes simplex virus 1 VP11/12 tyrosine-based binding motifs for Src family kinases, p85, Grb2 and Shc in activation of the phosphoinositide 3-kinase-Akt pathway.* Virology, 2016. **498**: p. 31-5.

All experiments presented within this chapter were performed by U. Strunk, with the following exception: the generation of the KOS37-UL46 GFP Y519F/Y633F mutant, the co-immunoprecipitation assay displayed in figure 5.7 as well as the Akt activation assay displayed in figure 5.8 were generated in collaboration with Daniel Gomez Ramos.

Preface

After investigating Melany Wagner's key question as to the role of tyrosine-based binding motifs within VP11/12 in the association with Lck, p85, Grb2 and Shc, I sought to address three remaining questions arising from her research. Specifically, does VP11/12 recruitment of Lck lead to Lck activation? If so, does the VP11/12 induced activation of Lck induce tyrosine phosphorylation within the binding motifs for Grb2, Shc and p85? Lastly, is the recruitment of SFKs and p85 essential for VP11/12 dependent activation of Akt?

The Wagner-Smiley model suggested that VP11/12 mimics an activated growth factor receptor. It was predicted that VP11/12 recruits and activates SFKs [266] to induce further tyrosine phosphorylation within the YTHM motif in order to associate with p85, leading to Akt activation [229]. We therefore hypothesized that the KOS37-UL46 Y613F/Y624F mutant (that no longer associates with SFKs) would also display a significantly decreased activation of Lck as well as no association with the remaining identified binding partners. We further hypothesized that the mutants that lack the ability to bind Lck and p85 would fail to activate Akt. We were unsure if inhibiting the association of VP11/12 with Grb2 or Shc would have an impact on VP11/12-dependent Akt activation or not.

Data presented in this chapter supports the Wagner-Smiley model demonstrating that indeed VP11/12 mimics an activated growth factor receptor [289] in that VP11/12 associates with cellular host proteins that are directly involved in the stimulation of the PI3K/Akt signal transduction pathway.

5.1 Results

5.1.1 VP11/12 recruits and activates the SFK Lck through the consensus YEEI and YETV motif

As mentioned in the preface of this chapter Melany Wagner proposed that VP11/12 activates Lck by binding its Sh2 domain [266]. To test this possibility, I examined the effects of inactivating the various tyrosine-based motifs present in VP11/12 on its ability induce the activation of Lck during Jurkat T-cell infection. Cell lysates harvested at 11 hpi were analyzed by western blotting for total Lck and for SFKs phosphorylated on the activation loop tyrosine (Lck residue Y394). The results were quantified on an Odyssey infrared imager (Fig. 5.1).

Given that the activation loop of SFKs is highly conserved, the antibody used to detect active SFK reacts with the active forms of all SFKs. However, Dr. Wagner's previous results have shown that the signal observed with the active SFK antibody in HSV-infected Jurkat cells arises predominantly, if not entirely, from Lck [266]. As shown previously, Lck is detected as two distinct species with a molecular masses of ca. 56 and 60 kDa in both control as well as infected cells. In addition, both species react with the active SFK antibody suggesting that the mobility shift is not due to phosphorylation of the activation loop. Although HSV infection does not alter the total Lck signal, it does increase the proportion of the higher molecular mass species (60 kDa) [266] (Fig. 5.1). Also in line with previously reported data, HSV-1 KOS37 induces a three to four fold increase in the total active SFK signal. That activation is eliminated by the VP11/12 null mutation in ΔUL46.

I found that inactivating either the YENV (Grb2, Y633) or the NPLY (Shc, Y657) binding motifs had little or no effect on Lck activation. Inactivating the YTHM motif (p85, Y519) induced a small but statistically significant increase. In contrast, inactivating the YEEI (SFK, Y634) motif significantly reduced but did not eliminate Lck activation, while mutating the YETV (SFK, Y613) motif had no significant effect. Inactivating both of the SFK Sh2 binding motifs, on the other hand, eliminated Lck activation. The observed phenotype was similar to that of the VP11/12 null mutant ΔUL46. Nevertheless, the Y613F/Y624F mutant consistently displayed lower levels of the 60 kDa Lck species than did ΔUL46. This observation perhaps indicates that this form of VP11/12 actively interferes with the function of other viral or cellular protein(s) that induce the mobility shift.

Overall, my results indicate that the predicted Lck Sh2-domain binding motifs at positions Y613 and Y624 both contribute towards the activation of Lck, with the Y624 motif playing a more dominant role. This data stands in contrast to the VP11/12-Lck protein association data, where I was able to demonstrate that both binding motifs contribute equally to the association (chapter 4.1.2.4, figure 4.10 and figure 4.11).

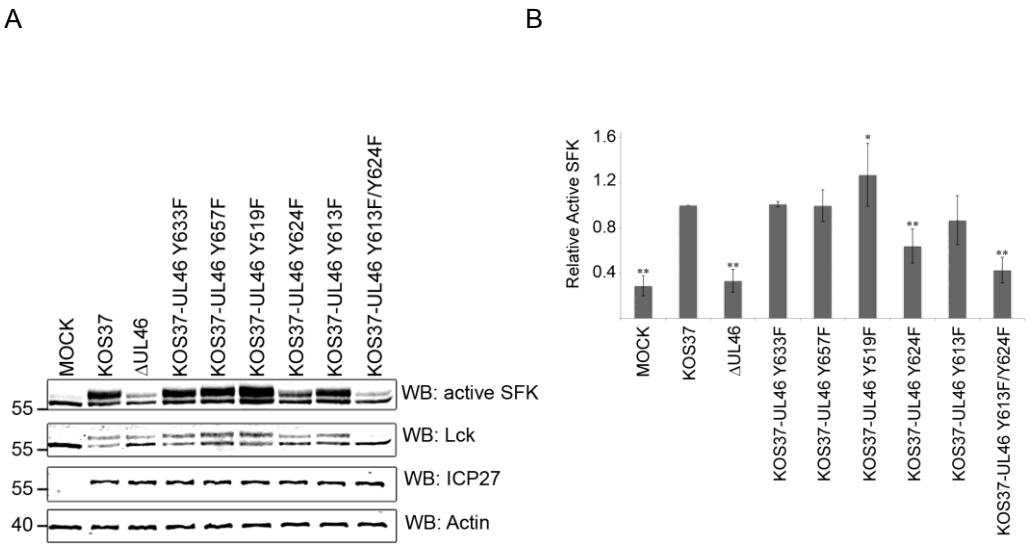

Fig. 5.1: Both Sh2-Lck binding motifs YEEI and YETV contribute to Lck activation.

Jurkat E6-1 cells were infected for 11 h with the indicated viruses. (A) Extracts were analyzed by western blot using antibodies directed against the indicated proteins and the results were visualized using an Odyssey infrared imager. Shown is one representative experiment out of four. (B) Quantification of the results obtained in four independent experiments are shown. The signal obtained with the active SFK antibody (56 kDA and 60 kDa species) was divided by the total Lck signal, and then normalized to the ratio obtained with KOS37, which was set to 1.0. The statistical significance of the differences between KOS37 and the other samples were evaluated using a two-tailed T-test (*p<0.05, ** p<0.01).

5.1.2 VP11/12 induced activation of Lck is necessary for the binding of p85, Grb2 and Shc

Wagner and Smiley showed that pharmacological inhibition of SFK activity strongly blocked the interaction between VP11/12 and p85 in HEL fibroblast cells [229], leading to the hypothesis that VP11/12-induced SFK activation leads to phosphorylation of the p85-binding YTHM motif [229]. In order to determine if SFK activity is similarly required for the interactions between Grb2 and Shc, I analyzed the effects of the SFK inhibitor PP2 in a co-immunoprecipitation assay (Fig. 5.2). In line with the previous work performed by Dr. Wagner, I demonstrated that PP2 had no effect on the interaction

between VP11/12 and Lck but strongly inhibited tyrosine phosphorylation of VP11/12 and the association with p85. Importantly, the inactive PP2 analogue PP3 had no effect. PP2 also completely eliminated the interactions between VP11/12 and Grb2 and Shc, consistent with the hypothesis that SFK activity is required for the phosphorylation of the Grb2 and Shc tyrosine-based binding motifs.

Taking Dr. Wagner's and my research in combination, I next thought to address the hypothesis that VP11/12 induced SFK activity is essential for phosphorylation of the Grb2, Shc and p85 binding motifs. I therefore hypothesized that the KOS37-UL46 GFP Y613F/Y624F virus would fail to associate with Grb2, Shc and p85 due to the lack of YETV/YEEI-dependent SFK activation. To address this question, I subjected the double-point mutated virus to a co-immunoprecipitation assay and investigated the ability of VP11/12 to associate with its identified cellular binding partners by western blotting (Fig. 5.3). In support of my hypothesis, the Y613F/Y624F double substitution had the predicted effects on these protein-protein interactions: The mutant VP11/12 failed to associate with Grb2 or Shc, supporting my model that the association of VP11/12 with Grb2 or Shc solely depends on the identified tyrosine-based binding motifs. In addition, the association of VP11/12 and p85 was significantly reduced, but not eliminated. Interestingly, the VP11/12-p85 association was reduced to a similar amount as seen previously after inactivation of the p85 tyrosine binding motif YTHM (Y519) (chapter 4.1.2.3, figure 4.7 and figure 4.8). This result might indicate that VP11/12 and p85 could interact using an additional tyrosine-independent association. It might also be possible that VP11/12 and p85 associate through an additional unidentified binding partner. Inactivating either the YEEI or the YETV motif only had a minor effect on VP11/12-Shc

association, whereas no impact was observed on the remaining VP11/12 protein associations.

Taken in combination, my data strongly indicates that the binding of p85, Grb2 and Shc by VP11/12 requires VP11/12-induced activation of SFKs. Further, my findings suggest that the activated SFK then leads to phosphorylation of the tyrosine-based motifs at Y519, Y633 and Y657; however, it remains unclear if the phosphorylation occurs directly or indirectly by the VP11/12-associated SFK. Briefly, it is possible that non-SFKs (Zap70 and or Syk) contribute to the phosphorylation of VP11/12 despite the fact that our laboratory was not successful in detecting an association of VP11/12 and Zap70/Syk.

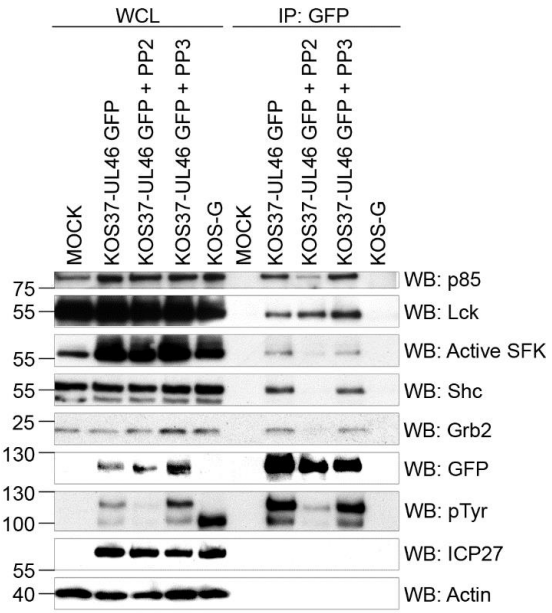

Fig. 5.2: Chemical inhibition of SFK activation inhibits the association of VP11/12 with Lck, p85, Grb2 and Shc.

Jurkat E6-1 cells were infected with the indicated viruses in the presence and absence of PP2 (active SFK-inhibitor) or PP3 (inactive analog). Cell lysates were then precipitated with an anti-GFP antibody (IP: GFP) and analyzed by western blot for the indicated proteins. Shown is one representative experiment out of three.

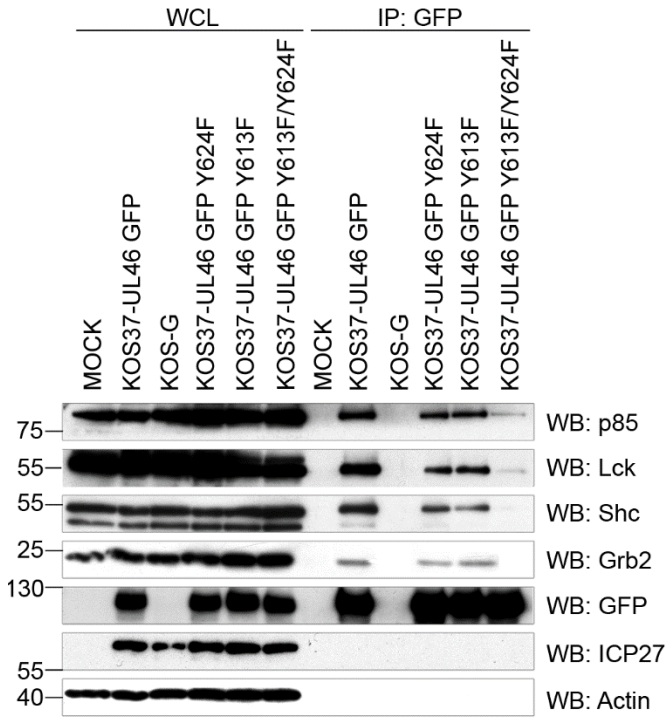

Fig. 5.3: The YEEI and YETV motifs are necessary for the association of VP11/12 with p85, Grb2 and Shc.

Jurkat E6-1 cells were infected with the indicated viruses for 13 h. Cell lysates were then precipitated with an anti-GFP antibody (IP: GFP) and analyzed by western blot for the indicated proteins. Shown is one representative experiment out of three.

5.1.3 VP11/12 induced SFK activation is required for global induction of tyrosine-phosphorylation

One of the first reports published on VP11/12 demonstrated that HSV infection of Jurkat cells triggers a dramatic increase in total phosphotyrosine levels [230]. The increase is VP11/12-dependent, and it appeared that VP11/12 is one of the major phosphotyrosine-reactive species [230]. To investigate the hypothesis that the phosphotyrosine increase correlates directly to the VP11/12-induced activation of SFKs, I infected Jurkat E6-1 cells

with viruses bearing mutations that inactivate each of the VP11/12 tyrosine-based motifs for SFKs, p85, Grb2 and Shc in the context of untagged VP11/12.

I generated untagged point-mutated viruses in order to avoid a possible impact of the GFP-tag on VP11/12's signaling capacity. Cells were harvested at 11 hpi and lysates were analyzed for total tyrosine phosphorylation by western blotting (Fig. 5.4). Consistent with previous data [230], cells infected with KOS37 displayed strikingly enhanced tyrosine phosphorylation of three prominent species relative to uninfected cells: a ca. 110 kDa band that corresponds to tyrosine phosphorylated VP11/12, a doublet migrating at ca. 56 and 60 kDa that most likely corresponds to Lck, as well as a ca. 40 kDa species that has yet to be identified. In contrast, the VP11/12 null mutant ΔUL46 displayed a pattern similar to uninfected cells, with the exception that the ca. 60 kDa Lck species increased in abundance while the ca. 56 kDa Lck species correspondingly declined. Inactivating the YENV motif (Grb2, Y633) or the NPLF motif (Shc, Y657) had little effect on the overall pattern of tyrosine phosphorylation. Inactivating the YTHM motif (p85, Y516), on the other hand, consistently led to enhanced tyrosine phosphorylation. In contrast, simultaneous inactivation of the YETV (SFK, Y613) and YEEI (SFK, Y624) motifs virtually eliminated enhanced tyrosine phosphorylation. Instead, the observed protein pattern of tyrosine phosphorylation was similar to that observed in uninfected cells. Each of the single mutants displayed an intermediate phenotype, whereas the Y624F mutant showed a greater decline than did the Y613 mutant. This observation is in line with my observation that the activation of Lck is predominantly YEEI driven (chapter 5.1.1, figure 5.1). Overall my data support the hypothesis that VP11/12-induced activation of SFKs is required for the tyrosine phosphorylation observed in infected Jukat T-cells.

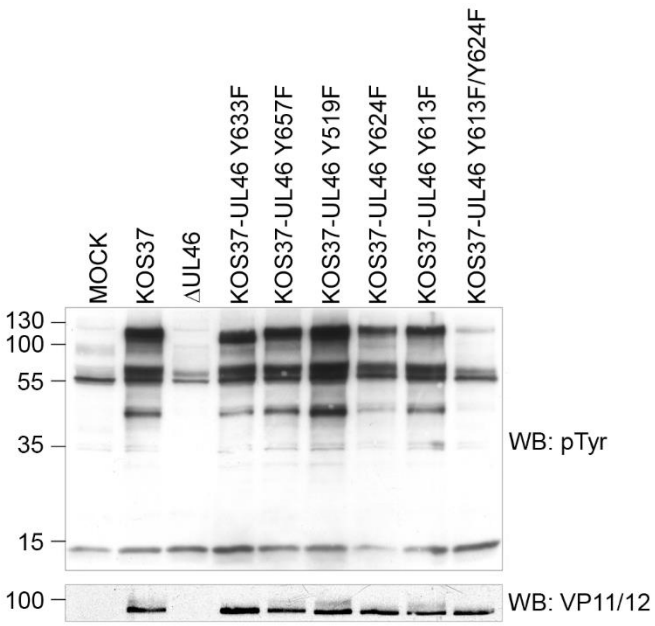

Fig. 5.4: VP11/12-dependent recruitment and activation of SFK through the YETV/YEEI motif is necessary for global tyrosine phosphorylation.

Jurkat E6-1 cells were infected with the indicated viruses for 11 h. Cell lysates were then analyzed by western blot for global tyrosine phosphorylation (WB:pTyr) and VP11/12. Shown is one representative experiment out of four.

5.1.4 Akt activation by VP11/12 depends on the interactions between VP11/12 and SFKs, p85 and Grb2

As mentioned earlier, Melany Wagner presented data that VP11/12 is required for the activation of Akt during HSV-1 infection [229]. My research provided data that VP11/12 interacts with SFKs, p85, Grb2 and Shc [229, 266, 279] by utilizing specific tyrosine-based binding motifs within its C-terminal region [279]. Wagner and Smiley proposed that VP11/12 interacts with p85 in order to activate the PI3K/Akt-pathway.

To test this remaining key question, I investigated whether Akt activation by VP11/12 depends on its ability to bind some or all of the cellular signaling proteins (SFK, p85, Grb2, Shc). To address this question I examined Akt activation in human foreskin fibroblast (HFF) cells following infection with viral mutants bearing mutations that inactivate each of the VP11/12 tyrosine-based motifs (Fig. 5.5). Wagner and Smiley previously showed a VP11/12-dependent Akt activation in Jurkat T-cells as well as human fibroblast cells (HFF) [229]. In contrast, I decided to perform the Akt activation assay only in HFF cells based on the fact that Jurkat T-cells display a high basal level of active Akt due to the deficiency in the PI3K antagonist PTEN [290].

I serum-starved HFF cells to eliminate growth factor signaling in order to lower active Akt levels, and then infected the cells with the indicated viruses (Fig. 5.5). Samples were harvested 15 h pi and then analyzed for Akt activation by western blotting using antibodies that detect total and phosphorylated Akt (S473 or T308). Actin served as a loading control, whereas VP11/12 and VP16 served as infection controls. In line with previously published data, infection of HFF cells with wild-type HSV-1 KOS37 led to activation of Akt (as judged by phosphorylation of Akt residues S473 and T308). In addition, VP11/12 was essential for this effect.

As predicted [266, 279], mutations that reduced the VP11/12-p85 interaction (KOS37-UL46 Y519F) or inhibited SFK binding (KOS37-UL46 Y613F, KOS37-UL46 Y624F, and KOS37-UL46 Y613F/Y624F) reduced Akt activation to levels similar to those observed in mock-infected samples. In addition, mutating the VP11/12-Grb2 interaction motif in KOS37-UL46 Y633F decreased Akt activation, suggesting that Grb2 also contributes to activation of the PI3K/Akt-pathway. In contrast, blocking the interaction between

VP11/12 and Shc (KOS37-UL46 Y657F) did not reduce Akt activation; instead it stimulated Akt activation even further than that observed in KOS37 infected cells.

Given that I consistently observed a marginal increase in Akt activation with this mutant, I decided to generate a second KOS37-UL46 Y657F mutant (KOS37-UL46 Y657F #2). I predicted that the odds of duplicating a spontaneous mutation in a second mutant would be low and it is therefore assumed that an independently derived mutant displays the same phenotype if the observed phenotype directly correlates to the Y657 mutation. I mock infected serum-starved HFF cells or infected with the indicated viruses. Samples were harvested 15 hpi and then analyzed for Akt activation by western blotting (Fig. 5.6) as described for figure 5.5. I observed the same phenotype for both Y657 mutated viruses. At this point we are unsure of the biological relevance of this observation.

Overall, my results imply that SFKs, p85, and Grb2 are involved in the Akt activation triggered by VP11/12, which supports the previous suggestion that VP11/12 activates Akt by mimicking an activated growth factor receptor [266, 279].

A

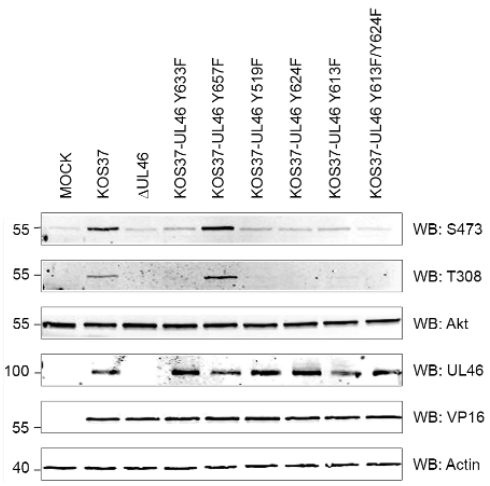

B

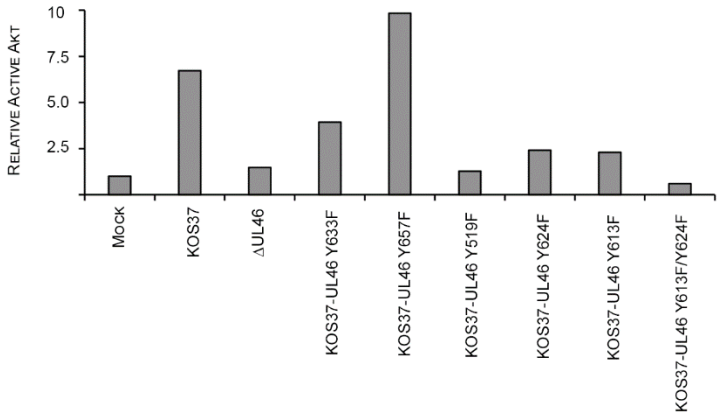

Fig. 5.5: VP11/12 mimics an activated growth factor receptor.

Serum starved HFF cells were mock infected or infected with the indicated viruses for 15 h. (A) Cell lysates were harvested and analyzed by western blotting using antibodies against phosphorylated Akt (S473 and T308), total Akt (Akt), VP11/12, VP16 and actin. Shown is one representative experiment out of four. (B) Quantification of the results obtained in one experiment is shown. The signals obtained with the S473 or total Actin antibody were normalized to actin. The normalized value was then used to determine the relative phosphorylation of S473 and the value obtained for mock was set to 1.0.

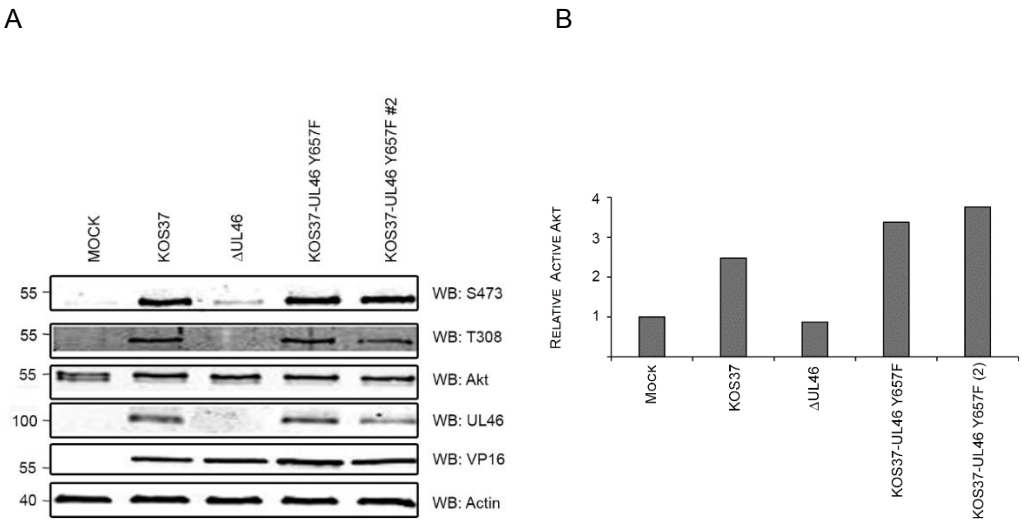

Fig. 5.6: The VP11/12-Shc association boosts Akt activation.

Serum starved HFF cells were mock infected or infected with the indicated viruses for 15 h. (A) Cell lysates were harvested and analyzed by western blotting as described for figure 5.5. Shown is one representative experiment out of three. (B) Quantification of the results obtained in one experiment is shown. The quantification was carried out as described in figure 5.5.

5.1.4.1 Grb2 contributes to the VP11/12-p85 association

I previously found that inactivating the YTHM tyrosine-based binding motif for the Sh2 domain of p85 (YTMH at Y519) reduced, but did not eliminate, the interaction between p85 and VP11/12. This data suggested that another protein-interaction domain in VP11/12 contributes to the p85-binding [279]. Also, I observed that inactivating the YTHM motif decreased the VP11/12-Grb2 association (Fig. 4.7 and Fig. 4.8**B**; displayed in chapter 4) as well as that inactivating the Grb2 binding motif decreased Akt activation (Fig. 5.5). Based on this cumulative data, I asked if the Grb2 motif contributes to the interaction between VP11/12 and p85.

Daniel Gomez Ramos and I investigated this possibility by generating a VP11/12 mutant in which both the p85 and Grb2 motifs were simultaneously inactivated (Y519F/Y633F). The effects of this double mutation on the interactions between VP11/12 and its cellular partners were then assessed using a co-immunoprecipitation assay. We infected Jurkat E6 cells with HSV-1 recombinants expressing wild-type or mutant forms of VP11/12 C-terminally tagged with EGFP, as described in chapter 4. We then used an anti-GFP antibody to precipitate VP11/12 and any associated cellular binding partners from cell extracts prepared 13 h post-infection. KOS-G expressing free GFP was used as a negative control. Co-immunoprecipitates were analyzed by western blotting using antibodies against p85, Lck, Shc, Grb2 and GFP (Figure 5.7). In line with my previous data, Danny Gomez Ramos found that mutating the Grb2 binding motif YENV (KOS37-UL46 GFP Y633F) inhibited the interaction with Grb2 without greatly affecting binding of p85, Lck and Shc. Inactivating the p85 Sh2 domain binding motif YTHM (KOS37-UL46 GFP Y519F) reduced but did not eliminate the interaction with p85 and reduced the VP11/12-Grb2 interaction. Using the double-point mutated virus KOS37-UL46 GFP Y519F/Y633F, Daniel Gomez Ramos showed that the association of VP11/12 with p85 was further reduced without obviously affecting the interactions with Lck or Shc. His result suggests that Grb2 contributes to the interaction between VP11/12 and p85.

We also assessed the ability of KOS37-UL46 Y519F/Y633F to activate Akt in the context of HFF infected cells. Based on the observation that single mutations at Y519 or Y633 inhibited Akt activation (Fig. 5.5), I assumed that KOS37-UL46 Y519F/Y633F would display a similar phenotype. To test this possibility, I infected HFF cells as described earlier (Fig. 5.5 and Fig. 5.6) and observed the activation of Akt by western blot analysis

(Fig. 5.8). As predicted, KOS37-UL46 Y519F/Y633F showed a similar phenotype as the single-point mutated viruses KOS37-UL46 Y519F and KOS37-UL46 Y633F. Overall, this data suggest that Grb2 contributes towards the VP11/12-p85 association.

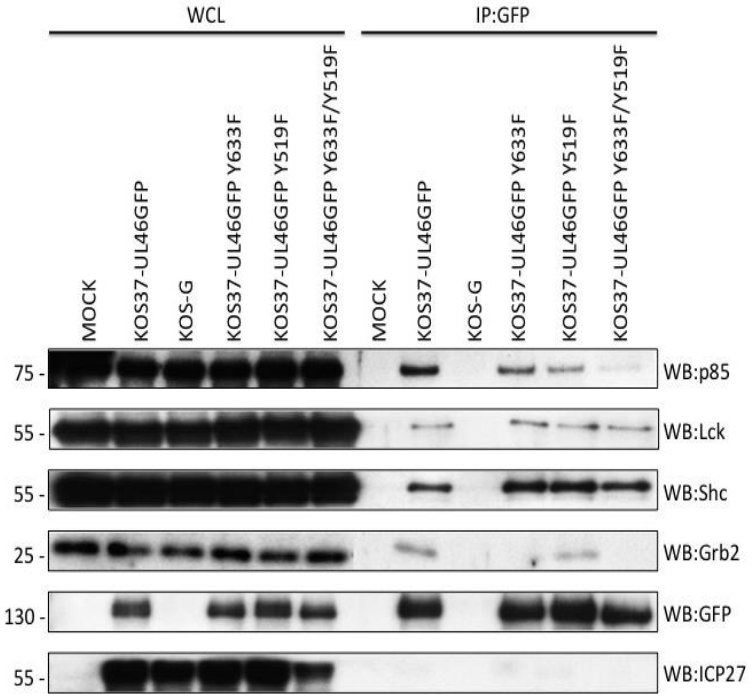

Fig. 5.7: The Grb2-binding motif YENV contributes to the VP11/12-p85 interaction.

Jurkat E6-1 cells were mock infected or infected with the indicated viruses for 13 h. Whole cell lysates (WCL) were co-immunoprecipitated using an antibody against GFP (IP:GFP) and analyzed via Western blotting (WB) for p85, Lck, Shc, Grb2, GFP and ICP27. The virus KOS37-UL46 GFP Y633F/Y519F and this figure was generated by Daniel Gomez Ramos. Shown is one representative experiment out of three.

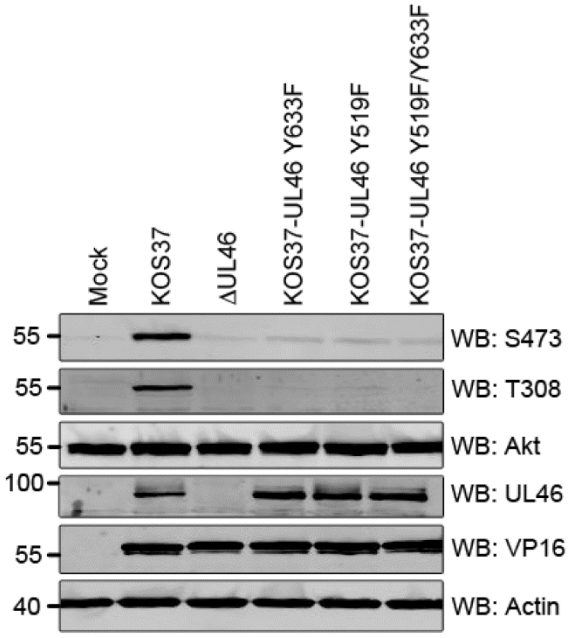

Fig. 5.8: Effects of inactivating the p85 and Grb2 binding motifs on VP11/12-dependent Akt activation.

Serum starved HFF cells were mock infected or infected with the indicated viruses for 15 h. (A) Cell lysates were harvested and analyzed by western blotting as described for figure 5.5. Shown is one representative experiment out of three.

5.2 Summary

The results presented in this chapter are summarized in figure 5.9 and show that HSV-1 VP11/12 recruits and activates the SFK member Lck in Jurkat T-cells to induce its activation (Fig. 5.1). Activated Lck will then, directly or indirectly, lead to further tyrosine-phosphorylation of tyrosine residues within the Grb-binding motif YENV, the Shc binding motif NPLY, as well as the p85 binding motif YTHM (Fig. 5.3). These phosphorylation events are necessary for enabling VP11/12 to associate with its cellular binding partners.

Data also presented in this chapter clearly demonstrates that, as predicted previously [229, 266], VP11/12 needs to associate with Lck as well as p85 to activate Akt in HFF

cells (Fig. 5.5). I also found that the association of VP11/12 with Grb2 is critical for the activation of Akt. Based on this observation, Danny Gomez Ramos and I investigated whether the Grb2-binding motif YENV contributes to the VP11/12-p85 association. We were able to demonstrate that simultaneous inactivation of the Grb2 and p85 binding motifs within VP11/12 further reduced, but did not fully inhibit, the p85-VP11/12 interaction (Fig. 5.7). Taken together, I was able to answer the key questions raised by Dr. Wagner about how VP11/12 recruits SFKs in order to enable further VP11/12- host cell protein associations and how protein-protein interactions enable VP11/12 to activate the PI3K/Akt-pathway.

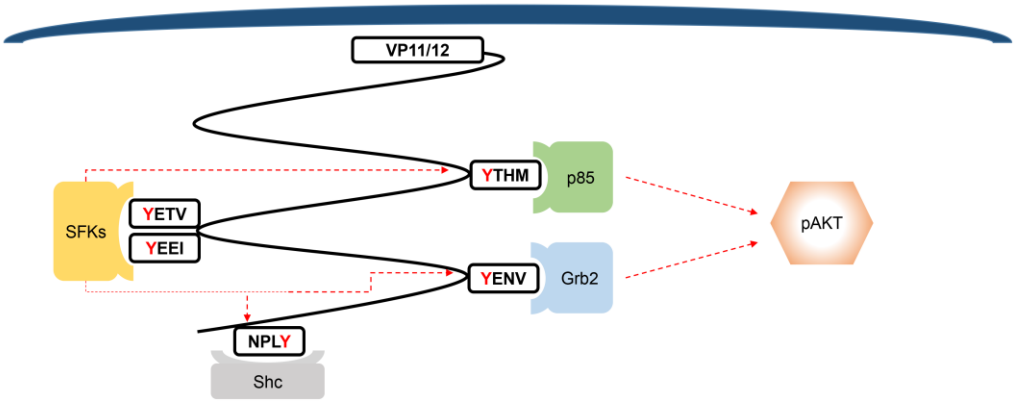

Fig. 5.9: VP11/12 recruits and activates SFKs before additional protein associations and triggers Akt activation through a SFK/p85/Grb2-dependent mechanism.

Chapter 6

The role of tyrosine-based binding motifs for recruitment and binding of SFKs, p85, Grb2 and Shc in inhibition of TCR signaling events

All experiments presented within this chapter were performed by U. Strunk, with the exception of the construction of the pcDNA-UL46 GFP Y613F/Y624F plasmid which was generated by Holly Saffran.

Preface

While the role of VP11/12 in activating the PI3K/Akt-pathway is becoming more elucidated, the role of VP11/12 in regulating TCR signaling events remains mainly unknown. As briefly mentioned in the introduction (section 1.2.2), the T-cell mediated cellular immune response plays an important role in controlling HSV-1 acute infection and HSV-1 specific T-cells inactivation stems from inhibition of signaling events at the level of LAT [208].

Our laboratory found in collaboration with the Jerome laboratory that deletion of VP11/12 does not restore Erk1/2 activation following TCR ligation during infection [230]; however, unpublished data by the Jerome group (personal conversation between James R. Smiley and Keith Jerome) suggest that VP11/12 is sufficient to block Erk1/2 phosphorylation and calcium flux upon overexpression in Jurkat T-cells. Based on the Jerome data I hypothesized that expression of VP11/12 as only viral protein in Jurkat T-cells is sufficient to block TCR signaling events. I further hypothesized that inhibiting the ability of VP11/12 to interact with SFKs would restore TCR signaling events (as previously seen by K. Jerome). Lastly, I investigated if the associations of VP11/12 with Grb2, Shc and p85 are also involved in the VP11/12-dependent inhibition of TCR signaling.

Data presented in this chapter supports the Jerome data demonstrating that indeed VP11/12 is capable of reducing TCR signaling events if it is expressed as only viral protein.

6.1 Results

As mentioned in the preface of this chapter, deletion of UL46 did not restore the phosphorylation of Erk1/2 in infected Jurkat cells [230]. Additional, unpublished studies in the Jerome lab, on the other hand suggested that overexpression of VP11/12 is sufficient to block the phosphorylation of Erk1/2 as well as calcium flux post TCR stimulation. Combining these previous studies, it is possible that VP11/12 is involved in dampening TCR signaling events; however, HSV-1 does not solely rely on VP11/12 to modify this pathway.

To confirm the findings of the Jerome lab, we constructed pcDNA3.1-UL46 expression constructs to express VP11/12 in transfected Jurkat T-cells. I aimed to investigate if WT VP11/12 is able to block the phosphorylation of Erk1/2 as well as the calcium flux post TCR stimulation when expressed as the only viral protein in Jurkat cells. If VP11/12 is able to do so, I hypothesized that VP11/12 requires its active SFK binding motifs YETV and YEEI to block the signaling events. This hypothesis is based on the following previous observations: First, inactivation of the SFK binding motifs inhibits the association of VP11/12 with the cellular proteins as well as VP11/12 activation (SFKs, p85, Grb2, Shc; chapter 4 and chapter 5; [279]). Second, inactivation of the SFK binding motifs inhibits the ability of VP11/12 to activate Akt (chapter 5; [289]). In addition, I aimed to investigate if VP11/12 must associate with p85, Grb2 and/or Shc to inhibit TCR signaling events.

The VP11/12-pcDNA3.1 based expression constructs were generated by site-directed mutagenesis as described in chapter 2.7, and the presence of each mutation was verified by sequencing across the UL46 region. The sequence validations can be found

in the appendix for this chapter (Fig. A6.1-A6.4). In more detail, the expression constructs are based on the same VP11/12 C-terminal GFP fusion proteins that I analyzed in viral mutants in the chapters 4 and 5. We inactivated the tyrosine-based-binding motifs for SFKs, p85, Grb2 and Shc in the same fashion as described for the viruses (chapter 3). Briefly, we replaced the relevant tyrosine codon with a phenylalanine codon to prevent phosphorylation and therefore activation of the binding motif.

I used three different control plasmids for my transfection studies. First, I used pcDNA3.1 as a mock control as well as gating control for the GFP-positive population. Second, I used pcDNA3.1-GFP as a GFP-expression control to provide proof that expression of GFP itself does not alter TCR signaling. Lastly, I used pC1-Neo paxillin-GFP as an additional GFP-expression control that expresses a GFP-fusion protein of roughly the same size as VP11/12. Of note, Hanne Ostergaard (University of Alberta) provided the pC1-neo paxillin-GFP construct [291] and verified that the expression of paxillin had no impact on the tyrosine phosphorylation or degranulation of cytotoxic T-cells (personal conversation). In addition, paxillin was previously identified as a direct target of Erk [292], but Robertson and Ostergaard demonstrated and that mutating the Erk phosphorylation target sites within paxillin did not alter the cellular location of paxillin [291].

To test our assumption that expression of VP11/12 in isolation is sufficient to block TCR signaling events, I transfected the constructs into Jurkat T-cells. Twenty-four hours after the transfection, I utilized flow-based assays to detect TCR signaling events post TCR stimulation with OKT3. OKT3 is a monoclonal antibody that reacts with an epitope on the human CD3 complex and is therefore leads to *in vitro* activation of T-cells. In more detail, the CD3 complex is crucial for transducing antigen-recognition signals into the cytoplasm of T-cells and in regulating the cell surface expression of the TCR complex.

T-cell activation through the TCR involves the cytoplasmic tails of the CD3 subunits (section 1.2.1).

6.1.1 VP11/12 reduces phosphorylation of Erk1/2 in transfected Jurkat T-cells

To investigate the possible interference of VP11/12 with the phosphorylation of Erk1/2 following TCR stimulation, I transfected Jurkat E-6.1 cells with the expression constructs for 24 hours and subsequently stimulated with OKT3. Unstimulated cells served as a negative control. Cells were then fixed/permeabilized and stained with an anti-phospho Erk1/2 (T202/Y204)-APC antibody (Fig. 6.3). As mentioned above, OKT3 binds CD3 and therefore triggers TCR signaling events. Erk1/2 phosphorylation was then assessed by flow cytometry.

My gating strategy was as follows: First, I selected my T-cell population based on the forward and sideward scatter plot (Fig. 6.1A). Second, I excluded dead cells based on live-dead stain (Molecular Probes, L34955) (Fig. 6.1B). Third, I gated on GFP-positive as well as GFP-negative cells within the same sample based on pcDNA3.1 transfected cells (Fig. 6.1C). In order to set a GFP+ gate, I used cells transfected with pcDNA3.1 as negative control and set the GFP+ gate within this population to 1 % GFP-positive. Importantly, I required an at least 5 % GFP-positive transfection efficiency in cells transfected with GFP-fusion proteins/free GFP. Experiments where one or more samples displayed a transfection efficiency of less than 5 % GFP-positive cells were excluded. Lastly, I determined the amount phosphoErk1/2 relative to the isotype control in both populations (Fig. 6.1D).

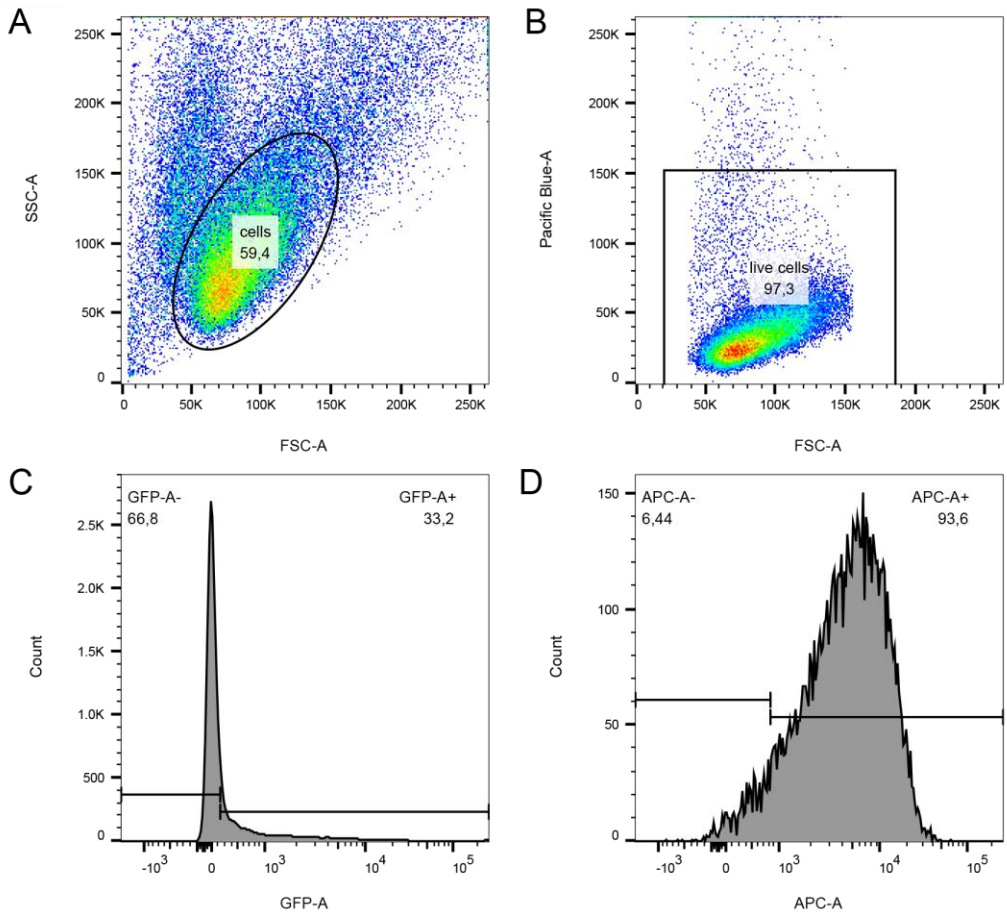

Fig. 6.1: Gating strategy for detecting intracellular pErk1/2 in T-cells.

This figure explains the gating strategy used to determine intracellular pErk1/2 levels for the pcDNA3.1-GFP sample in figure 6.2. Jurkat E-6.1 cells were transfected with pcDNA3.1-GFP for 24h and stimulated with OKT3 for 5 min. Cells were then fixed and permeabilized before staining. Shown are the histograms of the frequency of parent, which is defined as the percentage of events in the gate out of the parent gate (one level up). (A) First, cells were gated based on the SSC and FSC. (B) Cells were further gated based on the live/dead stain to exclude dead cells. (C) Next, cells were gated on GFP positive as well as GFP negative population based on 1% GFP expression in cells transfected with pcDNA3.1. (D) Lastly, the detection of pErk1/2-APC was gated relative to the isotype control in both populations.

I found that neither expression of free GFP by pcDNA3.1-EGFP or the expression of pC1-neo paxillin-GFP had any effect on the Erk1/2 phosphorylation level (Fig. 6.2A). In contrast, expression of WT VP11/12 by pcDNA3.1-UL46 GFP reduced, but did not fully eliminate the phosphorylation of Erk1/2 (Fig. 6.2A). Inactivation of the SFK binding motifs YETV/YEEI had the predicted effect, as it restored Erk1/2 phosphorylation (Fig. 6.2A).It further appeared that the inactivation of the Grb2 binding motif YENV, the Shc binding motif NPLY, or the p85 binding motif YTHM had only minor effects on the inhibition of Erk1/2 phosphorylation by VP11/12 (Fig. 6.2B). My data overall agrees with Keith Jerome's unpublished work; however, I was not able to detect a full inhibition of the phosphorylation of Erk1/2 as it was detected by Keith Jerome and colleagues. Using a chemical inhibitor of Erk1/2 activation in follow-up experiments could help defining the basal phosphoErk1/2 expression and therefore help quantify the inhibition efficiency of VP11/12.

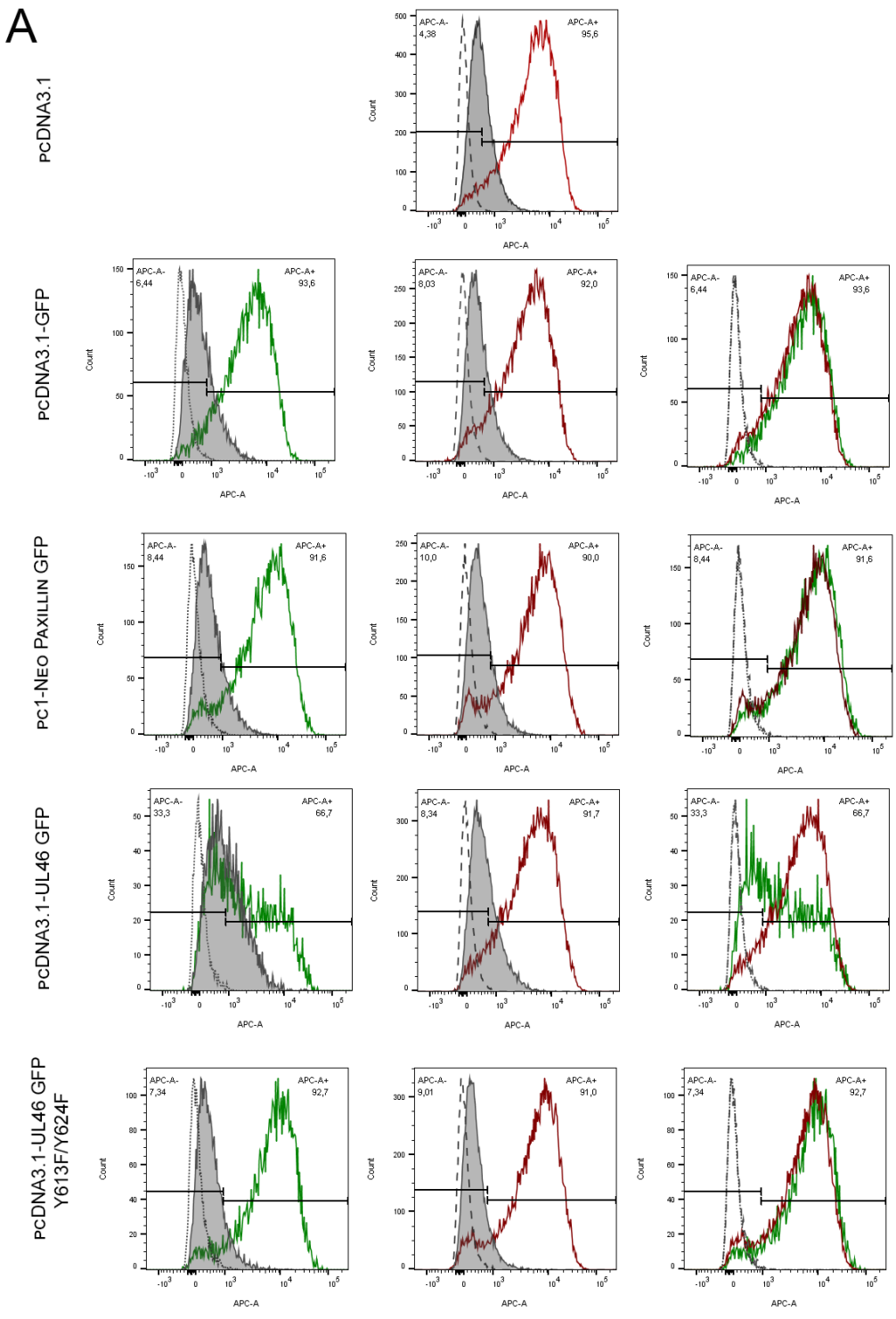
A
pcDNA3.1
pcDNA3.1-GFP
pc1-Neo Paxillin GFP
pcDNA3.1-UL46 GFP
pcDNA3.1-UL46 GFP Y613F/Y624F
APC-A-
APC-A+
Count
APC-A

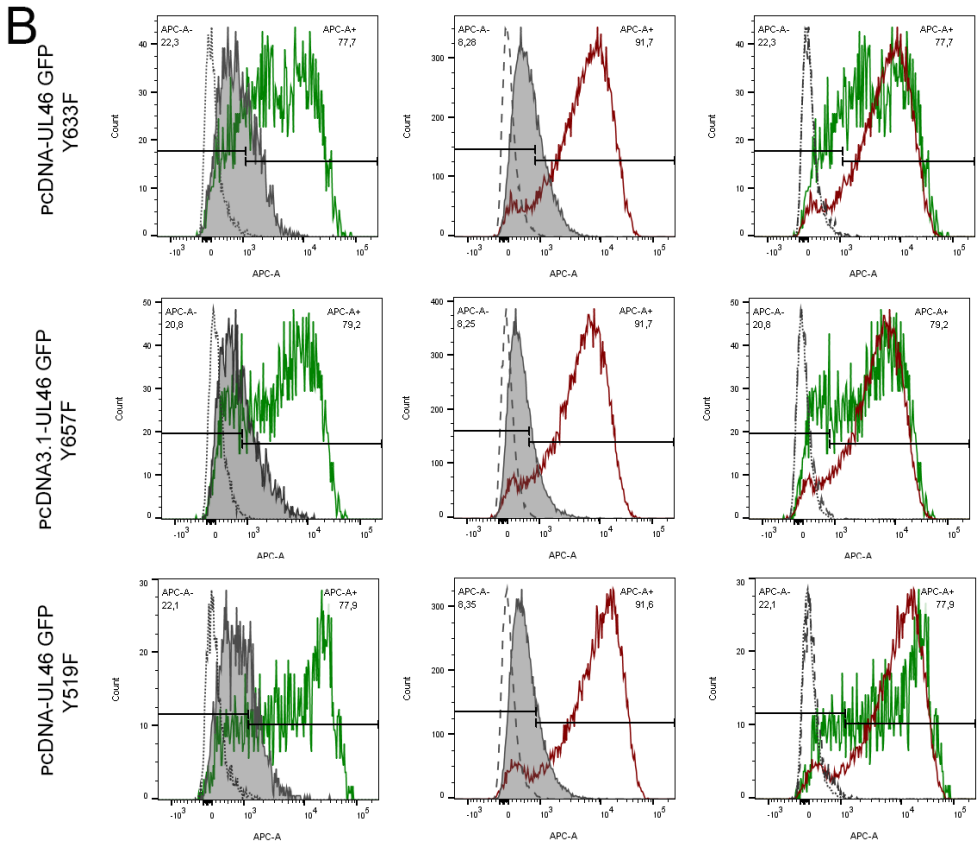

Fig. 6.2: The SFK-binding motifs are essential for VP11/12-dependent inhibition of Erk phosphorylation in Jurkat T-cells.

Jurkat E-6.1 cells were transfected with the indicated constructs for 24h and stimulated with OKT3 for 5 min or left unstimulated. Cells were fixed and permeabilized before staining with the indicated antibodies. Shown are the representative histograms of the frequency of parent (percentage of events in the gate out of the parent gate) relative to the isotype control (dotted/dashed gray line is isotype control stained, filled gray is unstimulated pErk stained, the green solid line is GFP-expressing cells OKT3 stimulated pErk stained, red solid line is non-GFP expressing cells OKT3 stimulated pErk stained). (A) WT VP11/12 strongly inhibits the activation of Erk1/2 and this effect was counteracted by the inactivation of the SFK binding motifs. In contrast, expression of free GFP or a control GFP-fusion protein had no impact on the activation of Erk1/2. (B) Mutation of the p85, Grb2 and Shc binding motif within VP11/12 had only a minor effect on Erk1/2 inhibition by VP11/12. Shown is one representative experiment out of three.

In order to quantify the effects, I then calculated the signal to noise ratio (S/N) (Fig. 6.3A) based on the median fluorescence intensity (MFI) of OKT3-stimulated cells stained with anti-human pErk1/2 antibody over non-stimulated cells stained with anti-human pErk1/2 antibody. Finally, these data were then used to calculate the ratio of the pErk1/2 signal in GFP expressing cells to that observed in GFP negative cells in the same sample providing a measure of degree to which the expressed protein interferes with the phosphorylation of Erk1/2 (Fig. 6.3B). Quantification of the results indicates that, as predicted, expression of VP11/12 as only viral protein strongly inhibited the activation of Erk1/2 and that inactivation of the SFK binding motifs restored the activation of Erk1/2. Further, mutating the Grb2, Shc or p85 binding motif increased the phosphorylation of Erk1/2 slightly; however, it did not restore the phosphorylation as seen with the SFK VP11/12 mutant (Fig. 6.3B). Overall these data suggest, that, most likely, only the SFK binding motifs play a major role in the ability of VP11/12 to reduce Erk1/2 phosphorylation.

The inhibition of Erk1/2 phosphorylation by WT VP11/12, as well as the restoration of Erk1/2 phosphorylation by pcDNA3.1-UL46 GFP Y613F/Y624F was observed in five independent experiments and the data was consistent. I only performed two informative experiments that included the p85, Grb2 and Shc mutants. My data support our hypothesis that the VP11/12-SFK association is essential for VP11/12 ability to interfere with TCR signaling events.

A

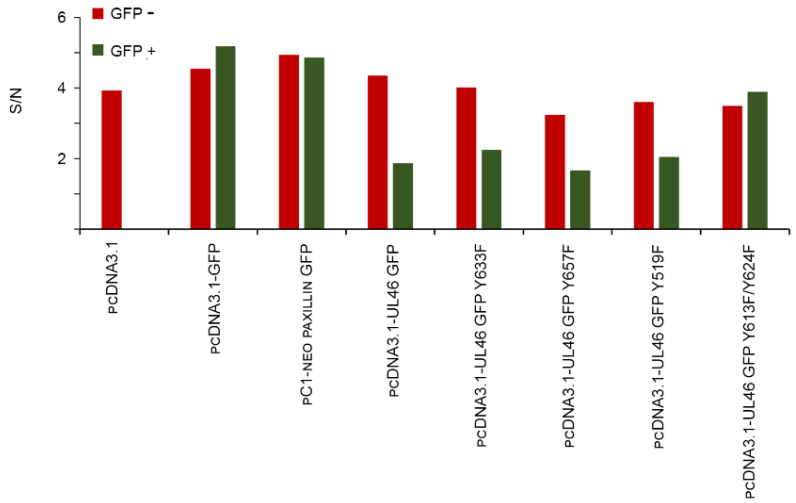

B

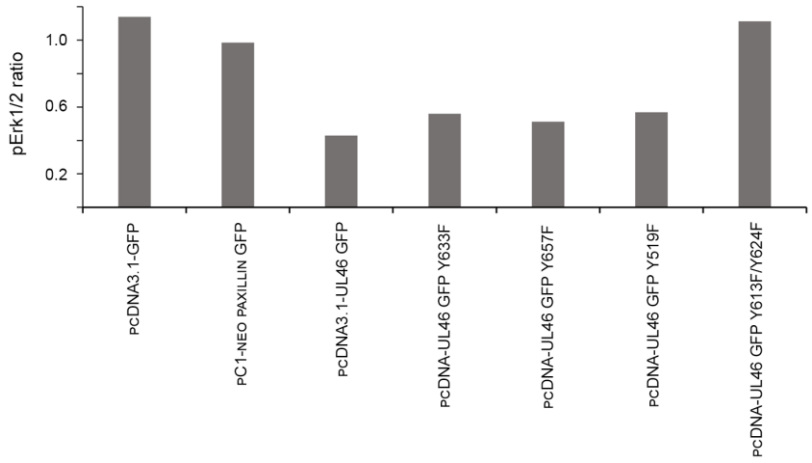

Fig. 6.3: The association of VP11/12 with SFKs through the YETV/YEEI motifs is essential to the ability of VP11/12 to block Erk1/2 phosphorylation.

(A) The signal to noise graph (S/N) is based on the median fluorescence intensity (MFI) of OKT3-stimulated cells stained with anti-human pErk1/2 antibody divided by non-stimulated cells stained with anti-human pErk1/2 antibody. (B) The pErk1/2 ratio is based on the S/N value of GFP-expressing cells divided by non-GFP expressing cells within the same sample. If the expression of free GFP or a GFP-fusion protein had no impact on the phosphorylation of Erk1/2, a ratio of 1 is expected. If the phosphorylation of Erk1/2 was limited in cells expressing free GFP or a GFP-fusion protein, a value smaller than one is expected. Shown is the data for the representative experiment in figure 6.2. In total three independent experiments were carried out and similar results were obtained.

6.1.2 VP11/12 reduces calcium flux in transfected Jurkat T-cells

As reviewed in the introduction, T-cells show an increased amount of calcium influx post TCR stimulation. It was suggested that overexpression of VP11/12 is sufficient to block this calcium flux (unpublished data K. Jerome).

To confirm this, I transfected T-cells with the plasmid constructs for 24 hours and loaded the cells with Indo1-AM before OKT3 stimulation. Indo1-AM is a calcium sensor dye that crosses the plasma-membrane. Within the cell, esterases cleave the AM group yielding a membrane-impermeable Indo-1 dye, which changes emission based on if it is bound to calcium or not. I measured this emission shift over time before and after the stimulation with OKT3 (Fig. 6.4 and Fig. 6.5; shown are the results of two calcium flux kinetic analysis). As a negative control, I loaded transfected cells with Indo1-AM in the presence of EGTA. EGTA is a chelating agent that will chelate calcium ions present in the sample buffer. Once the loaded cells were washed, I detected the baseline emission and then stimulated the cells with OKT3 before placing the sample back into the flow machine. The gating strategy was similar for the one described above (Fig. 6.1), with the exception that I did not gate on live cells using on a live-dead stain, due to technical limitations.

In both independent assays, I demonstrated that neither expression of free GFP by pcDNA3.1-EGFP or the expression of paxillin-GFP by pC1-neo paxillin-GFP had any effect on calcium flux kinetics (Fig. 6.4 and Fig. 6.5). These data suggest that the effect observed by the VP11/12-GFP constructs occur independently of the GFP tag.

T-cells expressing WT VP11/12 (pcDNA3.1-UL46 GFP) showed a strongly reduced, but not fully inhibited, calcium flux upon expression (Fig. 6.4 and Fig. 6.5). Interestingly, the reduced calcium flux in WT VP11/12 expressing cells is delayed relative to control cells

and occurs in an irregular pattern. Inactivation of both SFK-binding motifs, YEEI and YETV (pcDNA3.1-UL46 GFP Y613F/Y624F) (Fig. 6.4 and Fig. 6.5), restored the calcium flux, as previously predicted. Inactivation of the Grb2 tyrosine-based binding motif YENV (pcDNA3.1-UL46 GFP Y633F) leads to an intermediate phenotype, whereas inactivation of the p85 tyrosine-based binding motif YTHM (pcDNA3.1-UL46 GFP Y519F) had no effect on VP11/12 ability to reduce the calcium flux in Jurkat T-cells upon transfection induced expression (Fig. 6.4 and Fig. 6.5). Unexpectedly, the calcium flux phenotype upon expression of pcDNA3.1-UL46 GFP Y657 was inconsistent. Inhibition of the VP11/12-Shc interaction had no effect on the calcium flux in one assay (Fig. 6.4), but expression of the same construct leads to an intermediate phenotype in a second independent assay (Fig. 6.5).

Table 6.1 displays the transfection efficiencies for both experiments and provides evidence suggesting that the inconsistent results obtained with pcDNA3.1-UL46 GFP Y657F are most likely not due transfection inefficiency in one of the two experiments.

The inhibition of calcium flux by WT VP11/12 as well as the restoration by pcDNA3.1-UL46 GFP Y613F/Y624F was observed in five independent experiments and the data was consistent. I only performed two informative experiments that also included the additional mutants for p85, Grb2 and Shc.

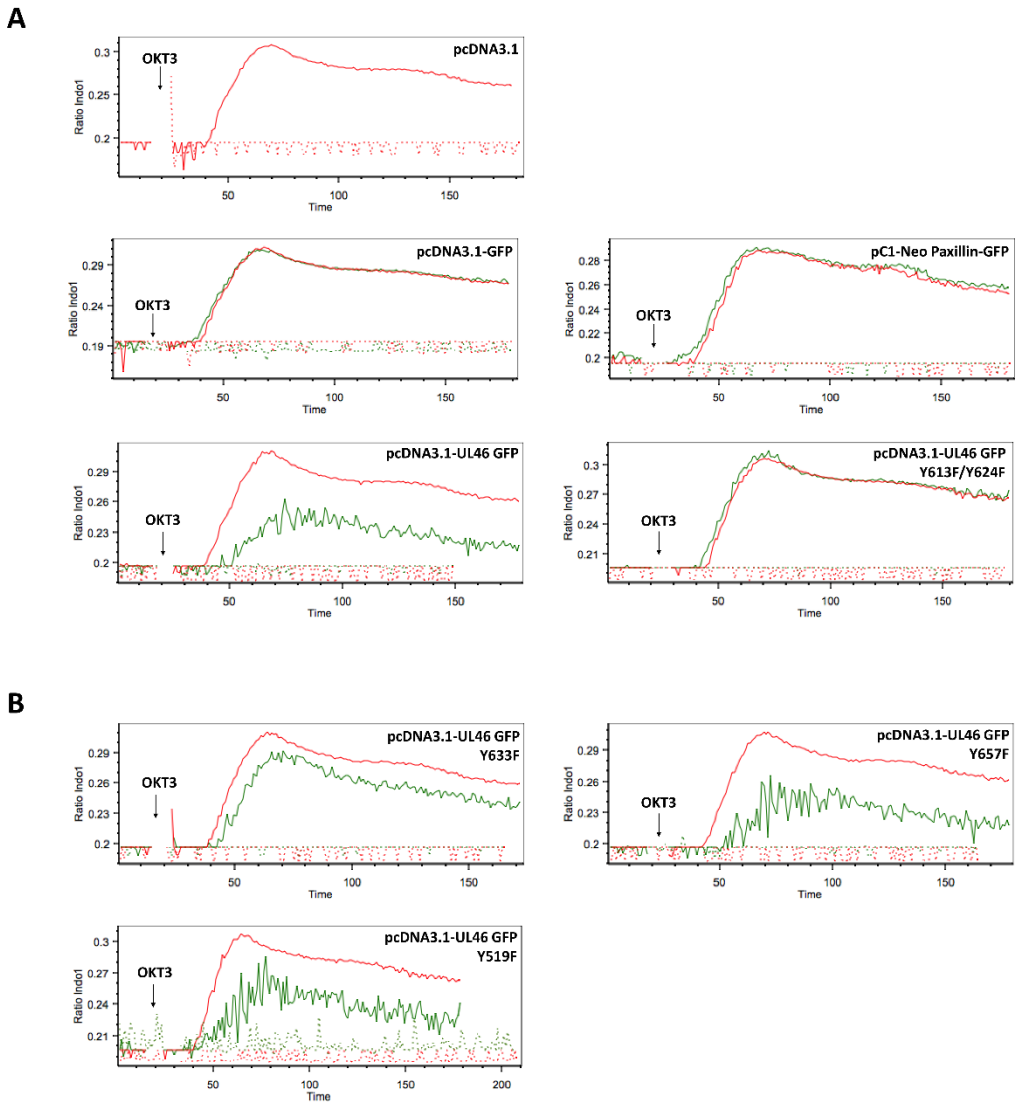

Fig. 6.4: VP11/12 inhibits the calcium flux post TCR stimulation.

The calcium flux (Ratio Indo1) was measured over time (sec). All cells were transfected for 24h with the indicated plasmids and the Indo1 emission background was monitored for 30 sec before OKT3 was directly added to the sample (red solid line: GFP-negative population, green solid line: GFP-positive population, red dotted line: GFP-negative population in presence of EGTA, green solid line: GFP-positive population in presence of EGTA). (A) Expression of free GFP or Paxillin-GFP had no impact on the calcium after TCR stimulation. WT VP11/12 delays and reduces the calcium flux and this impact is counteracted by inactivating both SFK-binding motifs. (B) Inactivating the VP11/12-Grb2 association (Y633F) leads to an intermediated phenotype and inactivating of either the VP11/12-Shc association (Y657) or the VP11/12-p85 association (Y519) displayed a calcium flux similar to WT-VP11/12.

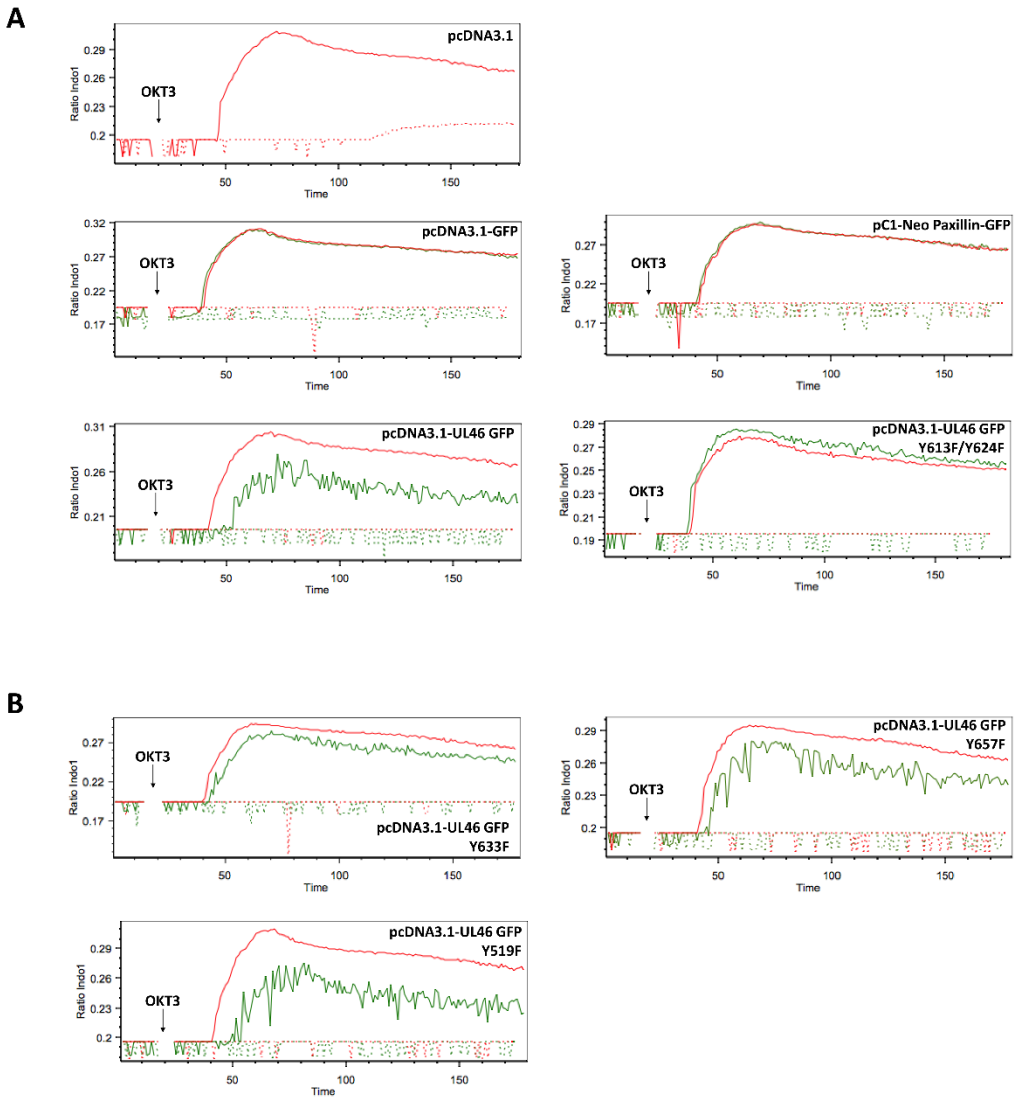

Fig. 6.5: VP11/12 inhibits the calcium flux post TCR stimulation.

The calcium flux was measured over time as described in figure legend 6.4. (A) Expression of free GFP or Paxillin-GFP had no impact on the calcium after TCR stimulation. WT VP11/12 delays as well as reduces the calcium flux and this impact is counteracted by inactivating both SFK-binding motifs. (B) Inactivation of the VP11/12-Grb2 association (Y633F) as well as of the VP11/12-Shc association (Y657F) lead to an intermediated phenotype. In contrast, inactivating the VP11/12-p85 association (Y519) displayed a similar calcium flux to WT-VP11/12.

Tabell 6.1: Transfection efficiency of plasmid constructs in Jurkat T-cells.

Construct	Transfection efficiency in % for Fig. 6.4	Transfection efficiency in % for Fig. 6.5
pcDNA3.1-GFP	33	36
pC1-neo paxillin-GFP	39	45
pcDNA3.1-UL46 GFP	10	14
pcDNA3.1-UL46 GFP Y613F/Y624F	17	23
pcDNA3.1-UL46 GFP Y633F	9	20
pcDNA3.1-UL46 GFP Y519F	6	13
pcDNA3.1-UL46 GFP Y657F	10	9

6.2 Summary

The results presented in this chapter show that HSV-1 VP11/12 is capable of reducing two major signaling events that occur post TCR stimulation (Fig. 6.6).

In the case of the phosphorylation of Erk1/2, I found that expression of WT VP11/12 reduced, but did not fully eliminate, the phosphorylation of Erk1/2. Further supporting my model that the YEEI/YETV-based VP11/12-SFK association is essential to VP11/12's signaling ability, inactivation of the YETV/YEEI motifs eliminated the negative impact of VP11/12 on the phosphorylation of Erk1/2. It further appeared that the inactivation of the Grb2 binding motif YENV, the Shc binding motif NPLY, or the p85 binding motif YTHM had a minor effect on the inhibition of Erk phosphorylation.

In line with the phosphoErk1/2 data, I found that expression of WT VP11/12 reduced, but did not fully eliminate, the calcium flux post OKT3 stimulation. Further, inactivation of the YETV/YEEI motifs restored the calcium flux, supporting our model that VP11/12 requires phosphorylation of both motifs to recruit and activate SFKs in order to be

become activated. Whereas the VP11/12-p85 association is not essential for reducing the calcium flux, the VP11/12-Grb2 association might play an important for reducing the calcium flux. In addition, the role of the interaction between VP11/12 and Shc remains uncertain. More data are necessary to draw a conclusion addressing the involvement of the associations of VP11/12 with Grb2 as well as Shc.

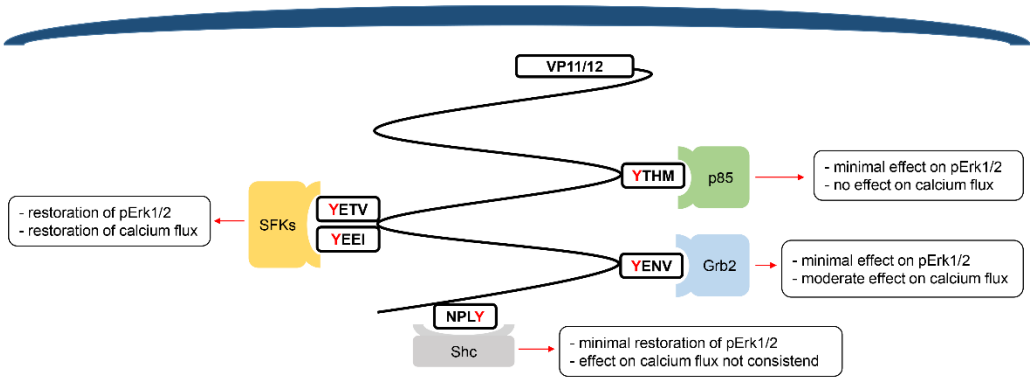

Fig. 6.6: Role of tyrosine-based binding motifs on reducing TCR signaling events.

WT VP11/12 inhibits but does not fully block the phosphorylation of Erk1/2 as well as calcium mobility. Shown in this illustration are the effects of inactivating each tyrosine-based binding motif on the ability of VP11/12 to inhibit the two signaling events.

Chapter 7

Discussion

7.1 Discussion

In this thesis, I studied the role of tyrosine-based binding motifs of the HSV-1 tegument protein VP11/12 for the cellular proteins SFK, p85, Grb2 and Shc. Before I began this project, it was proposed that VP11/12 associates with SFKs as well as with p85 through specific tyrosine-based binding motifs that are located within the C-terminal region of VP11/12 [229, 266]. It was further proposed by Smiley and Saffran that VP11/12 also interacts with Grb2 as well as Shc using the same tyrosine-based binding approach [279].

I started my project by generating mutant viruses with inactive binding motifs for SFKs, p85, Grb2 and Shc (Chapter 3). In chapter 4, I determined that inactivation of the predicted binding motifs for SFKs, Grb2 and Shc eliminated the protein-VP11/12 associations. In the case of p85, I was able to demonstrate that inactivation of the predicted p85-binding motif significantly reduced, but did not eliminate, the VP11/12-p85 interaction. From the experiments presented in chapter 4, it became evident that VP11/12 requires the phosphorylation of specific tyrosine-based binding motifs within its C-terminal region in order to associate with SFKs, p85, Grb2 and Shc.

In chapter 5, I determined the downstream effects of eliminating these protein-protein associations. First, I was able to demonstrate that VP11/12 requires the recruitment and activation of SFKs to further associate with Grb2, Shc and p85, as well as to induce global phosphorylation of VP11/12. Secondly, I was able to demonstrate that mutant viruses that fail to associate with Lck, Grb2 or p85 also fail to activate Akt. It was previously reported by my lab and others that Akt becomes activated during infection, and that the activation occurs in a VP11/12-dependent fashion [235, 266]. My data fully

supports the Wagner-Smiley model demonstrating that VP11/12 mimics an activated growth factor receptor in that VP11/12 associates with cellular proteins that are directly involved in the stimulation of the PI3K/Akt signaling pathway. Lastly, we were able to demonstrate that Grb2 contributes to the VP11/12-p85 association.

In chapter 6, I sought to address the question of whether VP11/12 interferes with the T-cell signaling pathway in addition to the PI3K/Akt signaling pathway. I also aimed to investigate the role of the protein-protein interactions between VP11/12 and the cellular proteins on the ability of VP11/12 to interfere with the TCR pathway. Before I started my project it was known that infiltration of HSV-1 into cytotoxic T-cells leads to an inhibition of TCR signaling events (e.g. inhibition of Erk1/2 phosphorylation) [208]. Deletion of VP11/12 did not restore Erk1/2 phosphorylation post TCR stimulation [230]; however, unpublished data by the Jerome group (personal conversation between James R. Smiley and Keith Jerome) suggests that VP11/12 is sufficient to block Erk1/2 phosphorylation, as well as calcium flux, upon overexpression of VP11/12 in Jurkat T-cells. I was able to demonstrate that transfection based expression of VP11/12 reduced, but not did eliminate, the phosphorylation of Erk1/2, as well as the calcium flux post-TCR stimulation. It further appeared that mutating the binding motifs for SFKs, p85, Grb2 and Shc had different effects on the inhibition of the phosphorylation of Erk1/2 or calcium flux.

In this chapter, I will discuss my results in the light of defining the role of VP11/12 as a complex receptor mimic that can activate the PI3K/Akt-pathway but can also inactivate TCR-signaling. Finally, I will outline possible future directions that have arisen from my research.

7.1.1 On the associations of VP11/12 with cellular host cell proteins

As reviewed in the introduction, our laboratory has previously proposed that VP11/12 utilizes specific tyrosine-based motifs in its C-terminal region (Y624 or Y613) to recruit and activate SFKs including Lck [266]. Activation of SKFs in turn was thought to directly or indirectly lead to phosphorylation of the YTHM motif at Y519, and downstream activation of Akt [229]. Jim Smiley also noted that the C-terminal region of VP11/12 contains tyrosine-based motifs predicted to bind the Sh2 domain of Grb2 and the PTB domain of Shc (Fig. 1.9). Holly Saffran then verified that VP11/12 indeed interacts with these proteins in co-immunoprecipitation assays. The major goal of the first part of my thesis research was to test the predicted roles of the tyrosine-based motifs in the interactions between VP11/12 and SFKs, p85, Grb2 and Shc. I conducted these studies in lymphocyte-like Jurkat E6.1 T-cells, which support substantially higher levels of VP11/12 tyrosine phosphorylation than do fibroblasts [230, 266]. Overall, my results confirm that specific binding motifs play key roles in the interaction of VP11/12 with Grb2 (Fig. 4.2 and Fig. 4.3), Shc (Fig. 4.5 and Fig. 4.6), p85 (Fig. 4.7, Fig. 4.8B and Fig. 5.7) and Lck (Fig. 4.9-4.11).

7.1.1.1 Association of VP11/12 with SFKs and consequences on downstream signaling events

Wagner and Smiley previously predicted that the interaction between VP11/12 and Lck most likely depends on the phosphorylation of the YEEI motif at position 624 [229, 230, 266]. This prediction was based on two observations. First, the phospho-YEEI appeared to be the optimal ligand for the Sh2-domain of Lck [268]. Second, the hamster polyoma

virus middle T antigen utilizes a Sh2-YEEI interaction mechanism to activate the SFK Fyn [269]. In addition, it was previously demonstrated that other viruses are expressing proteins that directly target SFKs. For example, the Herpesvirus saimiri encodes for the tyrosine kinase interacting protein that can binds Lck through multiple sequence motifs to control Lck activity [293], and the Hepatitis C Virus encodes for the essential non-structural protein 5A protein that interacts with several SFK members [294, 295].

In contrast to the previous prediction, my data indicated that the adjacent YETV motif at position Y613 also contributes to the VP11/12-Lck interaction. It appears that both motifs must be inactivated to severely impair the interaction with Lck (Fig. 4.10 and Fig. 4.11), as well as the activation of Lck (Fig. 5.1). Thus, the YETV and YEEI motifs appear to be largely redundant. The VP11/12-Lck interaction depends equally on both motifs, and the activation is mainly YEEI-driven.

As briefly mentioned in the introduction, SFK activity is based on the conformation of the kinase (Fig. 7.1A) [296]. SFKs are kept in an autoinhibited state through an intramolecular interaction between the inhibitory tyrosine, which is located in the C-terminal tail, and the Sh2 domain. Further, the SH3 domain also interacts with the linker region, which is located between the Sh2 domain and the catalytic domain [297, 298]. Activation can either occur due to dephosphorylation of the inhibitory tyrosine [299-301] or by ligand binding to the Sh3 and/or Sh2 domain [267]. Once the enzyme switches over to its open conformation, the regulatory tyrosine residue Y394 within the catalytic activation loop becomes exposed and undergoes auto-phosphorylation [297, 298, 301]. Phosphorylation of Y394 has a dominant role in full kinase activation [302] and this activating tyrosine residue is dephosphorylated by several phosphatases, including

CD45. The negatively regulated phosphorylation of SFKs is carried out by the C-terminal SRC kinase (CSK) and dephosphorylated by CD45 [303-306].

Data obtained in my studies [236, 279] strongly suggest that VP11/12 binds the Sh2 domain of SFKs through either YEEI or YETV, disrupting the inhibitory intramolecular associations and therefore enforcing SFK activation (Fig. 7.1B). Of note, Melany Wagner previously investigated the phosphorylation status of the inhibitory tyrosine and she found that viral infection had no impact on the dephosphorylation of the inhibitory tyrosine residue [236, 266]. It is less likely that both tyrosine based binding motifs bind the Sh2 domain at the same time because the Sh2 domain only has one binding pocket, as shown in crystal structures for Src [307]. Nevertheless, it is biochemically possible that both motifs in close proximity provide a greater binding affinity. By increasing the binding energy, VP11/12 might have a greater likelihood of competing with the inhibitory intermolecular associations within Lck. The association of VP11/12 with Lck is mediated via YEEI or YETV (Fig. 4.10 and Fig. 4.11), whereas the activation of Lck seems to be mediated predominantly through YEEI (Fig. 5.1).

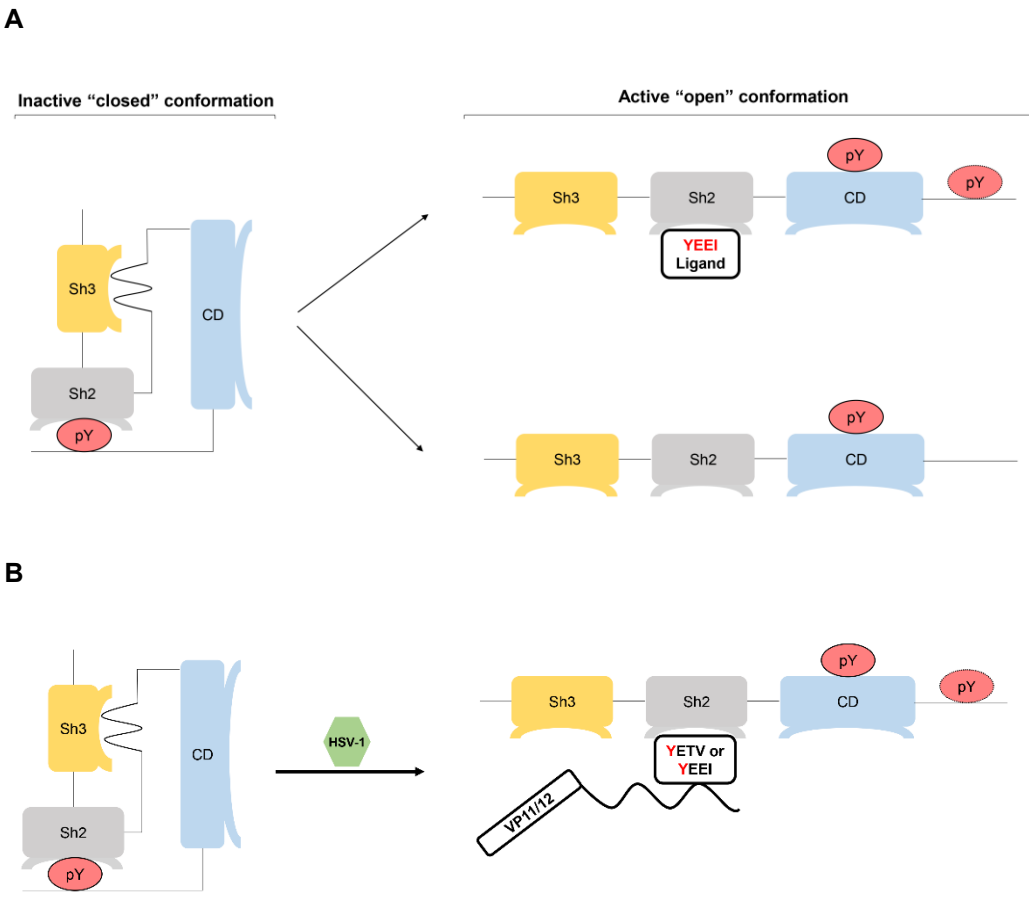

Fig. 7.1: Activation of SFKs through VP11/12.

SFKs are kept in an autoinhibited state through intramolecular interactions between the inhibitory tyrosine (pY), located downstream of the catalytic domain (CD), and the Sh2 domain as well as the Sh3 domain within the linker region. Activation can either occur by dephosphorylation of the inhibitory tyrosine or by ligand binding to the Sh3 and/or SH2 domain. (B) Our data suggest that VP11/12 interacts with the Sh2 domain of SFKs through YEEI or YETV, replacing the low-affinity intramolecular interactions and therefore lead to activation of SFKs.

It was further predicted before I started this project that VP11/12 recruits and activates SFKs upstream of the recruitment of p85, Grb2 and Shc (Fig. 7.2). I provided evidence supporting this model by conducting co-immunoprecipitations assays while either

chemically inhibiting the activation of SFKs (Fig. 5.2) or by infecting cells with the Y613F/Y624F double substitution mutant (Fig. 5.3). I demonstrated that the recruitment and activation of SFKs by VP11/12 is essential for the recruitment of the remaining cellular binding partners. In addition, the co-immunoprecipitation assays carried out with a chemical inhibitor to block the activation of SFKs (Fig. 5.2) indirectly suggested that the YEEI and YETV motifs are phosphorylated by a non-SFK, because inhibiting SFK activity did not eliminate the association between VP11/12 and Lck in T-cells. The identity of the kinase that leads to phosphorylation of the SFK binding motifs YEEI and YETV remains unknown. Mass spectrometry analysis of proteins that associate with VP11/12 could assist in identifying the responsible kinase.

Although I have shown that active SFKs are required for the phosphorylation of additional tyrosine-based motifs on VP11/12 (Fig. 5.2 and Fig. 5.3), my results do not necessarily imply that the activated SFKs themselves directly phosphorylate the motifs required for the interactions with p85, Grb2 and Shc. In this context, it was brought to our attention by Deborah Burshtyn that the seven amino acid residue separation between the critical YETV and YEEI sequences is similar to the one found in immunoreceptor tyrosine-based activation motifs (ITAMs). ITAMs are normally located in the cytoplasmic tails of a variety of immune receptors and are used to link the receptor to downstream signaling cascades (reviewed in [308]). Briefly, ITAMs consist of two YXXL/I sequences separated by six to eight residues. Following phosphorylation of the tyrosine residues by SFKs, the motif recruits members of the tandem Sh2 domain containing Syk family of tyrosine kinases (reviewed in [308]). Following this interaction, additional signaling events are stimulated (reviewed in [308]). Although the YETV sequence does not fully match the YXXL/I consensus, it is possible that valine can

functionally substitute for leucine or isoleucine, as all three share similar hydrophobic side chains. Although Holly Saffran was not previously able to detect an interaction between VP11/12 and Syk in co-immunoprecipitation assays, it is nevertheless possible that Syk contribute to phosphorylating the p85, Grb2 and Shc binding motifs. Interaction studies conducted in cells where Syk has been knocked down could assist in solving this question. Interestingly, the Epstein Barr virus (EBV) LMP2a protein contains an ITAM and it sequesters Syk through its ITAM sequence, which stimulates signaling through the B-cell receptor (BCR) [309].

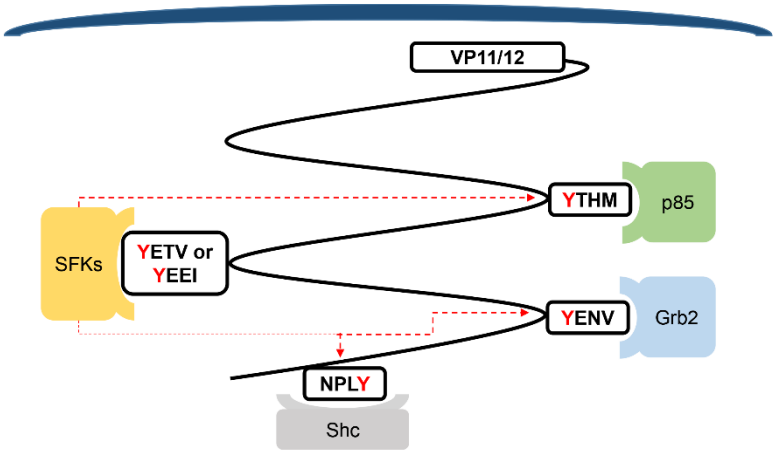

Fig. 7.2: Model of VP11/12 protein-protein associations.

VP11/12 requires the recruitment and activation of SFKs in order to further associate with p85, Grb2 and Shc. VP11/12 recruits and activates SKFs through the YEEI or YETV motif. Activated SFKs then, directly or indirectly, induces additional tyrosine phosphorylation of VP11/12, enabling the direct association with Grb2 (YENV) and Shc (NPLY). The p85-tyrosine based binding motif (YTHM) also becomes phosphorylated; however, the VP11/12-p85 interaction does not solely depend on one interaction interface. The interaction of VP11/12 and p85 may also require proline-rich sequences to enable an additional interaction with the Sh3 domain of p85 (not shown).

7.1.1.2 Association of VP11/12 with Grb2 and Shc

The interaction of VP11/12 with the Sh2 domain of Grb2 was predicted to be mediated by the cognate tyrosine-based motif YENV at position 633. I found that inactivation of the tyrosine-based motif fully abolished the VP11/12-Grb2 association without affecting the remaining protein associations (Fig. 4.2 and Fig. 4.3). My data strongly suggest that the VP11/12-Grb2 association depends on the phosphorylation of the tyrosine within the YENV motif.

In the case of the VP11/12-Shc interaction, I was able to demonstrate that inactivation of the predicted tyrosine-based motif NPLY at position 657 fully inhibited the association (Fig. 4.5). In addition, I provided evidence suggesting that this interaction is mediated by the PTB domain of Shc (Fig. 4.6). Taken together, my thesis research addressing the interactions of VP11/12 with Grb2 and Shc indicate that the interactions are most likely direct. Of note, inactivation of the NPLY motif also slightly impacted the ability of VP11/12 to associate with p85. At this point I am unsure of the biological relevance of this observation, but it is possible that inactivation of the NPLF motif induces an alteration of the global protein conformation that might affect the p85 binding motif. To test this, one could determine the crystal structure of WT VP11/12 and mutant VP11/12.

7.1.1.3 Association of VP11/12 with p85

In contrast to the VP11/12-Grb2 or VP11/12-Shc interactions, the interaction with p85 appears to be more complex than predicted. Inactivation of the YTHM motif at Y519 reduced, but did not fully eliminate, the interaction of VP11/12 with p85 (Fig. 4.7). My findings were supported by a chemical SFK inhibition assay, in that the chemical

inhibition of SFKs had effects similar to inactivating the YTHM motif (Fig. 5.2). Taken together, these data indicated that the interaction between VP11/12 and p85 does not solely depend on binding of the p85 Sh2 domain to the YTHM motif. It also worth mentioning that inactivation of the YTHM motif also negatively impacted the association between VP11/12 and Lck. I am unsure of the mechanism behind this observation, but it is possible that inactivation of the YTHM motif induces an alteration of the global protein conformation that reduces the ability of VP11/12 to associate with Lck. As mentioned in section 7.1.1.2, one could determine the crystal structure to investigate this possibility.

Melany Wagner previously published that VP11/12 contains two proline-rich potential Sh3 binding motifs for p85 [236]. We therefore thought that VP11/12 may require more than one interaction interface in order to associate with p85. Our hypothesis was supported by studies on the Influenza A virus NS1 protein. This protein contains one Sh2-binding motif and two SH3-binding motifs and all three motifs contribute to binding p85, although the interaction is mainly driven by the SH3-binding motifs [259]. Inactivation of all three motifs within NS1 produced a recombinant virus that is no longer able to interact with p85 or activate the Akt-pathway [259]. I performed an additional test to determine if VP11/12 uses a similar mechanism as NS1 does to interact with p85. Inactivation of one potential proline-rich SH3 binding motif in combination with inactivation of the Sh2 tyrosine-based binding motif did not further reduce the VP11/12-p85 interactions (Fig. 4.8B). This observation indicates that if VP11/12 interacts with the SH3 domain of p85, both proline-rich sequences are required for the association. To test this assumption, I inactivated both potential proline-rich SH3 binding motifs in combination with inactivation of the Sh2 tyrosine-based binding motif. Unfortunately, this

virus failed to produce any VP11/12 protein (Fig. 4.8B) and I was therefore not able to determine whether VP11/12 interacts with p85 in a proline-dependent manner. It remains unclear if the mutant virus fails to produce VP11/12 protein, or if the produced protein is unstable.

I also decided to investigate a possible contribution of Grb2 on the VP11/12-p85 association. This investigation originated from the observations that inactivation of the YTHM motif (p85, Y519) decreased the VP11/12-Grb2 interaction (Fig. 4.8B and 4.9), and that inactivation of the YENV motif (Grb2, Y633) reduced the ability of VP11/12 to induce Akt activation (Fig. 5.5). We therefore generated a point-mutated virus with inactive YENV as well as YTHM motifs to investigate if Grb2 contributes towards the p85-VP11/12 interactions. As shown as in figure 5.7, we were able to demonstrate that simultaneous inactivation of both binding motifs further reduced, but still did not fully eliminate, the VP11/12-p85 interactions. These data added to the observation that the association of VP11/12 with p85 appeared to be far more complex than previously predicted. To this date, I was not able to completely determine how VP11/12 interacts with p85. It is possible that unknown cellular or viral proteins stimulate a multi-protein complex in addition to the described interactions (please see next section for this possibility).

7.1.2 On the ability of VP11/12 to induce Akt activation

As mentioned above, Wagner and Smiley predicted that VP11/12 interacts with p85 in order to stimulate Akt activation [229]. This assumption was supported by the observation that the varicella-zoster virus (VZV) VP11/12 orthologue ORF12 was later shown by Jeffrey Cohen's laboratory to display similar activity, as it interacts with p85

[310]. However, we were unsure as to the biological consequences of the interactions between VP11/12 and Grb2 as well as Shc on the ability of VP11/12 to activate Akt. Grb2 and Shc are multifunctional signaling adaptors that play key roles in a variety of signaling pathways [311-313]. Both proteins are best characterized as positive effectors of the Ras/mitogen-activated protein kinase (MAPK)/Erk-pathway (Fig. 1.7). However, studies have also demonstrated the PI3K/Akt- and MAPK/Erk-pathway can cross-interact. For example, Ras can associate with the p110 subunit of PI3K, leading to stimulation of the PI3K/Akt-pathway (reviewed in [314]), and Erk can, similar to Akt, phosphorylate TSC2 in order to stimulate mTORC1 signaling [315].

Results presented in chapter 5 demonstrate that VP11/12-induced Akt activation requires the tyrosine-based binding motifs for the Sh2 domains of SFKs and p85 (Fig. 7.2). These observations fully support the previous suggestion that VP11/12 activates the PI3K/Akt pathway by binding and activating SFKs, which then leads to phosphorylation of the p85 binding motif and recruitment of p85 [229, 279].

This study unexpectedly revealed that the Grb2 binding motif YENV at residue Y633 is also required for Akt activation by VP11/12 (Fig. 5.5), and it contributes to p85 recruitment (Fig. 5.7).

As mentioned in the introduction (section 1.2.2.1), Grb2 is best characterized as a positive effector of the MAPK/Erk-pathway, and I therefore did not expect an effect on the ability of VP11/12 to activate Akt. While it is possible that inactivating the Grb2 binding motif impairs Akt activation and recruitment of p85 by altering the global conformation of the VP11/12 C-terminal region, this seems unlikely as binding of Lck and Shc are not affected. We therefore concluded that the effect likely originates from eliminating Grb2 from the VP11/12 complex. It has been previously reported that Grb2

and p85 can directly interact with each other *via* the Sh3 domain of Grb2 and the p85 proline-rich sequences [316]. In addition, it is possible that Grb2 facilitates p85 recruitment through an associated adaptor protein. It is well known in the literature that Grb2 binds members of the Grb2-associated binding (GAB) family of proteins through its SH3 domain (reviewed in [317-319]). GABs such as GAB1 and GAB2 bear tyrosine-based binding motifs for the Sh2 domain of p85, and an N-terminal PH domain involved in membrane targeting. Thus, it is possible that one or more GABs bind VP11/12-associated Grb2, providing an alternative binding site for p85 in the VP11/12 complex, and perhaps facilitating membrane targeting of VP11/12 (Fig. 7.3). Further studies are required to test this possibility. One approach to test a possible role of GABs is to knock down GAB-expression using siRNA prior to co-immunopreciptation assays. If GABs are involved in creating a secondary interaction between VP11/12 and p85, we would assume that a knockdown of the involved GAB(s) in cells infected with KOS37-UL46 GFP Y519F (p85, YTHM motif) will lead to a VP11/12-p85 association phenotype similar to the one observed in the p85/Grb2 mutant KOS37-UL46 GFP Y519F/Y633F without the GAB(s) knockdown (Fig. 5.7).

This study also unexpectedly revealed that the inactivation of the Shc binding motif increased the ability of VP11/12 to activate Akt. The marginal increase of Akt activation was observed in samples infected with independently derived mutants (Fig. 5.5). As described in chapter 3 of this thesis, I only sequenced the mutant virus along the UL46 gene locus and not the entire genome. It is therefore possible that the KOS37-UL46 GFP Y657F mutant virus harboured an additional undetected spontaneous mutation outside the UL46 sequence. By generating the second independently derived mutant KOS37-UL46 GFP Y657F #2, we minimized the possibility of the same spontaneous mutation.

It is possible that inactivating the Shc binding motif altered the global conformation of the VP11/12 C-terminal region such that the mutant interacts with p85 and/or Grb2 with increased affinity; however, this was not observed in any interaction assay (Fig. 4.1, Fig, 4.2 and Fig. 4.7). Perhaps VP11/12 associates through Shc with a negative regulator of the PI3K/Akt-pathway. Another possibility is that this particular mutation changes the interplay between VP11/12 and the viral kinase US3. The relationship between VP11/12 and US3 is highly complex, as outlined in the section below (7.1.2.1). To date, it remains unclear how the inactivation of the Shc binding motif increased the ability of VP11/12 to activate Akt.

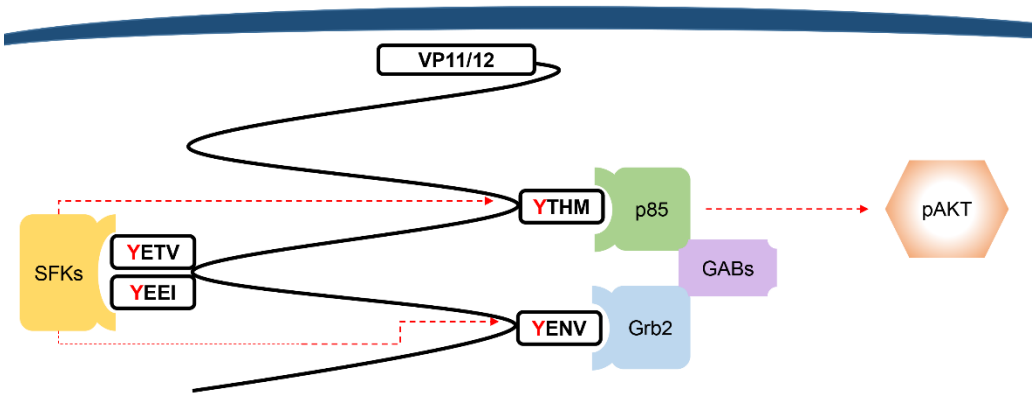

Fig. 7.3: VP11/12 activates Akt through association with p85.

Melany Wagner previously suggested that VP11/12 interacts with p85 in order to activate Akt. Here I presented data supporting her model. I was also able to demonstrate that Grb2 contributes indirectly to the VP11/12-p85 signaling axis. It is possible that Grb2 associates with GAB proteins that then further associate with p85, leading to a secondary pathway that can activate Akt.

7.1.2.1 The interplay between US3 and VP11/12

Deciphering the role of VP11/12-dependent signaling in the HSV life cycle is challenging because VP11/12 and the viral US3 protein kinase appear to collaborate to provide redundant coverage of the PI3K/Akt pathway: VP11/12 activates Akt [229] while the serine/threonine-protein kinase US3 phosphorylates many Akt substrates and thus serves as an Akt mimic [226]. In addition, Akt activation is enhanced in cells infected with a US3-null mutant [228, 235].

A study conducted by Matsuzaki *et al* provided the first evidence that US3 regulates VP11/12. Data presented in this publication showed that US3 is required for the stability as well as the packaging of VP11/12 during HSV-2 infection [320].

In the case of HSV-1 infection, studies carried out in our lab showed in detail that US3 collaborates with the protein kinase UL13 in order to modulate VP11/12 phosphorylation, virion packaging and Akt signaling activity [228]. This recently published work highlighted that VP11/12 is subjected to two different sets of phosphorylation events; whereas SFK-dependent phosphorylation triggers Akt activation, UL13-dependent phosphorylation induces a mobility shift of VP11/12 and inhibits the packaging of VP11/12 into virions [228]. Of note, a distinct study also showed that the interplay between US3 and UL13 is critical to the efficient assembly as well as the release of infectious virions from HSV-1-infected cells [321]. Importantly, US3 inhibits both types of phosphorylation events of VP11/12 and is therefore accountable for inhibiting VP11/12 induced PI3K/Akt-signaling as well packaging VP11/12 into virions [228]. In addition, the data presented in this paper showed that VP11/12 is essential for the activation of Akt when US3 is not present; as also, US3 negatively regulates VP11/12-induced Akt activation [228]. Specifically, our

lab and others observed that US3 null mutants display a marginal increase in Akt activation [228]. Given that I observed a marginal increase in Akt activation in a mutant that is no longer able to interact with Shc (Fig. 5.5 and Fig. 5.6), it is possible that US3 somehow utilizes the VP11/12-Shc association to inhibit VP11/12 dependent Akt activation.

Overall, these data indicate that VP11/12 stimulates the PI3K/Akt-signaling pathway if US3 activity is limited. The detailed mechanism used by US3 or other viral or cellular proteins to coordinate US3 and VP11/12 remains to be determined. It also remains to be determined what sites on VP11/12 are phosphorylated by US3. Combining all the current data, it is thought that VP11/12 utilizes the tyrosine-based binding motifs for SFKs, p85 and Grb2 to stimulate the Akt pathway if US3 fails to inactivate VP11/12.

Interestingly, the biological relevance of VP11/12 induced Akt activation remains unknown. Melany Wagner demonstrated that VP11/12 is required for the activation of Akt during infection; however, VP11/12 is not required for the activation of the downstream Akt targets such as S6K or GSK-3β [229, 236]. Additional work carried out in our lab investigated whether US3 blocks VP11/12-dependent Akt target phosphorylation, but it was observed that the phosphorylation of Akt targets depends only on US3 (unpublished data from Holly Saffran and Heather Eaton). Future studies investigating the biological relevance of VP11/12 induced Akt activation are outlined below (section 7.2).

7.1.2.2 Orthologues of VP11/12

Every tyrosine-based motif that we have implicated in the signaling activity of VP11/12 is located within the C-terminal region of VP11/12 (Fig. 1.9), which is conserved only in

HSV-1, HSV-2, and closely related members of the *Simplexvirus* genus of the *Alphaherpesvirinae* (Fig. 1.9) [279]. It is therefore intriguing that the VP11/12 orthologues of the Varicella Zoster viruses (VZV) and pseudorabies virus (PrV), which bear unrelated C-terminal regions with no homology to VP11/12, also activate cell signaling pathways. The VZV VP11/12 orthologue ORF12 activates the PI3K/Akt pathway [310] as well as the MAPK/Erk pathway [322] in non-lymphocytic cells. The PrV VP11/12 orthologue UL46 fails to activate Akt but activates the MAPK/Erk pathway [323] in non-lymphocytic cells. This observation stands in contrast to HSV-1, where Akt becomes activated [235] but MAPK/Erk signaling is downregulated. In more detail,VP11/12 fails to activate Erk1/2 in transient transfection assays [323] in fibroblast cells, and HSV-1 infection suppresses Erk1/2 activation during infection in fibroblast cells [227] and T-cells [209]. Overall, these data suggest that all alphaherpesvirus VP11/12 orthologues display a distinct signaling profile.

The mechanisms employed by VZV ORF12 and PrV UL46 to activate signaling pathways have not been defined in detail, although VZV ORF12 has been shown to bind p85 [310]. It will be interesting to determine if SFKs and the C-terminal regions and tyrosine-based motifs in VP11/12 play important roles in mediating the signaling activity of these proteins. It is important to mention that VZV ORF12 (accession number AAY57754, version AAY57754.1) codes for one predicted p85 binding motif (YGWM at Y249) as well as one predicted Grb2 binding motif (YENI at Y598). In contrast, PrV UL46 (accession number AID18727, version AID18727.1) does not encode any highly predicted potential binding motifs for p85 and/or Grb2.

7.1.3 On the ability of VP11/12 to reduce TCR signaling events upon expression in transfected T-cells

When I started my project, little was known about the possible involvement of VP11/12 in TCR signaling events. As reviewed in the introduction, early studies demonstrated that T-cells infected with HSV-1 displayed modified TCR-signaling events. Sloan *et al* demonstrated that *de novo* protein synthesis was not required for inhibiting cytotoxic T-cells, and that the signaling cascade was suppressed downstream of LAT, as phosphorylation of ZAP-70 by Lck occurred normally but phosphorylation of LAT was decreased [208]. In addition, certain TCR signaling events such as the p38-dependent IL-10 synthesis, which further suppresses cellular immunity, remained active [209]. Previous data indicated that deletion of VP11/12 did not restore Erk1/2 phosphorylation [230]; however, unpublished data by the Jerome group suggested that VP11/12 is sufficient to block Erk1/2 phosphorylation as well as calcium flux upon overexpression in Jurkat T-cells. We therefore sought to investigate if VP11/12 inhibits TCR signaling in isolation. I decided to investigate two downstream events in TCR signaling. First, I determined the phosphorylation of Erk1/2, and second I determined the calcium mobility. For both experiments, Jurkat T-cells were transfected with plasmids expressing WT-VP11/12, mutant VP11/12 or control plasmids for 24 hours.

I found that WT VP11/12 reduced, but did not fully inhibit, both signaling events (Fig. 6.3- Fig. 6.6). Further, I was able to demonstrate that inactivating the SFK binding motifs YEEI and YETV restored the phosphorylation of Erk1/2 as well as calcium mobility. This observation supported our previous hypothesis, which stated that the SFK binding motifs are essential to the activation of VP11/12.

Before discussing my results in more detail, it is important to mention that I determined VP11/12 function on TCR signaling events in a transfection model. Transfection studies do not necessarily mirror the mechanism used during viral infection.

7.1.3.1 On the ability of VP11/12 to reduce Erk1/2 phosphorylation

In line with our previous data, I observed that WT VP11/12 reduced the phosphorylation of Erk1/2 and inactivation of both SFK binding motifs restored the phosphorylation of Erk1/2. In the case of the phosphorylation of Erk1/2 I found that mutating the Grb2 binding motif (YENV, Y633), Shc binding motif (NPLY, Y657), or the p85 binding motif (YTHM, Y519), had a minor effect on the ability of VP11/12 to block the phosphorylation of Erk1/2. This observation leads to three possible mechanisms.

First, it is possible that VP11/12 binds and sequesters Lck away from TCR signaling complexes, in order to block all downstream signaling events to avoid signal transduction. To test this, one could determine if expression of VP11/12 as only viral protein in T-cells inhibits the phosphorylation of ZAP-70 and/or LAT. If this is indeed the case, then these results might indicate that VP11/12 sequesters Lck in order to control the phosphorylation of signaling proteins. Nevertheless, this possible mechanism does not account for the potential involvement of the VP11/12-Grb2-binding motif on calcium mobility, as described below.

Second, it is possible that VP11/12 recruits two or more of the cellular proteins that we have identified in order to control the phosphorylation of Erk1/2. This would imply that VP11/12 might shut down redundant pathways that lead to the activation of Erk1/2. For example, that Erk1/2 can become activated through the SOS/Grb2-complex or through RasGRP, as mentioned in the preface of chapter 6. Nevertheless, this possibility seems

less likely due to the observed phenotype as that none of the mutations fully restored the phosphorylation of Erk1/2 as shown with the YEEI/YETV-mutant. Every mutant only showed a slight restoration of pErk1/2 post TCR stimulation, indicating that protein-protein interactions might only play minor roles in regulating the phosphorylation of Erk1/2 and/or that a secondary Grb2/Shc/p85-independent pathway induces Erk1/2 phosphorylation. As mentioned in the preface of chapter 6 (Fig. 6.1), the phosphorylation of Erk1/2 can be induced through the Grb2/SOS-complex or through the PLCγ-DAG-RasGRP axis. It would be interesting to determine if this secondary axis plays a role in the reduced phosphorylation of Erk1/2 during expression of VP11/12. For example, if RasGRP stimulates phosphorylation of Erk1/2, knock down of RasGRP or chemical inhibition of PLCγ should reduce the phosphorylation of Erk1/2. Nevertheless, it is further possible that multiple protein associations are necessary for the ability of VP11/12 to inhibit the phosphorylation of Erk1/2. It is therefore of interest to determine if, for example, a mutant with an inactive Grb2 binding motif as well as an inactive Shc binding motif shows a similar phenotype to the one observed after inactivating both SFK binding motifs.

Third, it is also possible that VP11/12 recruits other, yet unknown, cellular proteins via the same or additional binding motifs to regulate the phosphorylation of Erk1/2. This possibility is based on the observation that only the YEEI/YETV-double mutation fully restored Erk1/2 phosphorylation. Overall, the data suggests that VP11/12 must be tyrosine phosphorylated in order to interfere with the TCR pathway; however, the protein(s) involved still need to be determined. Such unidentified proteins could be identified by mass spectrometry analysis of proteins that interact with VP11/12 in pulldown experiments.

7.1.3.2 On the ability of VP11/12 to reduce the calcium flux

In the case of calcium mobility, I found that transfection based expression of VP11/12 severely reduced as well as delayed the calcium flux after TCR stimulation. Interestingly, the reduced calcium flux in WT VP11/12 expressing cells occurs in an irregular pattern. It is important to mention that we cannot exclude the possibility that the irregular pattern is based on the lower cell count of VP11/12 expressing cells (Tab. 6.1) and/or the FlowJo programming (section 2.11.3). In general, comparing the kinetics of a small population to a larger population, FlowJo is programmed to represent the kinetics of the smaller population in a less smooth line because of the smaller amount of available data points. Nevertheless, my literature review has failed to identify a similar pattern, and the cause of this pattern remains unknown.

The delay in calcium flux after VP11/12 expression might indicate that the depletion of intracellular ER calcium is limited. It is known that intracellular calcium stores have to be depleted in order to induce a massive calcium influx. In more detail, activation of the TCR leads to stimulation of PLCγ and PLCγ generates DAG and IP3. IP3 then binds to IP3-receptors (IP3Rs), which are located at the endoplasmic reticulum (ER) membrane. IP3R releases calcium from the ER and induce CRAC channel activation [324]. The link between store depletion and CRAC channel opening remained unknown for many years, but research over the past ten years demonstrated that the STIM1 protein is essential for the activation of CRAC channels [325, 326]. To test if the depletion of intracellular ER calcium is limited, one should first repeat the experiments while crosslinking OKT3, in order to strengthen the stimulation, and only adding EGTA immediately before the flow detection, in order to avoid possible EGTA-stimulated intracellular store depletion.

Additionally, one could observe the activation of PLCγ by either directly measuring its activation using fluorogenic assay systems or by measuring IP3 production.

The observed irregular pattern might additionally indicate that transfected cells fail to induce the secondary extracellular calcium influx through CRAC channels. Future studies should investigate if, for example, cells transfected with VP11/12 display a decreased amount of CRAC channels or abnormal location of STIM proteins. The CRAC channel itself consist(s) of a hexameric complex formed by plasma membrane proteins called ORAIs (ORAI1, ORAI2, ORAI3) [327]. The exact mechanism behind the insertion of ORAIs as well as relocation of STIMs within the ER membrane are not clear, but it is suggested that both mechanisms play an important role in the calcium influx [324, 328-332]. Antibodies against ORAIs are available and could be used to determine the amount as well as location of CRAC channels. Similar to this, antibodies against STIM proteins could be used to determine the location of STIM proteins.

In the case of the VP11/12-p85 association, I found that inactivation of the p85 binding motif (YTHM, Y519) had no impact on the calcium mobility. This observation is in line with our expectations, based on the general understanding that p85 does not stimulate calcium signaling in T-cells under physiological conditions (Fig. 6.1).

As mentioned above, I found that inactivation of the Grb2 binding motif (YENV, Y519) almost restored the calcium mobility to levels similar to those detected in the SFK double mutant (YEEI/YETV, Y613 and Y624). This observation suggests that VP11/12 recruits Grb2 in order to control the calcium flux; however, VP11/12 may need to recruit an additional protein to gain full control over the calcium signaling axis. An interesting

possibility is that VP11/12 might sequester Grb2 away from LAT in order to inhibit TCR signaling. This possibility originates from the observation that Grb2 showed a reduced binding to LAT during HSV-1 infection [208, 209] as well as that Grb2, in combination with SOS, induces LAT oligomerization [333]. A recent study also demonstrated that Grb2 is essential for the recruitment and formation of large signaling clusters that are critical for the induction of PLCγ1 and therefore calcium signaling in T-cells [334]. In more detail, Bilal and Houtman presented data suggesting that Grb2 regulates the formation of LAT microclusters. Those microclusters directly drive the activation and recruitment of PLCγ1 to LAT [334]. Overall, it is possible that VP11/12 sequesters Grb2 in order to block the formation of microclusters that then could stimulate calcium signaling. To test this hypothesis, one could observe the formation of LAT microclusters upon expression of VP11/12 as only viral protein through immunofluorescent total internal reflection fluorescence (TIRF) microscopy, as described and carried out by Bilal and Houtman [334].

Lastly, I found that the result of inactivating the Shc binding motif (NPLY, Y657) were inconsistent between experiments. In one experiment this mutation had no effect on the calcium flux (Fig. 6.5), whereas it showed the same phenotype as the Grb2-mutant in a second experiment (Fig. 6.6). Grb2 and Shc can interact with other (Fig. 1.7) and it is therefore possible that both proteins are recruited by VP11/12 to inhibit the calcium flux in order to silence TCR signaling. In future experiments, it will be of interest to further explore the possibility that the Shc-mutant is able to interfere with calcium signaling. In addition, future research should investigate if a simultaneous inactivation of the Grb2- and Shc-binding motifs fully restores calcium mobility. Figure 6.7 outlines the effects of

point-mutations within the C-terminal region of VP11/12 on TCR signaling events. In summary, our data suggest that VP11/12 sequesters proteins away from the TCR in order to block TCR signaling events.

7.1.3.3 The interplay between VP11/12 and US3

While I was performing my TCR signaling experiments, Yang *et al.* published that US3, in transfection as well as infection assays, directly inhibits TCR signaling by inhibiting the activation of LAT [335]. This recently published work provided evidence that US3 suppresses TCR signaling events such as the phosphorylation of LAT, Erk1/2 and PLCγ1, and calcium mobility. In their model, US3 interferes with the stability of LAT as well as TRAF6, resulting in a suboptimal activation of LAT. Of note, TRAF6 induces the ubiquitination of LAT and has been therefore suggested to coordinate T-cell activation [336].

These studies stand in contrast to unpublished data from our lab, in that Holly Saffran did not observe that US3 inhibits Erk1/2 phosphorylation. She infected cells with WT HSV-1, ΔUS3, ΔUL46 or ΔUS3/ΔUL46, and none of the deletions had any impact on the inhibition of Erk1/2 phosphorylation post TCR stimulation. Her data therefore indicates that the inhibition of Erk1/2 phosphorylation during infection occurs independent of US3 and VP11/12. It remains unclear, how two different studies observed an opposite effect, but it is worth mentioning that Yang *et al.* used the HSV-1 F-strain, and our lab used the HSV-1 KOS strain. It is possible that the observed effects of US3 are strain specific.

Nevertheless, the recent study is of interest in combination with data presented in chapter 6, because it suggests that US3 and VP11/12 might target the same pathway. As mentioned in section 7.1.2.1 in this discussion, US3 and VP11/12 are already

characterized to target the PI3K/Akt-pathway; although, it appears that both proteins collaborate to provide redundant coverage. Further, the current data suggest that VP11/12 stimulates the Akt pathway only if US3 fails to inactivate VP11/12 [228]. It is therefore possible that VP11/12 and US3 function similarly during the inhibition of TCR signaling events. More research needs to be carried out addressing the relationship between US3 and VP11/12 during T-cell infection. For example, one should determine a possible role for US3 in hindering the activation of VP11/12 in T-cells, as previously seen in HeLa cells and Vero cells [228]. It is also of interest to determine if VP11/12 interferes with the TRAF6-LAT association, similar to US3, or if VP11/12 developed a different mechanism to block TCR signaling events.

7.2 Concluding remarks and future directions

I made significant contributions to our overall understanding of the mechanism involved in the VP11/12 dependent interference with PI3K/Akt- as well as the TCR-signaling pathway by investigating the role of tyrosine-based binding motifs within VP11/12. In summary, I was able to demonstrate that VP11/12 mimics a cell surface receptor, as it directly recruits and activates cellular proteins that are involved in signal transduction. Three major key questions have arisen from my research project and should be addressed in future research.

First, regarding the phosphorylation of VP11/12, it remains unknown what non-SFK kinase initially phosphorylates the SFK binding motifs YEEI and YETV. Related to this, it remains unknown if the recruited SFK (Lck in the case of Jurkat T-cells) directly phosphorylates the remaining tyrosine-based binding motifs or if that phosphorylation

occurs indirectly for example by ZAP-70 and/or Syk. Based on my SFK-inhibition assay (Fig. 5.2) it seems less likely that ZAP-70 triggers the phosphorylation of the SFK binding motifs because its activation depends on Lck (Fig. 1.7). However, both questions could be addressed in future infection studies that are carried out in cell lines that do not express certain kinases or that were treated with specific kinase inhibitors. Given the evidence suggesting that VP11/12 and US3 serve redundant roles in targeting the PI3K/Akt-pathway [226, 228] as well as that US3 inhibits tyrosine-phosphorylation of VP11/12 [228], it is of high interest to further investigate if US3 inhibits the tyrosine-phosphorylation of the tyrosine-based binding motifs in VP11/12.

Second, I was able to demonstrate that VP11/12 interacts with the Sh2 domain of p85 through the YTHM motif located at position Y519; however, this interaction interface is not the only interface used by VP11/12 to associate with p85. We were further able to provide evidence for the contribution of Grb2 to the VP11/12-p85 interaction; nevertheless, inactivation of both interaction points did not fully inhibit the VP11/12-p85 association. Further research is required to fully elucidate the VP11/12-p85 interaction. Such research could be based on a mass spectrometry analysis of proteins that associate with VP11/12 in immunoprecipitation assays. Results might indicate additional secondary interaction partners.

Lastly, when I started my thesis project the biological function of VP11/12 remained unknown. As mentioned in the section 1.2.1 of my thesis introduction, a recent report indicated that VP11/12 inhibits the early antiviral immune response by inactivating the STING DNA sensing pathway [183]. In addition to manipulating the innate immune response, two lines of evidence suggest additional potential biological functions for VP11/12. The first line of evidence is based on the observation that VP11/12-null viruses

do not show a phenotype under cell culture conditions in most studies [23, 90, 183, 230]. This overall indicates that VP11/12 might influence a viral pathway(s) that is not easy to determine under cell culture conditions such as latency and/or reactivation. This future direction is further supported by the observation that nerve growth factor-dependent signaling through the PI3K/Akt/mTOR axis is essential for maintaining viral latency [165, 167-170], as mentioned in the introduction in section 1.1.4. It therefore seems especially important to determine if VP11/12 influences latency establishment and/or reactivation. Future research should investigate the establishment of latency as well as the reactivation out of latency focussing on VP11/12 in the primary neuron culture system described by Ian Mohr and colleagues [166]. If VP11/12 is involved in latency establishment and/or reactivation out of latency, we would expect that cells infected with mutant viruses that lacked the ability to activate Akt show a different phenotype than cells that were infected with a WT virus.

The second line of evidence was most recently discovered by Pascale Duplay's laboratory in collaboration with us. They found that VP11/12 induces phosphorylation of Dok proteins during Jurkat T-cell infection and that the phosphorylation requires the active SFK binding motifs as well as the Shc binding motif [337]. Dok-1 and Dok-2 are negative regulators of TCR signaling events and they become tyrosine phosphorylated in a Lck-dependent fashion upon T-cell activation [338, 339]. Studies carried out in a murine model previously demonstrated that Dok-1/2 double knockouts lead to hyper-proliferation/activation of T-cells [340]. Our collaborators also previously established a link between Dok proteins and viral infection, as in the absence of Dok proteins the number of cytotoxic effector as well as memory cells generated in the response of HSV-1 infection is significantly lower [341]. Taken together, the current data suggests that

Dok proteins are directly targeted by VP11/12 to create a negative feedback loop in order to prevent hyper-activation of cytotoxic T-cells. In the same report the Duplay group also demonstrated that VP11/12 interacts with the Dok-2, most likely associating with the PTB domain of Dok-2, through a SFK/Shc-tyrosine based binding motif dependant mechanism and that VP11/12 stimulates Dok-2 degradation [337]. Even though it seems contradictory to induce Dok-2 degradation, previous research by our collaborator indicated that Dok-2 expression returns to a basal level after activation [342] and that Dok-2 re-expression is most likely necessary to hinder a possible harmful T-cell over-activation [341, 342]. In the Duplay model, VP11/12 degrades Dok-2 to prevent its re-expression and to create quiescence in infected T-cells [337]. In summary, this study describes a novel strategy by HSV-1 to inactivate T-cells; however, their data does not fully agree with our observations concerning the role of the Shc binding motif in VP11/12 driven T-cell inactivation.

My data present in chapter 6 does not indicate that the Shc-binding motif alone is essential for the VP11/12 controlled reduction of Erk1/2 phosphorylation (Fig. 6.3 and Fig. 6.4) and calcium flux (Fig. 6.5 and Fig. 6.6). This stands in contrast to the observations made in the Duplay group, where inactivation of the Shc-binding motif alone was sufficient to block the effects of VP11/12 on Dok-2. To distinguish between events that originate from Shc and/or Dok-2 binding to VP11/12, one could hinder the expression of Shc or Dok-2 using siRNA before determining TCR-signaling events. In addition, future research should investigate what signaling pathway is controlled by the VP11/12 associated Dok-2 during HSV-1 infection in order to alter T-cell function. Earlier reports suggest that Dok-2 inhibits signaling events by recruiting the RAS p21 protein activator 1 (RasGAP) [343-345] and RasGAP then inactivates Ras by replacing its

bound GTP with GDP. One could therefore determine the location of RasGAP and the activation state of Ras during infection with WT virus compared to the infection with mutant VP11/12 that no longer associate with SFKs and/or Dok-2. Even though I did not observe that the Shc-binding motif is essential for TCR-signaling events downstream of Ras, such as the phosphorylation of Erk1/2 and calcium flux, it is possible that VP11/12 bound Dok-2 effects T-cell signaling events other than the ones we observed.

Chapter 8

References

1. Roizman, B., Knipe, D. M., Whitley R. J., *Herpes simplex viruses*, ed. P.M. Howley. Vol. 5th edition. 2007, Fields Virology: Williams and Wilkins, Philadelphia, PA.
2. WHO, *Herpes Simplex Viruses.* *http://www.who.int/mediacentre/factsheets/fs400/en/.* 2017.
3. Baringer, J.R., *Herpes simplex infections of the nervous system.* Neurol Clin, 2008. **26**(3): p. 657-74, viii.
4. Harris, J.B. and A.P. Holmes, *Neonatal Herpes Simplex Viral Infections and Acyclovir: An Update.* J Pediatr Pharmacol Ther, 2017. **22**(2): p. 88-93.
5. Cohen, J.I., *Clinical practice: Herpes zoster.* N Engl J Med, 2013. **369**(3): p. 255-63.
6. Ablashi, D., et al., *Classification of HHV-6A and HHV-6B as distinct viruses.* Arch Virol, 2014. **159**(5): p. 863-70.
7. Diehl, V., et al., *Demonstration of a herpes group virus in cultures of peripheral leukocytes from patients with infectious mononucleosis.* J Virol, 1968. **2**(7): p. 663-9.
8. Chang, Y., et al., *Identification of herpesvirus-like DNA sequences in AIDS-associated Kaposi's sarcoma.* Science, 1994. **266**(5192): p. 1865-9.
9. Pertel, P.E., et al., *Cell fusion induced by herpes simplex virus glycoproteins gB, gD, and gH-gL requires a gD receptor but not necessarily heparan sulfate.* Virology, 2001. **279**(1): p. 313-24.
10. Turner, A., et al., *Glycoproteins gB, gD, and gHgL of herpes simplex virus type 1 are necessary and sufficient to mediate membrane fusion in a Cos cell transfection system.* J Virol, 1998. **72**(1): p. 873-5.
11. Heine, J.W., et al., *Proteins specified by herpes simplex virus. XII. The virion polypeptides of type 1 strains.* J Virol, 1974. **14**(3): p. 640-51.
12. Loret, S., G. Guay, and R. Lippe, *Comprehensive characterization of extracellular herpes simplex virus type 1 virions.* J Virol, 2008. **82**(17): p. 8605-18.
13. Luxton, G.W., et al., *Targeting of herpesvirus capsid transport in axons is coupled to association with specific sets of tegument proteins.* Proc Natl Acad Sci U S A, 2005. **102**(16): p. 5832-7.
14. Maurer, U.E., B. Sodeik, and K. Grunewald, *Native 3D intermediates of membrane fusion in herpes simplex virus 1 entry.* Proc Natl Acad Sci U S A, 2008. **105**(30): p. 10559-64.
15. Wolfstein, A., et al., *The inner tegument promotes herpes simplex virus capsid motility along microtubules in vitro.* Traffic, 2006. **7**(2): p. 227-37.
16. Kelly, B.J., et al., *Functional roles of the tegument proteins of herpes simplex virus type 1.* Virus Res, 2009. **145**(2): p. 173-86.

17. Gibson, W. and B. Roizman, *Proteins specified by herpes simplex virus. 8. Characterization and composition of multiple capsid forms of subtypes 1 and 2.* J Virol, 1972. **10**(5): p. 1044-52.
18. Spear, P.G. and B. Roizman, *Proteins specified by herpes simplex virus. V. Purification and structural proteins of the herpesvirion.* J Virol, 1972. **9**(1): p. 143-59.
19. Grunewald, K., et al., *Three-dimensional structure of herpes simplex virus from cryo-electron tomography.* Science, 2003. **302**(5649): p. 1396-8.
20. Bohannon, K.P., et al., *Differential protein partitioning within the herpesvirus tegument and envelope underlies a complex and variable virion architecture.* Proc Natl Acad Sci U S A, 2013. **110**(17): p. E1613-20.
21. Owen, D.J., C.M. Crump, and S.C. Graham, *Tegument Assembly and Secondary Envelopment of Alphaherpesviruses.* Viruses, 2015. **7**(9): p. 5084-114.
22. Schmid, M.F., et al., *A tail-like assembly at the portal vertex in intact herpes simplex type-1 virions.* PLoS Pathog, 2012. **8**(10): p. e1002961.
23. Zhang, Y. and J.L. McKnight, *Herpes simplex virus type 1 UL46 and UL47 deletion mutants lack VP11 and VP12 or VP13 and VP14, respectively, and exhibit altered viral thymidine kinase expression.* J Virol, 1993. **67**(3): p. 1482-92.
24. Gibson, W. and B. Roizman, *Proteins specified by herpes simplex virus. Staining and radiolabeling properties of B capsid and virion proteins in polyacrylamide gels.* J Virol, 1974. **13**(1): p. 155-65.
25. Newcomb, W.W., et al., *The UL6 gene product forms the portal for entry of DNA into the herpes simplex virus capsid.* J Virol, 2001. **75**(22): p. 10923-32.
26. Newcomb, W.W., F.P. Booy, and J.C. Brown, *Uncoating the herpes simplex virus genome.* J Mol Biol, 2007. **370**(4): p. 633-42.
27. Macdonald, S.J., et al., *Genome sequence of herpes simplex virus 1 strain KOS.* J Virol, 2012. **86**(11): p. 6371-2.
28. McGeoch, D.J., et al., *The complete DNA sequence of the long unique region in the genome of herpes simplex virus type 1.* J Gen Virol, 1988. **69 (Pt 7)**: p. 1531-74.
29. McGeoch, D.J., et al., *Complete DNA sequence of the short repeat region in the genome of herpes simplex virus type 1.* Nucleic Acids Res, 1986. **14**(4): p. 1727-45.
30. McGeoch, D.J., et al., *Sequence determination and genetic content of the short unique region in the genome of herpes simplex virus type 1.* J Mol Biol, 1985. **181**(1): p. 1-13.
31. Szpara, M.L., L. Parsons, and L.W. Enquist, *Sequence variability in clinical and laboratory isolates of herpes simplex virus 1 reveals new mutations.* J Virol, 2010. **84**(10): p. 5303-13.

32. Kieff, E.D., S.L. Bachenheimer, and B. Roizman, *Size, composition, and structure of the deoxyribonucleic acid of herpes simplex virus subtypes 1 and 2.* J Virol, 1971. **8**(2): p. 125-32.
33. Hayward, G.S., et al., *Anatomy of herpes simplex virus DNA: evidence for four populations of molecules that differ in the relative orientations of their long and short components.* Proc Natl Acad Sci U S A, 1975. **72**(11): p. 4243-7.
34. Wadsworth, S., G.S. Hayward, and B. Roizman, *Anatomy of herpes simplex virus DNA. V. Terminally repetitive sequences.* J Virol, 1976. **17**(2): p. 503-12.
35. Wadsworth, S., R.J. Jacob, and B. Roizman, *Anatomy of herpes simplex virus DNA. II. Size, composition, and arrangement of inverted terminal repetitions.* J Virol, 1975. **15**(6): p. 1487-97.
36. Locker, H. and N. Frenkel, *BamI, KpnI, and SalI restriction enzyme maps of the DNAs of herpes simplex virus strains Justin and F: occurrence of heterogeneities in defined regions of the viral DNA.* J Virol, 1979. **32**(2): p. 429-41.
37. Wagner, M.J. and W.C. Summers, *Structure of the joint region and the termini of the DNA of herpes simplex virus type 1.* J Virol, 1978. **27**(2): p. 374-87.
38. Mocarski, E.S. and B. Roizman, *Structure and role of the herpes simplex virus DNA termini in inversion, circularization and generation of virion DNA.* Cell, 1982. **31**(1): p. 89-97.
39. Spaete, R.R. and N. Frenkel, *The herpes simplex virus amplicon: analyses of cis-acting replication functions.* Proc Natl Acad Sci U S A, 1985. **82**(3): p. 694-8.
40. Varmuza, S.L. and J.R. Smiley, *Signals for site-specific cleavage of HSV DNA: maturation involves two separate cleavage events at sites distal to the recognition sequences.* Cell, 1985. **41**(3): p. 793-802.
41. Friedmann, A., J. Shlomai, and Y. Becker, *Electron microscopy of herpes simplex virus DNA molecules isolated from infected cells by centrifugation in CsCl density gradients.* J Gen Virol, 1977. **34**(3): p. 507-22.
42. Murchie, M.J. and D.J. McGeoch, *DNA sequence analysis of an immediate-early gene region of the herpes simplex virus type 1 genome (map coordinates 0.950 to 0.978).* J Gen Virol, 1982. **62 (Pt 1)**: p. 1-15.
43. Stow, N.D., *Localization of an origin of DNA replication within the TRS/IRS repeated region of the herpes simplex virus type 1 genome.* EMBO J, 1982. **1**(7): p. 863-7.
44. Weller, S.K., et al., *Cloning, sequencing, and functional analysis of oriL, a herpes simplex virus type 1 origin of DNA synthesis.* Mol Cell Biol, 1985. **5**(5): p. 930-42.
45. Banfield, B.W., et al., *Evidence for an interaction of herpes simplex virus with chondroitin sulfate proteoglycans during infection.* Virology, 1995. **208**(2): p. 531-9.

46. Herold, B.C., et al., *Glycoprotein C-independent binding of herpes simplex virus to cells requires cell surface heparan sulphate and glycoprotein B.* J Gen Virol, 1994. **75 (Pt 6)**: p. 1211-22.
47. Herold, B.C., et al., *Glycoprotein C of herpes simplex virus type 1 plays a principal role in the adsorption of virus to cells and in infectivity.* J Virol, 1991. **65**(3): p. 1090-8.
48. Shieh, M.T., et al., *Cell surface receptors for herpes simplex virus are heparan sulfate proteoglycans.* J Cell Biol, 1992. **116**(5): p. 1273-81.
49. Spear, P.G., et al., *Heparan sulfate glycosaminoglycans as primary cell surface receptors for herpes simplex virus.* Adv Exp Med Biol, 1992. **313**: p. 341-53.
50. WuDunn, D. and P.G. Spear, *Initial interaction of herpes simplex virus with cells is binding to heparan sulfate.* J Virol, 1989. **63**(1): p. 52-8.
51. Montgomery, R.I., et al., *Herpes simplex virus-1 entry into cells mediated by a novel member of the TNF/NGF receptor family.* Cell, 1996. **87**(3): p. 427-36.
52. Whitbeck, J.C., et al., *Glycoprotein D of herpes simplex virus (HSV) binds directly to HVEM, a member of the tumor necrosis factor receptor superfamily and a mediator of HSV entry.* J Virol, 1997. **71**(8): p. 6083-93.
53. Krummenacher, C., et al., *Herpes simplex virus glycoprotein D can bind to poliovirus receptor-related protein 1 or herpesvirus entry mediator, two structurally unrelated mediators of virus entry.* J Virol, 1998. **72**(9): p. 7064-74.
54. Cocchi, F., et al., *Cell-to-cell spread of wild-type herpes simplex virus type 1, but not of syncytial strains, is mediated by the immunoglobulin-like receptors that mediate virion entry, nectin1 (PRR1/HveC/HIgR) and nectin2 (PRR2/HveB).* J Virol, 2000. **74**(8): p. 3909-17.
55. Warner, M.S., et al., *A cell surface protein with herpesvirus entry activity (HveB) confers susceptibility to infection by mutants of herpes simplex virus type 1, herpes simplex virus type 2, and pseudorabies virus.* Virology, 1998. **246**(1): p. 179-89.
56. Shukla, D., et al., *A novel role for 3-O-sulfated heparan sulfate in herpes simplex virus 1 entry.* Cell, 1999. **99**(1): p. 13-22.
57. Yoon, M., et al., *Mutations in the N termini of herpes simplex virus type 1 and 2 gDs alter functional interactions with the entry/fusion receptors HVEM, nectin-2, and 3-O-sulfated heparan sulfate but not with nectin-1.* J Virol, 2003. **77**(17): p. 9221-31.
58. Jackson, J.O. and R. Longnecker, *Reevaluating herpes simplex virus hemifusion.* J Virol, 2010. **84**(22): p. 11814-21.
59. Luby-Phelps, K., *Physical properties of cytoplasm.* Curr Opin Cell Biol, 1994. **6**(1): p. 3-9.
60. Sodeik, B., M.W. Ebersold, and A. Helenius, *Microtubule-mediated transport of incoming herpes simplex virus 1 capsids to the nucleus.* J Cell Biol, 1997. **136**(5): p. 1007-21.

61. Radtke, K., et al., *Plus- and minus-end directed microtubule motors bind simultaneously to herpes simplex virus capsids using different inner tegument structures.* PLoS Pathog, 2010. **6**(7): p. e1000991.
62. Hancock, W.O., *Bidirectional cargo transport: moving beyond tug of war.* Nat Rev Mol Cell Biol, 2014. **15**(9): p. 615-28.
63. Schipke, J., et al., *The C terminus of the large tegument protein pUL36 contains multiple capsid binding sites that function differently during assembly and cell entry of herpes simplex virus.* J Virol, 2012. **86**(7): p. 3682-700.
64. Abaitua, F., et al., *A Nuclear localization signal in herpesvirus protein VP1-2 is essential for infection via capsid routing to the nuclear pore.* J Virol, 2012. **86**(17): p. 8998-9014.
65. Ojala, P.M., et al., *Herpes simplex virus type 1 entry into host cells: reconstitution of capsid binding and uncoating at the nuclear pore complex in vitro.* Mol Cell Biol, 2000. **20**(13): p. 4922-31.
66. Copeland, A.M., W.W. Newcomb, and J.C. Brown, *Herpes simplex virus replication: roles of viral proteins and nucleoporins in capsid-nucleus attachment.* J Virol, 2009. **83**(4): p. 1660-8.
67. Pasdeloup, D., et al., *Herpesvirus capsid association with the nuclear pore complex and viral DNA release involve the nucleoporin CAN/Nup214 and the capsid protein pUL25.* J Virol, 2009. **83**(13): p. 6610-23.
68. Bauer, D.W., et al., *Herpes virus genome, the pressure is on.* J Am Chem Soc, 2013. **135**(30): p. 11216-21.
69. Fay, N. and N. Pante, *Nuclear entry of DNA viruses.* Front Microbiol, 2015. **6**: p. 467.
70. Garber, D.A., S.M. Beverley, and D.M. Coen, *Demonstration of circularization of herpes simplex virus DNA following infection using pulsed field gel electrophoresis.* Virology, 1993. **197**(1): p. 459-62.
71. Poffenberger, K.L. and B. Roizman, *A noninverting genome of a viable herpes simplex virus 1: presence of head-to-tail linkages in packaged genomes and requirements for circularization after infection.* J Virol, 1985. **53**(2): p. 587-95.
72. Strang, B.L. and N.D. Stow, *Circularization of the herpes simplex virus type 1 genome upon lytic infection.* J Virol, 2005. **79**(19): p. 12487-94.
73. Lu, X. and S.J. Triezenberg, *Chromatin assembly on herpes simplex virus genomes during lytic infection.* Biochim Biophys Acta, 2010. **1799**(3-4): p. 217-22.
74. Placek, B.J. and S.L. Berger, *Chromatin dynamics during herpes simplex virus-1 lytic infection.* Biochim Biophys Acta, 2010. **1799**(3-4): p. 223-7.
75. Gerster, T. and R.G. Roeder, *A herpesvirus trans-activating protein interacts with transcription factor OTF-1 and other cellular proteins.* Proc Natl Acad Sci U S A, 1988. **85**(17): p. 6347-51.

76. Herrera, F.J. and S.J. Triezenberg, *VP16-dependent association of chromatin-modifying coactivators and underrepresentation of histones at immediate-early gene promoters during herpes simplex virus infection.* J Virol, 2004. **78**(18): p. 9689-96.
77. Katan, M., et al., *Characterization of a cellular factor which interacts functionally with Oct-1 in the assembly of a multicomponent transcription complex.* Nucleic Acids Res, 1990. **18**(23): p. 6871-80.
78. O'Hare, P. and C.R. Goding, *Herpes simplex virus regulatory elements and the immunoglobulin octamer domain bind a common factor and are both targets for virion transactivation.* Cell, 1988. **52**(3): p. 435-45.
79. O'Hare, P., C.R. Goding, and A. Haigh, *Direct combinatorial interaction between a herpes simplex virus regulatory protein and a cellular octamer-binding factor mediates specific induction of virus immediate-early gene expression.* EMBO J, 1988. **7**(13): p. 4231-8.
80. Cordingley, M.G., M.E. Campbell, and C.M. Preston, *Functional analysis of a herpes simplex virus type 1 promoter: identification of far-upstream regulatory sequences.* Nucleic Acids Res, 1983. **11**(8): p. 2347-65.
81. Kristie, T.M. and B. Roizman, *Separation of sequences defining basal expression from those conferring alpha gene recognition within the regulatory domains of herpes simplex virus 1 alpha genes.* Proc Natl Acad Sci U S A, 1984. **81**(13): p. 4065-9.
82. Mackem, S. and B. Roizman, *Structural features of the herpes simplex virus alpha gene 4, 0, and 27 promoter-regulatory sequences which confer alpha regulation on chimeric thymidine kinase genes.* J Virol, 1982. **44**(3): p. 939-49.
83. Gu, H. and Y. Zheng, *Role of ND10 nuclear bodies in the chromatin repression of HSV-1.* Virol J, 2016. **13**: p. 62.
84. Boutell, C. and R.D. Everett, *Regulation of alphaherpesvirus infections by the ICP0 family of proteins.* J Gen Virol, 2013. **94**(Pt 3): p. 465-81.
85. Orzalli, M.H., N.A. DeLuca, and D.M. Knipe, *Nuclear IFI16 induction of IRF-3 signaling during herpesviral infection and degradation of IFI16 by the viral ICP0 protein.* Proc Natl Acad Sci U S A, 2012. **109**(44): p. E3008-17.
86. Mavromara-Nazos, P., et al., *Regulation of herpes simplex virus 1 genes: alpha gene sequence requirements for transient induction of indicator genes regulated by beta or late (gamma 2) promoters.* Virology, 1986. **149**(2): p. 152-64.
87. Kato, K., et al., *Synthesis, subcellular localization and VP16 interaction of the herpes simplex virus type 2 UL46 gene product.* Arch Virol, 2000. **145**(10): p. 2149-62.
88. McKnight, J.L., et al., *Characterization and nucleotide sequence of two herpes simplex virus 1 genes whose products modulate alpha-trans-inducing factor-dependent activation of alpha genes.* J Virol, 1987. **61**(4): p. 992-1001.

89. Vittone, V., et al., *Determination of interactions between tegument proteins of herpes simplex virus type 1.* J Virol, 2005. **79**(15): p. 9566-71.
90. Zhang, Y., D.A. Sirko, and J.L. McKnight, *Role of herpes simplex virus type 1 UL46 and UL47 in alpha TIF-mediated transcriptional induction: characterization of three viral deletion mutants.* J Virol, 1991. **65**(2): p. 829-41.
91. Everett, R.D., *Trans activation of transcription by herpes virus products: requirement for two HSV-1 immediate-early polypeptides for maximum activity.* EMBO J, 1984. **3**(13): p. 3135-41.
92. Gelman, I.H. and S. Silverstein, *Identification of immediate early genes from herpes simplex virus that transactivate the virus thymidine kinase gene.* Proc Natl Acad Sci U S A, 1985. **82**(16): p. 5265-9.
93. O'Hare, P. and G.S. Hayward, *Evidence for a direct role for both the 175,000- and 110,000-molecular-weight immediate-early proteins of herpes simplex virus in the transactivation of delayed-early promoters.* J Virol, 1985. **53**(3): p. 751-60.
94. Sze, P. and R.C. Herman, *The herpes simplex virus type 1 ICP6 gene is regulated by a 'leaky' early promoter.* Virus Res, 1992. **26**(2): p. 141-52.
95. Boehmer, P.E. and I.R. Lehman, *Herpes simplex virus DNA replication.* Annu Rev Biochem, 1997. **66**: p. 347-84.
96. Hardwicke, M.A. and P.A. Schaffer, *Cloning and characterization of herpes simplex virus type 1 oriL: comparison of replication and protein-DNA complex formation by oriL and oriS.* J Virol, 1995. **69**(3): p. 1377-88.
97. Olivo, P.D., N.J. Nelson, and M.D. Challberg, *Herpes simplex virus DNA replication: the UL9 gene encodes an origin-binding protein.* Proc Natl Acad Sci U S A, 1988. **85**(15): p. 5414-8.
98. Boehmer, P.E., M.S. Dodson, and I.R. Lehman, *The herpes simplex virus type-1 origin binding protein. DNA helicase activity.* J Biol Chem, 1993. **268**(2): p. 1220-5.
99. Boehmer, P.E. and I.R. Lehman, *Physical interaction between the herpes simplex virus 1 origin-binding protein and single-stranded DNA-binding protein ICP8.* Proc Natl Acad Sci U S A, 1993. **90**(18): p. 8444-8.
100. Crute, J.J., E.S. Mocarski, and I.R. Lehman, *A DNA helicase induced by herpes simplex virus type 1.* Nucleic Acids Res, 1988. **16**(14A): p. 6585-96.
101. Sherman, G., J. Gottlieb, and M.D. Challberg, *The UL8 subunit of the herpes simplex virus helicase-primase complex is required for efficient primer utilization.* J Virol, 1992. **66**(8): p. 4884-92.
102. Jacob, R.J., L.S. Morse, and B. Roizman, *Anatomy of herpes simplex virus DNA. XII. Accumulation of head-to-tail concatemers in nuclei of infected cells and their role in the generation of the four isomeric arrangements of viral DNA.* J Virol, 1979. **29**(2): p. 448-57.

103. Weller, S.K. and J.A. Sawitzke, *Recombination promoted by DNA viruses: phage lambda to herpes simplex virus.* Annu Rev Microbiol, 2014. **68**: p. 237-58.
104. Conley, A.J., et al., *Molecular genetics of herpes simplex virus. VII. Characterization of a temperature-sensitive mutant produced by in vitro mutagenesis and defective in DNA synthesis and accumulation of gamma polypeptides.* J Virol, 1981. **37**(1): p. 191-206.
105. Huang, C.J. and E.K. Wagner, *The herpes simplex virus type 1 major capsid protein (VP5-UL19) promoter contains two cis-acting elements influencing late expression.* J Virol, 1994. **68**(9): p. 5738-47.
106. Lieu, P.T. and E.K. Wagner, *Two leaky-late HSV-1 promoters differ significantly in structural architecture.* Virology, 2000. **272**(1): p. 191-203.
107. Baines, J.D., *Herpes simplex virus capsid assembly and DNA packaging: a present and future antiviral drug target.* Trends Microbiol, 2011. **19**(12): p. 606-13.
108. Desai, P. and S. Person, *Molecular interactions between the HSV-1 capsid proteins as measured by the yeast two-hybrid system.* Virology, 1996. **220**(2): p. 516-21.
109. Hong, Z., et al., *Identification of a minimal hydrophobic domain in the herpes simplex virus type 1 scaffolding protein which is required for interaction with the major capsid protein.* J Virol, 1996. **70**(1): p. 533-40.
110. Thomsen, D.R., et al., *Assembly of the herpes simplex virus capsid: requirement for the carboxyl-terminal twenty-five amino acids of the proteins encoded by the UL26 and UL26.5 genes.* J Virol, 1995. **69**(6): p. 3690-703.
111. Zhou, Z.H., et al., *Identification of the sites of interaction between the scaffold and outer shell in herpes simplex virus-1 capsids by difference electron imaging.* Proc Natl Acad Sci U S A, 1998. **95**(6): p. 2778-83.
112. Gao, M., et al., *The protease of herpes simplex virus type 1 is essential for functional capsid formation and viral growth.* J Virol, 1994. **68**(6): p. 3702-12.
113. Nicholson, P., et al., *Localization of the herpes simplex virus type 1 major capsid protein VP5 to the cell nucleus requires the abundant scaffolding protein VP22a.* J Gen Virol, 1994. **75 (Pt 5)**: p. 1091-9.
114. Preston, V.G., J.A. Coates, and F.J. Rixon, *Identification and characterization of a herpes simplex virus gene product required for encapsidation of virus DNA.* J Virol, 1983. **45**(3): p. 1056-64.
115. Rixon, F.J. and D. McNab, *Packaging-competent capsids of a herpes simplex virus temperature-sensitive mutant have properties similar to those of in vitro-assembled procapsids.* J Virol, 1999. **73**(7): p. 5714-21.
116. Newcomb, W.W., et al., *Assembly of the herpes simplex virus capsid: identification of soluble scaffold-portal complexes and their role in formation of portal-containing capsids.* J Virol, 2003. **77**(18): p. 9862-71.

117. Singer, G.P., et al., *Identification of a region in the herpes simplex virus scaffolding protein required for interaction with the portal.* J Virol, 2005. **79**(1): p. 132-9.
118. Dasgupta, A. and D.W. Wilson, *ATP depletion blocks herpes simplex virus DNA packaging and capsid maturation.* J Virol, 1999. **73**(3): p. 2006-15.
119. Bubeck, A., et al., *Comprehensive mutational analysis of a herpesvirus gene in the viral genome context reveals a region essential for virus replication.* J Virol, 2004. **78**(15): p. 8026-35.
120. Chang, Y.E. and B. Roizman, *The product of the UL31 gene of herpes simplex virus 1 is a nuclear phosphoprotein which partitions with the nuclear matrix.* J Virol, 1993. **67**(11): p. 6348-56.
121. Reynolds, A.E., et al., *U(L)31 and U(L)34 proteins of herpes simplex virus type 1 form a complex that accumulates at the nuclear rim and is required for envelopment of nucleocapsids.* J Virol, 2001. **75**(18): p. 8803-17.
122. Roller, R.J., et al., *Herpes simplex virus type 1 U(L)34 gene product is required for viral envelopment.* J Virol, 2000. **74**(1): p. 117-29.
123. Bjerke, S.L. and R.J. Roller, *Roles for herpes simplex virus type 1 UL34 and US3 proteins in disrupting the nuclear lamina during herpes simplex virus type 1 egress.* Virology, 2006. **347**(2): p. 261-76.
124. Leach, N.R. and R.J. Roller, *Significance of host cell kinases in herpes simplex virus type 1 egress and lamin-associated protein disassembly from the nuclear lamina.* Virology, 2010. **406**(1): p. 127-37.
125. Reynolds, A.E., L. Liang, and J.D. Baines, *Conformational changes in the nuclear lamina induced by herpes simplex virus type 1 require genes U(L)31 and U(L)34.* J Virol, 2004. **78**(11): p. 5564-75.
126. Park, R. and J.D. Baines, *Herpes simplex virus type 1 infection induces activation and recruitment of protein kinase C to the nuclear membrane and increased phosphorylation of lamin B.* J Virol, 2006. **80**(1): p. 494-504.
127. Mou, F., T. Forest, and J.D. Baines, *US3 of herpes simplex virus type 1 encodes a promiscuous protein kinase that phosphorylates and alters localization of lamin A/C in infected cells.* J Virol, 2007. **81**(12): p. 6459-70.
128. Simpson-Holley, M., et al., *Herpes simplex virus 1 U(L)31 and U(L)34 gene products promote the late maturation of viral replication compartments to the nuclear periphery.* J Virol, 2004. **78**(11): p. 5591-600.
129. Trus, B.L., et al., *Allosteric signaling and a nuclear exit strategy: binding of UL25/UL17 heterodimers to DNA-Filled HSV-1 capsids.* Mol Cell, 2007. **26**(4): p. 479-89.
130. Cockrell, S.K., et al., *Residues of the UL25 protein of herpes simplex virus that are required for its stable interaction with capsids.* J Virol, 2011. **85**(10): p. 4875-87.

131. Toropova, K., et al., *The herpes simplex virus 1 UL17 protein is the second constituent of the capsid vertex-specific component required for DNA packaging and retention.* J Virol, 2011. **85**(15): p. 7513-22.
132. Bigalke, J.M. and E.E. Heldwein, *Have NEC Coat, Will Travel: Structural Basis of Membrane Budding During Nuclear Egress in Herpesviruses.* Adv Virus Res, 2017. **97**: p. 107-141.
133. Bigalke, J.M., et al., *Membrane deformation and scission by the HSV-1 nuclear egress complex.* Nat Commun, 2014. **5**: p. 4131.
134. Klupp, B.G., et al., *Vesicle formation from the nuclear membrane is induced by coexpression of two conserved herpesvirus proteins.* Proc Natl Acad Sci U S A, 2007. **104**(17): p. 7241-6.
135. Mou, F., E. Wills, and J.D. Baines, *Phosphorylation of the U(L)31 protein of herpes simplex virus 1 by the U(S)3-encoded kinase regulates localization of the nuclear envelopment complex and egress of nucleocapsids.* J Virol, 2009. **83**(10): p. 5181-91.
136. Granzow, H., et al., *Egress of alphaherpesviruses: comparative ultrastructural study.* J Virol, 2001. **75**(8): p. 3675-84.
137. Bucks, M.A., et al., *Herpes simplex virus type 1 tegument proteins VP1/2 and UL37 are associated with intranuclear capsids.* Virology, 2007. **361**(2): p. 316-24.
138. Diefenbach, R.J., *Conserved tegument protein complexes: Essential components in the assembly of herpesviruses.* Virus Res, 2015. **210**: p. 308-17.
139. Hollinshead, M., et al., *Endocytic tubules regulated by Rab GTPases 5 and 11 are used for envelopment of herpes simplex virus.* EMBO J, 2012. **31**(21): p. 4204-20.
140. Sugimoto, K., et al., *Simultaneous tracking of capsid, tegument, and envelope protein localization in living cells infected with triply fluorescent herpes simplex virus 1.* J Virol, 2008. **82**(11): p. 5198-211.
141. Turcotte, S., J. Letellier, and R. Lippe, *Herpes simplex virus type 1 capsids transit by the trans-Golgi network, where viral glycoproteins accumulate independently of capsid egress.* J Virol, 2005. **79**(14): p. 8847-60.
142. Alconada, A., et al., *Intracellular traffic of herpes simplex virus glycoprotein gE: characterization of the sorting signals required for its trans-Golgi network localization.* J Virol, 1999. **73**(1): p. 377-87.
143. Farnsworth, A. and D.C. Johnson, *Herpes simplex virus gE/gI must accumulate in the trans-Golgi network at early times and then redistribute to cell junctions to promote cell-cell spread.* J Virol, 2006. **80**(7): p. 3167-79.
144. Farnsworth, A., T.W. Wisner, and D.C. Johnson, *Cytoplasmic residues of herpes simplex virus glycoprotein gE required for secondary envelopment and binding of tegument proteins VP22 and UL11 to gE and gD.* J Virol, 2007. **81**(1): p. 319-31.

145. McMillan, T.N. and D.C. Johnson, *Cytoplasmic domain of herpes simplex virus gE causes accumulation in the trans-Golgi network, a site of virus envelopment and sorting of virions to cell junctions.* J Virol, 2001. **75**(4): p. 1928-40.
146. Cardone, G., et al., *The UL36 tegument protein of herpes simplex virus 1 has a composite binding site at the capsid vertices.* J Virol, 2012. **86**(8): p. 4058-64.
147. Zhou, Z.H., et al., *Visualization of tegument-capsid interactions and DNA in intact herpes simplex virus type 1 virions.* J Virol, 1999. **73**(4): p. 3210-8.
148. Coller, K.E., et al., *The capsid and tegument of the alphaherpesviruses are linked by an interaction between the UL25 and VP1/2 proteins.* J Virol, 2007. **81**(21): p. 11790-7.
149. Fan, W.H., et al., *The large tegument protein pUL36 is essential for formation of the capsid vertex-specific component at the capsid-tegument interface of herpes simplex virus 1.* J Virol, 2015. **89**(3): p. 1502-11.
150. Laine, R.F., et al., *Structural analysis of herpes simplex virus by optical super-resolution imaging.* Nat Commun, 2015. **6**: p. 5980.
151. Jambunathan, N., et al., *Herpes simplex virus 1 protein UL37 interacts with viral glycoprotein gK and membrane protein UL20 and functions in cytoplasmic virion envelopment.* J Virol, 2014. **88**(11): p. 5927-35.
152. Maringer, K., J. Stylianou, and G. Elliott, *A network of protein interactions around the herpes simplex virus tegument protein VP22.* J Virol, 2012. **86**(23): p. 12971-82.
153. Stevens, J.G. and M.L. Cook, *Latent herpes simplex virus in spinal ganglia of mice.* Science, 1971. **173**(3999): p. 843-5.
154. Kubat, N.J., et al., *Specific histone tail modification and not DNA methylation is a determinant of herpes simplex virus type 1 latent gene expression.* J Virol, 2004. **78**(3): p. 1139-49.
155. Kubat, N.J., et al., *The herpes simplex virus type 1 latency-associated transcript (LAT) enhancer/rcr is hyperacetylated during latency independently of LAT transcription.* J Virol, 2004. **78**(22): p. 12508-18.
156. Neumann, D.M., et al., *In vivo changes in the patterns of chromatin structure associated with the latent herpes simplex virus type 1 genome in mouse trigeminal ganglia can be detected at early times after butyrate treatment.* J Virol, 2007. **81**(23): p. 13248-53.
157. Wang, Q.Y., et al., *Herpesviral latency-associated transcript gene promotes assembly of heterochromatin on viral lytic-gene promoters in latent infection.* Proc Natl Acad Sci U S A, 2005. **102**(44): p. 16055-9.
158. Hill, J.M., et al., *Herpes simplex virus latent phase transcription facilitates in vivo reactivation.* Virology, 1990. **174**(1): p. 117-25.
159. Leib, D.A., et al., *A deletion mutant of the latency-associated transcript of herpes simplex virus type 1 reactivates from the latent state with reduced frequency.* J Virol, 1989. **63**(7): p. 2893-900.

160. Roizman, B. and R.J. Whitley, *An inquiry into the molecular basis of HSV latency and reactivation.* Annu Rev Microbiol, 2013. **67**: p. 355-74.
161. Decman, V., et al., *Gamma interferon can block herpes simplex virus type 1 reactivation from latency, even in the presence of late gene expression.* J Virol, 2005. **79**(16): p. 10339-47.
162. Khanna, K.M., et al., *Herpes simplex virus-specific memory CD8+ T cells are selectively activated and retained in latently infected sensory ganglia.* Immunity, 2003. **18**(5): p. 593-603.
163. Liu, T., et al., *Gamma interferon can prevent herpes simplex virus type 1 reactivation from latency in sensory neurons.* J Virol, 2001. **75**(22): p. 11178-84.
164. Liu, T., et al., *CD8(+) T cells can block herpes simplex virus type 1 (HSV-1) reactivation from latency in sensory neurons.* J Exp Med, 2000. **191**(9): p. 1459-66.
165. Camarena, V., et al., *Nature and duration of growth factor signaling through receptor tyrosine kinases regulates HSV-1 latency in neurons.* Cell Host Microbe, 2010. **8**(4): p. 320-30.
166. Kobayashi, M., et al., *A primary neuron culture system for the study of herpes simplex virus latency and reactivation.* J Vis Exp, 2012(62).
167. Kobayashi, M., et al., *Control of viral latency in neurons by axonal mTOR signaling and the 4E-BP translation repressor.* Genes Dev, 2012. **26**(14): p. 1527-32.
168. Wilcox, C.L. and E.M. Johnson, Jr., *Nerve growth factor deprivation results in the reactivation of latent herpes simplex virus in vitro.* J Virol, 1987. **61**(7): p. 2311-5.
169. Wilcox, C.L. and E.M. Johnson, Jr., *Characterization of nerve growth factor-dependent herpes simplex virus latency in neurons in vitro.* J Virol, 1988. **62**(2): p. 393-9.
170. Wilcox, C.L., et al., *Nerve growth factor-dependence of herpes simplex virus latency in peripheral sympathetic and sensory neurons in vitro.* J Neurosci, 1990. **10**(4): p. 1268-75.
171. Dobson, A.T., et al., *Identification of the latency-associated transcript promoter by expression of rabbit beta-globin mRNA in mouse sensory nerve ganglia latently infected with a recombinant herpes simplex virus.* J Virol, 1989. **63**(9): p. 3844-51.
172. Bloom, D.C., *Alphaherpesvirus Latency: A Dynamic State of Transcription and Reactivation.* Adv Virus Res, 2016. **94**: p. 53-80.
173. Frappier, L., *Regulation of herpesvirus reactivation by host microRNAs.* J Virol, 2015. **89**(5): p. 2456-8.
174. Jiang, X., et al., *Increased neurovirulence and reactivation of the herpes simplex virus type 1 latency-associated transcript (LAT)-negative mutant dLAT2903 with a disrupted LAT miR-H2.* J Neurovirol, 2016. **22**(1): p. 38-49.

175. Jiang, X., et al., *A herpes simplex virus type 1 mutant disrupted for microRNA H2 with increased neurovirulence and rate of reactivation.* J Neurovirol, 2015. **21**(2): p. 199-209.
176. Pan, D., et al., *A neuron-specific host microRNA targets herpes simplex virus-1 ICP0 expression and promotes latency.* Cell Host Microbe, 2014. **15**(4): p. 446-56.
177. Dempsey, P.W., S.A. Vaidya, and G. Cheng, *The art of war: Innate and adaptive immune responses.* Cell Mol Life Sci, 2003. **60**(12): p. 2604-21.
178. Chew, T., K.E. Taylor, and K.L. Mossman, *Innate and adaptive immune responses to herpes simplex virus.* Viruses, 2009. **1**(3): p. 979-1002.
179. McNab, F., et al., *Type I interferons in infectious disease.* Nat Rev Immunol, 2015. **15**(2): p. 87-103.
180. Su, C. and C. Zheng, *Herpes Simplex Virus 1 Abrogates the cGAS/STING-Mediated Cytosolic DNA-Sensing Pathway via Its Virion Host Shutoff Protein, UL41.* J Virol, 2017. **91**(6).
181. Kalamvoki, M. and B. Roizman, *HSV-1 degrades, stabilizes, requires, or is stung by STING depending on ICP0, the US3 protein kinase, and cell derivation.* Proc Natl Acad Sci U S A, 2014. **111**(5): p. E611-7.
182. Christensen, M.H., et al., *HSV-1 ICP27 targets the TBK1-activated STING signalsome to inhibit virus-induced type I IFN expression.* EMBO J, 2016. **35**(13): p. 1385-99.
183. Deschamps, T. and M. Kalamvoki, *Evasion of the STING DNA-Sensing Pathway by VP11/12 of Herpes Simplex Virus 1.* J Virol, 2017. **91**(16).
184. Cuchet-Lourenco, D., et al., *The viral ubiquitin ligase ICP0 is neither sufficient nor necessary for degradation of the cellular DNA sensor IFI16 during herpes simplex virus 1 infection.* J Virol, 2013. **87**(24): p. 13422-32.
185. Johnson, K.E., L. Chikoti, and B. Chandran, *Herpes simplex virus 1 infection induces activation and subsequent inhibition of the IFI16 and NLRP3 inflammasomes.* J Virol, 2013. **87**(9): p. 5005-18.
186. Xing, J., et al., *Herpes simplex virus 1 tegument protein US11 downmodulates the RLR signaling pathway via direct interaction with RIG-I and MDA-5.* J Virol, 2012. **86**(7): p. 3528-40.
187. Peri, P., et al., *Herpes simplex virus type 1 Us3 gene deletion influences toll-like receptor responses in cultured monocytic cells.* Virol J, 2008. **5**: p. 140.
188. Poppers, J., et al., *Inhibition of PKR activation by the proline-rich RNA binding domain of the herpes simplex virus type 1 Us11 protein.* J Virol, 2000. **74**(23): p. 11215-21.
189. Dauber, B., et al., *The Herpes Simplex Virus Virion Host Shutoff Protein Enhances Translation of Viral True Late mRNAs Independently of Suppressing Protein Kinase R and Stress Granule Formation.* J Virol, 2016. **90**(13): p. 6049-57.

190. Pasieka, T.J., et al., *Herpes simplex virus virion host shutoff attenuates establishment of the antiviral state.* J Virol, 2008. **82**(11): p. 5527-35.
191. Sciortino, M.T., et al., *The virion host shutoff RNase plays a key role in blocking the activation of protein kinase R in cells infected with herpes simplex virus 1.* J Virol, 2013. **87**(6): p. 3271-6.
192. Wang, S., et al., *Herpes simplex virus 1 serine/threonine kinase US3 hyperphosphorylates IRF3 and inhibits beta interferon production.* J Virol, 2013. **87**(23): p. 12814-27.
193. Xing, J., et al., *Herpes simplex virus 1-encoded tegument protein VP16 abrogates the production of beta interferon (IFN) by inhibiting NF-kappaB activation and blocking IFN regulatory factor 3 to recruit its coactivator CBP.* J Virol, 2013. **87**(17): p. 9788-801.
194. Lin, R., et al., *The herpes simplex virus ICP0 RING finger domain inhibits IRF3- and IRF7-mediated activation of interferon-stimulated genes.* J Virol, 2004. **78**(4): p. 1675-84.
195. Wang, S., et al., *Herpes simplex virus 1 ubiquitin-specific protease UL36 inhibits beta interferon production by deubiquitinating TRAF3.* J Virol, 2013. **87**(21): p. 11851-60.
196. Deshpande, S.P., U. Kumaraguru, and B.T. Rouse, *Dual role of B cells in mediating innate and acquired immunity to herpes simplex virus infections.* Cell Immunol, 2000. **202**(2): p. 79-87.
197. Lubinski, J.M., et al., *The herpes simplex virus 1 IgG fc receptor blocks antibody-mediated complement activation and antibody-dependent cellular cytotoxicity in vivo.* J Virol, 2011. **85**(7): p. 3239-49.
198. Para, M.F., L. Goldstein, and P.G. Spear, *Similarities and differences in the Fc-binding glycoprotein (gE) of herpes simplex virus types 1 and 2 and tentative mapping of the viral gene for this glycoprotein.* J Virol, 1982. **41**(1): p. 137-44.
199. Cunningham, A.L., et al., *Evolution of recurrent herpes simplex lesions. An immunohistologic study.* J Clin Invest, 1985. **75**(1): p. 226-33.
200. Cunningham, A.L., et al., *Interferon gamma production by herpes simplex virus antigen-specific T cell clones from patients with recurrent herpes labialis.* J Gen Virol, 1985. **66 (Pt 2)**: p. 249-58.
201. Koelle, D.M., et al., *Clearance of HSV-2 from recurrent genital lesions correlates with infiltration of HSV-specific cytotoxic T lymphocytes.* J Clin Invest, 1998. **101**(7): p. 1500-8.
202. Zhu, J., et al., *Virus-specific CD8+ T cells accumulate near sensory nerve endings in genital skin during subclinical HSV-2 reactivation.* J Exp Med, 2007. **204**(3): p. 595-603.
203. Hill, A. and H. Ploegh, *Getting the inside out: the transporter associated with antigen processing (TAP) and the presentation of viral antigen.* Proc Natl Acad Sci U S A, 1995. **92**(2): p. 341-3.

204. York, I.A., et al., *A cytosolic herpes simplex virus protein inhibits antigen presentation to CD8+ T lymphocytes.* Cell, 1994. **77**(4): p. 525-35.
205. Hill, A., et al., *Herpes simplex virus turns off the TAP to evade host immunity.* Nature, 1995. **375**(6530): p. 411-5.
206. Imai, T., et al., *Us3 kinase encoded by herpes simplex virus 1 mediates downregulation of cell surface major histocompatibility complex class I and evasion of CD8+ T cells.* PLoS One, 2013. **8**(8): p. e72050.
207. Aubert, M., et al., *The virological synapse facilitates herpes simplex virus entry into T cells.* J Virol, 2009. **83**(12): p. 6171-83.
208. Sloan, D.D., et al., *Inhibition of TCR signaling by herpes simplex virus.* J Immunol, 2006. **176**(3): p. 1825-33.
209. Sloan, D.D. and K.R. Jerome, *Herpes simplex virus remodels T-cell receptor signaling, resulting in p38-dependent selective synthesis of interleukin-10.* J Virol, 2007. **81**(22): p. 12504-14.
210. Gao, G.F. and B.K. Jakobsen, *Molecular interactions of coreceptor CD8 and MHC class I: the molecular basis for functional coordination with the T-cell receptor.* Immunol Today, 2000. **21**(12): p. 630-6.
211. Straus, D.B. and A. Weiss, *Genetic evidence for the involvement of the lck tyrosine kinase in signal transduction through the T cell antigen receptor.* Cell, 1992. **70**(4): p. 585-93.
212. Veillette, A., et al., *The CD4 and CD8 T cell surface antigens are associated with the internal membrane tyrosine-protein kinase p56lck.* Cell, 1988. **55**(2): p. 301-8.
213. Chan, A.C., et al., *ZAP-70: a 70 kd protein-tyrosine kinase that associates with the TCR zeta chain.* Cell, 1992. **71**(4): p. 649-62.
214. Iwashima, M., et al., *Sequential interactions of the TCR with two distinct cytoplasmic tyrosine kinases.* Science, 1994. **263**(5150): p. 1136-9.
215. van Oers, N.S., N. Killeen, and A. Weiss, *Lck regulates the tyrosine phosphorylation of the T cell receptor subunits and ZAP-70 in murine thymocytes.* J Exp Med, 1996. **183**(3): p. 1053-62.
216. Zhang, W., et al., *LAT: the ZAP-70 tyrosine kinase substrate that links T cell receptor to cellular activation.* Cell, 1998. **92**(1): p. 83-92.
217. Finco, T.S., et al., *LAT is required for TCR-mediated activation of PLCgamma1 and the Ras pathway.* Immunity, 1998. **9**(5): p. 617-26.
218. Shim, E.K., S.H. Jung, and J.R. Lee, *Role of two adaptor molecules SLP-76 and LAT in the PI3K signaling pathway in activated T cells.* J Immunol, 2011. **186**(5): p. 2926-35.
219. Dower, N.A., et al., *RasGRP is essential for mouse thymocyte differentiation and TCR signaling.* Nat Immunol, 2000. **1**(4): p. 317-21.
220. Ravichandran, K.S., et al., *Interaction of Shc with the zeta chain of the T cell receptor upon T cell activation.* Science, 1993. **262**(5135): p. 902-5.

221. Osman, N., et al., *A comparison of the interaction of Shc and the tyrosine kinase ZAP-70 with the T cell antigen receptor zeta chain tyrosine-based activation motif.* J Biol Chem, 1995. **270**(23): p. 13981-6.
222. Fukushima, A., et al., *Lck couples Shc to TCR signaling.* Cell Signal, 2006. **18**(8): p. 1182-9.
223. Zhang, W., et al., *Association of Grb2, Gads, and phospholipase C-gamma 1 with phosphorylated LAT tyrosine residues. Effect of LAT tyrosine mutations on T cell angigen receptor-mediated signaling.* J Biol Chem, 2000. **275**(30): p. 23355-61.
224. Wagner, M.J., et al., *Molecular mechanisms of SH2- and PTB-domain-containing proteins in receptor tyrosine kinase signaling.* Cold Spring Harb Perspect Biol, 2013. **5**(12): p. a008987.
225. Sloan, D.D., et al., *CTL are inactivated by herpes simplex virus-infected cells expressing a viral protein kinase.* J Immunol, 2003. **171**(12): p. 6733-41.
226. Chuluunbaatar, U., et al., *Constitutive mTORC1 activation by a herpesvirus Akt surrogate stimulates mRNA translation and viral replication.* Genes Dev, 2010. **24**(23): p. 2627-39.
227. Chuluunbaatar, U., R. Roller, and I. Mohr, *Suppression of extracellular signal-regulated kinase activity in herpes simplex virus 1-infected cells by the Us3 protein kinase.* J Virol, 2012. **86**(15): p. 7771-6.
228. Eaton, H.E., et al., *Herpes simplex virus protein kinases US3 and UL13 modulate VP11/12 phosphorylation, virion packaging, and phosphatidylinositol 3-kinase/Akt signaling activity.* J Virol, 2014. **88**(13): p. 7379-88.
229. Wagner, M.J. and J.R. Smiley, *Herpes simplex virus requires VP11/12 to activate Src family kinase-phosphoinositide 3-kinase-Akt signaling.* J Virol, 2011. **85**(6): p. 2803-12.
230. Zahariadis, G., et al., *Cell-type-specific tyrosine phosphorylation of the herpes simplex virus tegument protein VP11/12 encoded by gene UL46.* J Virol, 2008. **82**(13): p. 6098-108.
231. Hargett, D., T. McLean, and S.L. Bachenheimer, *Herpes simplex virus ICP27 activation of stress kinases JNK and p38.* J Virol, 2005. **79**(13): p. 8348-60.
232. McLean, T.I. and S.L. Bachenheimer, *Activation of cJUN N-terminal kinase by herpes simplex virus type 1 enhances viral replication.* J Virol, 1999. **73**(10): p. 8415-26.
233. Zachos, G., B. Clements, and J. Conner, *Herpes simplex virus type 1 infection stimulates p38/c-Jun N-terminal mitogen-activated protein kinase pathways and activates transcription factor AP-1.* J Biol Chem, 1999. **274**(8): p. 5097-103.
234. Gregory, D., et al., *Efficient replication by herpes simplex virus type 1 involves activation of the IkappaB kinase-IkappaB-p65 pathway.* J Virol, 2004. **78**(24): p. 13582-90.

235. Benetti, L. and B. Roizman, *Protein kinase B/Akt is present in activated form throughout the entire replicative cycle of deltaU(S)3 mutant virus but only at early times after infection with wild-type herpes simplex virus 1.* J Virol, 2006. **80**(7): p. 3341-8.
236. Wagner, M.J., *Herpes Simplex Virus Requires VP11/12 to Activate Src Family Kinase-PI3 Kinase-Akt Signalling.* Ph.D. Thesis, 2010.
237. Huang, G., L.Z. Shi, and H. Chi, *Regulation of JNK and p38 MAPK in the immune system: signal integration, propagation and termination.* Cytokine, 2009. **48**(3): p. 161-9.
238. Rojas, J.M., et al., *IL-10: A Multifunctional Cytokine in Viral Infections.* J Immunol Res, 2017. **2017**: p. 6104054.
239. Zachos, G., et al., *Herpes simplex virus type 1 blocks the apoptotic host cell defense mechanisms that target Bcl-2 and manipulates activation of p38 mitogen-activated protein kinase to improve viral replication.* J Virol, 2001. **75**(6): p. 2710-28.
240. Goodkin, M.L., A.T. Ting, and J.A. Blaho, *NF-kappaB is required for apoptosis prevention during herpes simplex virus type 1 infection.* J Virol, 2003. **77**(13): p. 7261-80.
241. Hargett, D., S. Rice, and S.L. Bachenheimer, *Herpes simplex virus type 1 ICP27-dependent activation of NF-kappaB.* J Virol, 2006. **80**(21): p. 10565-78.
242. Corcoran, J.A., W.L. Hsu, and J.R. Smiley, *Herpes simplex virus ICP27 is required for virus-induced stabilization of the ARE-containing IEX-1 mRNA encoded by the human IER3 gene.* J Virol, 2006. **80**(19): p. 9720-9.
243. Gillis, P.A., L.H. Okagaki, and S.A. Rice, *Herpes simplex virus type 1 ICP27 induces p38 mitogen-activated protein kinase signaling and apoptosis in HeLa cells.* J Virol, 2009. **83**(4): p. 1767-77.
244. Panday, A., et al., *Transcription Factor NF-kappaB: An Update on Intervention Strategies.* Arch Immunol Ther Exp (Warsz), 2016. **64**(6): p. 463-483.
245. Amici, C., et al., *Activation of I kappa b kinase by herpes simplex virus type 1. A novel target for anti-herpetic therapy.* J Biol Chem, 2001. **276**(31): p. 28759-66.
246. Patel, A., et al., *Herpes simplex type 1 induction of persistent NF-kappa B nuclear translocation increases the efficiency of virus replication.* Virology, 1998. **247**(2): p. 212-22.
247. Leoni, V., et al., *Herpes simplex virus glycoproteins gH/gL and gB bind Toll-like receptor 2, and soluble gH/gL is sufficient to activate NF-kappaB.* J Virol, 2012. **86**(12): p. 6555-62.
248. Cai, M., et al., *The herpes simplex virus 1-encoded envelope glycoprotein B activates NF-kappaB through the Toll-like receptor 2 and MyD88/TRAF6-dependent signaling pathway.* PLoS One, 2013. **8**(1): p. e54586.

249. Liu, X., et al., *Herpesvirus tegument protein activates NF-kappaB signaling through the TRAF6 adaptor protein.* Proc Natl Acad Sci U S A, 2008. **105**(32): p. 11335-9.
250. Amici, C., et al., *Herpes simplex virus disrupts NF-kappaB regulation by blocking its recruitment on the IkappaBalpha promoter and directing the factor on viral genes.* J Biol Chem, 2006. **281**(11): p. 7110-7.
251. Kelly, J.D., et al., *Platelet-derived growth factor (PDGF) stimulates PDGF receptor subunit dimerization and intersubunit trans-phosphorylation.* J Biol Chem, 1991. **266**(14): p. 8987-92.
252. Wu, H., et al., *YXXM motifs in the PDGF-beta receptor serve dual roles as phosphoinositide 3-kinase binding motifs and tyrosine-based endocytic sorting signals.* J Biol Chem, 2003. **278**(42): p. 40425-8.
253. Liu, P., et al., *Targeting the phosphoinositide 3-kinase pathway in cancer.* Nat Rev Drug Discov, 2009. **8**(8): p. 627-44.
254. Alessi, D.R., et al., *Characterization of a 3-phosphoinositide-dependent protein kinase which phosphorylates and activates protein kinase Balpha.* Curr Biol, 1997. **7**(4): p. 261-9.
255. Sarbassov, D.D., et al., *Phosphorylation and regulation of Akt/PKB by the rictor-mTOR complex.* Science, 2005. **307**(5712): p. 1098-101.
256. Manning, B.D. and L.C. Cantley, *AKT/PKB signaling: navigating downstream.* Cell, 2007. **129**(7): p. 1261-74.
257. Roux, P.P. and I. Topisirovic, *Regulation of mRNA translation by signaling pathways.* Cold Spring Harb Perspect Biol, 2012. **4**(11).
258. Mannova, P. and L. Beretta, *Activation of the N-Ras-PI3K-Akt-mTOR pathway by hepatitis C virus: control of cell survival and viral replication.* J Virol, 2005. **79**(14): p. 8742-9.
259. Shin, Y.K., et al., *Influenza A virus NS1 protein activates the phosphatidylinositol 3-kinase (PI3K)/Akt pathway by direct interaction with the p85 subunit of PI3K.* J Gen Virol, 2007. **88**(Pt 1): p. 13-8.
260. Ichaso, N. and S.M. Dilworth, *Cell transformation by the middle T-antigen of polyoma virus.* Oncogene, 2001. **20**(54): p. 7908-16.
261. Chuluunbaatar, U. and I. Mohr, *A herpesvirus kinase that masquerades as Akt: you don't have to look like Akt, to act like it.* Cell Cycle, 2011. **10**(13): p. 2064-8.
262. Munger, J. and B. Roizman, *The US3 protein kinase of herpes simplex virus 1 mediates the posttranslational modification of BAD and prevents BAD-induced programmed cell death in the absence of other viral proteins.* Proc Natl Acad Sci U S A, 2001. **98**(18): p. 10410-5.
263. Nozawa, N., et al., *Formation of aggresome-like structures in herpes simplex virus type 2-infected cells and a potential role in virus assembly.* Exp Cell Res, 2004. **299**(2): p. 486-97.

264. Willard, M., *Rapid directional translocations in virus replication.* J Virol, 2002. **76**(10): p. 5220-32.
265. Murphy, M.A., et al., *The HSV-1 tegument protein pUL46 associates with cellular membranes and viral capsids.* Virology, 2008. **376**(2): p. 279-89.
266. Wagner, M.J. and J.R. Smiley, *Herpes simplex virus requires VP11/12 to induce phosphorylation of the activation loop tyrosine (Y394) of the Src family kinase Lck in T lymphocytes.* J Virol, 2009. **83**(23): p. 12452-61.
267. Engen, J.R., et al., *Structure and dynamic regulation of Src-family kinases.* Cell Mol Life Sci, 2008. **65**(19): p. 3058-73.
268. Songyang, Z., et al., *SH2 domains recognize specific phosphopeptide sequences.* Cell, 1993. **72**(5): p. 767-78.
269. Dunant, N.M., A.S. Messerschmitt, and K. Ballmer-Hofer, *Functional interaction between the SH2 domain of Fyn and tyrosine 324 of hamster polyomavirus middle-T antigen.* J Virol, 1997. **71**(1): p. 199-206.
270. Bresnahan, W.A., G.E. Hultman, and T. Shenk, *Replication of wild-type and mutant human cytomegalovirus in life-extended human diploid fibroblasts.* J Virol, 2000. **74**(22): p. 10816-8.
271. Tischer, B.K., G.A. Smith, and N. Osterrieder, *En passant mutagenesis: a two step markerless red recombination system.* Methods Mol Biol, 2010. **634**: p. 421-30.
272. Minaker, R.L., K.L. Mossman, and J.R. Smiley, *Functional inaccessibility of quiescent herpes simplex virus genomes.* Virol J, 2005. **2**: p. 85.
273. Gierasch, W.W., et al., *Construction and characterization of bacterial artificial chromosomes containing HSV-1 strains 17 and KOS.* J Virol Methods, 2006. **135**(2): p. 197-206.
274. Zagursky, R.J. and J.B. Hays, *Expression of the phage lambda recombination genes exo and bet under lacPO control on a multi-copy plasmid.* Gene, 1983. **23**(3): p. 277-92.
275. Sakaki, Y., et al., *Purification and properties of the gamma-protein specified by bacteriophage lambda: an inhibitor of the host RecBC recombination enzyme.* Proc Natl Acad Sci U S A, 1973. **70**(8): p. 2215-9.
276. Kovall, R. and B.W. Matthews, *Toroidal structure of lambda-exonuclease.* Science, 1997. **277**(5333): p. 1824-7.
277. Weissbach, A. and D. Korn, *The effect of lysogenic induction on the deoxyribonucleases of Escherichia coli K12 lambda.* J Biol Chem, 1962. **237**: p. PC3312-PC3314.
278. Colleaux, L., et al., *Universal code equivalent of a yeast mitochondrial intron reading frame is expressed into E. coli as a specific double strand endonuclease.* Cell, 1986. **44**(4): p. 521-33.
279. Strunk, U., et al., *Role of herpes simplex virus VP11/12 tyrosine-based motifs in binding and activation of the Src family kinase Lck and recruitment of p85, Grb2, and Shc.* J Virol, 2013. **87**(20): p. 11276-86.

280. Obenauer, J.C., L.C. Cantley, and M.B. Yaffe, *Scansite 2.0: Proteome-wide prediction of cell signaling interactions using short sequence motifs.* Nucleic Acids Res, 2003. **31**(13): p. 3635-41.
281. McNemar, C., et al., *Thermodynamic and structural analysis of phosphotyrosine polypeptide binding to Grb2-SH2.* Biochemistry, 1997. **36**(33): p. 10006-14.
282. Ogura, K., et al., *Solution structure of the SH2 domain of Grb2 complexed with the Shc-derived phosphotyrosine-containing peptide.* J Mol Biol, 1999. **289**(3): p. 439-45.
283. McGlade, C.J., et al., *SH2 domains of the p85 alpha subunit of phosphatidylinositol 3-kinase regulate binding to growth factor receptors.* Mol Cell Biol, 1992. **12**(3): p. 991-7.
284. Piccione, E., et al., *Phosphatidylinositol 3-kinase p85 SH2 domain specificity defined by direct phosphopeptide/SH2 domain binding.* Biochemistry, 1993. **32**(13): p. 3197-202.
285. Kavanaugh W.M., T.C.W., Williams L.T., *PTB domain binding to signaling proteins through a sequence motif containing phosphotyrosine.* Science, 1995. **268**(5214): p. 1177-9.
286. Warming, S., et al., *Simple and highly efficient BAC recombineering using galK selection.* Nucleic Acids Res, 2005. **33**(4): p. e36.
287. Feng, S., et al., *Two binding orientations for peptides to the Src SH3 domain: development of a general model for SH3-ligand interactions.* Science, 1994. **266**(5188): p. 1241-7.
288. Lim, W.A., F.M. Richards, and R.O. Fox, *Structural determinants of peptide-binding orientation and of sequence specificity in SH3 domains.* Nature, 1994. **372**(6504): p. 375-9.
289. Strunk, U., et al., *Role of Herpes simplex virus 1 VP11/12 tyrosine-based binding motifs for Src family kinases, p85, Grb2 and Shc in activation of the phosphoinositide 3-kinase-Akt pathway.* Virology, 2016. **498**: p. 31-5.
290. Shan, X., et al., *Deficiency of PTEN in Jurkat T cells causes constitutive localization of Itk to the plasma membrane and hyperresponsiveness to CD3 stimulation.* Mol Cell Biol, 2000. **20**(18): p. 6945-57.
291. Robertson, L.K. and H.L. Ostergaard, *Paxillin associates with the microtubule cytoskeleton and the immunological synapse of CTL through its leucine-aspartic acid domains and contributes to microtubule organizing center reorientation.* J Immunol, 2011. **187**(11): p. 5824-33.
292. Ku, H. and K.E. Meier, *Phosphorylation of paxillin via the ERK mitogen-activated protein kinase cascade in EL4 thymoma cells.* J Biol Chem, 2000. **275**(15): p. 11333-40.
293. Bauer, F., et al., *Characterization of Lck-binding elements in the herpesviral regulatory Tip protein.* Biochemistry, 2004. **43**(47): p. 14932-9.

294. Pagano, M.A., et al., *Viral proteins and Src family kinases: Mechanisms of pathogenicity from a "liaison dangereuse".* World J Virol, 2013. **2**(2): p. 71-8.
295. Shelton, H. and M. Harris, *Hepatitis C virus NS5A protein binds the SH3 domain of the Fyn tyrosine kinase with high affinity: mutagenic analysis of residues within the SH3 domain that contribute to the interaction.* Virol J, 2008. **5**: p. 24.
296. Roskoski, R., Jr., *Src kinase regulation by phosphorylation and dephosphorylation.* Biochem Biophys Res Commun, 2005. **331**(1): p. 1-14.
297. Sicheri, F., I. Moarefi, and J. Kuriyan, *Crystal structure of the Src family tyrosine kinase Hck.* Nature, 1997. **385**(6617): p. 602-9.
298. Xu, W., S.C. Harrison, and M.J. Eck, *Three-dimensional structure of the tyrosine kinase c-Src.* Nature, 1997. **385**(6617): p. 595-602.
299. Cooper, J.A., et al., *Tyr527 is phosphorylated in pp60c-src: implications for regulation.* Science, 1986. **231**(4744): p. 1431-4.
300. Kmiecik, T.E. and D. Shalloway, *Activation and suppression of pp60c-src transforming ability by mutation of its primary sites of tyrosine phosphorylation.* Cell, 1987. **49**(1): p. 65-73.
301. Xu, W., et al., *Crystal structures of c-Src reveal features of its autoinhibitory mechanism.* Mol Cell, 1999. **3**(5): p. 629-38.
302. D'Oro, U., et al., *Mutational analysis of Lck in CD45-negative T cells: dominant role of tyrosine 394 phosphorylation in kinase activity.* Mol Cell Biol, 1996. **16**(9): p. 4996-5003.
303. Brownlie, R.J. and R. Zamoyska, *T cell receptor signalling networks: branched, diversified and bounded.* Nat Rev Immunol, 2013. **13**(4): p. 257-69.
304. Hermiston, M.L., Z. Xu, and A. Weiss, *CD45: a critical regulator of signaling thresholds in immune cells.* Annu Rev Immunol, 2003. **21**: p. 107-37.
305. Schmedt, C., et al., *Csk controls antigen receptor-mediated development and selection of T-lineage cells.* Nature, 1998. **394**(6696): p. 901-4.
306. Schmedt, C. and A. Tarakhovsky, *Autonomous maturation of alpha/beta T lineage cells in the absence of COOH-terminal Src kinase (Csk).* J Exp Med, 2001. **193**(7): p. 815-26.
307. Waksman, G., et al., *Binding of a high affinity phosphotyrosyl peptide to the Src SH2 domain: crystal structures of the complexed and peptide-free forms.* Cell, 1993. **72**(5): p. 779-90.
308. Isakov, N., *Immunoreceptor tyrosine-based activation motif (ITAM), a unique module linking antigen and Fc receptors to their signaling cascades.* J Leukoc Biol, 1997. **61**(1): p. 6-16.
309. Fruehling, S. and R. Longnecker, *The immunoreceptor tyrosine-based activation motif of Epstein-Barr virus LMP2A is essential for blocking BCR-mediated signal transduction.* Virology, 1997. **235**(2): p. 241-51.

310. Liu, X. and J.I. Cohen, *Varicella-zoster virus ORF12 protein activates the phosphatidylinositol 3-kinase/Akt pathway to regulate cell cycle progression.* J Virol, 2013. **87**(3): p. 1842-8.
311. Jang, I.K., J. Zhang, and H. Gu, *Grb2, a simple adapter with complex roles in lymphocyte development, function, and signaling.* Immunol Rev, 2009. **232**(1): p. 150-9.
312. Tari, A.M. and G. Lopez-Berestein, *GRB2: a pivotal protein in signal transduction.* Semin Oncol, 2001. **28**(5 Suppl 16): p. 142-7.
313. Wills, M.K. and N. Jones, *Teaching an old dogma new tricks: twenty years of Shc adaptor signalling.* Biochem J, 2012. **447**(1): p. 1-16.
314. Castellano, E. and J. Downward, *RAS Interaction with PI3K: More Than Just Another Effector Pathway.* Genes Cancer, 2011. **2**(3): p. 261-74.
315. Winter, J.N., L.S. Jefferson, and S.R. Kimball, *ERK and Akt signaling pathways function through parallel mechanisms to promote mTORC1 signaling.* Am J Physiol Cell Physiol, 2011. **300**(5): p. C1172-80.
316. Wang, J., et al., *Direct association of Grb2 with the p85 subunit of phosphatidylinositol 3-kinase.* J Biol Chem, 1995. **270**(21): p. 12774-80.
317. Gu, H. and B.G. Neel, *The "Gab" in signal transduction.* Trends Cell Biol, 2003. **13**(3): p. 122-30.
318. Wohrle, F.U., R.J. Daly, and T. Brummer, *Function, regulation and pathological roles of the Gab/DOS docking proteins.* Cell Commun Signal, 2009. **7**: p. 22.
319. Adams, S.J., I.T. Aydin, and J.T. Celebi, *GAB2--a scaffolding protein in cancer.* Mol Cancer Res, 2012. **10**(10): p. 1265-70.
320. Matsuzaki, A., et al., *US3 protein kinase of herpes simplex virus type 2 is required for the stability of the UL46-encoded tegument protein and its association with virus particles.* J Gen Virol, 2005. **86**(Pt 7): p. 1979-85.
321. Gershburg, S., et al., *The UL13 and US3 Protein Kinases of Herpes Simplex Virus 1 Cooperate to Promote the Assembly and Release of Mature, Infectious Virions.* PLoS One, 2015. **10**(6): p. e0131420.
322. Liu, X., et al., *Varicella-Zoster virus ORF12 protein triggers phosphorylation of ERK1/2 and inhibits apoptosis.* J Virol, 2012. **86**(6): p. 3143-51.
323. Schulz, K.S., et al., *Pseudorabies virus pUL46 induces activation of ERK1/2 and regulates herpesvirus-induced nuclear envelope breakdown.* J Virol, 2014. **88**(11): p. 6003-11.
324. Clapham, D.E., *Calcium signaling.* Cell, 2007. **131**(6): p. 1047-58.
325. Roos, J., et al., *STIM1, an essential and conserved component of store-operated Ca2+ channel function.* J Cell Biol, 2005. **169**(3): p. 435-45.
326. Zhang, S.L., et al., *STIM1 is a Ca2+ sensor that activates CRAC channels and migrates from the Ca2+ store to the plasma membrane.* Nature, 2005. **437**(7060): p. 902-5.
327. Hou, X., et al., *Crystal structure of the calcium release-activated calcium channel Orai.* Science, 2012. **338**(6112): p. 1308-13.

328. Joseph, N., B. Reicher, and M. Barda-Saad, *The calcium feedback loop and T cell activation: how cytoskeleton networks control intracellular calcium flux.* Biochim Biophys Acta, 2014. **1838**(2): p. 557-68.
329. Quintana, A., et al., *Calcium microdomains at the immunological synapse: how ORAI channels, mitochondria and calcium pumps generate local calcium signals for efficient T-cell activation.* EMBO J, 2011. **30**(19): p. 3895-912.
330. Quintana, A., et al., *Sustained activity of calcium release-activated calcium channels requires translocation of mitochondria to the plasma membrane.* J Biol Chem, 2006. **281**(52): p. 40302-9.
331. Vaeth, M., et al., *ORAI2 modulates store-operated calcium entry and T cell-mediated immunity.* Nat Commun, 2017. **8**: p. 14714.
332. Zhou, Y., et al., *Pore architecture of the ORAI1 store-operated calcium channel.* Proc Natl Acad Sci U S A, 2010. **107**(11): p. 4896-901.
333. Houtman, J.C., et al., *Oligomerization of signaling complexes by the multipoint binding of GRB2 to both LAT and SOS1.* Nat Struct Mol Biol, 2006. **13**(9): p. 798-805.
334. Bilal, M.Y. and J.C. Houtman, *GRB2 Nucleates T Cell Receptor-Mediated LAT Clusters That Control PLC-gamma1 Activation and Cytokine Production.* Front Immunol, 2015. **6**: p. 141.
335. Yang, Y., et al., *The Us3 Protein of Herpes Simplex Virus 1 Inhibits T Cell Signaling by Confining Linker for Activation of T Cells (LAT) Activation via TRAF6 Protein.* J Biol Chem, 2015. **290**(25): p. 15670-8.
336. Xie, J.J., et al., *TNFR-associated factor 6 regulates TCR signaling via interaction with and modification of LAT adapter.* J Immunol, 2013. **190**(8): p. 4027-36.
337. Lahmidi, S., et al., *Herpes simplex virus 1 infection of T cells causes VP11/12-dependent phosphorylation and degradation of the cellular protein Dok-2.* Virology, 2017. **511**: p. 66-73.
338. Dong, S., et al., *T cell receptor for antigen induces linker for activation of T cell-dependent activation of a negative signaling complex involving Dok-2, SHIP-1, and Grb-2.* J Exp Med, 2006. **203**(11): p. 2509-18.
339. Nemorin, J.G. and P. Duplay, *Evidence that Llck-mediated phosphorylation of p56dok and p62dok may play a role in CD2 signaling.* J Biol Chem, 2000. **275**(19): p. 14590-7.
340. Yasuda, T., et al., *Dok-1 and Dok-2 are negative regulators of T cell receptor signaling.* Int Immunol, 2007. **19**(4): p. 487-95.
341. Lahmidi, S., et al., *Dok-1 and Dok-2 Are Required To Maintain Herpes Simplex Virus 1-Specific CD8+ T Cells in a Murine Model of Ocular Infection.* J Virol, 2017. **91**(15).
342. Laroche-Lefebvre, C., et al., *Dok-1 and Dok-2 Regulate the Formation of Memory CD8+ T Cells.* J Immunol, 2016. **197**(9): p. 3618-3627.

343. Di Cristofano, A., et al., *Molecular cloning and characterization of p56dok-2 defines a new family of RasGAP-binding proteins.* J Biol Chem, 1998. **273**(9): p. 4827-30.
344. Jones, N. and D.J. Dumont, *Recruitment of Dok-R to the EGF receptor through its PTB domain is required for attenuation of Erk MAP kinase activation.* Curr Biol, 1999. **9**(18): p. 1057-60.
345. Mihrshahi, R., A.N. Barclay, and M.H. Brown, *Essential roles for Dok2 and RasGAP in CD200 receptor-mediated regulation of human myeloid cells.* J Immunol, 2009. **183**(8): p. 4879-86.

Chapter A3

Appendix to: Generation of point mutated viruses via *en passant* mutagenesis

All experiments presented within this chapter were performed by U. Strunk with the following exceptions: The viruses KOS37-UL46 GFP, KOS37-GFP UL46, KOS37-UL46 Y624F and KOS37-UL46 GFP Y624F were generated by Holly Saffran. The viruses KOS37-UL46 Y519F/Y633F and KOS37-UL46 GFP Y519F/Y633F were generated by Danny Gomez Ramos.

Preface

The data presented in this chapter documents the final sequence validation of point mutated viruses, which were generated using *en passant* mutagenesis.

3A.1 Results

After the generation of BAC constructs harbouring the mutated UL46 sequence as described in chapter 3.1.2.1, the infectious virus was reconstructed as described in chapter 3.1.2.2. Briefly, the BAC construct was transfected into Cre Vero cells and single plaques were purified. The infectious virus was grown in Vero cells and a sequencing across the UL46 locus was carried with the primers indicated in each figure legend. The sequencing results were aligned to WT HSV-1 KOS VP11/12 (accession number JQ673480; version JQ673480.1) using Clustal Omega.

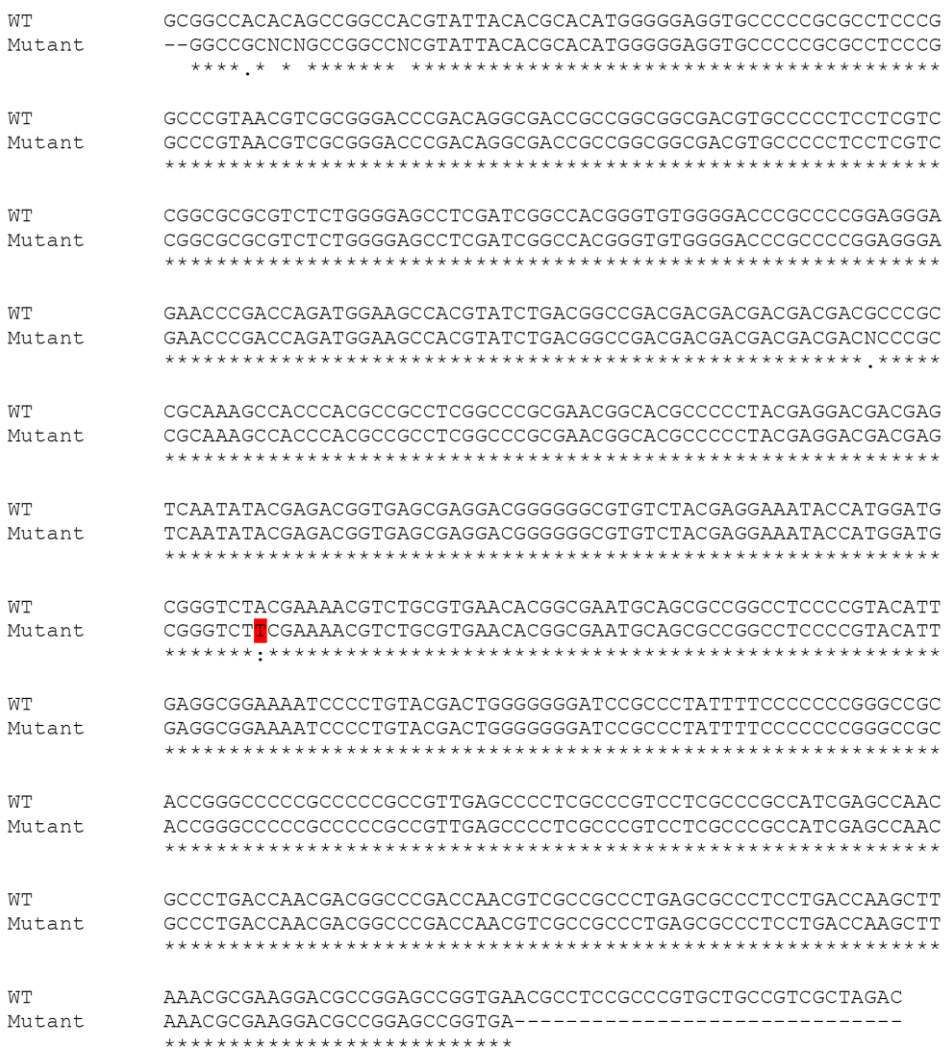

Fig A3.1: Sequence validation of KOS37-UL46 Y633F.

The UL46-PCR product was purified and sequenced using JRS 754. The sequence was aligned to WT UL46 in order to verify the point mutation (red). Sequences were aligned using Clustal Omega.

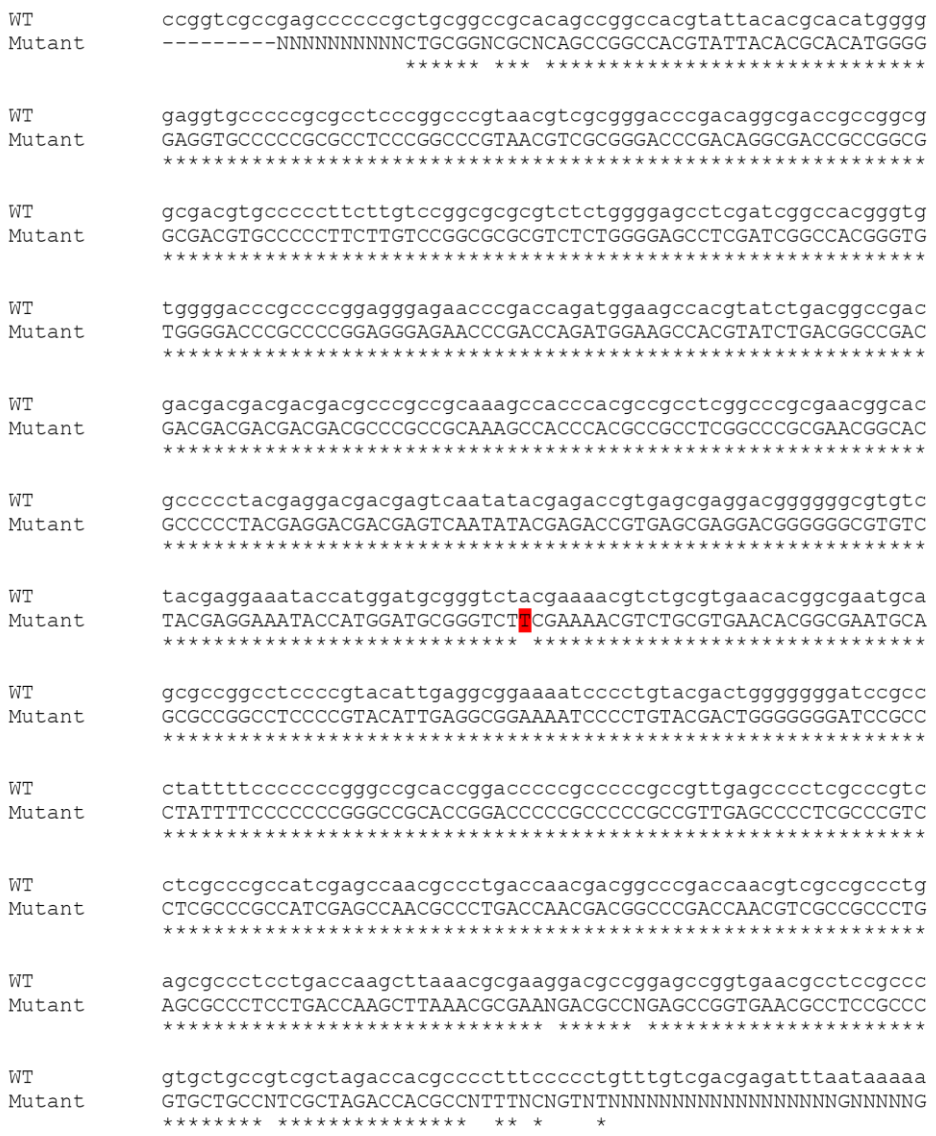

Fig A3.2: Sequence validation of KOS37- GFP UL46 Y633F.

The UL46-PCR product was purified and sequenced using JRS 754. The sequence was aligned to WT UL46 in order to verify the point mutation (red). Sequences were aligned using Clustal Omega.

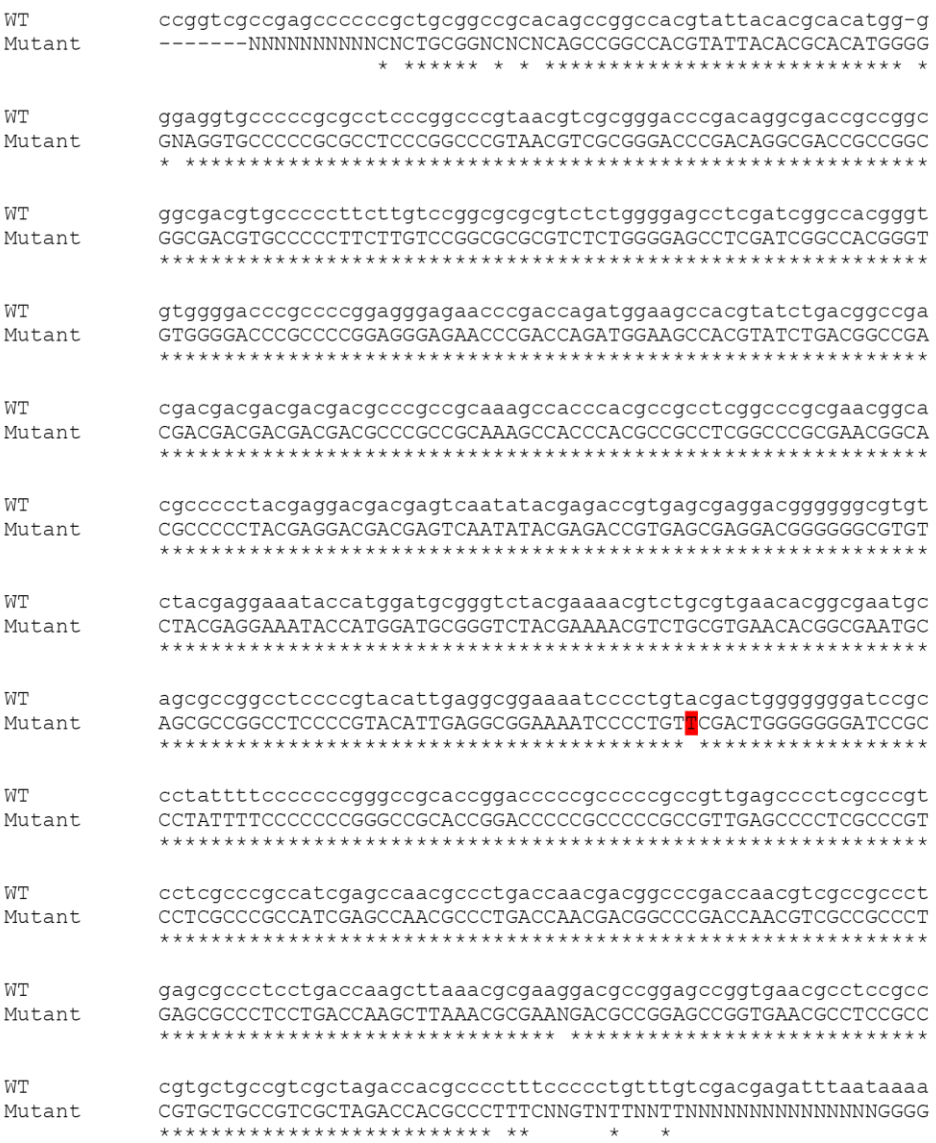

Fig A3.3: Sequence validation of KOS37-UL46 Y657F.

The UL46-PCR product was purified and sequenced using JRS 754. The sequence was aligned to WT UL46 in order to verify the point mutation (red). Sequences were aligned using Clustal Omega.

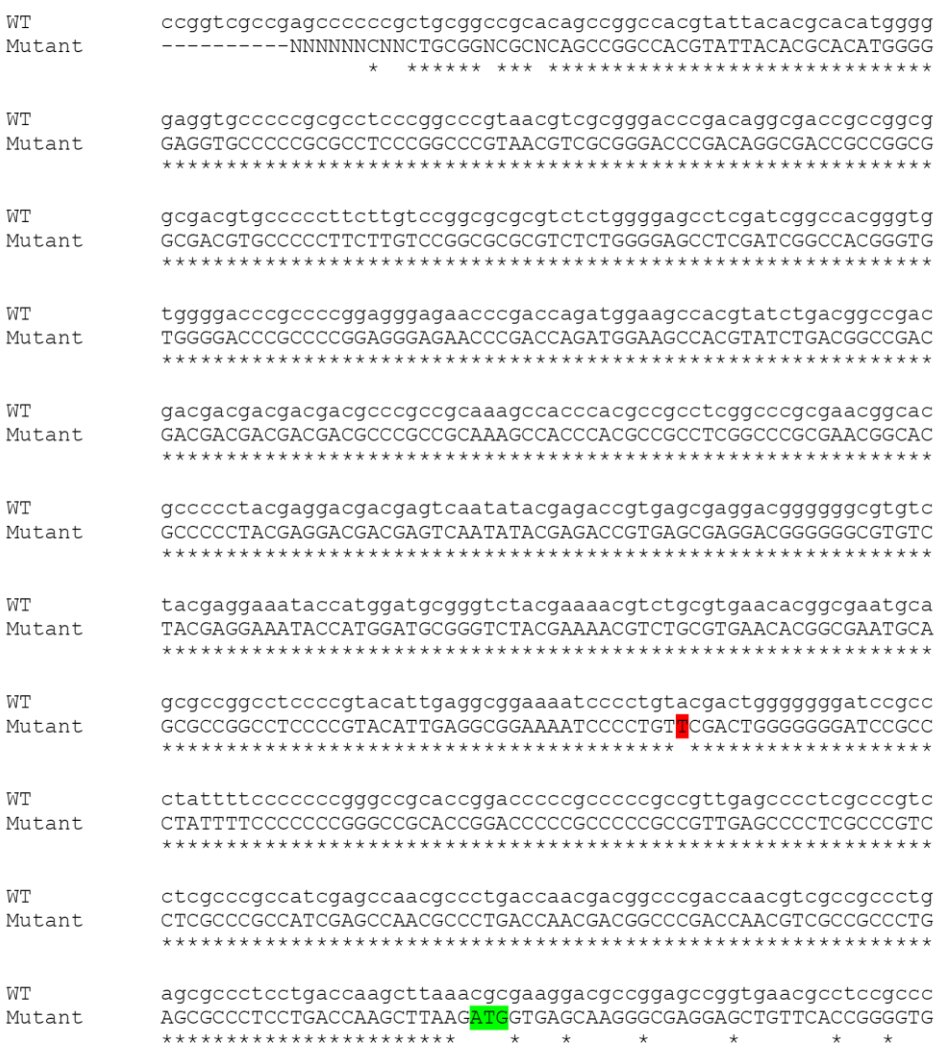

Fig A3.4: Sequence validation of KOS37-UL46 GFP Y657F.

The UL46-PCR product was purified and sequenced using JRS 754. The sequence was aligned to WT UL46 in order to verify the point mutation (red). The start codon of the C-terminal GFP-tag is in green. Sequences were aligned using Clustal Omega.

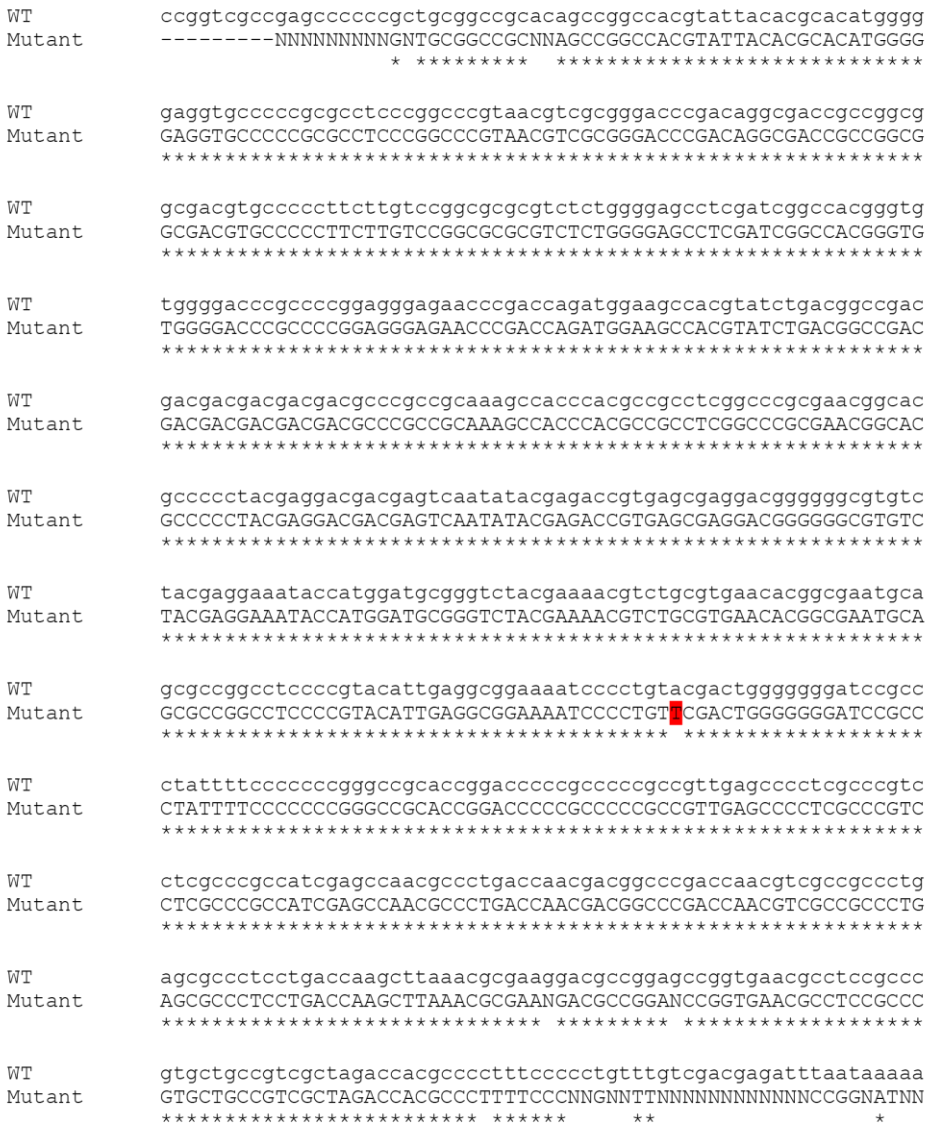

Fig A3.5: Sequence validation of KOS37-GFP UL46 Y657F.

The UL46-PCR product was purified and sequenced using JRS 754. The sequence was aligned to WT UL46 in order to verify the point mutation (red). Sequences were aligned using Clustal Omega.

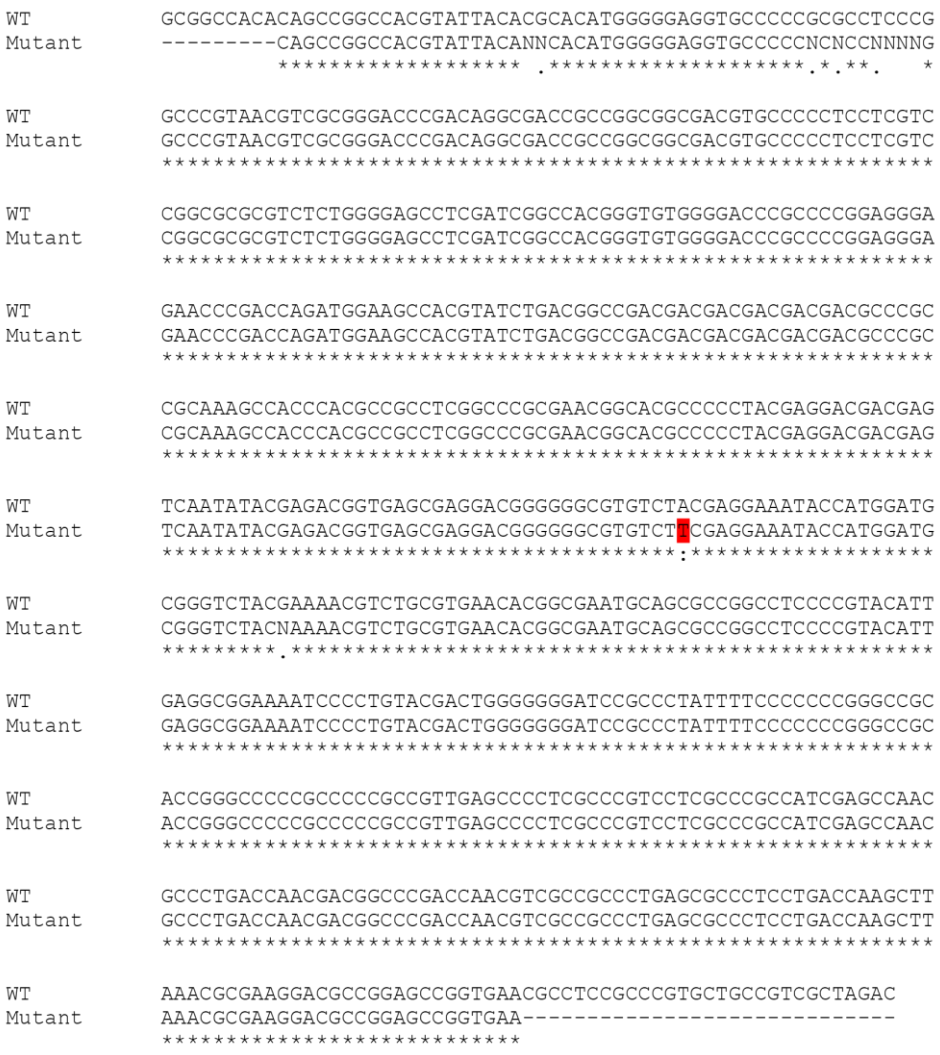

Fig A3.6: Sequence validation of KOS37-UL46 Y624F.

The UL46-PCR product was purified and sequenced using JRS 754. The sequence was aligned to WT UL46 in order to verify the point mutation (red). Sequences were aligned using Clustal Omega.

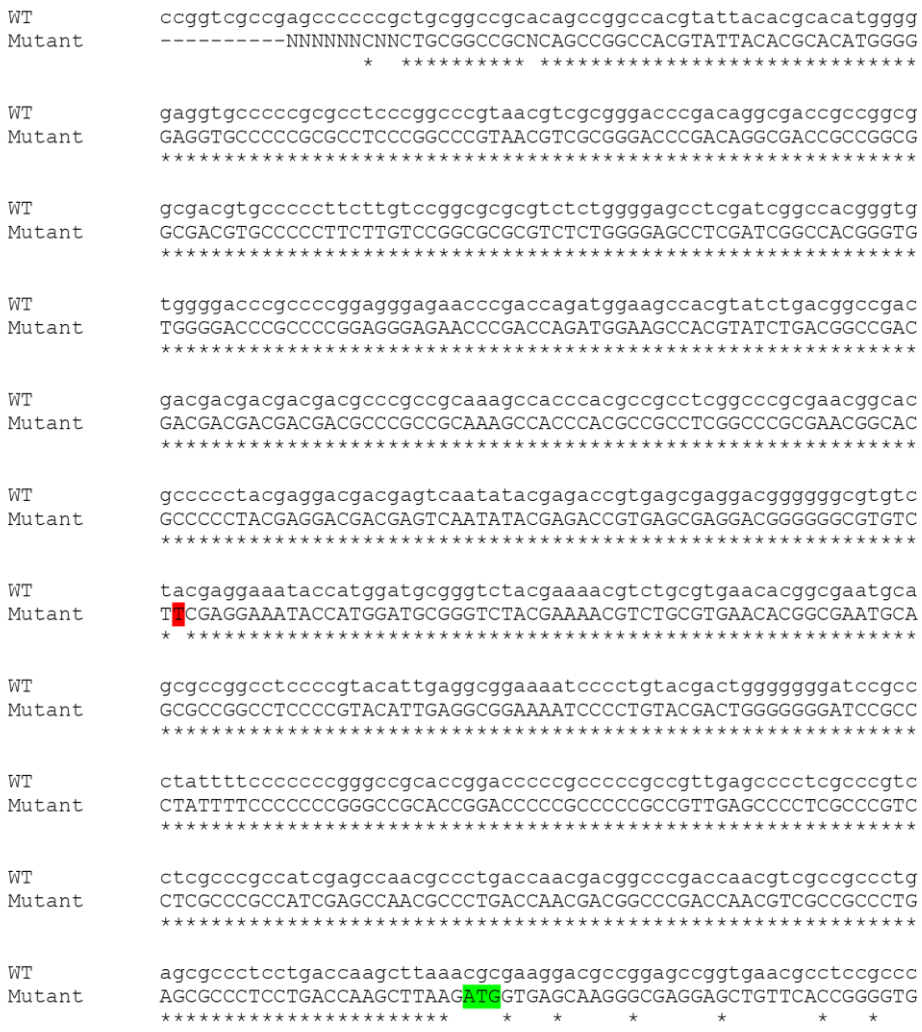

Fig A3.7: Sequence validation of KOS37-UL46 GFP Y624F.

The UL46-PCR product was purified and sequenced using JRS 754. The sequence was aligned to WT UL46 in order to verify the point mutation (red). The start codon of the C-terminal GFP-tag is in green. Sequences were aligned using Clustal Omega.

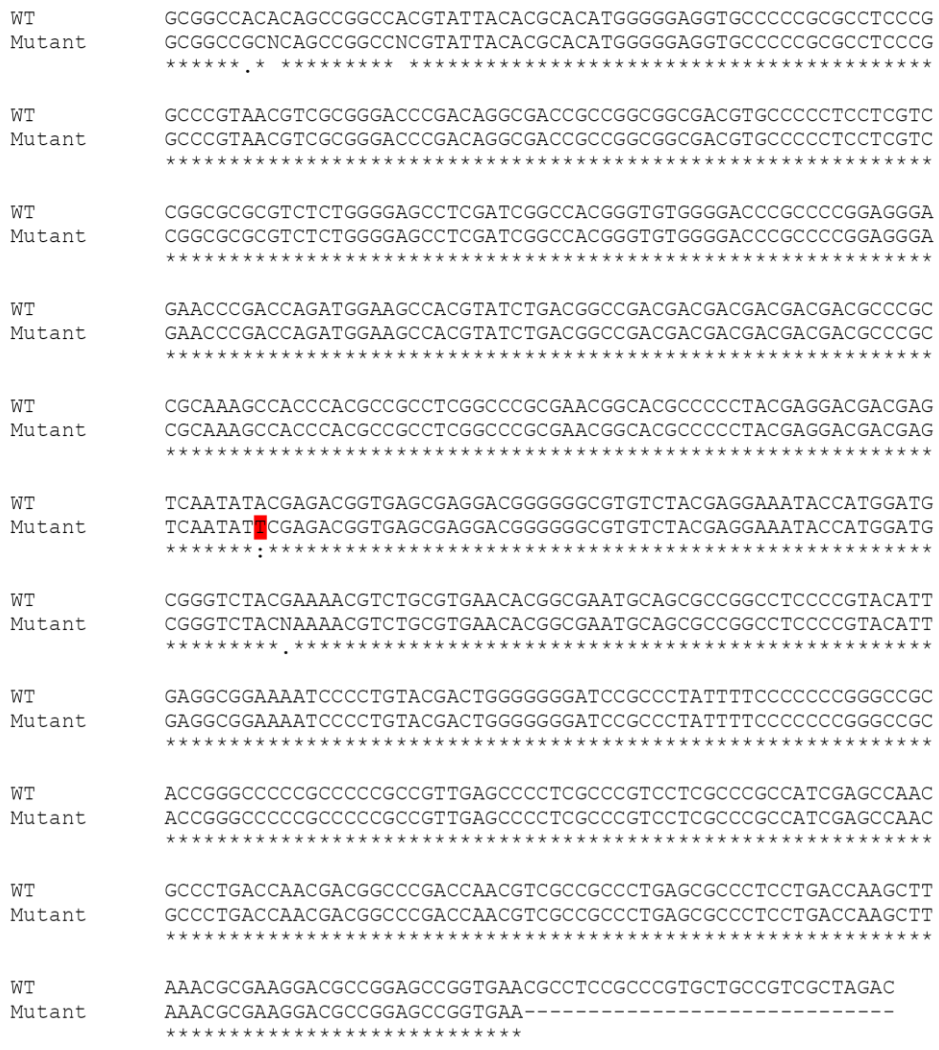

Fig A3.8: Sequence validation of KOS37-UL46 Y613F.

The UL46-PCR product was purified and sequenced using JRS 754. The sequence was aligned to WT UL46 in order to verify the point mutation (red). Sequences were aligned using Clustal Omega.

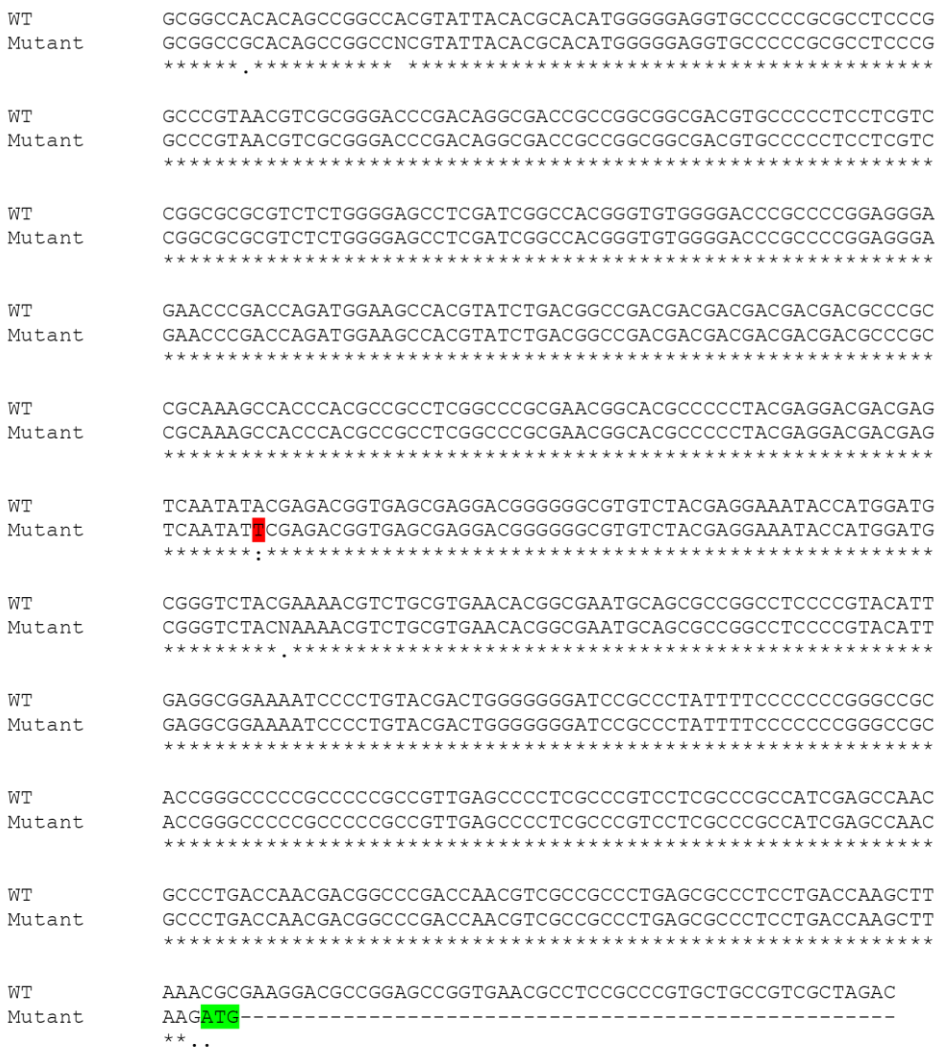

Fig A3.9: Sequence validation of KOS37-UL46 GFP Y613F.

The UL46-PCR product was purified and sequenced using JRS 754. The sequence was aligned to WT UL46 in order to verify the point mutation (red). The start codon of the C-terminal GFP-tag is in green. Sequences were aligned using Clustal Omega.

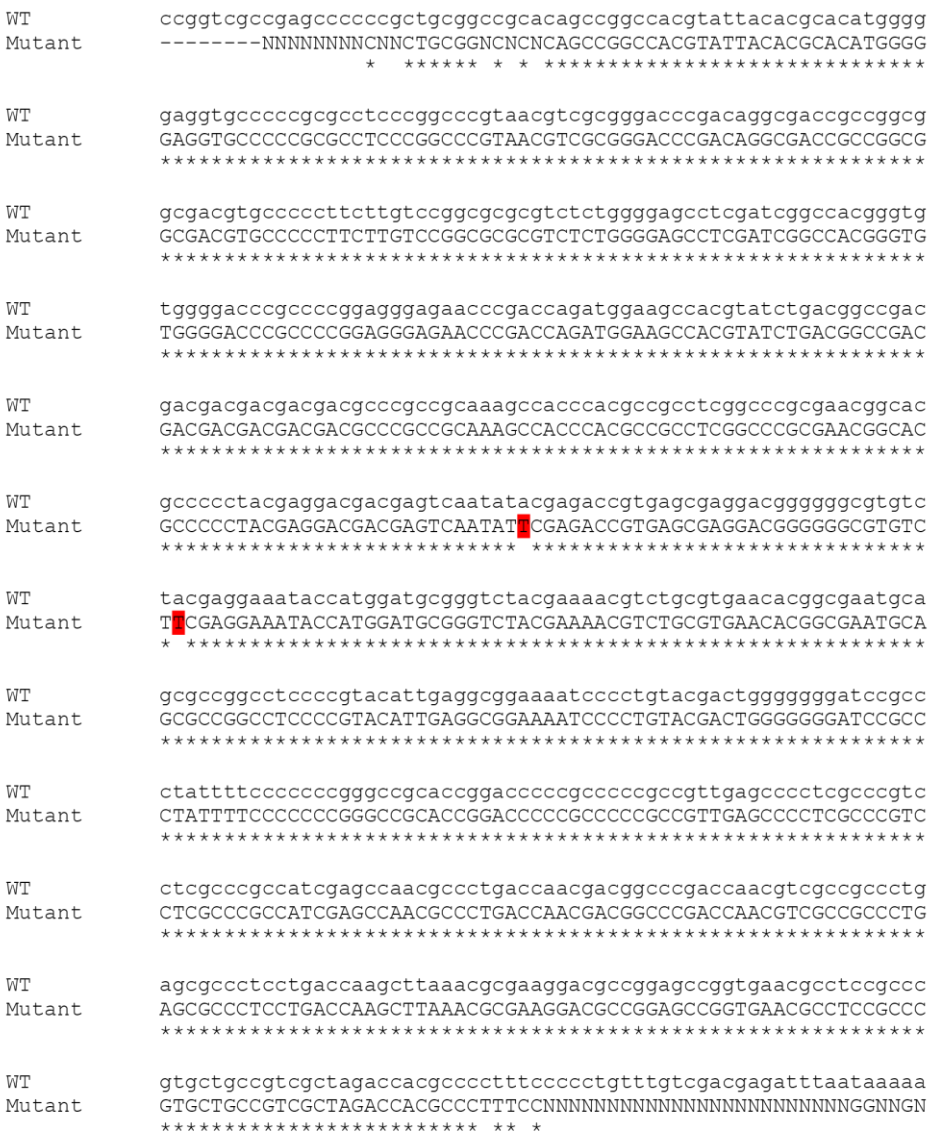

Fig A3.10: Sequence validation of KOS37-UL46 Y613F/Y624F.

The UL46-PCR product was purified and sequenced using JRS 754. The sequence was aligned to WT UL46 in order to verify the point mutations (red). Sequences were aligned using Clustal Omega.

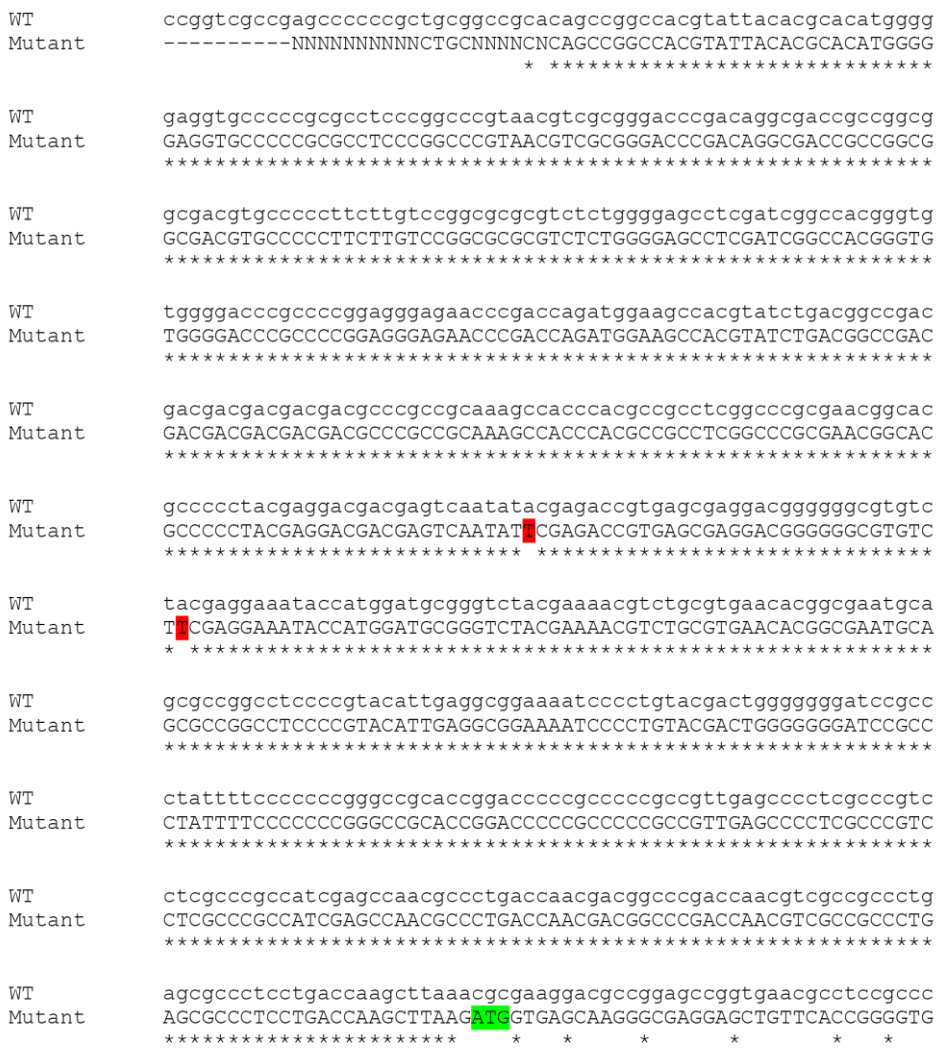

Fig A3.11: Sequence validation of KOS37-UL46 GFP Y613F/Y624F.

The UL46-PCR product was purified and sequenced using JRS 754. The sequence was aligned to WT UL46 in order to verify the point mutations (red). The start codon of the C-terminal GFP-tag is in green. Sequences were aligned using Clustal Omega.

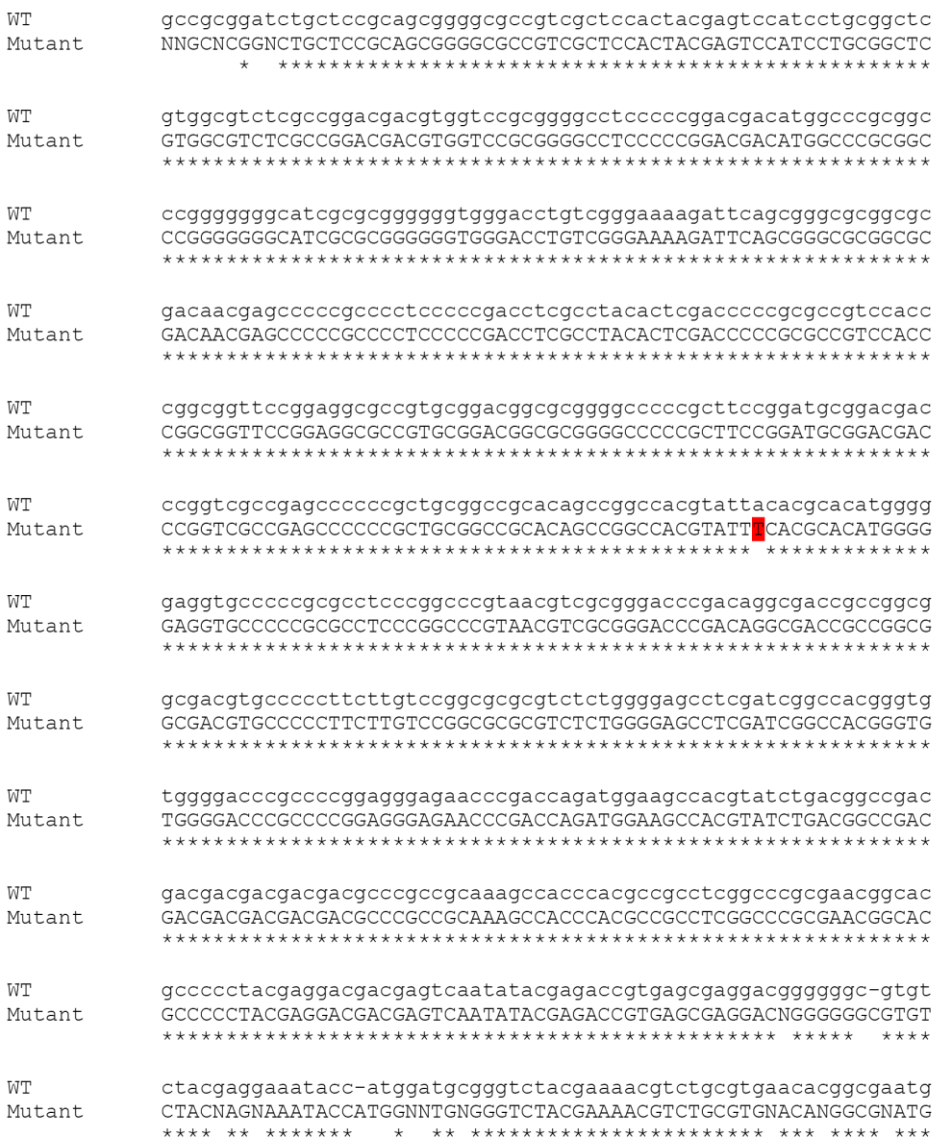

Fig A3.12: Sequence validation of KOS37-UL46 Y519F.

The UL46-PCR product was purified and sequenced using JRS 1033. The sequence was aligned to WT UL46 in order to verify the point mutation (red). Sequences were aligned using Clustal Omega.

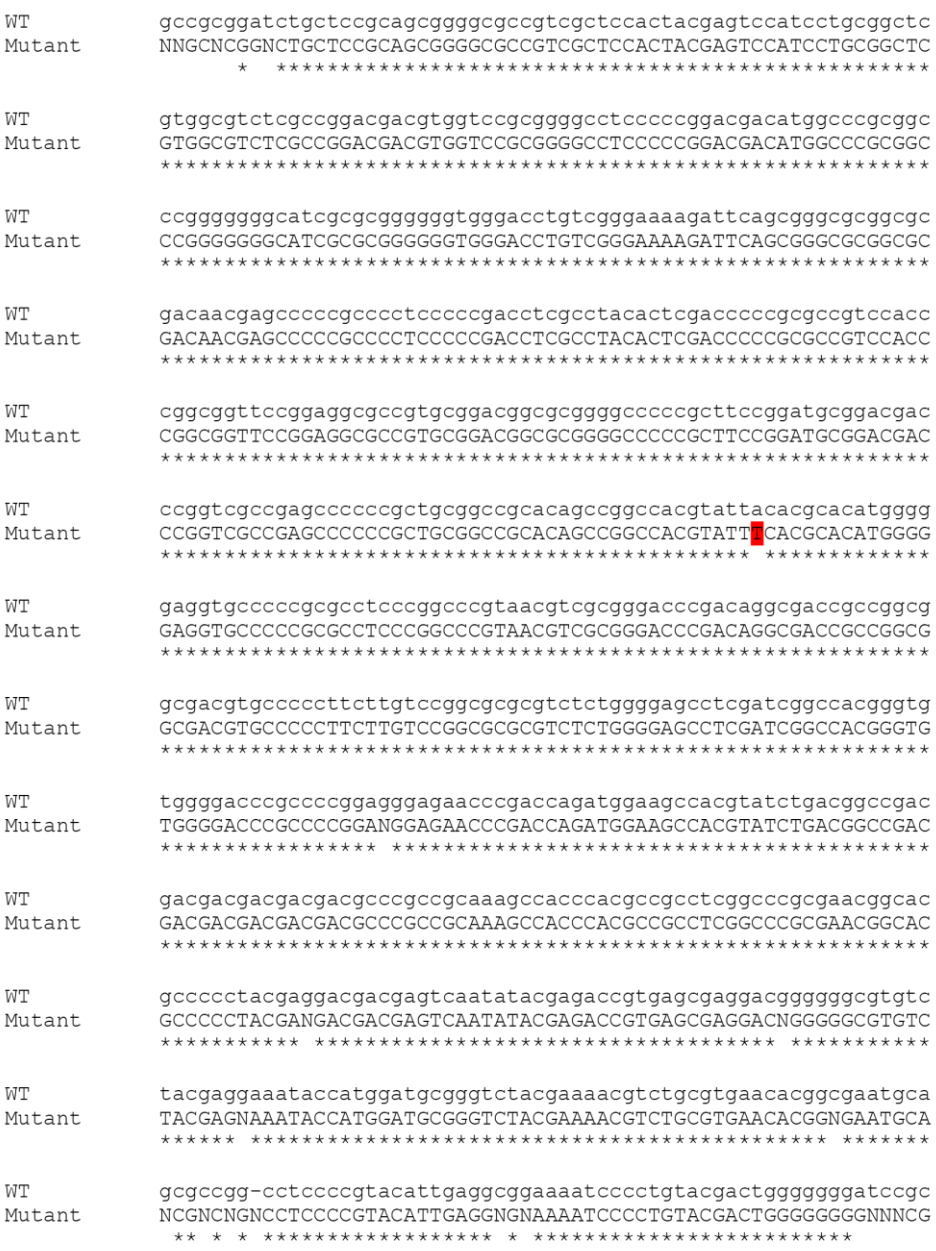

Fig A3.13: Sequence validation of KOS37-UL46 GFP Y519F.

The UL46-PCR product was purified and sequenced using JRS 1033. The sequence was aligned to WT UL46 in order to verify the point mutation (red). The start codon of the C-terminal GFP-tag is in green. Sequences were aligned using Clustal Omega.

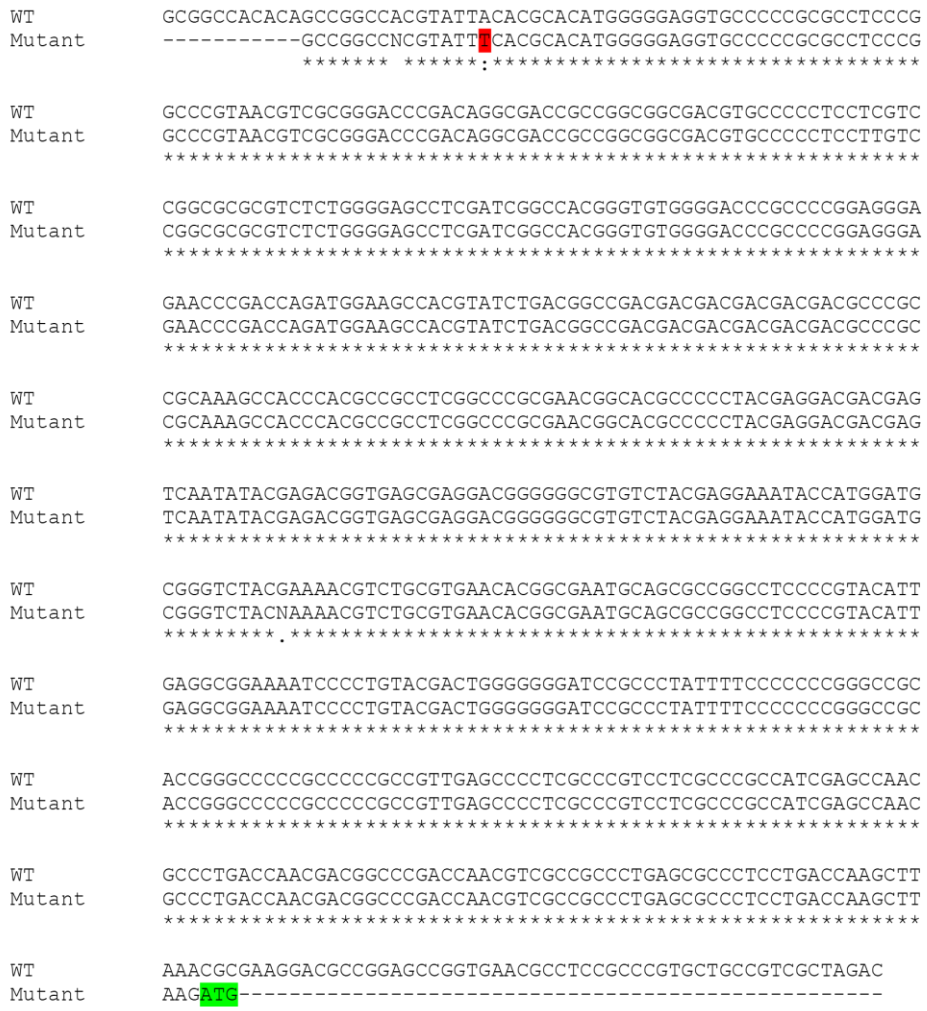

Fig A3.14: Sequence validation of KOS37-UL46 GFP Y519F.

The UL46-PCR product was purified and sequenced using JRS 754. The sequence was aligned to WT UL46 in order to verify the point mutation (red). The start codon of the C-terminal GFP-tag is in green. Sequences were aligned using Clustal Omega.

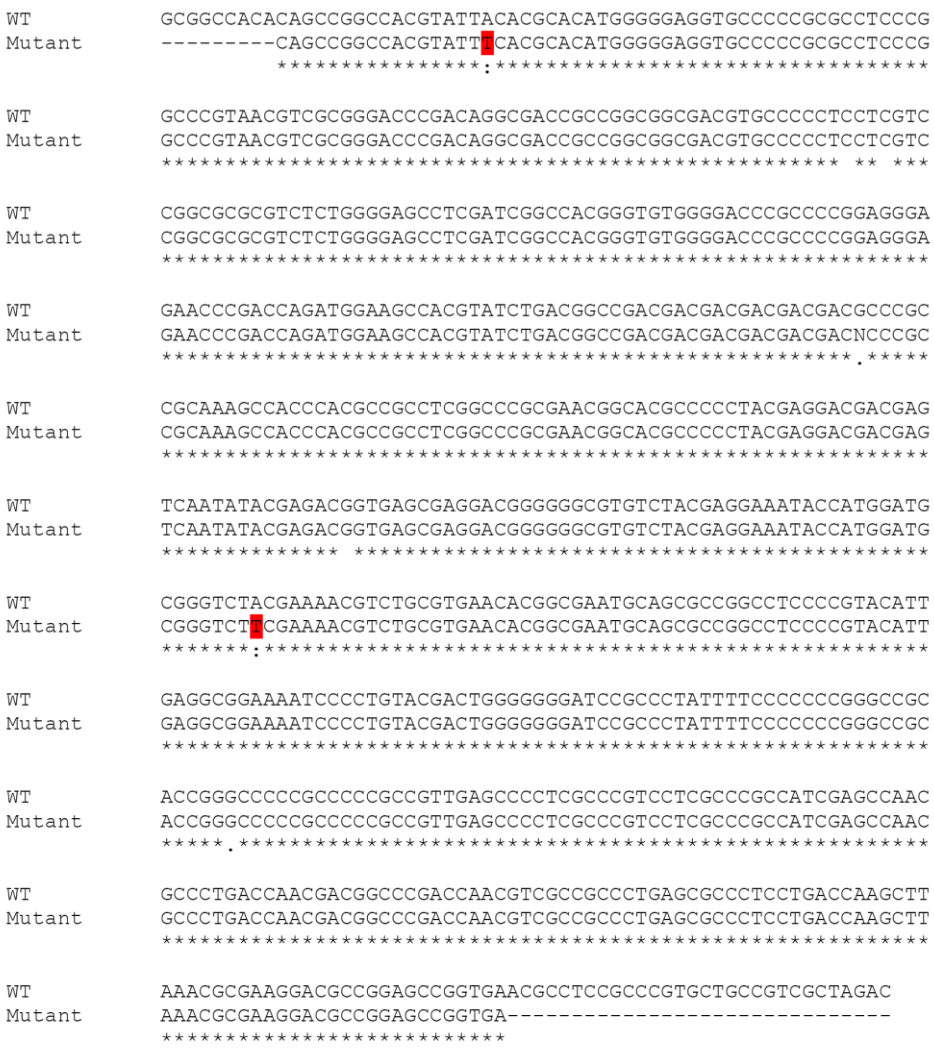

Fig A3.15: Sequence validation of KOS37-UL46 Y519F/Y633F.

The UL46-PCR product was purified and sequenced using JRS 754. The sequence was aligned to WT UL46 in order to verify the point mutations (red). Sequences were aligned using Clustal Omega.

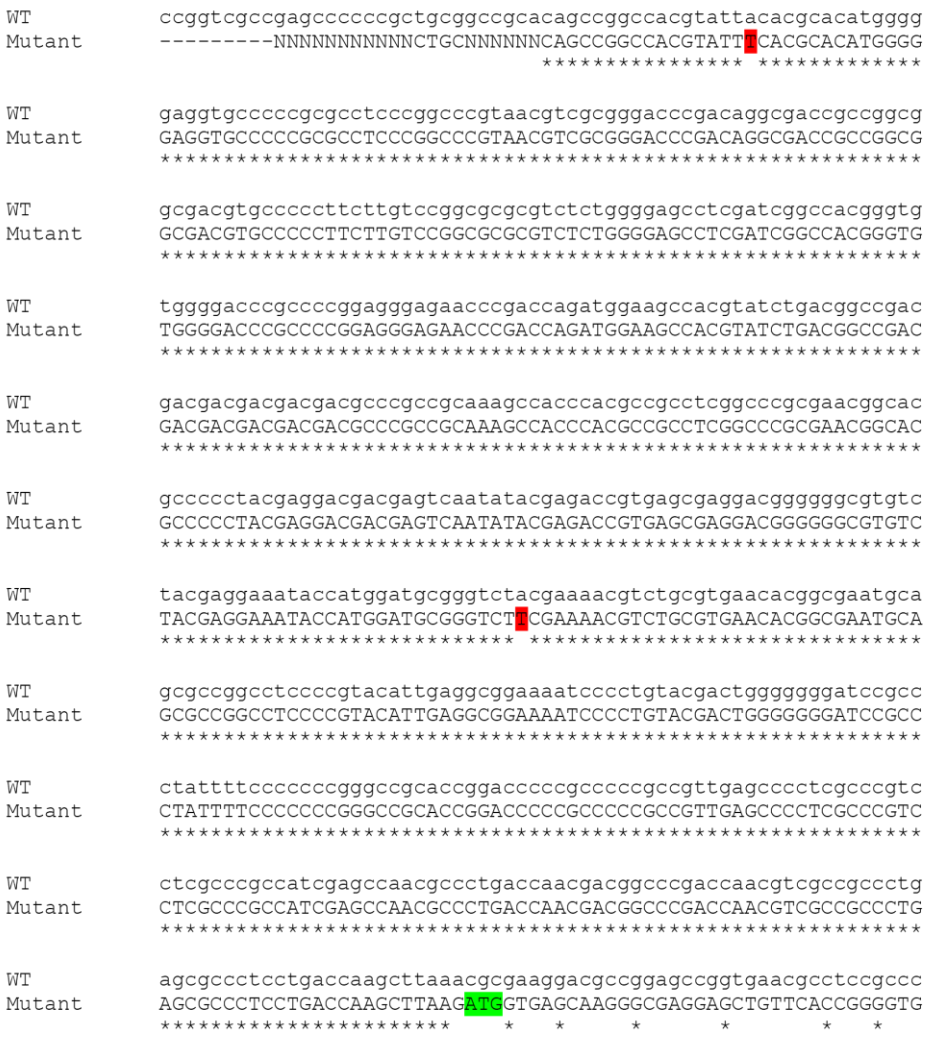

Fig A3.16: Sequence validation of KOS37-UL46 GFP Y519F/Y633F.

The UL46-PCR product was purified and sequenced using JRS 754. The sequence was aligned to WT UL46 in order to verify the point mutations (red). The start codon of the C-terminal GFP-tag is in green. Sequences were aligned using Clustal Omega.

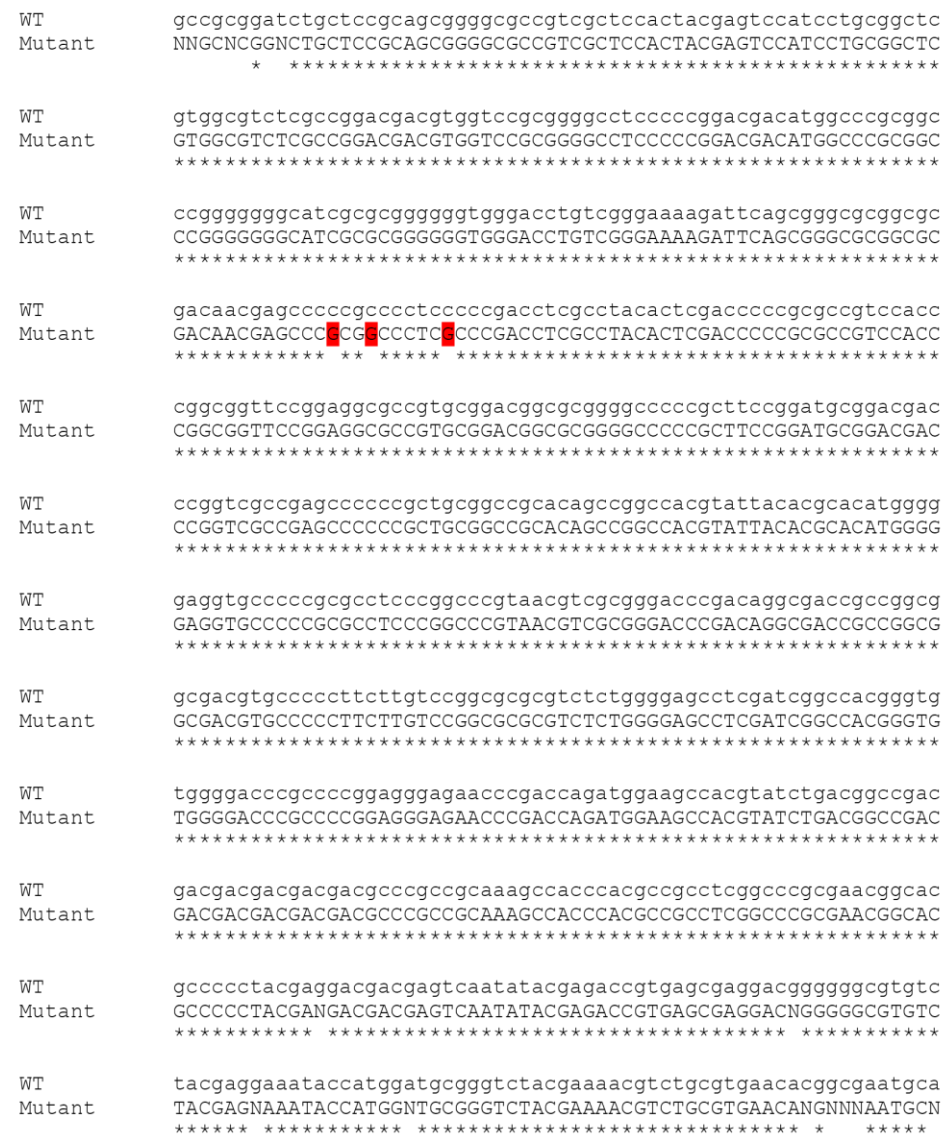

Fig A3.17: Sequence validation of KOS37-UL46 AALA.

The UL46-PCR product was purified and sequenced using JRS 1033. The sequence was aligned to WT UL46 in order to verify the point mutations (red). Sequences were aligned using Clustal Omega.

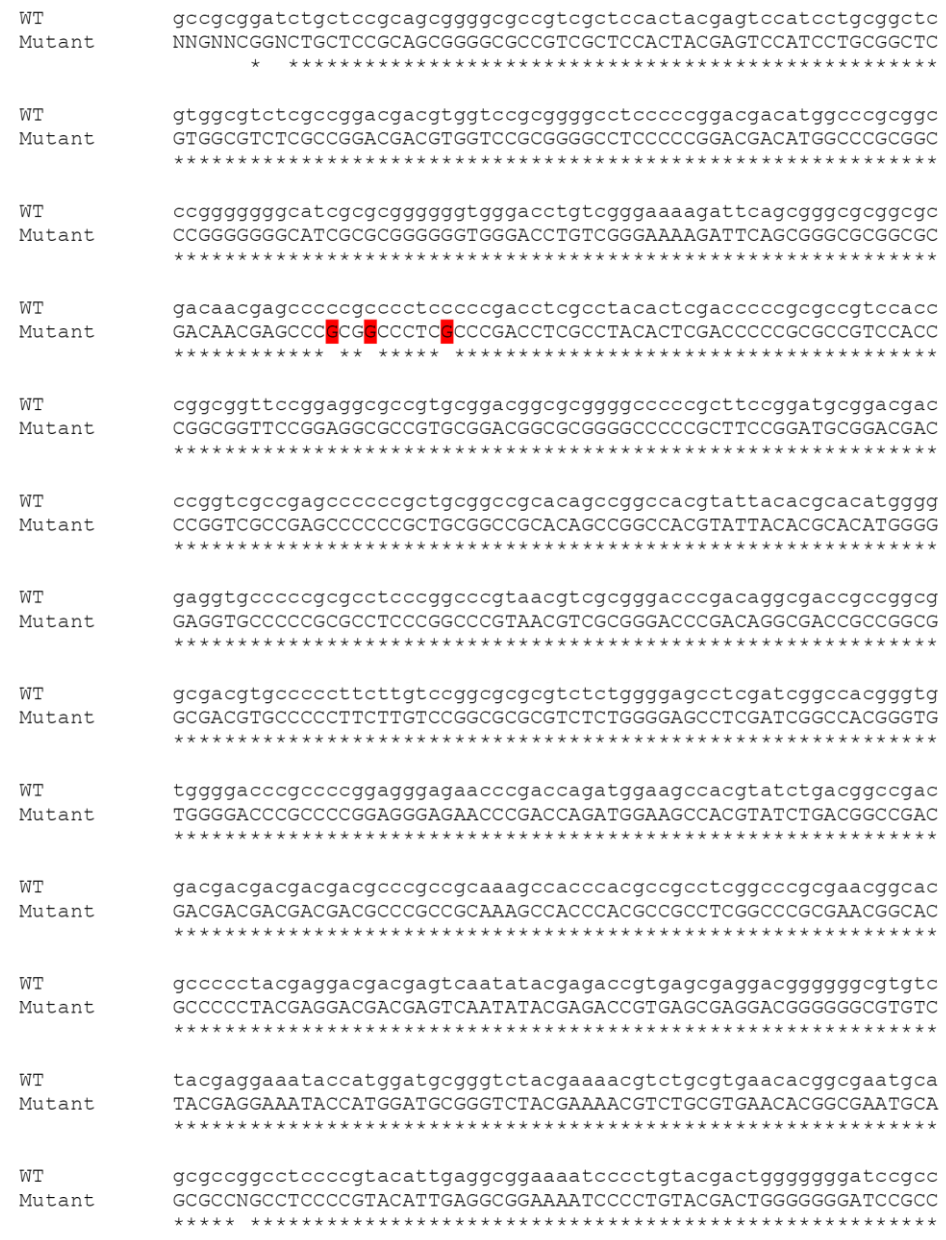

Fig A3.18: Sequence validation of KOS37-UL46 GFP AALA.

The UL46-PCR product was purified and sequenced using JRS 1033. The sequence was aligned to WT UL46 in order to verify the point mutations (red). Sequences were aligned using Clustal Omega.

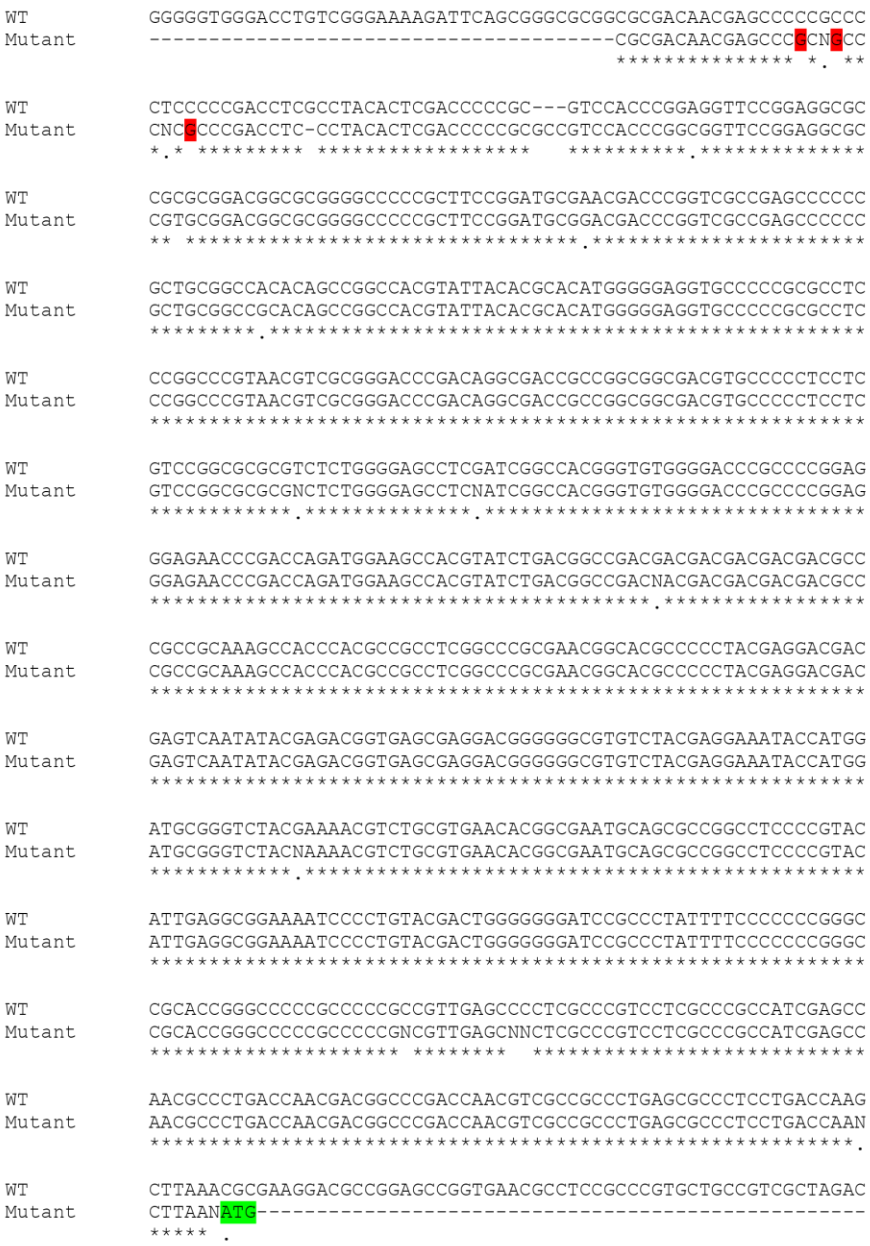

Fig A3.19: Sequence validation of KOS37-UL46 GFP AALA.

The UL46-PCR product was purified and sequenced using JRS 860. The sequence was aligned to WT UL46 in order to verify the point mutations (red). The start codon of the C-terminal GFP-tag is in green. Sequences were aligned using Clustal Omega.

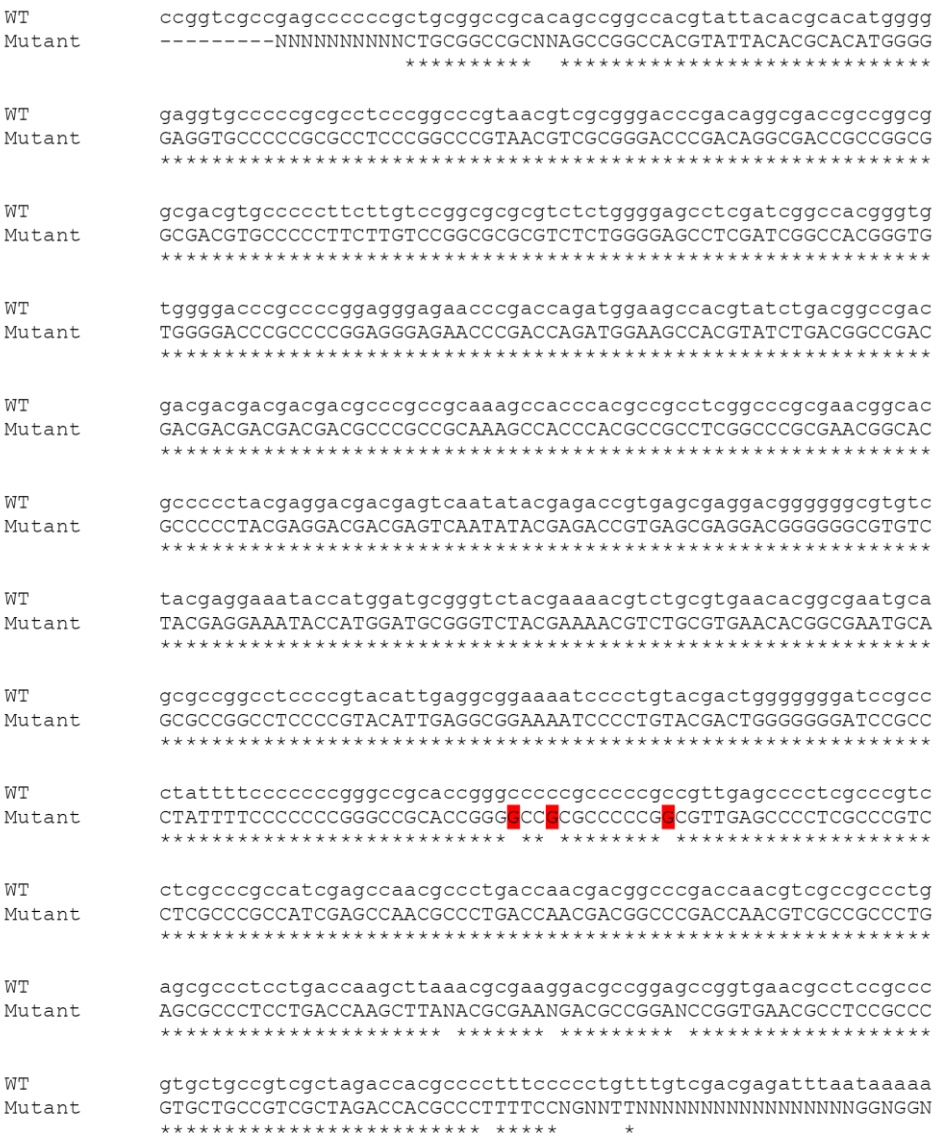

Fig A3.20: Sequence validation of KOS37-UL46 AAPPA.

The UL46-PCR product was purified and sequenced using JRS 754. The sequence was aligned to WT UL46 in order to verify the point mutations (red). Sequences were aligned using Clustal Omega.

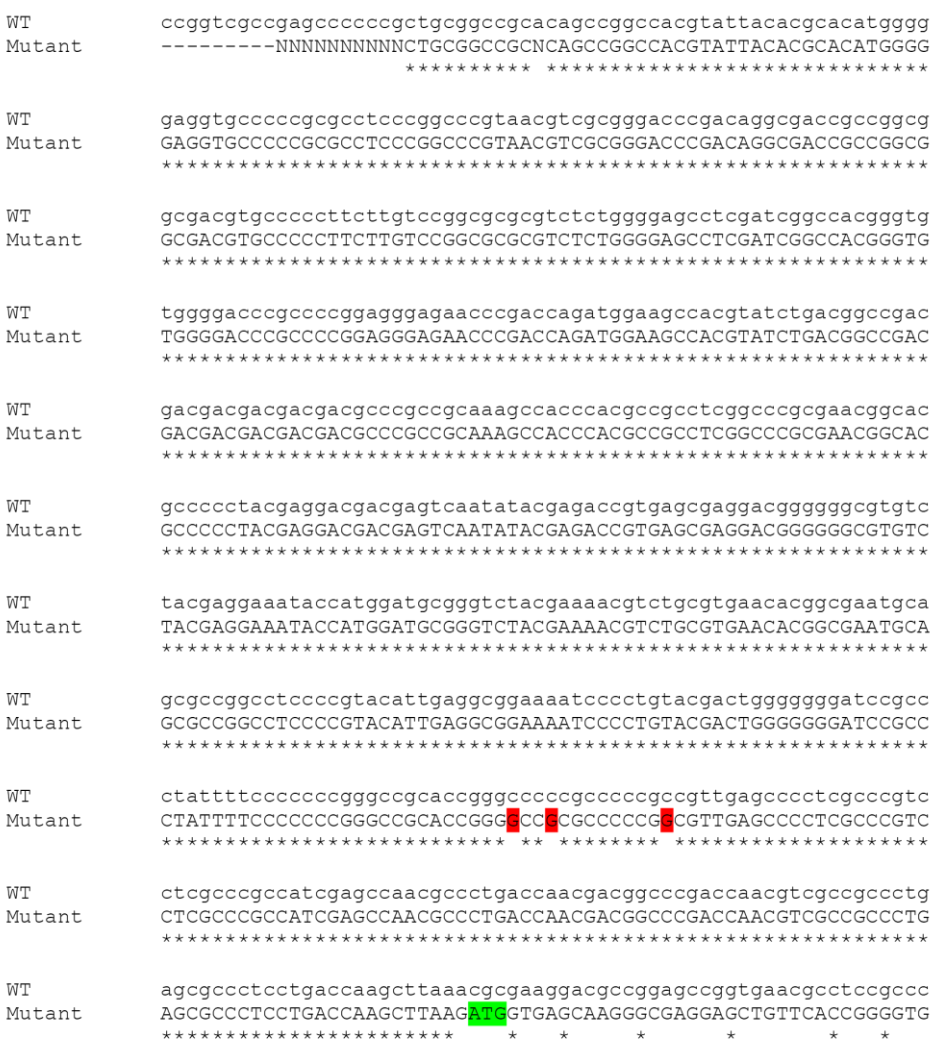

Fig A3.21: Sequence validation of KOS37-UL46 GFP AAPPA.

The UL46-PCR product was purified and sequenced using JRS 754. The sequence was aligned to WT UL46 in order to verify the point mutations (red). The start codon of the C-terminal GFP-tag is in green. Sequences were aligned using Clustal Omega.

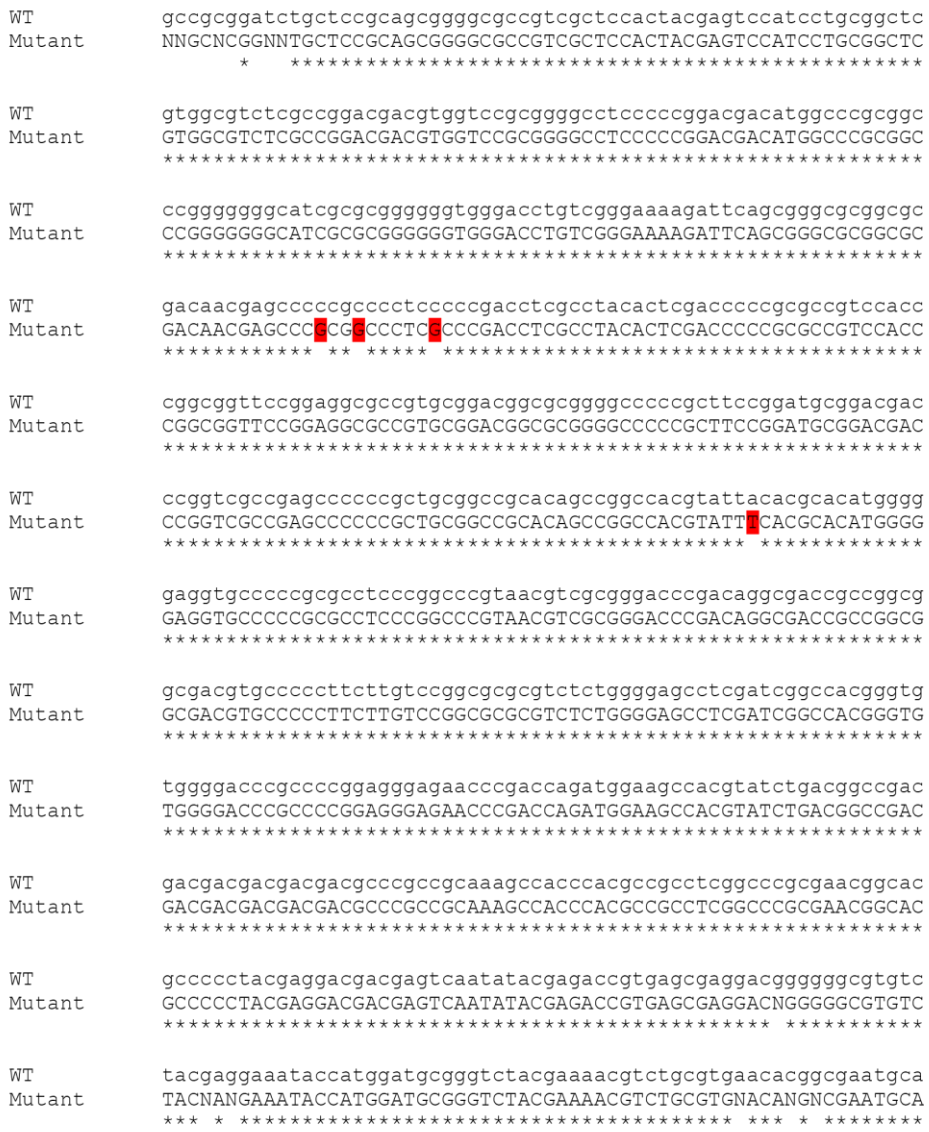

Fig A3.22: Sequence validation of KOS37-UL46 AALA/Y519F.

The UL46-PCR product was purified and sequenced using JRS 1033. The sequence was aligned to WT UL46 in order to verify the point mutations (red). Sequences were aligned using Clustal Omega.

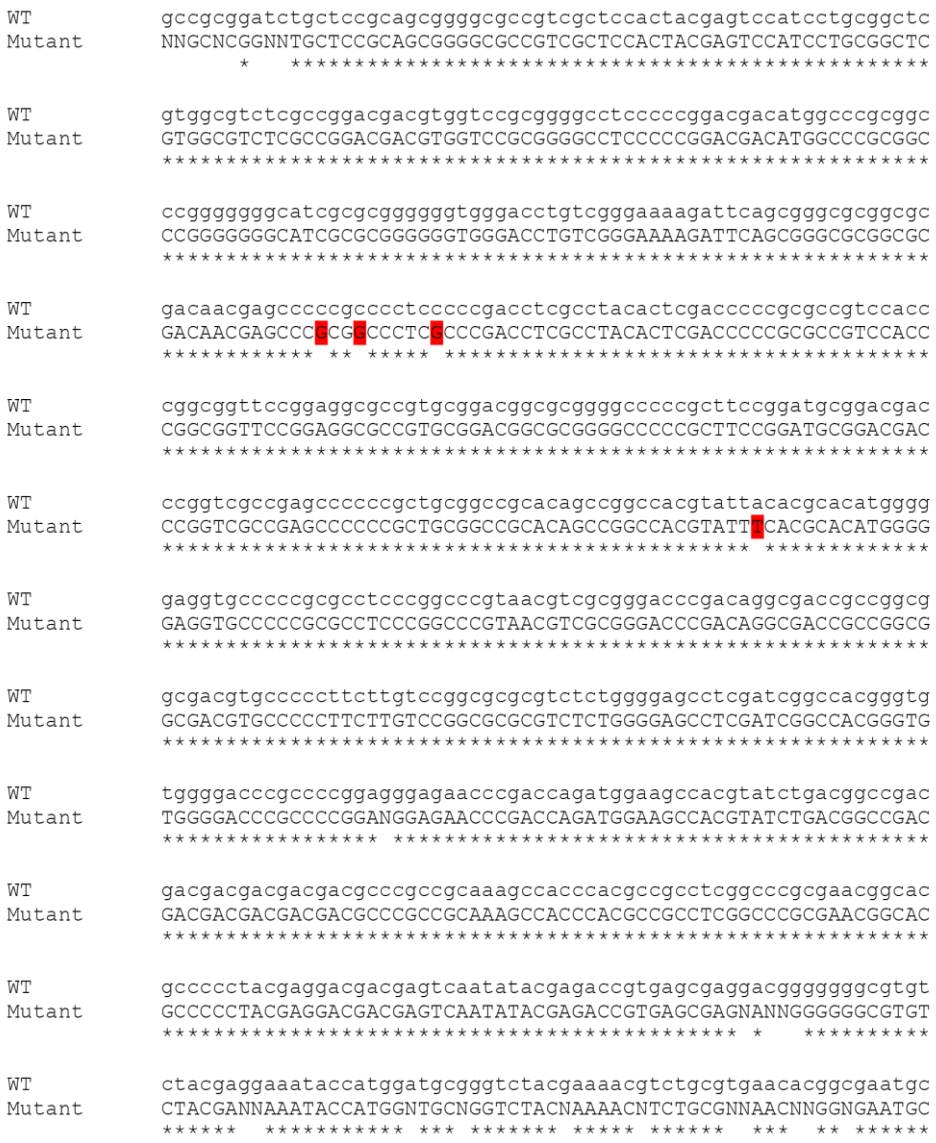

Fig A3.23: Sequence validation of KOS37-UL46 GFP AALA/Y519F.

The UL46-PCR product was purified and sequenced using JRS 1033. The sequence was aligned to WT UL46 in order to verify the point mutations (red). The start codon of the C-terminal GFP-tag is in green. Sequences were aligned using Clustal Omega.

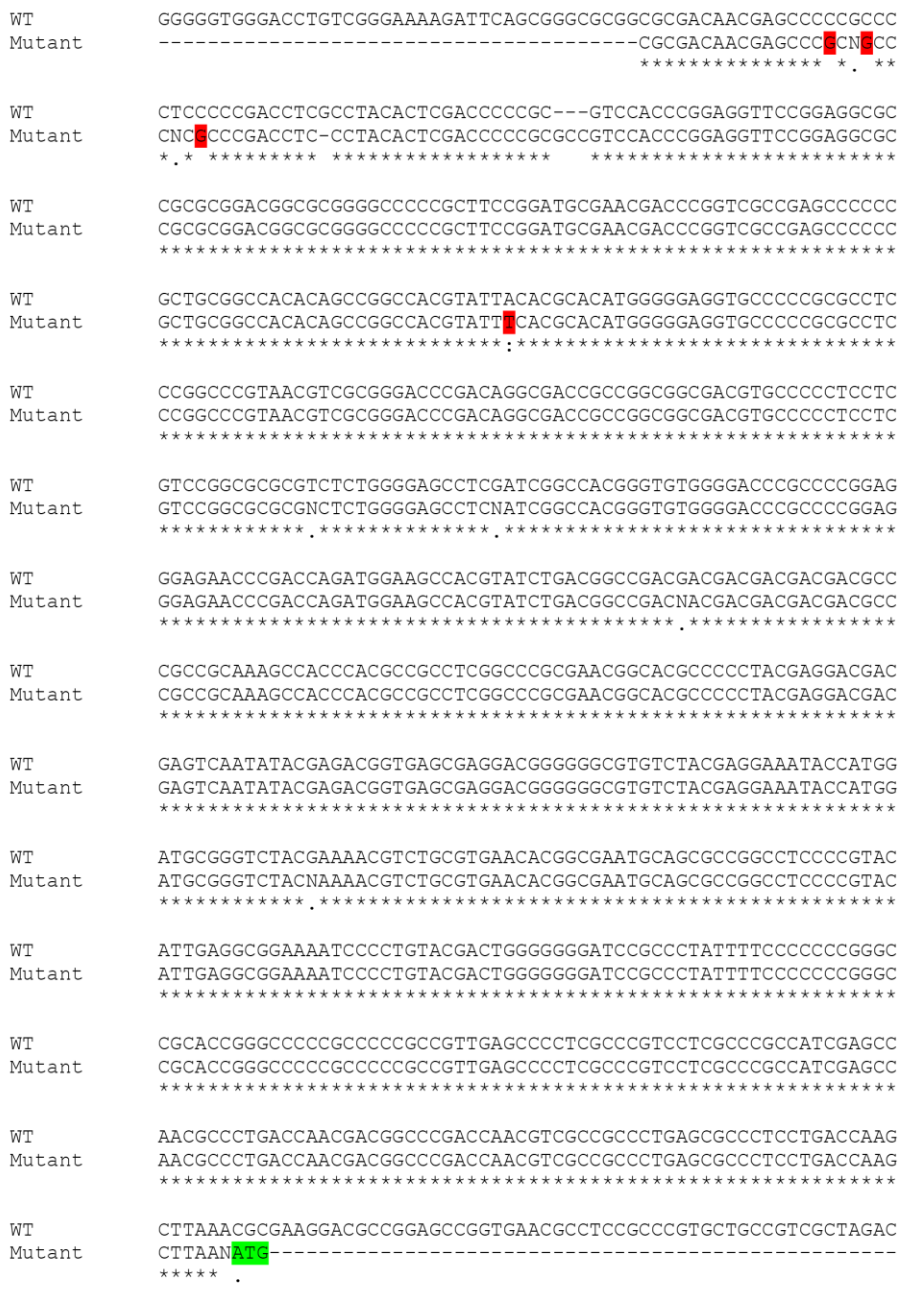

Fig A3.24: Sequence validation of KOS37-UL46 GFP AALA/Y519F.

The UL46-PCR product was purified and sequenced using JRS 860. The sequence was aligned to WT UL46 in order to verify the point mutations (red). The start codon of the C-terminal GFP-tag is in green. Sequences were aligned using Clustal Omega.

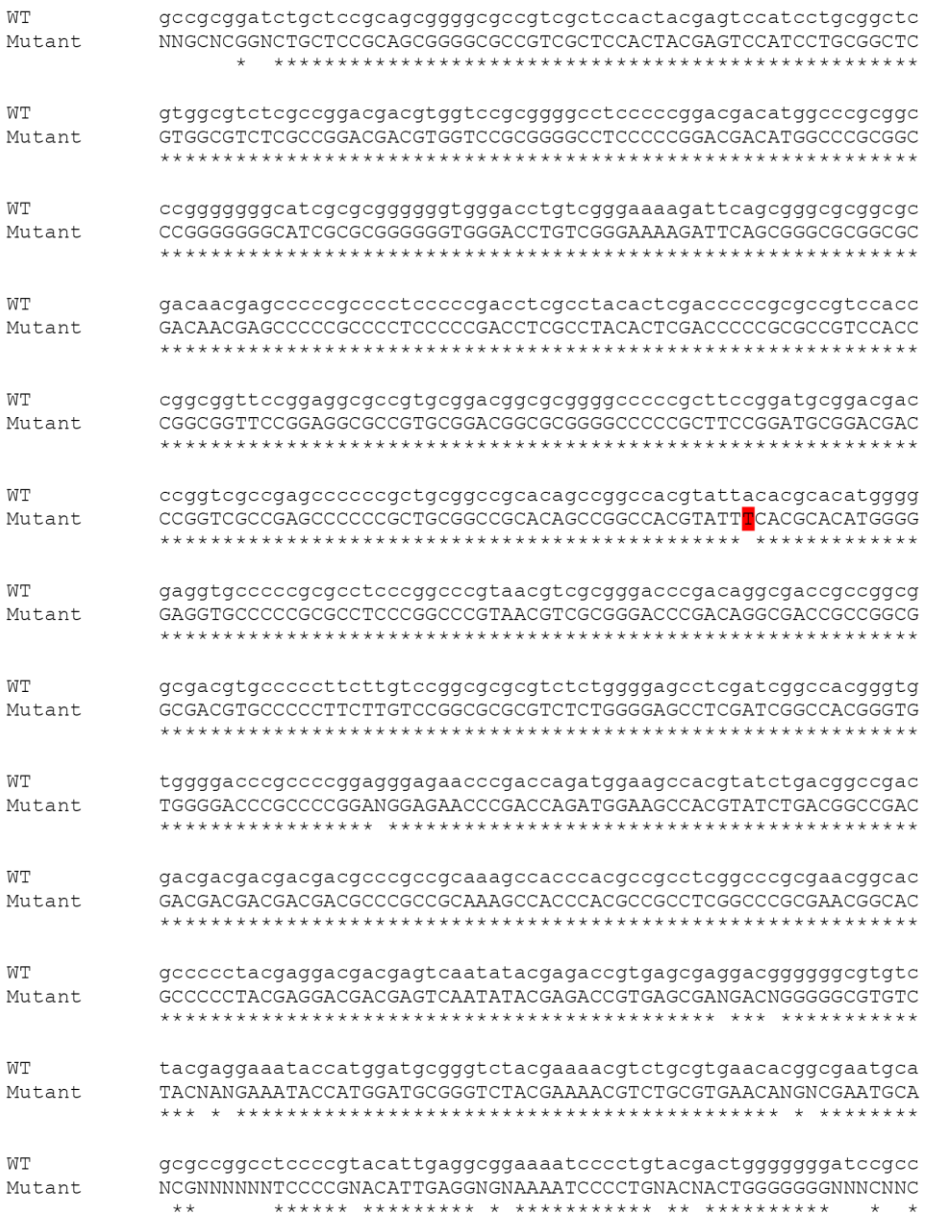

Fig A3.25: Sequence validation of KOS37-UL46 GFP Y519F/AAPPA.

The UL46-PCR product was purified and sequenced using JRS 1033. The sequence was aligned to WT UL46 in order to verify the point mutations (red). The start codon of the C-terminal GFP-tag is in green. Sequences were aligned using Clustal Omega.

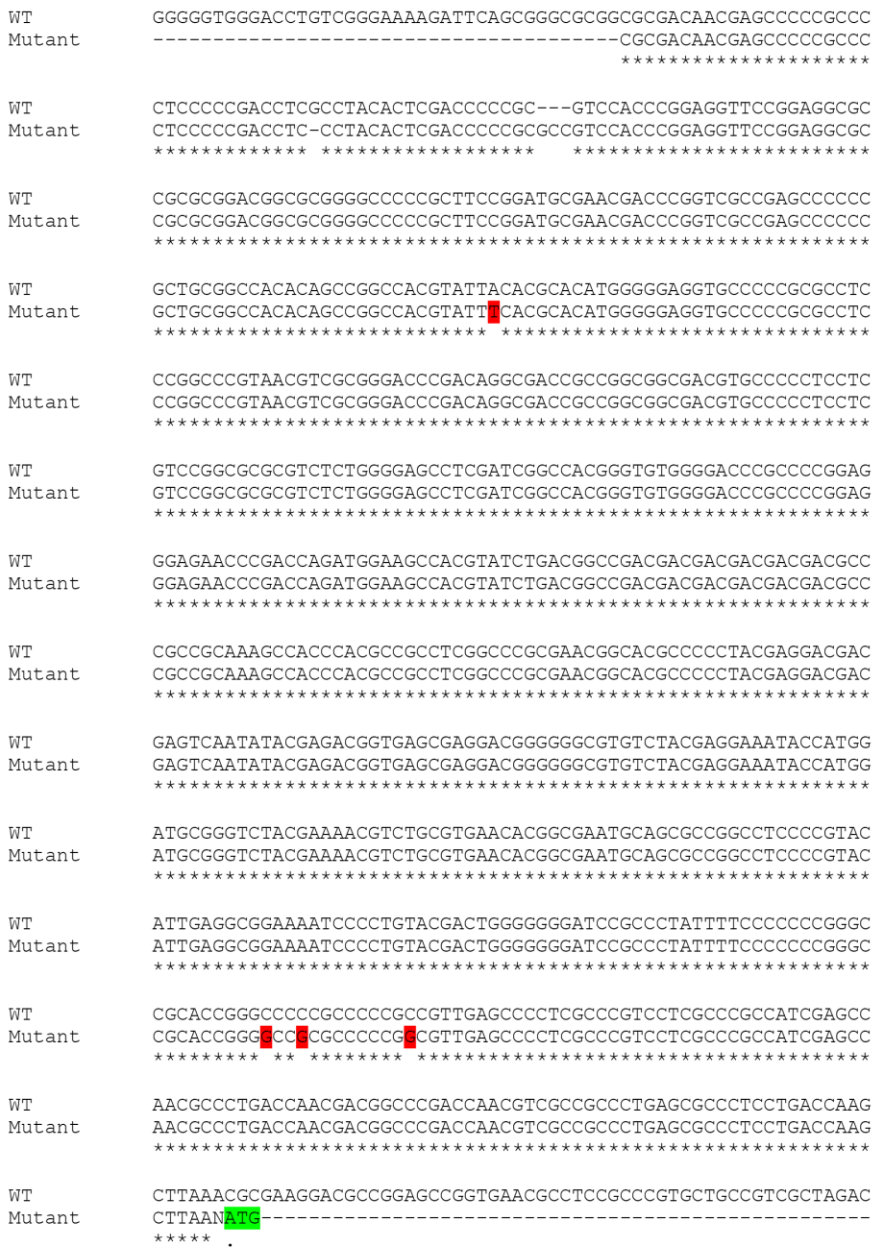

Fig A3.26: Sequence validation of KOS37-UL46 GFP Y519F/AAPPA.

The UL46-PCR product was purified and sequenced using JRS 754. The sequence was aligned to WT UL46 in order to verify the point mutations (red). The start codon of the C-terminal GFP-tag is in green. Sequences were aligned using Clustal Omega.

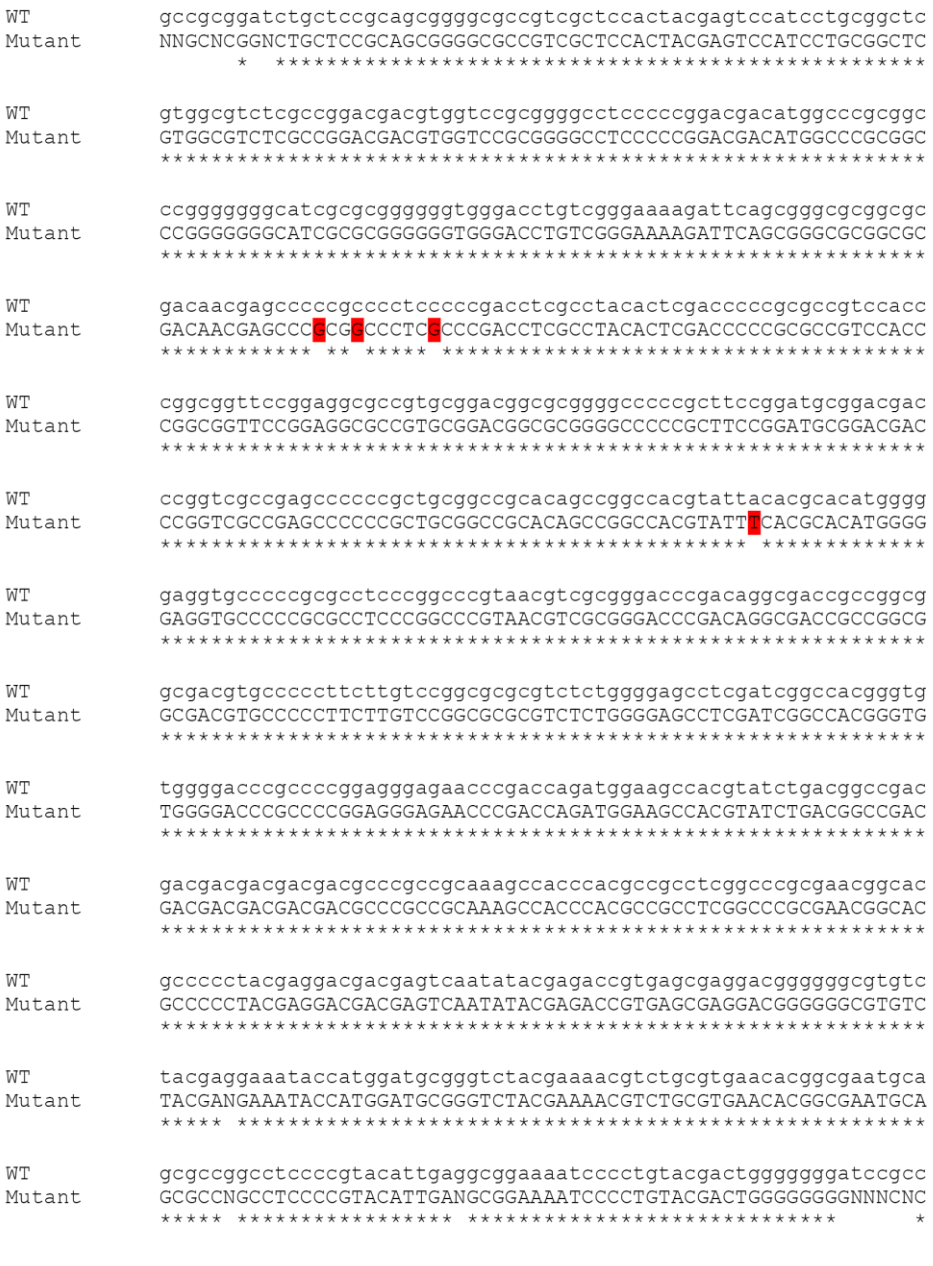

Fig A3.27: Sequence validation of KOS37-UL46 GFP AALA/Y519/AAPPA.

The UL46-PCR product was purified and sequenced using JRS 1033. The sequence was aligned to WT UL46 in order to verify the point mutations (red). The start codon of the C-terminal GFP-tag is in green. Sequences were aligned using Clustal Omega.

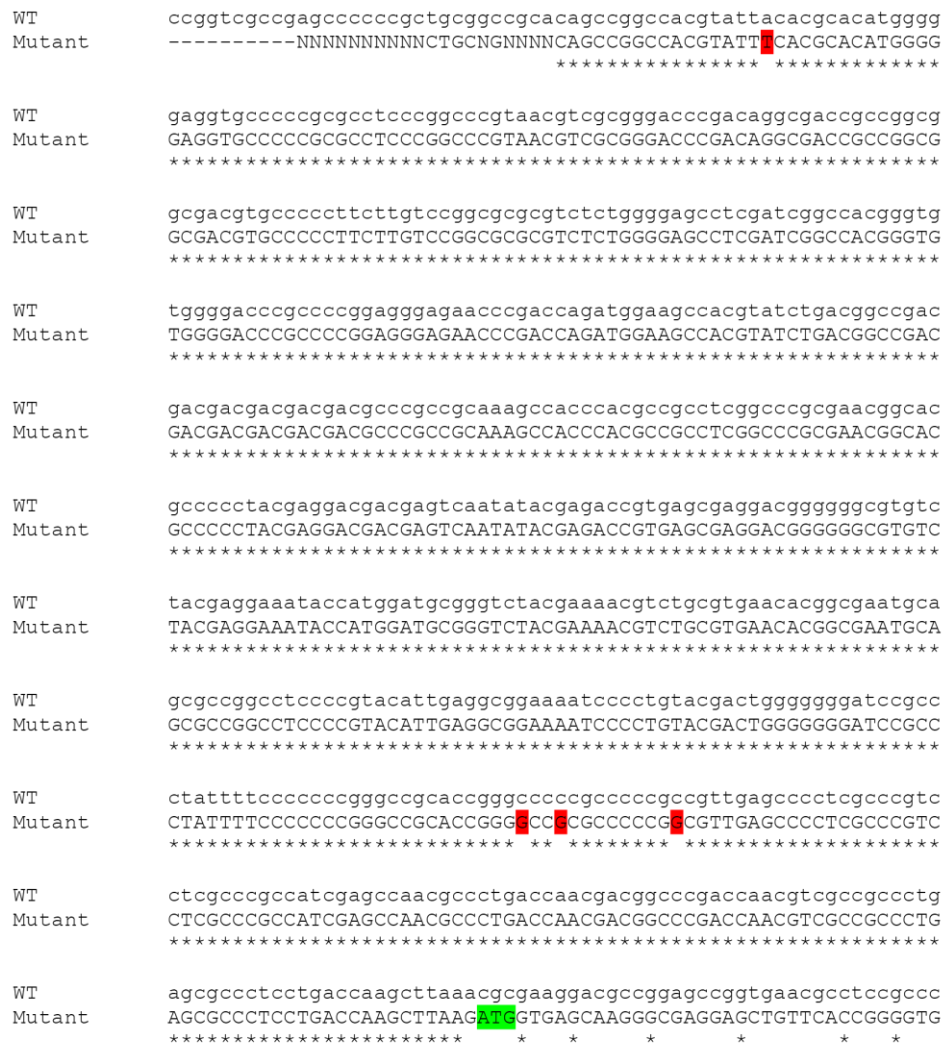

Fig A3.28: Sequence validation of KOS37-UL46 GFP AALA/Y519/AAPPA.

The UL46-PCR product was purified and sequenced using JRS 754. The sequence was aligned to WT UL46 in order to verify the point mutations (red). The start codon of the C-terminal GFP-tag is in green. Sequences were aligned using Clustal Omega.

Chapter A6

Appendix for: The role of tyrosine-based binding motifs for recruitment and binding of SFKs, p85, Grb2 and Shc in inhibition of TCR receptor signaling events

All experiments presented within this chapter were performed by U. Strunk, with the exception of the construction of the pcDNA-UL46 GFP Y613F/Y624F plasmid which was generated by Holly Saffran.

Preface

This appendix contains the sequencing results for the generated pcDNA-UL46 GFP constructs.

6A.1 Results

After generating the pcDNA3.1-UL46 constructs, we sequencing across the UL46 locus with the JRS754. The sequencing results were aligned to WT HSV-1 KOS (accession number JQ673480; version JQ673480.1) VP11/12 using Clustal Omega.

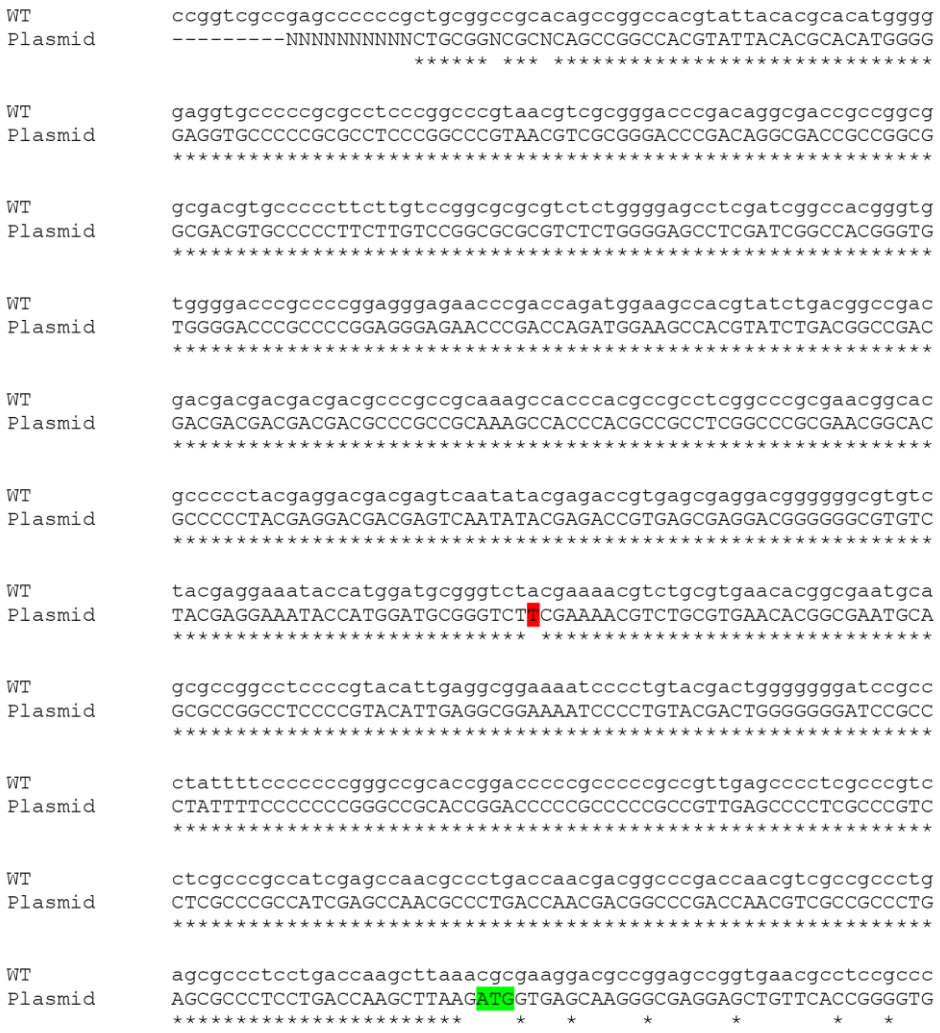

Fig A6.1: Sequence validation of pcDNA3.1-UL46 GFP Y633F.

The UL46-PCR product was purified and sequenced using JRS 754. The sequence was aligned to WT UL46 in order to verify the point mutation (red). Sequences were aligned using Clustal Omega.

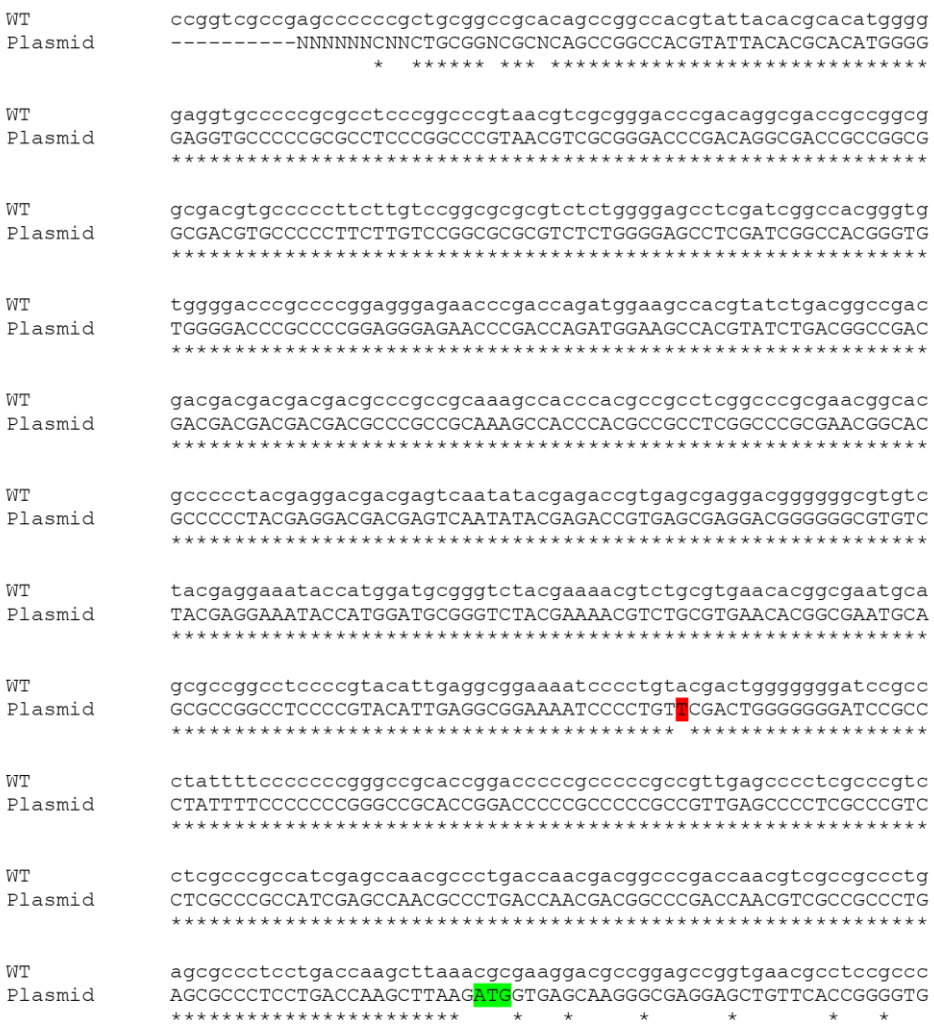

Fig A6.2: Sequence validation of pcDNA3.1-UL46 GFP Y657F.

The UL46-PCR product was purified and sequenced using JRS 754. The sequence was aligned to WT UL46 in order to verify the point mutation (red). Sequences were aligned using Clustal Omega.

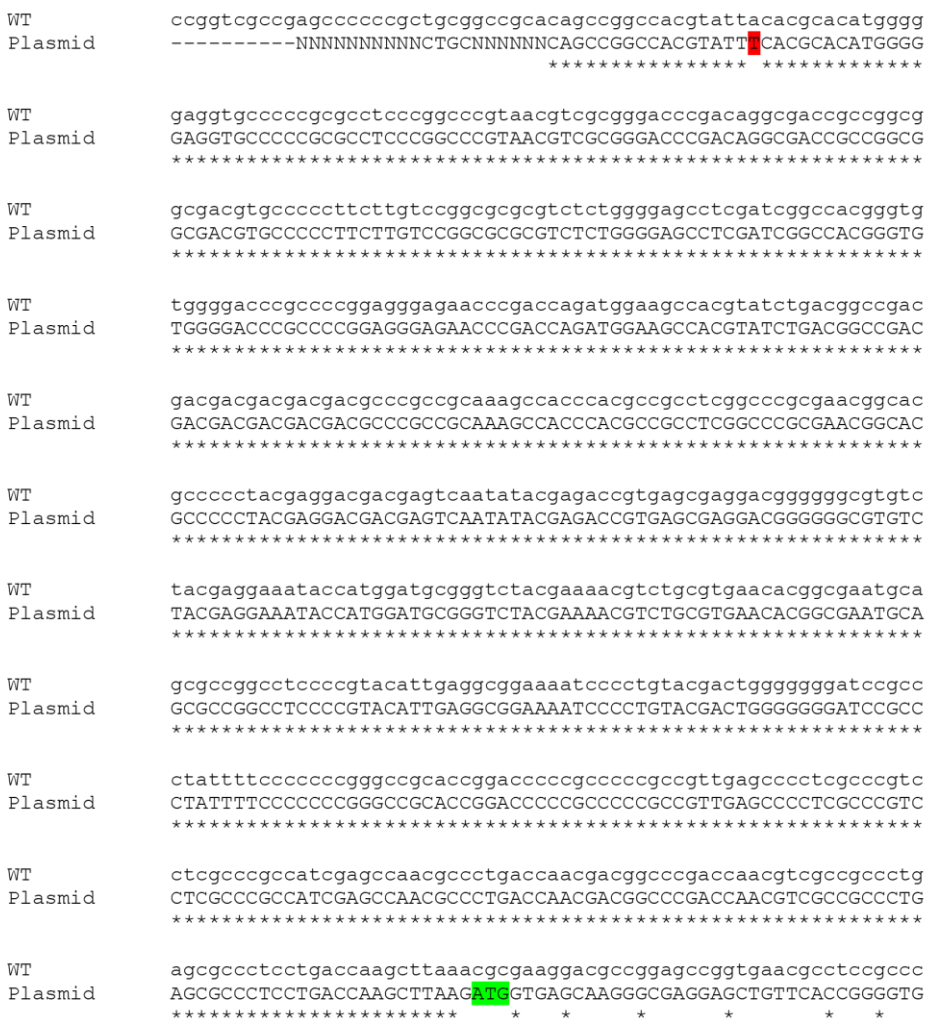

Fig A6.3: Sequence validation of pcDNA3.1-UL46 GFP Y519F.

The UL46-PCR product was purified and sequenced using JRS 754. The sequence was aligned to WT UL46 in order to verify the point mutation (red). Sequences were aligned using Clustal Omega.

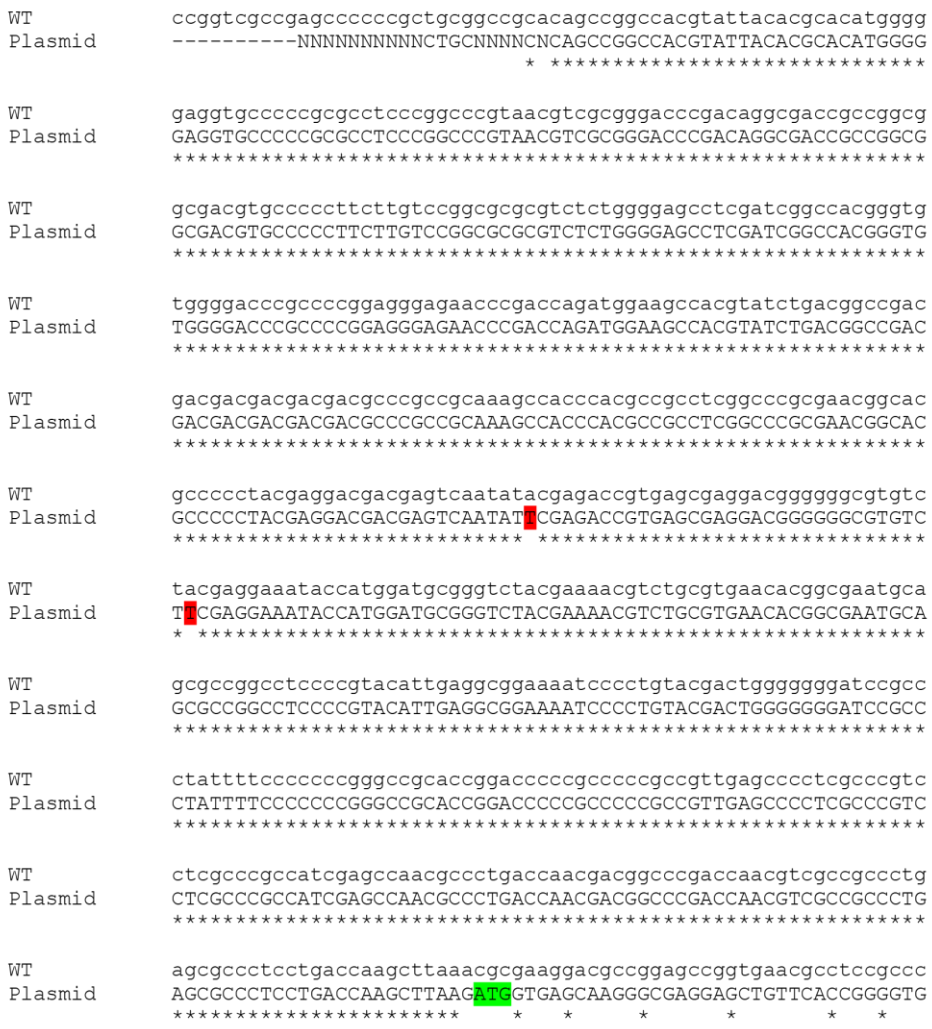

Fig A6.4: Sequence validation of pcDNA3.1-UL46 GFP Y613F/Y624F.

The UL46-PCR product was purified and sequenced using JRS 754. The sequence was aligned to WT UL46 in order to verify the point mutation (red). Sequences were aligned using Clustal Omega.